ITRI-148
December 1996
CATEGORY: UC-408

INHALATION TOXICOLOGY RESEARCH INSTITUTE ANNUAL REPORT

1995 - 1996

by the Staff of the
Inhalation Toxicology Research institute

INHALATION TOXICOLOGY RESEARCH INSTITUTE
LOVELACE BIOMEDICAL & ENVIRONMENTAL RESEARCH INSTITUTE
P.O. Box 5890 Albuquerque, NM 87185-5890

Prepared for
THE OFFICE OF HEALTH & ENVIRONMENTAL RESEARCH
U.S. DEPARTMENT OF ENERGY
UNDER CONTRACT NUMBER DE-AC04-76EV01013

The research described in this report involved animals maintained in animal care facilities fully accredited by the American Association for Accreditation of Laboratory Animal Care. The research described in this report that involved humans was conducted in compliance with government regulations protecting human subjects.

Printed in the United States of America

Available to DOE and DOE contractors from the Office of Scientific and Technical Information, P. O. Box 62, Oak Ridge, TN 37831: prices available from (615) 576-8401.

Available to the public from the National Technical Information Service, U.S. Department of Commerce, 5285 Port Royal Rd., Springfield, VA 22161.

ITRI-148
December 1996
Category: UC-408

Annual Report of the Inhalation Toxicology Research Institute Operated for the United States Department of Energy by the Lovelace Biomedical and Environmental Research Institute

October 1, 1995 through September 30, 1996

by the Staff of the
Inhalation Toxicology Research Institute
Joe L. Mauderly, DVM, Director

Scientific Editors
David E. Bice, PhD
Fletcher F. Hahn, DVM, PhD
Rogene F. Henderson, PhD
Mark D. Hoover, PhD
Robin E. Neft, PhD
Johannes Tesfaigzi, PhD
Janice R. Thornton-Manning, PhD

Paula L. Bradley, MA, Technical Editor

December 1996

Prepared for the Office of Health and Environmental Research of the
U.S. Department of Energy Under Contract Number DE-AC04-76EV01013

DISCLAIMER

TABLE OF CONTENTS

INTRODUCTION

The Institute

The Inhalation Toxicology Research Institute (ITRI) is a Government-owned facility leased and operated by the Lovelace Biomedical and Environmental Research Institute (LBERI) as a private, nonprofit research and testing laboratory. LBERI is an operating subsidiary of the Lovelace Respiratory Research Institute. Through September 30, 1996, ITRI was a Federally Funded Research and Development Center operated by Lovelace for the U.S. Department of Energy (DOE) as a "Single Program Laboratory" within the DOE Office of Health and Environmental Research, Office of Energy Research. Work for DOE continues in the privatized ITRI facility under a Cooperative Agreement. At the time of publication, approximately 70% of the Institute's research is funded by DOE, and the remainder is funded by a variety of Federal agency, trade association, individual industry, and university customers.

The principal mission of ITRI is to conduct basic and applied research to improve our understanding of the nature and magnitude of the human health impacts of inhaling airborne materials in the home, workplace, and general environment. Institute research programs have a strong basic science orientation with emphasis on the nature and behavior of airborne materials, the fundamental biology of the respiratory tract, the fate of inhaled materials and the mechanisms by which they cause disease, and the means by which data produced in the laboratory can be used to estimate risks to human health. Disorders of the respiratory tract continue to be a major health concern, and inhaled toxicants are thought to contribute substantially to respiratory morbidity. As the country's largest facility dedicated to the study of basic inhalation toxicology, ITRI provides a national resource of specialized facilities, personnel, and educational activities serving the needs of government, academia, and industry.

The Institute's multidisciplinary staff works in specialized facilities and takes a collaborative research approach to resolving scientific issues. ITRI is located on Kirtland Air Force Base East, approximately 10 miles southeast of Albuquerque, New Mexico. The more than 280,000 square feet of laboratory and support facilities include unique facilities and equipment for basic biological research and exposures of animals to all types of airborne toxicants. The staff of approximately 150 includes doctoral-level scientists in physical, chemical, biological, medical, and mathematical disciplines. Working with the scientists are highly trained scientific technicians, laboratory animal technicians, and a full range of support staff. The entire range of biological systems is employed, including macromolecules, cells, tissues, laboratory animals, and humans. The research includes both field and laboratory studies. Strong emphasis is placed on the quality of research and resulting data; the Institute has a Quality Assurance Unit and is fully capable of research in adherence to Good Laboratory Practices guidelines.

The Report

The papers in this report consist of extended abstracts organized along topical lines. The papers include summaries of non-proprietary research funded by both DOE and other sources, to represent the full scope of Institute activities. The source of funding is acknowledged for each paper. The appendices summarize the Institute's staff, publications, and presentations, seminars by visiting scientists, collaborations with scientists in other institutions, and a description of ITRI's educational activities.

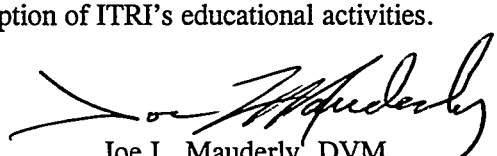

Joe L. Mauderly, DVM
President, Lovelace Biomedical and
Environmental Research Institute

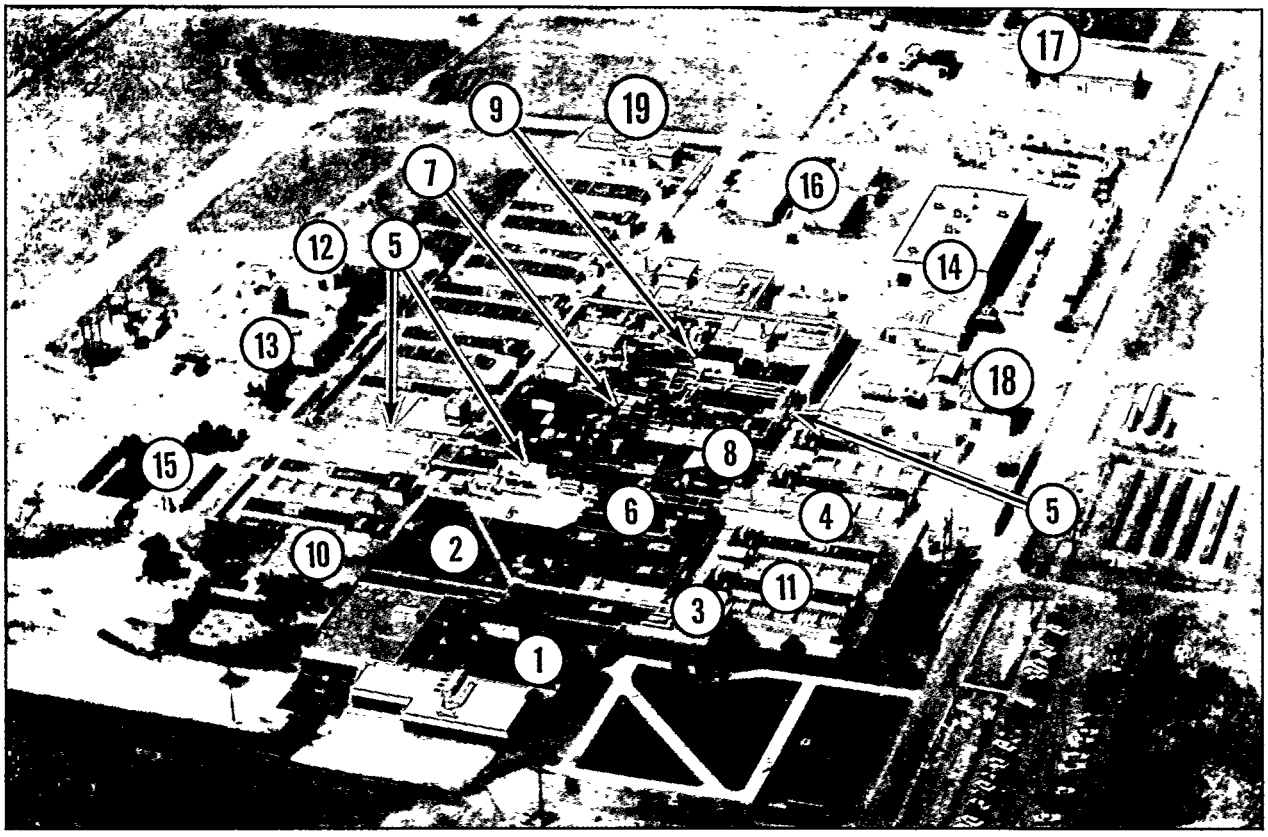

An aerial view of the Inhalation Toxicology Research Institute. The Institute's facilities, which were constructed in several increments starting in June 1962, consist of (1) administrative area, including the directorate, personnel, business, purchasing, and editorial offices, a cafeteria, conference rooms, and environment, safety and health operations; (2) central laboratory and office area, including aerosol science, radiobiology, pathology, chemistry, and toxicology laboratories; (3) cell toxicology laboratories; (4) pathophysiology laboratories; (5) chronic inhalation exposure complex with some laboratories suitable for use with carcinogenic materials; (6) exposure facility for acute inhalation exposures to chemical toxicants and beta- and gamma-radionuclides; (7) exposure facilities for acute inhalation exposures to alpha-emitting radionuclides; (8) veterinary hospital and facilities for detailed clinical observations; (9) small-animal barrier-type housing facilities; (10) library and quality assurance facilities; (11) kennel buildings; (12) analytical chemistry building; (13) engineering and maintenance support building; (14) property management, receiving, and storage building; (15) auxiliary office and classroom complex; (16) auxiliary laboratories; (17) waste storage and treatment facility; (18) standby power facility; and (19) animal quarantine facility.

LIST OF ANNUAL REPORTS

Selective Summary of Studies in the Fission Product Inhalation Program (July 1964 through June 1966):

LF-28, 1965
LF-33, 1966

Fission Product Inhalation Program Annual Report (1966–1972):

LF-38, 1967
LF-39, 1968
LF-41, 1969
LF-43, 1970
LF-44, 1971
LF-45, 1972

Inhalation Toxicology Research Institute Annual Report (1972–1996):

LF-46, 1973
LF-49, 1974
LF-52, 1975
LF-56, 1976
LF-58, 1977
LF-60, 1978
LF-69, 1979
LMF-84, 1980
LMF-91, 1981
LMF-102, 1982
LMF-107, 1983
LMF-113, 1984
LMF-114, 1985
LMF-115, 1986
LMF-120, 1987
LMF-121, 1988
LMF-126, 1989
LMF-129, 1990
LMF-134, 1991
LMF-138, 1992
ITRI-140, 1993
ITRI-144, 1994
ITRI-146, 1995
ITRI-148, 1996

Long-Term Dose-Response Studies of Inhaled or Injected Radionuclides (1988–1993):

LMF-128, 1989
LMF-130, 1990
LMF-135, 1991
ITRI-139, 1992–1993

I. AEROSOL TECHNOLOGY AND CHARACTERIZATION OF AIRBORNE MATERIALS

THE EFFECT OF RELATIVE HUMIDITY ON THE SIZE DISTRIBUTION OF DRY POWDER PARTICLES

Bijian Fan and Yung-Sung Cheng*

Of all the physical parameters that influence the delivery of dry powder medicine to the lung, particle aerodynamic diameter is the most critical. Only particles within the narrow size range of 0.5 to 5 μm can reach the deep lung to medicate this region (Gonda, I. *J. Pharm. Pharmacol. 33*:692, 1981); thus, all dry-powder inhalers attempt to present drug particles in this size range. Some dry powder particles absorb moisture and grow if exposed to a humid environment. This can change the location of deposition in the respiratory tract and the efficacy of drug delivery by inhalation. The purpose of this study was to investigate the size distribution of dry powder particles in a range of humid environments that might occur as particle enters the human respiratory tract. The knowledge derived could help us to understand the effect of humidity on the delivery of dry powder to the lung and suggest ways to reduce adverse effects.

The distribution of particle aerodynamic diameters for three different powders at relative humidity of 10%, 30%, 60%, and 90% was measured using an Aerosizer (Amherst Process Instruments, Hadley, MA). The powder included Bricanyle, a commercially available protein drug (Draco, Lund, Sweden), and industrial powders, titanium dioxide (TiO_2), and cobalt (Monsato, St. Louis, MO).

The built-in powder disperser module of the Aerosizer was used to suspend the powder particles in a stream of carrier air of known relative humidity. The measurement began by loading approximately 0.01 cm^3 of dry powder into the disperser cup. A jet of carrier air from the disperser nozzle caused the powder to become airborne. Relative humidity of the carrier air was controlled by adding an appropriate volumetric flow of humid air to a known flow of dry air. The duration of each test, from start of powder dispersion to completion of powder size measurement, was 3 min. Essentially all of the powder sample was dispersed from the cup during each test. The duration of powder dispersion was deliberately kept short to evaluate the short-term influence of relative humidity on particle size. Such a condition is representative of what may occur when dry powder is dispersed into a humid environment such as the human respiratory tract. Different results might have been obtained if the powder had been allowed to equilibrate in the humid environment prior to dispersion.

The changes in particle size as a function of relative humidity are presented in Figure 1 as mean geometric diameters for the three kinds of dry powders. The mean geometric diameter of three powders increased with increasing relative humidity. As the dry powders were dispersed, they apparently absorbed moisture and either grew or agglomerated.

To assist in quantifying the susceptibility of the different powders to hygroscopic growth, we defined a simple dimensionless growth parameter, $R = D_{90\%}/D_{10\%}$, where $D_{90\%}$ was the mean geometric diameter at 90% relative humidity, and $D_{10\%}$ was the mean geometric diameter at 10% relative humidity. As the relative humidity of the air changed from 10% to 90%, it was found that TiO_2 was more susceptible to particle growth, with a growth parameter of $R = 1.3$. Cobalt was somewhat less susceptible with $R = 1.2$, and Bricanyle was even less susceptible with $R = 1.1$. Note, that particle deposition within the human respiratory tract is likely to depend on both the initial particle size of the powder and the magnitude of the growth parameter R after the aerosol enters the nose or mouth.

This study provides information on the particle hygroscopic growth of three types of dry powders exposed to different levels of relative humidity during the dispersion process. Further work will address

*Postdoctoral Fellow

the variation of particle size distributions from longer exposures to a humid environment before and after dispersion.

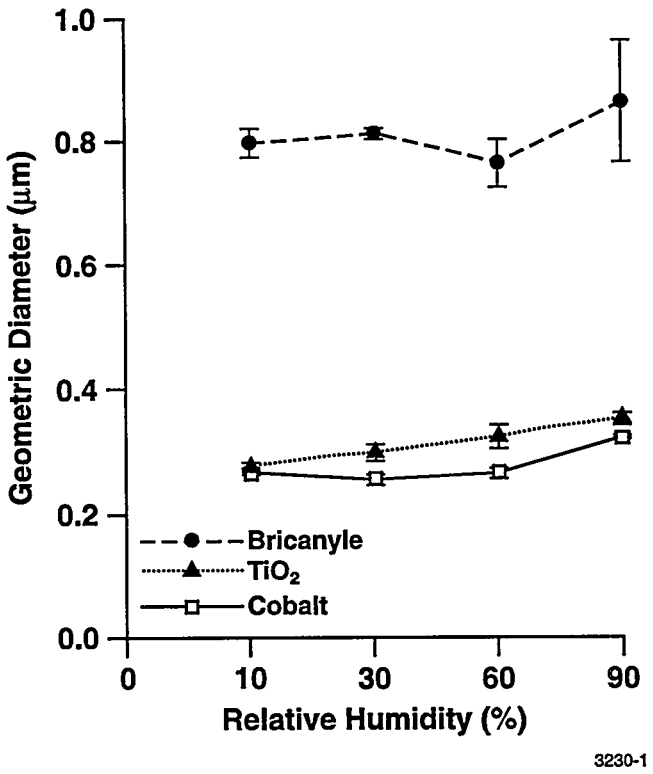

Figure 1. Influence of the relative humidity of the dispersion airjet on the mean geometric particle diameter of three powders resuspensed by the Aerosizer aerodynamic particle sizer.

(Research sponsored by the Office of Health and Environmental Research, U.S. Department of Energy, under Contract No. DE-AC04-76EV01013.)

PERFORMANCE QUALIFICATION TESTS OF THE MILLIPORE AW-19 MEMBRANE FILTER FOR USE IN MEASURING WORKPLACE AND EFFLUENT AEROSOLS

Mark D. Hoover, Alice F. Fencl, and George J. Newton

In previous annual reports (1990–91, p. 16 and 1991–92, p. 5), we described the technical bases for selection and use of filter media in continuous air monitors for alpha-emitting radionuclides. Four major requirements are that the filter (1) collects particles on its surface so that the alpha energy spectrum is not degraded by burial of particles in the filter matrix, (2) has a collection efficiency greater than 95% for all particle sizes so that results are not biased by sample losses, (3) is rugged enough to prevent breakage during normal handling, and (4) has a low pressure drop so that samples can be collected at a reasonably high flow rate of 25 to 60 L/min (1 to 2 cfm) through filters that are approximately 50 mm diameter (typical for collecting workplace and effluent aerosols). We recommended the Millipore Fluoropore 5-μm pore size, teflon membrane filter as having the best overall combination of front-surface collection, collection efficiency, durability, and low pressure drop, and we recommended the Millipore AW-19 mixed cellulose ester, supported membrane filter as an excellent alternative when it is desirable to use a filter that can be dissolved for chemical analyses. In addition, the "up" and "down" sides of the AW-19 filters (as they are packaged by the manufacturer) are essentially equivalent, which simplifies handling. We noted, however, that the pressure drop characteristics of the Fluoropore filter were substantially better that those of the AW-19 filter (59 L/min/cm^2 at 5 psi pressure drop for the Fluoropore, versus only 16 L/min/cm^2 for the AW-19 filter). The tradeoff of pressure drop versus chemical solubility is frequently required. Fortunately, the pressure drop of the rugged AW-19 filter is essentially the same as that of the fragile Millipore SMWP, 5-μm pore size, unsupported, mixed cellulose ester filter that was the previous choice for use in alpha continuous air monitors.

During this past year, we completed our qualification of the AW-19 filter for workplace and effluent sampling by conducting a formal evaluation of its collection efficiency for particles of 0.3 μm aerodynamic diameter and its pressure drop at flow rates of 28.3, 56.6, and 84.9 L/min (1, 2, and 3 cfm). The challenge diameter of 0.3 μm is used for such tests because filters typically have a minimum collection efficiency for particles that have diameters in the range of 0.2–0.5 μm. Above about 0.3 μm diameter, filtration efficiency increases due to inertial impaction, and below this size efficiency increases due to diffusion. A common misconception is that filters act as sieves, and that there is a direct relationship between the pore size of a filter and the minimum particle size that can be collected. In reality, filtration occurs by a complex combination of mechanisms including direct interception, inertial deposition, diffusional deposition, electrical attraction, and gravitational sedimentation. Filters with nominal pore sizes larger than 1 μm can be very efficient collectors of sub-micrometer particles. In fact, membrane filters show no serious degradation of collection efficiency until the pore diameters exceed 5 μm. Thus, filters with a 5-μm pore size are often preferred because they retain high-efficiency values, while providing lower pressure drops than smaller pore-size filters.

Figure 1 is a schematic diagram of the experimental setup for the filter efficiency tests, including the filter holder geometry for the tested and backup filters. The approach is based on the test methods described in the U.S. Nuclear Regulatory Commission technical resource document *Air Monitoring in the Workplace* (E. E. Hickey *et al.*, NUREG-1400, 1993). The filter to be evaluated is placed in front of a filter with known collection efficiency near 99.9%, and the collection efficiency (E) of the tested filter is calculated as:

$$E = A_1 / (A_1 + A_2)$$

where A_1 is the amount of aerosol collected on the first filter, and A_2 is the amount of aerosol collected on the backup filter. The sequential filter method can be used in the workplace to provide a test with actual workplace aerosols, or it can be used in the laboratory, as we have done. Use of the special filter holder is not required, but we found it convenient to place the primary filter on its own support screen and to use an o-ring to physically separate the primary filter and its support from the backup filter. This eliminated any concern that the efficiency of the backup filter would be affected by direct contact with the primary filter.

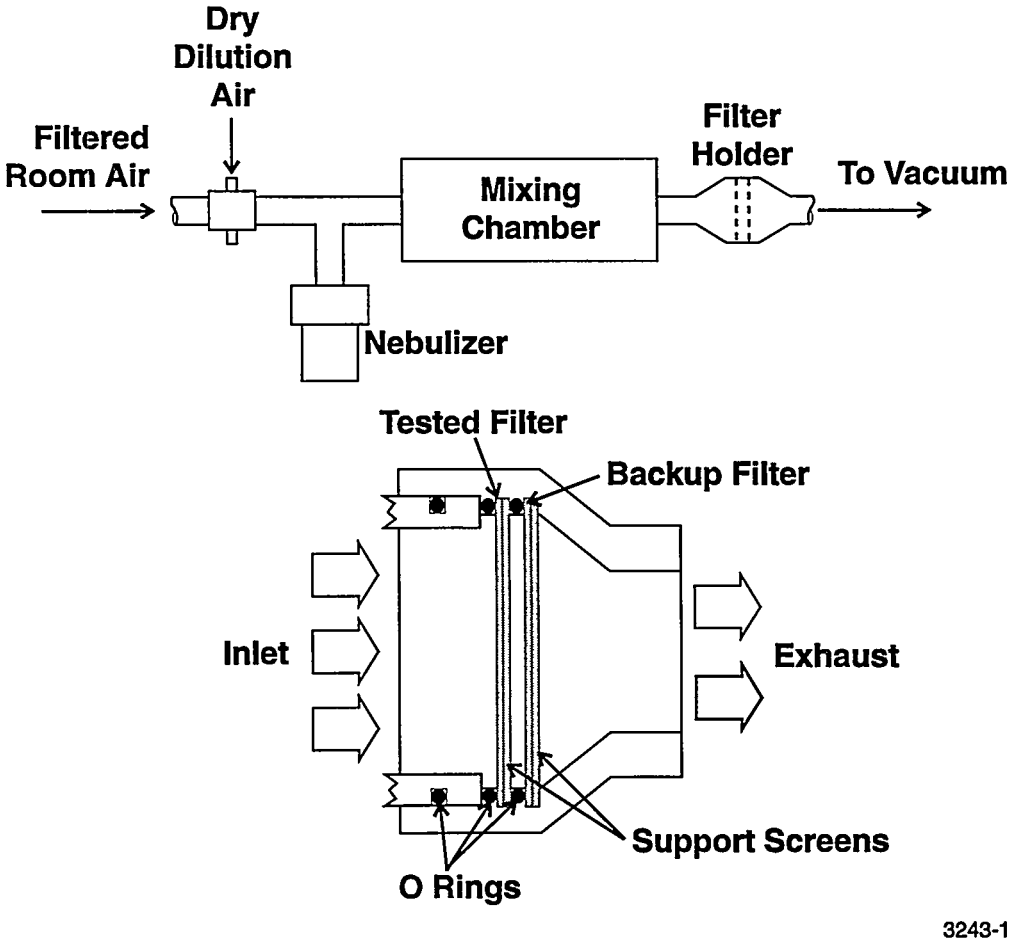

Figure 1. Schematic diagrams of the experimental setup for the filter efficiency tests (above) and the filter holder geometry for the tested and backup filters (below).

The challenge aerosol was prepared from green fluorescent, 0.3 μm monodisperse diameter, polymer microspheres (Duke Scientific Corp., Palo Alto, CA). A stable suspension of individual particles was achieved in a mixture of 50% ethyl alcohol, 50% ultra-pure water; aggregation of the particles was a problem if they were suspended in water alone. Aerosols were generated by a Lovelace nebulizer operated at 30 psi with a nominal flow rate of 1.5 L/min. Dry, compressed air was added to evaporate the carrier liquids, and a small amount of demand dilution air was provided to balance the generation and aerosol collection flow rates. Monodispersity and proper aerodynamic size of 0.3 μm were confirmed by cascade impaction using a Micro-Orifice, Uniform Deposit Impactor (MOUDI, MSP, Inc, St. Paul, MN). The amounts of fluorescent material on the primary filter, support screen, and backup filter were determined in a fluorometer (Model 111, Turner Corporation, Palo Alto, CA) following dissolution of the

fluorescent particles in 10 mL of 50% ethyl acetate, 50% ethyl alcohol. Collection efficiency of the support screen was approximately 3% of any material penetrating the primary filter. Fluoropore 5-μm pore size filters were used as the backup filters because they have a suitably high collection efficiency, and they contribute a negligible background to fluorometric analysis. Solutions from the backup filter were analyzed directly, and solutions from the primary filter were diluted by a factor of 100 prior to analysis. That provided approximately equal sensitivity for detection of fluorescence on the primary and backup filters.

Pressure drop was measured on 10 filters from each of three separate lots of AW-19 filters at flow rates of 28.3, 56.6, and 84.9 L/min. Collection efficiency tests were performed on six filters from lot one and five filters from lot two at 28.3 L/min and on five filters selected from the three lots at 84.9 L/min. These tests were performed on the nominal "collection" side of the AW-19 filters. Following the normal convention of filter packaging by Millipore Corporation, the collection side is the "down" side of the filter as it is removed from the box. Although both sides are essentially the same, the down side is slightly flatter than the up side, because the down side is in contact with smooth preparation surface during manufacturing. The up side has slightly more contour because the membrane tends to slump between the fiber support on the up side. We tested collection efficiency on the up side of one filter from each lot at 28.3 L/min, and we tested pressure drop on five filters from each lot at all three flow rates.

Table 1 summarizes the experimental results. The pressure drops for the collection side of 47-mm diameter AW-19 filters show (1) nominal linearity of pressure increase with flow rate, (2) reasonable uniformity of pressure drop within each lot, (3) excellent uniformity in the third lot, which was the most recent purchase, (4) close agreement between performance of lots 1 and 3, and (5) a slightly higher overall pressure drop in lot 2 as compared to lots 1 and 3. Although relatively modest, variations in pressure drop within and between lots indicate that the user must adjust the flow control valve whenever a new filter is installed. As noted by Millipore in its instructions to users, we noted a slight decrease of about 0.1 psi when the up side of the filter was used as the collection side. We attribute this to the possibility that the effective size of pore entry is slightly larger for the up side of the membrane than for the down side (which was in contact with the smooth preparation surface during manufacturing).

Filter collection efficiency for the collection (down) side of the AW-19 filters was greater than 99.9% at both 28.3 and 84.9 L/min. Modest differences in pressure drop performance between lots 1 and 2 did not result in differences in collection efficiency. In addition, the collection efficiency for the up side of the AW-19 filters was similarly excellent at 99.93 $\pm$ 0.03%. This confirms that any modest differences between the up and down sides of the AW-19 are not operationally significant.

In conjunction with earlier data on the performance of the AW-19 filter for alpha spectroscopy (1991–92 Annual Report, p. 5), these results provide a technical basis for selection of the AW-19 filter for use in sampling radioactive aerosols in the workplace and in effluent streams.

Table 1

Experimental Results at Three Flow Rates for Pressure Drop and Collection Efficiency for 0.3-μm Diameter Monodisperse Fluorescent Microspheres for the Millipore AW-19 Mixed Cellulose Ester, Supported Membrane Filter

Flow Rate	Face Velocity (cm/s)[a]	Pressure Drop (psi)[b]	Collection Efficiency (%)[c]
28.3 L/min (1 cfm)	34.1	0.8 ± 0.05 1.0 ± 0.04 0.8 ± 0.00	99.95 ± 0.04 99.98 ± 0.01
56.6 L/min (2 cfm)	68.1	1.7 ± 0.09 2.2 ± 0.08 1.8 ± 0.04	not tested
84.9 L/min (3 cfm)	102.2	2.9 ± 0.19 4.2 ± 0.24 2.9 ± 0.05	99.93 ± 0.04

[a]Face velocity is based on an active area of 13.85 cm^2 for a open diameter of 42 mm on a 47-mm diameter filter.

[b]Pressure drop results are given as the mean and standard deviation for the collection (down) side of 10 filters from each of three production lots. Pressure drops were slightly lower (0.1 psi, for example) for the up side of the filters.

[c]Collection efficiency results are given as the mean and standard deviation for six filters from lot 1 and five filters from lot 2 at 28.3 L/min, and for five filters (two from lot 1, two from lot 2, and one from lot 3) at 84.9 L/min. Collection efficiency for the up side of one filter each from the three lots was similar at 99.93 ± 0.03%.

(Research performed under funding from Westinghouse Hanford Company through memorandum purchase order MJW-SBL-A257723 with the U.S. Department of Energy under Contract No. DE-AC04-76EV01013.)

USE OF AMBIENT RADON PROGENY FOR IN-PLACE TESTING OF HIGH-EFFICIENCY PARTICULATE AIR FILTERS

*George J. Newton, Mark D. Hoover, Hsu-Chi Yeh, Dennis Yazzie, and Judith Velarde**

The purpose of this work was to evaluate the use of naturally occurring radon progeny for in-place testing of HEPA (high efficiency particulate air) filters. HEPA filters are routinely used to control emissions of radioactive particles from nuclear facilities. Because HEPA filters play a critical role in protecting members of the public and the environment, there are stringent requirements for verifying the efficiency of HEPA filters prior to their installation and during their use. Traditional methods for the performance tests involve introducing a challenge aerosol before the filter and comparing the concentration of particles before and after the filter. Special aerosol generation and characterization systems are required, the particle size distribution of the challenge aerosol must be confirmed, the test process can be tedious, and performance results are only available during the actual period of testing.

HEPA filters typically consist of a paper or fiberglass filter media approximately 0.038-cm thick (0.015-in) that is folded accordion-style around cardboard or aluminum-sheet separators. This design presents many square meters of surface area for filtration, distributes the buildup of dust over a large surface area, and prolongs the useful life of the filters. The folded filter is enclosed in a rigid frame that is air tight except through the filter media. Leaks through a HEPA filter system can occur in three ways: an inadequate seal between the filter frame and the filter housing, a separation or crack between the filter media and the filter frame, and a crack or hole in the filter media itself. The design of the test system was considered adequate to simulate any one of these leak pathways.

Prior to installation, HEPA filters are tested by DOE test facilities for verification of the 99.97% collection efficiency of the 0.3 μm diameter challenge aerosol. The challenge aerosol is typically a vaporization-condensation aerosol of di-octol-pthalate (DOP) or di-2-ethyl-hexyl-sebacate (DEHS). DEHS is the preferred material because of potential toxicity of DOP. The diameter of the challenge aerosol, 0.3 μm, is used because filters typically have a minimum collection efficiency for particles in the diameter range of 0.2–0.5 μm. Above about 0.3 μm diameter, filtration efficiency increases due to inertial impaction, and below this size efficiency increases due to diffusion. In the alternate method, the challenge aerosol consists of alpha-emitting radon progeny, attached to the ambient background room aerosol of about 0.2 μm diameter.

A simple calculation can be done to determine if a leakage rate of 0.05% can be detected within a reasonable sampling period. For example, if a 0.05% leak could be detected within 24 h, then it might be possible to detect a 1% leak within less than 1 h. Such a detection capability would provide a reasonable response time for a serious decrease in filter performance. The calculation begins by assuming that the typical indoor concentration of ^{222}Ra is 1 pCi/L. Taking into account the availability of one alpha decay from ^{218}Po and one alpha decay from ^{214}Po for each decay of ^{222}Ra, this provides an equilibrium concentration of 2 pCi/L of alpha-emitting, radon progeny radioactivity. A sampling rate of 42.5 L/min for 24 h, with a detection efficiency of 20% would result in an upstream accumulation of alpha counts as follows: (2 pCi/L) × (2.22 dpm/pCi) × (0.2 cpm/dpm) × (42.5 L/min) × (24 h) × (60 min/h) = 54,314 counts, and a downstream accumulation of alpha counts of 27 counts for a 0.05% leak. This would provide adequate counting statistics to meet the *de facto* sensitivity standard.

Figure 1 shows a schematic diagram of the setup used to evaluate the proposed test method. A standard housing for 30.5-cm × 30.5-cm × 15.3-cm (12-in × 12-in × 6-in) HEPA filters was mounted

*Department of Energy Teacher Research Associate Program (TRAC) Participant

Figure 1 shows a schematic diagram of the setup used to evaluate the proposed test method. A standard housing for 30.5-cm × 30.5-cm × 15.3-cm (12-in × 12-in × 6-in) HEPA filters was mounted between two, 2-m-long sections of 15.8-cm (6-in) inner diameter schedule 80, poly-vinyl-chloride (PVC) pipe. A bypass loop of 1.6-cm (5/8-in) inner diameter stainless steel tubing was installed between the filter inlet and outlet tubes. A variable-speed, rotary air pump in the loop was used to allow a controlled "leak" of unfiltered air to bypass the filter. The leak rate was controlled by adjusting the voltage of the rotary pump. Proper leak rate was periodically confirmed by connecting the output of the pump to a calibrated flow meter. A 110-V rotary blower was used to maintain a total flow rate of 8.21 m^3/s (290 cfm) through the HEPA filter. That provided a face velocity of 8.21 m/s (290 ft/min) which was in the manufacturer's suggested range of 75 to 150 m/s (250–500 ft/min). In practice, large arrays of HEPA filters are assembled to provide a total flow rate that is appropriate for the facility exhaust stream. Testing of penetration through a single filter was considered adequate to demonstrate the efficacy of the test method.

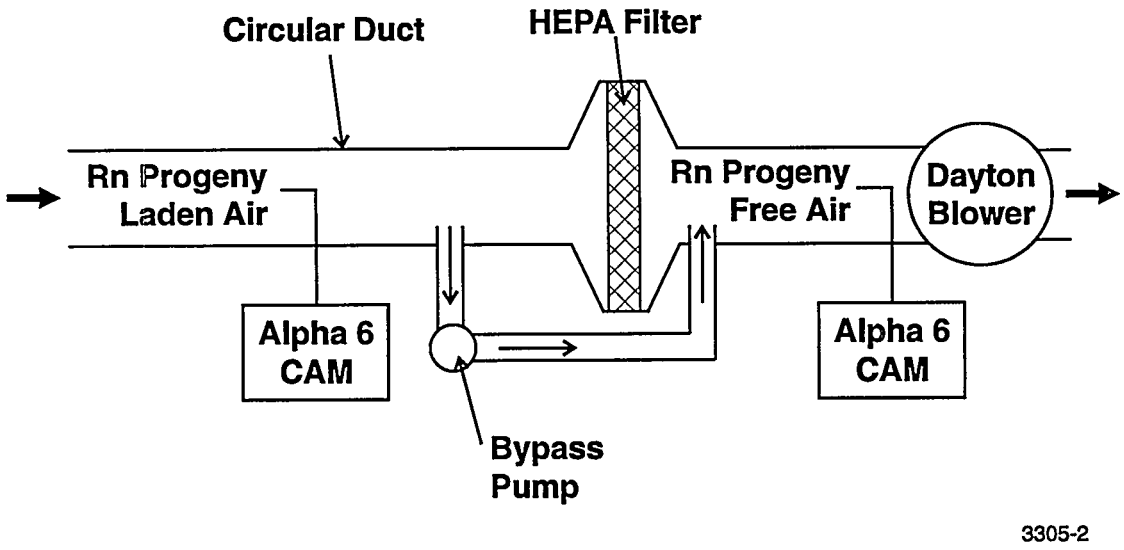

Figure 1. Schematic diagram of the experiment to demonstrate the efficacy of using ambient radon progeny to test the collection efficiency of HEPA filters. Shown are the filter housing with associated inlet and exhaust ducts, the air mover for drawing air through the filter, the variable-flow bypass line for allowing a controlled amount of ambient air to bypass the filter, and the upstream and downstream alpha continuous air monitors.

The concentration of ambient radon progeny radionuclides was measured simultaneously on both sides of the HEPA filter via two Eberline Alpha 6 inline continuous air monitors (CAMs) (Eberline Instrument Corp., Santa Fe, NM). The upstream CAM was located near the extraction location of the simulated leak. The downstream CAM was located far enough from the inleakage to allow good mixing of the filtered and unfiltered air. The CAMs were operated at a flow rate of 42.5 L/min (1.5 cfm). The detection efficiency for radon progeny was 20%. During a nonleaking condition, only radon gas itself should pass through the HEPA filter. Any radon progeny detected by the downstream CAM would be the result of ingrowth of the progeny during the time-of-flight of radon gas from the exit side of the HEPA filter to the probe and the CAM. The correction factor for this ingrowth can be estimated by calculation or determined empirically by operating the system in a leak-tight configuration. After the correction

factor is applied, the ratio of alpha radioactivity detected after and before the filter will be proportional to the leak rate.

Figure 2 shows the cumulative alpha counts detected both upstream and downstream of the HEPA filter for a range of bypass leaks used to test the concept. Bypass leak flow rates were 5, 4, 3, 2, 1, and 0.5%. Data shown are for the downstream counts divided by the upstream counts (percent) versus time in hours. The test system demonstrated that an alarm could have been set within 1–4 h for all leak flow rates shown. The counting system was stabilized after 4 h and indicated the proper ratio for the leak. Excellent agreement was found for bypass flow rates down to about 0.5%. For bypass flow rates less than 0.5%, we corrected the time-of-flight radon progeny ingrowth based on the geometry of the bypass system. For bypass flow rates <0.5%, the data were more erratic because of the inaccuracy in the correction algorithm. In an actual HEPA filter installation, such a correction calculation is not required. In an actual installation, the relative counts of radon progeny upstream and downstream are also empirical factors unique to the particular installation. In practice, continuous, on-line monitoring of the HEPA filter integrity would provide additional safety for operation of the facility.

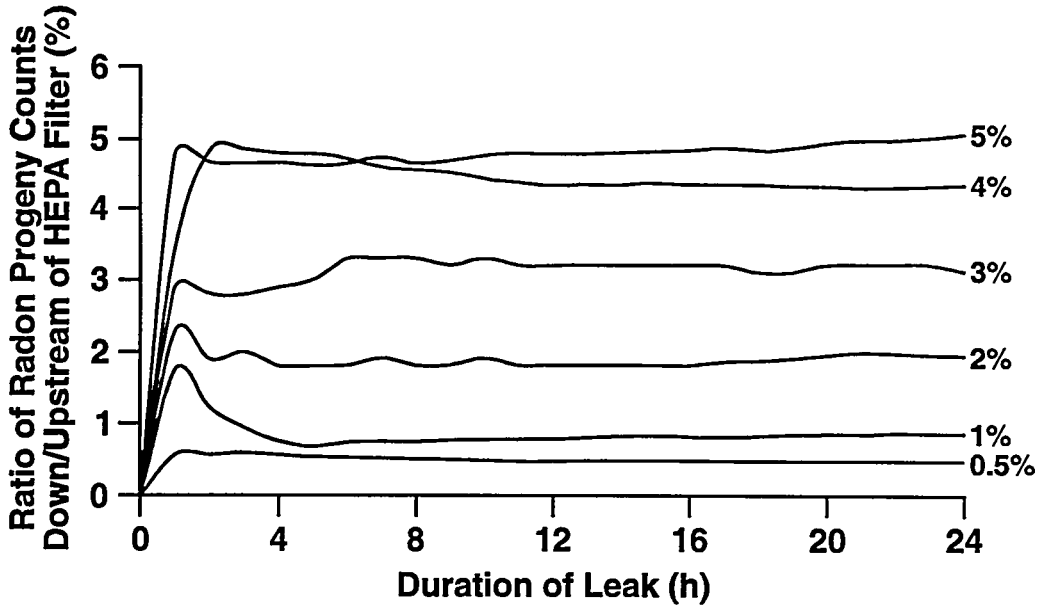

Figure 2. Plot of data from in-place HEPA filter testing using radon progeny. The family of curves shows the downstream/upstream (%) counts for six different tests as a function of time. The labels at the end of the curves (24 h) are for the bypass leak flow rates (%).

Based on these proof-of-principle tests and the calculations for sensitivity, it appears that radon progeny can be used to monitor HEPA filter integrity at the 0.05% leak criterion as long as the concentration of ^{222}Rn is above a minimum level. If the concentrations of radon progeny are too low to quantify the 0.05% leak criterion, the system can still be used to provide a continuous, on-line indication of HEPA filter integrity. This reassurance would be valuable to operational personnel in deciding when and if a facility should be shut down for traditional in-place HEPA filter testing using traditional challenge aerosols.

This work has demonstrated the feasibility of using naturally occurring radon progeny for in-place testing of HEPA filters. Following the installation of suitable extraction probes before and after the filters, it would be straightforward to temporarily install a pair of alpha CAMs for periodic testing, or to permanently install the monitors for continuous verification of filter performance. Permanent installation might be highly desirable on critical filtration systems. Future work should include demonstration tests in operating nuclear facilities.

(Research sponsored by the Office of Health and Environmental Research, U.S. Department of Energy, under Contract No. DE-AC04-76EV01013.)

CHARACTERIZATION OF BACTERIA AEROSOLS USED FOR LASER EXPERIMENTS

*Yung-Sung Cheng, Edward B. Barr, and Bijian Fan**

A Biosafety Level II Laboratory was set up at ITRI to conduct experiments on the use of fluorescent spectra of bioaerosols as a means to detect these particles in the air (1994–95 Annual Report, p. 1). Sandia National Laboratories (SNL) is developing the laser-based real-time detection technology, and ITRI is working with SNL scientists to evaluate this technology. This paper describes the methods we used in the generation and characterization of bacteria and presents some preliminary results.

The aerosol test system included an aerosol generator, a dryer, an aerosol test chamber, and instruments for collecting samples. A Hospitak air-blast nebulizer (Hospitak, Lindenhurst, NY) was used to resuspend bacteria from an aqueous suspension. The aerosol output from the nebulizer was 12 L min^{-1} using compressed air at 20 psig. A syringe pump was used to provide a constant input of liquid to the nebulizer at a uniform concentration and flow rate, resulting in stable aerosol production over a long period of time. The aerosol (1 L min^{-1}) passed through a warm diffusion dryer to remove water from the droplets. The rest of the output was removed through a filter. The dry aerosol entered a small cubic aerosol chamber (7 cm on each side) for fluorescent measurements. The test chamber was adapted from a stainless steel optical chamber. It had four windows (3.8 cm ID) with quartz lens for incoming laser light and for detection of fluorescent light from the particles. The aerosol entered the top via a 0.32 cm ID stainless steel tube and exited through a 0.64 cm ID tube. The aerosol flow was accelerated in the inlet nozzle to form an aerosol beam in the 2-cm distance between the nozzle and the outlet tube. The laser beam was focused at the center of the aerosol beam. The design of the aerosol chamber was based on results of preliminary tests in a much larger chamber. Design goals were to minimize aerosol deposition in the chamber and to allow better control of the aerosol beam inside the chamber. The inlet and outlet geometries were chosen based on computational fluid dynamics simulation studies. Results of the simulation studies predicted an optimal aerosol flow of 1 L min^{-1} with a sheath flow of 4 L min^{-1}. Sheath air was used to prevent the aerosol from depositing on the window. Less than 2% of 1 μm particles were deposited in the chamber when the sheath flow was used.

Both time-averaged (or grab) and real-time techniques were used to characterize the aerosol concentrations and particle size distributions. The time-averaged techniques involved collecting bacteria in impingers, filters, and impactors during an entire experiment. The impinger samples were plated in the Trypticase® Soy Agar with 5% sheep blood (Becton Dickinson Co., Cockeysville, MD) for viable bacterium counts. In addition, samples were taken from the impinger and filtered through a Nucleopore membrane filter for microscopic/image analysis of the bacteria particle size and morphology. Filter samples were weighed to determine the bacteria mass concentration. Real-time techniques, including optical methods (light scattering), differential mobility, and time-of-flight methods, were used to make instantaneous measurement of particle concentration or size distribution. Although the real-time instruments can be used to monitor the aerosol continuously during the experiment, they involve indirect measurements, which must be correlated/calibrated with measurements from the time-averaged samples. The high concentration ($>10^5$ bacteria per cm^3 of air) and small size (0.05–1.5 μm) range of some of the aerosols in our study place real-time techniques at the edge of their capabilities.

Four bacteria were evaluated in this study: *E. coli* (EC), *Bacillus thuringiensis* (BT), and *Bacillus globigii* (BG, also known as *Bacillus subtilis var niger*) which have elongated morphology, and *Staphylococcus aureus* (SA), which is spherically shaped. Table 1 shows the diameter and lengths of

*Postdoctoral Fellow

these materials determined from scanning electron microscopy (SEM). Figure 1 shows a SEM photo of BG.

Table 1

Geometric Mean (GM) Dimensions and Geometric Standard Deviation (GSD) of Four Bioaerosols Evaluated by Scanning Electron Microscopy in This Study

	Diameter		Length	
	GM (μm)	GSD	GM (μm)	GSD
E. coli	0.82	1.11	1.92	1.13
Staphylococcus aureus	1.00	1.11	–	–
Bacillus globigii	0.70	1.07	1.75	1.13
Bacillus thuringiensis	1.16	1.00	3.60	1.18

Figure 1. Scanning electron micrograph of bacillus gobilis on a 0.6 μm Nucleopore membrane filter.

Relatively high concentrations ranged from 80 mg m^{-3} for SA to about 300 mg m^{-3} for EC. Mass concentrations were then converted to number concentrations based on particle volumes determined as estimated from SEM photomicrographs. Number concentrations ranged from 4×10^4 per cm^3 of air for BT to 3×10^5 per cm^3 of air for EC. The viable concentrations were much lower than the number concentrations, indicating that the viability of these bacteria, especially BT and BG, was reduced in the generation and impinger sample collecting processes.

The aerodynamic particle size distributions of viable bacteria were obtained with the Andersen microbial impactor (Grasby GMW, Cleves, OH). The count mean aerodynamic particle diameters were between 0.73 and 0.91 μm with GSDs between 1.30 and 1.67. These results indicate that most viable aerosols were single bacteria. The aerodynamic diameters of the SA were close to the geometric diameter

determined from SEM because of its spherical shape and near-unit density. For elongated particles, the aerodynamic diameters were a function of dimensions and orientation of the bacteria in the flow field.

Our results indicate that the experimental setup can produce stable, highly concentrated bacteria aerosols which are suitable for laser experiments and that the characterization methods being used are appropriate for monitoring the bioaerosols and interpreting the data.

(Research performed under U.S. Department of Energy Contract No. DE-AC04-76EV01013 with funding from Sandia National Laboratories through Federal Agency Order AP-2829.)

AN IMPROVED METHOD TO PREPARE STABLE SUSPENSIONS OF MONTMORILLONITE CLAY FOR USE IN AEROSOL SCIENCE STUDIES

*George J. Newton, Mark D. Hoover, and Francesca Sisneros**

For many years, investigators at this Institute have used the predictable ion exchange and refractory properties of aluminosilicate clays to prepare "insoluble" forms of respirable particles with well-defined physical and chemical characteristics. Much of this work has involved the preparation of insoluble, radiolabeled, spherical particles for use in inhalation experiments with laboratory animals and in other basic aerosol science studies. The initial material for those studies was American Petroleum Institute (API) "Bayard, New Mexico, Montmorillonite Clay No. 30" obtained in 1963 from Ward Scientific (New York, NY). By the late 1980s, the Institute's supply of the original material was nearly exhausted, and no more clay was available from Ward Scientific. Newton, G. J. and Hoover, M. D. (1987–88 Annual Report, p. 39) obtained new stocks of the clay material from a geological formation near the original site in southwestern New Mexico. (The exact location of the original site had been obliterated by expansion of the adjacent Santa Rita Open Pit Copper Mine.)

Using cleaning and processing methods developed at the Institute over a number of years (see Newton, G. J. *et al.* In *Generation of Aerosols*, Ann Arbor Science, p. 399, 1980), similar action exchange capacities and particle size distributions were obtained with the new clay. However, an apparently greater content of nonclay inclusions in the new material required greater amounts of hydrogen peroxide (H_2O_2) to prepare the required stable colloidal suspensions of the clay. Because the historical method had used reagent-grade H_2O_2, the cost of preparing the clay for use increased concomitantly. Although the added cost was not significant for the small amounts of clay normally required for specialized aerosol studies, a recent project required substantial volumes of processed clay material which would have been prohibitively expensive and time-consuming to prepare. This provided an incentive to seek a more economical method for processing the raw clay. This report describes successful modifications of the clay preparation procedure to reduce costs and improve efficiency.

Table 1 compares the historical and improved procedures for preparing stable suspensions of the clay. As before, the raw clay was ground in a ball mill and sieved to prepare a powder that was free of pebbles and had a particle size smaller than 425 μm (40 mesh). The powder was suspended in water to form a slurry. However, instead of immediately decanting the suspension to obtain the small particle fraction for subsequent treatment with H_2O_2, NaCl was added to the suspension to further reduce the particle size distribution of the suspended clay. The Na^+ ions entered the clay matrix, displacing the naturally occurring Al^{+++}, Mg^{++}, and Ca^{++} ions. This increased the interlayer distances in the clay matrix, causing the clay to swell and separate into a finer suspension. Excess Na^+ was then removed by a running water dialysis. Clay suspensions were placed in dialysis tubing and suspended in a vessel having a few mL of tap water flowing into the vessel. Following running water dialysis, the stable suspension was decanted and treated with industrial grade H_2O_2.

Several kg of raw clay were prepared by grinding and sieving the clay through a 425 μm screen (40 mesh). The ground and sieved clay was separated into 200 g batches to investigate the results of varying the order of the clay preparation procedure. A batch was prepared using the historical method to yield a reference point for time, H_2O_2 requirements, and yield of the stable clay suspension. Nine, 200-g batches were used to investigate the preparation of Montmorillonite clay. Running water dialyses used Spectra/Por 7 (Spectrum, Houston, TX) dialysis tubing with a molecular weight cut-off (MWCO) of 1000.

---

*U.S. Department of Energy Summer Student Research Participant

Water used for these studies was Milli-Q (Millipore Corp., Bedford, MA) deionized water having a resistance of about 1.0×10^9 ohms/cm.

Table 1

A Change in the Historical Sequence of Steps for Processing Montmorillonite Clay Reduced the Requirements and Expense for H_2O_2 and Increased the Yield of a Stable Clay Suspension

Step	Historical Method	Improved Method
1	Grind and Sieve Raw Clay	Grind and Sieve Raw Clay
2	Suspend Clay in Water	Suspend Clay in Water
3	Decant Small Particle Fraction	Exchange Na into Clay Matrix
4	Treat with H_2O_2	Dialyze with Running Water to Remove Excess Na
5	Exchange Na into Clay Matrix	Decant Small Particle Fraction
6	Dialyze with Running Water to Remove Excess Na	Treat with H_2O_2
7	Resuspend Clay Suspension at Desired Concentration	Gentle Heat to Drive Off H_2O_2 and Resuspend Clay Suspension at Desired Concentration

Table 2 shows the results of the modifications of the clay preparation procedure. Substituting industrial grade H_2O_2 for reagent grade H_2O_2 resulted in a 90% savings in H_2O_2 on a per unit cost. Furthermore, by changing the order of the Na^+ packing to treat the clay immediately after making the clay slurry, the total requirement for H_2O_2 was reduced 95%. The yield was also increased when the running water dialysis was increased to 96 h. The final yield of stable clay suspension using the new clay was 23.1 ± 6.2% versus 25.3 ± 4.0% (mean ± SD) for the historical method.

Table 2

Comparison of the Relative Efficiencies and Costs of the Historical and Improved Methods for Preparing Stable Suspensions of Montmorillonite Clay

Attribute	Historical Method Original Clay	Historical Method New Clay	Improved Method, New Clay, 4-h Dialysis	Improved Method, New Clay, 96-h Dialysis
Percent Yield (Mass of Stable Suspension per Mass of Raw Clay)	25.3 ± 4.0 %	8.0 %	17.4 ± 9.1 %	23.1 ± 6.2 %
Unit requirement for Hydrogen Peroxide (Ml H_2O_2 per g stable clay in suspension)	4.0 mL/g clay	5.0 mL/g clay	0.2 mL/g clay	0.2 mL/g clay

The new method, adapted to the new source of clay, has produced a stable clay suspension with exchange capacities and particle size distribution that are similar to the original clay suspensions made from the American Petroleum Institute "Bayard, New Mexico, Montmorillonite Clay No. 30." Furthermore, the new method has reduced the total cost of preparing stable clay suspensions to about 5% of the costs of the historical method. Thus, a source of Montmorillonite clay is now available for aerosol and inhalation toxicological studies that can be related to the historical studies.

(Research sponsored by the Assistant Secretary for Defense Programs, U.S. Department of Energy Contract No. DE AC04-76EV01013.)

DESIGN AND EVALUATION OF AN AEROSOL WIND TUNNEL FOR APPLIED INDUSTRIAL HYGIENE AND HEALTH PHYSICS STUDIES

Mark D. Hoover, Edward B. Barr, George J. Newton,
Carlos Ortiz, N. K. Anand*, and Andrew R. McFarland**

A new aerosol wind tunnel has been designed, fabricated, and assembled for applied industrial hygiene and health physics studies at the ITRI. This project is part of a cooperative program with Texas A&M University that takes advantage of their significant experience with the design and operation of aerosol wind tunnels. This report describes the wind tunnel and presents results for its initial performance.

A schematic of the new aerosol wind tunnel is shown in Figure 1. The tunnel is constructed from stainless steel to facilitate cleaning and prevent corrosion of its internal surfaces. Each section of the tunnel is mounted on its own support frame with adjustable leveling feet to correctly align the tunnel over its length of 12.5 m. Clear polycarbonate windows allow observation of experiments, visualization of smokes and other flow-tracer media, still or video photography, and remote sensing of particle size or velocity. The windows also provide physical access for installing and removing experiments, and are exchangeable so that different configurations of access ports and penetrations can be used to mount external sampling equipment and insert pitot tubes, hot wire anemometer probes, or aerosol sampling probes.

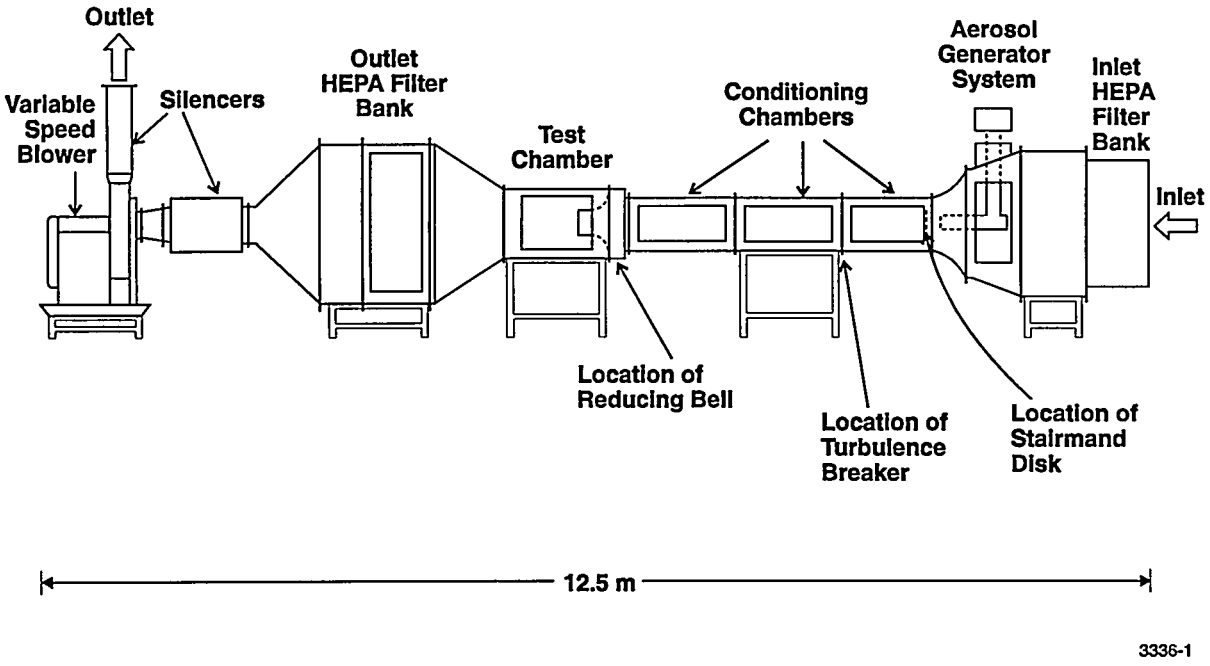

Figure 1. Schematic diagram of the Lovelace aerosol wind tunnel. A Stairmand Disk and a turbulence breaker provide conditioning of the aerosol flow, and clear polycarbonate windows allow access to and observation of the experiments.

The flow arrangement for the tunnel is an open-loop design in which incoming air is drawn from the laboratory, and filtered exhaust air is returned to the laboratory. This minimizes the facility requirements

*Department of Mechanical Engineering, Texas A&M University, College Station, Texas

for heating, ventilating, and air conditioning that would be necessary for an open-loop, once-through design in which incoming air is drawn from the laboratory, and filtered exhaust air is expelled to the outside environment. It also mitigates problems of heat buildup or humidity changes in a closed-loop, recirculating design. However, some care is needed to make proper background corrections, or to wait a suitable interval between tests with sulfur hexafluoride or other tracer gases that are not removed by filtration.

Air enters the tunnel through a 1.4-m wide by 1.4-m high section of high-efficiency particulate air (HEPA) filters. The filters provide particle-free room air for the experiments and prevent inadvertent release of test aerosols into the room. The HEPA filter module can be removed to accommodate studies that do not require particle-free air or do not involve the injection of special aerosols.

A 1.5-m long HEPA filter house with a 1.6-m by 1.6-m cross section is connected to the test section by a 0.8-m long transition duct. The filter house is serviced through a 0.55-m wide by 1.3-m tall stainless steel door and can accommodate two banks of HEPA filters in series, with a 1-m separation distance between banks. The tunnel is currently configured without the first HEPA bank, which provides adequate space for placement of a full-torso, anthropomorphic manikin in the filter house. The manikin can be equipped with personal samplers, surrogate oral and nasal airways, or a combination of both.

The clean exhaust air from the filter house is passed through a 1-m long silencer to isolate the experiment section from any noise produced by the blower section. Flow through the tunnel is provided by a belt-driven, 45-horse power (hp) blower, connected to a 15-hp, variable speed motor with digital frequency control. A second silencer is located on the exhaust side of the blower to minimize propagation of noise into the laboratory.

The filter module at the entrance of the tunnel is followed by an aerosol generation chamber (1.6-m high by 1.6-m wide by 1.4-m long) in which an aerosol generator can be placed, or into which aerosols can be injected. Replaceable, 0.4-m by 0.9-m windows at the top, bottom, and sides of the generation chamber provide access for inserting and operating the generator or injecting the aerosols. Initial studies are being conducted with a vibrating orifice monodisperse aerosol generator (VOMAG, Model 3053, TSI Inc, St. Paul, MN).

After leaving the generation chamber, the aerosol travels through three flow-conditioning chambers before entering the experiment test section. Each conditioning chamber is 1.2 m long and has a 0.6-m × 0.6-m cross section. The aerosol generation chamber is connected to the first conditioning chamber by a short (0.35-m long) transition section that includes a bulk-head plate with a 30-cm diameter opening. Aerosol entering the first conditioning chamber is dispersed by large-scale turbulence when the airflow contacts a 35-cm diameter disk mounted 13-cm downstream from the opening. This type of mixing plate (known as a "Stairmand disk") improves the spatial uniformity of aerosol leaving the generation chamber. Further mixing and straightening of the flow occurs when the air passes through a small-scale turbulent mixer as it enters the second conditioning chamber. This breaks up the large scale turbulence and creates a relatively flat velocity profile across the entire cross section of the duct. The small-scale turbulent mixer consists of a bulk-head plate with 64 equally spaced, 5-cm diameter holes. The flow is then allowed to establish a uniform profile as it proceeds, without further disturbance, through the second and third conditioning chambers. Particle behavior can be studied in the conditioning chambers, depending on the turbulent conditions being modeled. The Stairmand disk assembly and the small-scale turbulence plate can be reconfigured or removed through the access windows to provide different mixing conditions or to match the mixing conditions to a range of flow rates.

The experiment test section is 1.4 m long and has a 0.76-m by 0.76-m cross section. These dimensions are suitable for testing personal samplers, anthropomorphic manikins of the nose and head

areas, extractive stack-sampling probes, and most workplace aerosol collection devices. The conditioning chambers provide a uniformly mixed aerosol with a relatively uniform velocity profile over the cross section of the test chamber. A very uniform velocity profile can be achieved across the central region of the test chamber by placing a 0.3-m-long, bell-shaped, reducing inlet at the entrance to the test section. The bell can be inserted or removed through the access windows. The entrance diameter of the bell is 0.6 m, and the exit diameter of the bell is 0.3 m.

Performance tests are currently underway to meet the U.S. Environmental Protection Agency guidelines for aerosol wind tunnel performance (Ambient Air Monitoring Reference and Equivalence Methods, 40 CFR 53, Subpart D, 1995). Uniformity of aerosol concentration entering the first conditioning chamber is strongly dependent on proper positioning of the aerosol generator outlet on the centerline of the inlet to the Stairmand disk. The blower motor frequency has been tested between a minimum frequency of 10 Hz and a maximum line frequency of 60 Hz, resulting in nominal flow velocities at the outlet of the 0.3-m diameter flow reduction bell of 3.3 m/s to 24 m/s, respectively, with velocity coefficients of variation (COVs) less than 2%. For the 0.76-m × 0.76-m test section, the velocity is 0.7 m/s to 3.6 m/s for frequencies up to 43 Hz. Tracer gas concentration profiles had COVs less than 10% for the entire test section. For particle concentration profiles, the COV is less than 16% over a 20-cm × 20-cm cross sectional area in the test section just after the flow reduction bell and less than 11% over a 30-cm × 30-cm cross sectional area in the center of the 0.76-m × 0.76-m test section without the flow reduction bell. This performance is suitable for workplace aerosol studies and meets the EPA requirements. Velocity profiles and particle and tracer gas concentrations are also being evaluated at other locations in the tunnel, such as in the conditioning chambers, to provide a more complete description of tunnel performance.

As an initial application of the tunnel to a practical problem, inlet efficiency tests were conducted at a wind speed of 1 m/s with 10 μm aerodynamic diameter particles for the inline sampling head of the Eberline Alpha-6 continuous air monitor to qualify its use as a room area monitor. At a flowrate of 2 cfm, aerosol collection efficiencies (mean $\pm$ standard deviation for four tests at each orientation) were 84% $\pm$ 2% with the inlet tube facing toward the direction of flow, 84% $\pm$ 2% with the inlet tube perpendicular to the direction of flow in a horizontal direction, and 84% $\pm$ 6% with the inlet tube facing downstream of the direction of flow. As expected, particle collection efficiencies were slightly better at lower flowrates: 87% $\pm$ 3% at 1.5 cfm, and 89% $\pm$ 2% at 1 cfm, for the inlet tube facing toward the direction of flow. Note that previous work (1990–91 Annual Report, p. 9) found the internal delivery efficiency for the inline head (compared to an inline filter) to be essentially 100%, which indicates that particle collection losses for use of the inline head as a room area monitor are associated with aspiration of particles into the sampling inlet. These results far exceed the generally accepted minimum performance criteria of 50% efficiency for particles with 10 μm aerodynamic diameter. In addition, the performance of the inline sampling head as a room area monitor is very similar to the performance of the radial-inlet version of the Alpha-6 CAM, which is in the range of 83% to 90% collection efficiency for most orientations (A. R. McFarland *et al. Health Physics J. 61(1)*: 97, 1991).

The new aerosol wind tunnel provides a state-of-the-art capability for studying aerosol collection efficiencies and particle deposition patterns in room aerosol monitors, personal samplers, extractive sampling probes, and geometrical configurations representative of human oral and nasal breathing. It can also be used to study resuspension rates for particles attached to surfaces and patterns for aerosol mixing and movement around subscale models of workplace objects such as glovebox enclosures. Results from such studies are needed to improve the technical basis for measuring, modeling, and mitigating toxic aerosols in the workplace and environment.

(Research performed under U.S. Department of Energy Cooperative Agreement No. DE-FC04-96AL76406 with funding from the Assistant Secretary for Defense Programs and the Y-12 Plant.)

II. DEPOSITION, TRANSPORT, AND CLEARANCE OF INHALED TOXICANTS

ANATOMIC VARIABILITY IN ADULT HUMAN NASAL AIRWAY DIMENSIONS

Raymond A. Guilmette, Yung-Sung Cheng, and William C. Griffith

Respiratory tract models used in calculating radiation doses from exposure to inhaled radioactive aerosols have only recently focused attention on the importance of the nasal airways (NAs). Because the NAs are the first tissues of the respiratory tract available for aerosol deposition in nose-breathing people, any deposition of aerosol in this anatomical structure will reduce the amounts available to be deposited in the remainder of the respiratory tract. Thus, uncertainties in estimating the deposition fractions in the NAs will propagate throughout the remainder of the respiratory tract, creating errors in the calculated dose estimates.

Cheng, K. H. *et al.* (*J. Aerosol Sci. 27*: 785, 1996) and Cheng, Y. S. *et al.* (*Radiat. Prot. Dosim. 38*: 41, 1991) have summarized the human data on NA deposition of ultrafine and larger sized aerosols, respectively, and found substantial intersubject variability in the deposition fractions, particularly in the particle-size range from 1–10 μm. Because the NAs have complex shapes, adequate theoretical models for predicting aerosol deposition in NAs have not yet been developed. We, therefore, have hypothesized that much of the variability observed in measured NA deposition efficiencies is due to differences in the size and shape of individual NAs, and have undertaken to estimate the variability in NA size in a small population of humans.

To assess the variabilities in NA dimensions among different adult humans, we have conducted an anatomical study of adult, nonsmoking, male and female human subjects with no notable NA disease or structural pathology. All subjects received a magnetic resonance imaging (MRI) scan of their NAs using the 1.5 Tesla 55-cm-bore Siemens MRI unit. Before performing the MRI scan, several anthropometric measurements were also made on each subject: (1) height, (2) weight, (3) circumference of the head at the level of the glabella, (4) lateral head width at the glabella, and (5) anterior-posterior head width at the glabella. The perimeters of each NA taken from the 3-mm contiguous coronal MR images were traced by hand, digitized using a Grafpen (SAC, Southport, CT) sonic digitizer, and the perimeter maps stored and analyzed in a personal computer. For this analysis, the cross-sectional areas of all coronal sections from the anterior nares to the posterior end of the nasal airway just prior to the nasopharynx were summed, then multiplied by the thickness of each section (3 mm) to obtain a measure of the volume of both NAs. Likewise, the perimeter lengths for the same sections were summed and multiplied by the section thickness to obtain the NA surface area. These data were then compared with the various anthropometric measurements by simple linear regression (REG procedure, SAS/STAT software, Cary, NC).

Separate comparisons of the *in vivo* deposition efficiencies for ultrafine particles in nine subjects previously described in Cheng, K. H. *et al.* (1996) were made with the respective NA anatomy data from this study. Using an approach similar to that used by Cheng, Y. S. *et al.* (*Aerosol Sci. Technol. 23*: 541, 1995), the deposition efficiency for each subject was characterized by the respective coefficients, a_i, obtained by fitting each subject's deposition data to the relationship: $P_i = 1-E_i = \exp(-a_i D^{0.5} Q^{-0.12})$, where P_i is the penetration efficiency for subject i, E_i is the deposition efficiency, D is the particle-size-specific diffusion coefficient ($cm^2\ s^{-1}$), and Q is the flow rate ($cm^3\ s^{-1}$). Data obtained using particles with sizes of 4, 8, and 20 nm, and at flow rates of 167 and 333 $cm^3\ s^{-1}$ were used.

MRI scans of adequate quality for morphometric analysis were analyzed for 21 male and 24 female subjects. The results of regressing surface area and volume on the variables height, weight, head circumference, lateral head width, and dorsoventral head width are summarized in Table 1. The most statistically significant relationships for total NA volume and surface area were with subject height and dorsoventral head width. No relationships were apparent for weight, height/weight ratio, or lateral head

width. Head circumference was only marginally correlated. This was found to be due to a significant lack of correlation for the male subjects; the correlation for females was approximately the same as that for dorsoventral head width. With the limited data available, the uncertainties on the fitted parameter values were relatively large; nevertheless, the slopes of the fits for all anthropometric parameters except lateral head width were statistically significant. The average relative standard error for height, circumference, and dorsoventral head width was 25 $\pm$ 4%. These data indicate that, in general, the size of human nasal airways, as represented by the coarse measures of total airway surface area and volume, are related to the height and the dorsoventral head width of the individual.

Table 1

Regression of Anthropometric Measures on NA Surface Area and Volume

Variable	Intercept (± SE)	Surface Area Slope (± SE)	Pr (slope = 0)	R^2
		Surface Area		
Height	2.4 (45)	1.13 (0.26)	0.0001	0.304
Weight	171 (13)	0.354 (0.178)	0.054	0.0839
Circumference	–56 (83)	4.42 (1.46)	0.0041	0.176
Lateral Width	188 (26)	0.60 (1.69)	0.725	0.0029
Dorsoventral Width	7.4 (51)	9.91 (2.66)	0.0006	0.2434
		Volume		
Height	–20 (9.7)	0.25 (0.06)	0.0001	0.311
Weight	16 (2.8)	0.094 (0.038)	0.016	0.1275
Circumference	–47 (17)	1.22 (0.29)	0.0002	0.2845
Lateral Width	17 (5.6)	0.37 (0.36)	0.316	0.0234
Dorsoventral Width	–24 (10)	2.46 (0.55)	0.0001	0.3217

The deposition efficiencies of ultrafine aerosols (4–20 nm) in nine nonsmoking male humans (data taken from Cheng, K. H. *et al.*, 1996) were compared with their respective NA surface areas and volumes, as well as with their heights and dorsoventral head widths, the parameters previously shown to be most correlated with surface area and volume (Table 2). Regression analyses showed that the deposition efficiencies were highly correlated with both surface areas (R^2 = 0.6912) and volumes (R^2 = 0.7451) of the subjects. Conversely, it is interesting to note that both height and dorsoventral head width were not highly correlated with the deposition data. Thus, although correlation was found between the gross anthropometric measurements of subject height and dorsoventral head width and NA surface area and volume, it appears that this correlation does not provide satisfactory predictive power for individualized deposition efficiency. Whether this would also be the case for inhalation of larger aerosol particles typical of occupational exposures (0.5–20 μm) is not known, as human deposition studies using larger aerosol particles in which NA size and shape measurements were obtained have not been done. Nevertheless, it appears that NA size and shape factors are important in explaining the large variabilities observed in studies of NA aerosol deposition.

Table 2

Regression of Coefficients a_i[a] on Measures of NA Size

Variable	Intercept (± SE)	Slope (± SE)	R^2
Height	−12 (34)	0.153 (0.190)	0.0976
Dorsoventral Width	−16 (36)	0.160 (1.85)	0.1103
Surface Area	−16 (8.7)	0.15 (0.041)	0.6912
Volume	−6.8 (5.4)	0.85 (0.20)	0.7451

[a] a_i is the fitted regression coefficient in the equation $P_i = \exp(-a_i D^{0.5} Q^{-0.12})$.

(Research sponsored by the Office of Health and Environmental Research, U.S. Department of Energy, under Contract No. DE-AC04-76EV01013.)

AN EXPOSURE SYSTEM FOR MEASURING NASAL AND LUNG UPTAKE OF VAPORS IN NONHUMAN PRIMATES

*Terry A. Ahlert, Alan R. Dahl, and Per Gerde**

Inhaled gases and vapors often produce biological damage in the nasal cavity and lower respiratory tract. The specific site within the respiratory tract at which a gas or vapor is absorbed strongly influences the tissues at risk to potential toxic effects; to predict or to explain tissue or cell-specific toxicity of inhaled gases or vapors, the sites at which they are absorbed must be known. The purpose of the work reported here was to develop a system for determining nose and lung absorption of vapors in cynomolgus monkeys. Although these monkeys have nasal anatomies vastly different from those of rodents but similar to humans, the comparative uptake of vapors is of interest for comparing doses to nasal mucosa.

The system was based on one reported for dogs (Snipes, M. B. *et al. Fundam. Appl. Toxicol. 16*: 81, 1991) and for rats (1994–95 Annual Report, p. 40). Five major system modifications that facilitate accurate determinations of vapor uptake in a monkey's nose and lungs are outlined here. (1) In the previous work using dogs, a correction was made for the fact that airflow during breathing was approximately sinusoidal, whereas the sampling airflow was in the form of a square wave (Dahl, A. R. *et al. Toxicol. Appl. Pharmacol. 109*: 263, 1991; Gerde, P. and A. R. Dahl. *Toxicol. Appl. Pharmacol. 109*: 276, 1991). The reciprocating syringe system developed for the rat was modified by the addition of an offset mechanism that allows the proportional, sinusoidal sampling from a monkey's trachea to be synchronized with the actual expansion and contraction of the monkey's lung. Two main factors necessitated this development: (a) the lag time of air displacement in the respiratory box versus the actual expansion of the monkey's lungs, and (b) the time delay in the mechanical turning of the solenoid valves versus the electrical signal indicating power to the solenoid which was recorded on the Visicorder. (2) A pneumotach was installed inline with each sampling syringe to record the sinusoidal flow wave. (3) Component sizes were selected to maximize sampling and breathing flows while simultaneously minimizing dead space, thereby decreasing time to equilibrium. (4) Diffusion of vapor through the sampling lines was minimized by using stainless steel, Teflon™, or glass tubing wherever practical. (5) The development of a system patency test allowed us to confirm the accuracy of each sample taken. This system consists of a small Tedlar bag preceded by two non-rebreathing valves on either side of a charcoal column to take the place of a monkey's nose and lungs (Fig. 1).

The exposure system can sustain an apneic monkey for approximately 60 min at tidal volumes ranging from 95–120 mL and at frequencies ranging from 15–17 breaths/min.

The information gathered by the system patency testing is presented in Table 1. A pattern of decreasing recovery for the tracheal exhale sample can be seen with increasing degrees of offset until both exhale samples (total and trachea) are equal at 80° offset. When this condition is met, the system is deemed accurate. The experiment was repeated using a monkey to replace the bag and charcoal filter in the system and exposing the lung only (only 2-Butanone was used). Varying degrees of offset enabled us to determine the optimum offset for the monkeys' lungs. By using the rule of equal exhale samples, the system was accurate at 45° offset (Table 2). This knowledge will be useful to determine if the results obtained from exposures to both the lungs and nose are accurate.

*National Institute for Working Life, Solna, Sweden

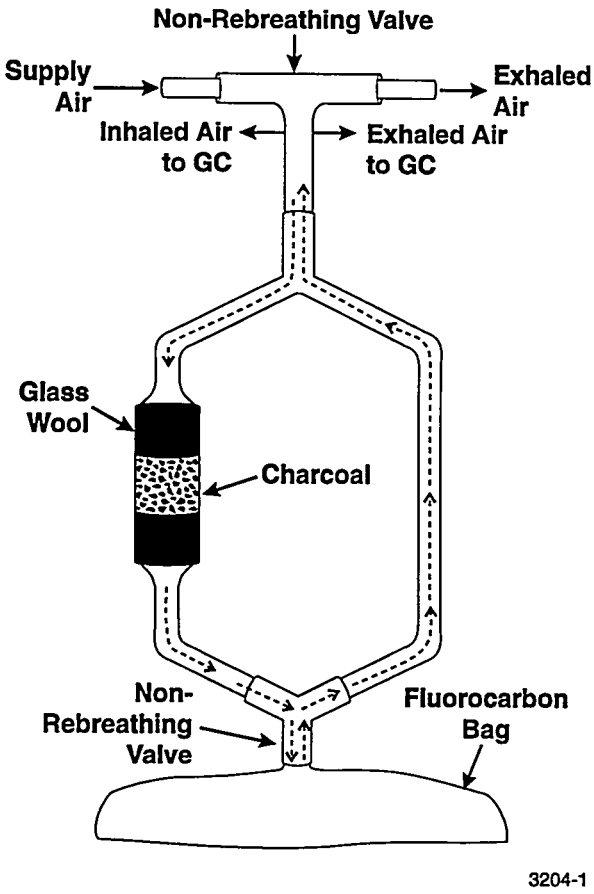

Figure 1. Schematic showing the orientation of non-rebreathing valves and charcoal column used in the system patency test.

Table 1

System Patency Recoveries with 1-Butanone

Number of Samples	n=2	n=1	n=3	n=1	n=3	n=1	n=3	n=7	n=4	n=3	n=2
[2-BUT][a]	92	115	100	118	99	56	64	69	58	57	91
TV[b]	108	106	107	106	108	115	108	110	112	111	108
Offset in Degrees	20	45	50	55	60	67.5	70	80	85	90	92.5
Trachea Inhale[c]	0.74	0.91	0.91	0.94	0.96	0.92	0.95	0.97	0.98	0.99	1.03
Trachea Exhale[d]	0.80	0.56	0.52	0.47	0.45	0.33	0.37	0.28	0.24	0.20	0.23
Total Exhale[e]	0.30	0.32	0.31	0.31	0.30	0.26	0.29	0.29	0.28	0.28	0.30
Total Uptake[f]	0.70	0.68	0.69	0.69	0.70	0.74	0.71	0.71	0.72	0.72	0.70

[a][2-BUT] = concentration of exposure from GC analysis in ppm.
[b]TV = Tidal volume.
[c]Trachea Inhale = GC peak area as fraction of baseline peak area.
[d]Trachea Exhale = GC peak area as fraction of baseline peak area.
[e]Total Exhale = GC peak area as fraction of baseline peak area.
[f]Total Uptake = 1 - Total Exhale.

Table 2

Lung Only Monkey Exposures to 2-Butanone

	Monkey 84							Monkey 201						
Number of Samples	n=1	n=1	n=1	n=3	n=1	n=1	n=1	n=1	n=1	n=1	n=3	n=1	n=1	n=1
[2-BUT][a]	59	58	56	57	56	57	57	56	56	54	56	54	57	57
TV[b]	112	115	100	104	100	100	99	108	107	98	102	94	98	97
Offset	35	40	42.5	45	47.5	50	55	35	40	42.5	45	47.5	50	55
Trachea Inhale[c]	0.93	0.92	0.93	0.97	0.99	1.01	1.01	0.92	0.96	0.97	0.96	0.94	1.00	1.01
Trachea Exhale[d]	0.62	0.57	0.57	0.57	0.53	0.57	0.56	0.63	0.61	0.63	0.60	0.57	0.61	0.59
Total Exhale[e]	0.52	0.52	0.54	0.56	0.55	0.60	0.60	0.56	0.59	0.61	0.60	0.60	0.62	0.63
Total Uptake[f]	0.48	0.48	0.46	0.44	0.45	0.40	0.40	0.44	0.41	0.39	0.40	0.40	0.38	0.37

[a][2-BUT] = concentration of exposure from GC analysis in ppm.
[b]TV = Tidal volume.
[c]Trachea Inhale = GC peak area as fraction of baseline peak area.
[d]Trachea Exhale = GC peak area as fraction of baseline peak area.
[e]Total Exhale = GC peak area as fraction of baseline peak area.
[f]Total Uptake = 1 – Total Exhale.

This exposure system is the first reported that can measure vapor uptake in monkeys in both the upper airways and lung during cyclic breathing. Both are important measurements in determining nasal uptake because the lung depletes the air that has passed through the trachea during inhalation. During exhalation, this air—now unsaturated relative to the vapor still absorbed in the outermost layer of the nasal airway mucosa—passes over and absorbs vapor from the nasal mucosa. This phenomenon was first quantitated in dogs (Dahl *et al.*, 1991); by extending the technique to monkeys, we can measure uptake of vapors in the nasal cavity of a species with a nasal anatomy similar to humans.

The system described will be used to produce data necessary to validate a mathematical model for calculating uptake of vapors in monkeys similar to the one developed for dogs (Gerde and Dahl, 1991). Although the model will be capable of calculating the nasal and lung uptake of gases when the concentration at the air/mucosa interface is larger than zero, only an average dose over the main airway nasal mucosal surfaces will be calculable. Calculation of local doses within the nasal cavity of vapors having > 0 concentrations in the mucosa at the air interface will require coupling of an airflow-dependent uptake model (e.g., Kimbell, J. S. *et al. Toxicol. Appl. Pharmacol. 121*: 253, 1993) with the model to be validated using the exposure system reported here.

In summary, the exposure system described allows us to measure in the monkey: (1) nasal absorption and desorption of vapors; (2) net lung uptake of vapors; and (3) the effects of changed breathing parameters on vapor uptake.

(Research sponsored by the PHS/NIH under Grant R01-ES04422 from the National Institute for Environmental Health Sciences with the U.S. Department of Energy, under Contract No. DE-AC04-76EV01013.)

PARTICLE DEPOSITION STUDIES IN A CAST OF HUMAN ORAL AND UPPER TRACHEOBRONCHIAL AIRWAYS

Yung-Sung Cheng, Hsu-Chi Yeh, Bean T. Chen, and David L. Swift***

Aerosol drugs are usually delivered by inhalation to the lung through the mouth (oral) rather than the nasal route because of lower aerosol deposition in the mouth. However, information is limited on oral deposition in humans, especially on the local deposition pattern in the oral cavity and the oral pharynx region. The purpose of this study was to investigate effects of particle size and breathing rate on the deposition pattern in a human oral airway cast with a defined geometry. Data from these studies are providing information on the deposition mechanism and the possible correlation of particle deposition with airway geometry.

The cast included the oral cavity, pharynx, larynx, trachea, and three generations of bronchi. The oral portion of the cast was molded from a dental impression of the oral cavity in a human volunteer, while the other airway portion of the cast was made from a cadaver (1993–94 Annual Report, p. 42). The production mold for this cast was made using Dow-E silicone rubber (Dow Corning, Midland, MI) to minimize the effect of electrostatic deposition. Wax was poured into the production model; after it was solidified in the mold, a solid wax was carefully taken out. An electrically conductive silicone rubber compound (KE-4576, one-component RTV, GemTech, Grapevine, TX) was applied to the wax mold to make the hollow cast. After a certain number of applications, time was allowed for the rubber to cure, and the hollow cast was obtained by removing the wax in boiling water. A number of identical wax molds were made from the same production mold. Each wax mold was used to make a separate hollow cast so that a fresh hollow cast could be used for each particle deposition study. In the deposition experiment, the inside wall of the cast was coated with silicon oil (Dow Corning 550) to minimize particle bounce.

Seven different sizes of polystyrene latex fluorescent particles in the size range of 0.93–16 μm were used in the study (0.93, 1.79, and 2.79 μm from Polysciences, Warrington, PA; 4.0 μm from Interfacial Dynamics, Portland, OR; and 6.07, 9.80, and 16.0 μm from Duke Scientific, Palo Alto, CA). Particles > 5 μm were generated as a dry powder from a small-scale powder disperser (SSPD) (Model 3433, TSI Inc., St Paul, MN), and particles < 5 μm were generated from a Respiraguard II nebulizer (Marquest Medical Products, Inc., Englewood, CO). About 35 mg of particles were placed into the aerosol generator in each run. The aerosol passed through a desiccator to remove moisture and a Kr-85 tube to bring the particle charge to Boltzmann equilibrium. The aerosol then entered a cast of the human oral cavity and the tracheobronchial (TB) tree. Each end-branch of the TB cast was connected to a filter (Versapore 3000, Gelman Sciences, Bedford, CT) and flow meter. The flow rate through each branch was determined prior to the particle deposition study with a velocity transducer (Model 8170, TSI Inc., St Paul, MN) at a total flow rate of 15, 30, and 60 L min^{-1}. The cast was cut into segments after the experiment. Fluorescent material in the particles deposited in the cast and in the filter was extracted by using ethyl acetate. The resultant solution was then filtered using a nylon membrane (0.2 μm nylon membrane, Corning Glass) and the fluorescent content of the filtered solution measured using a Fluorescence Spectrometer (Hitachi, Danbury, CT). From this measurement, the deposition fraction in each airway segment was calculated.

Figure 1 shows the total deposition in the oral airway and upper tracheobronchial airways. Total deposition in these airways appeared to be independent of flow rate for the smallest particle size tested

*Now at National Institute for Occupational Safety and Health, Morgantown, West Virginia
**School of Hygiene and Public Health, Johns Hopkins University, Baltimore, Maryland

(0.93 μm); for larger particle sizes, the particle deposition increased with increasing flow rate, suggesting that impaction was the dominant deposition mechanism for particles > 0.9 μm. Deposition at the highest flow rate of 60 L min^{-1} showed close to 100% of the particles > about 8 μm deposited in the oral and upper tracheobronchial airways. Figure 2 shows particle deposition in the oral airway including the oral cavity, pharynx, and larynx. Again, the deposition fraction shows the same effects of flow rate and particle size.

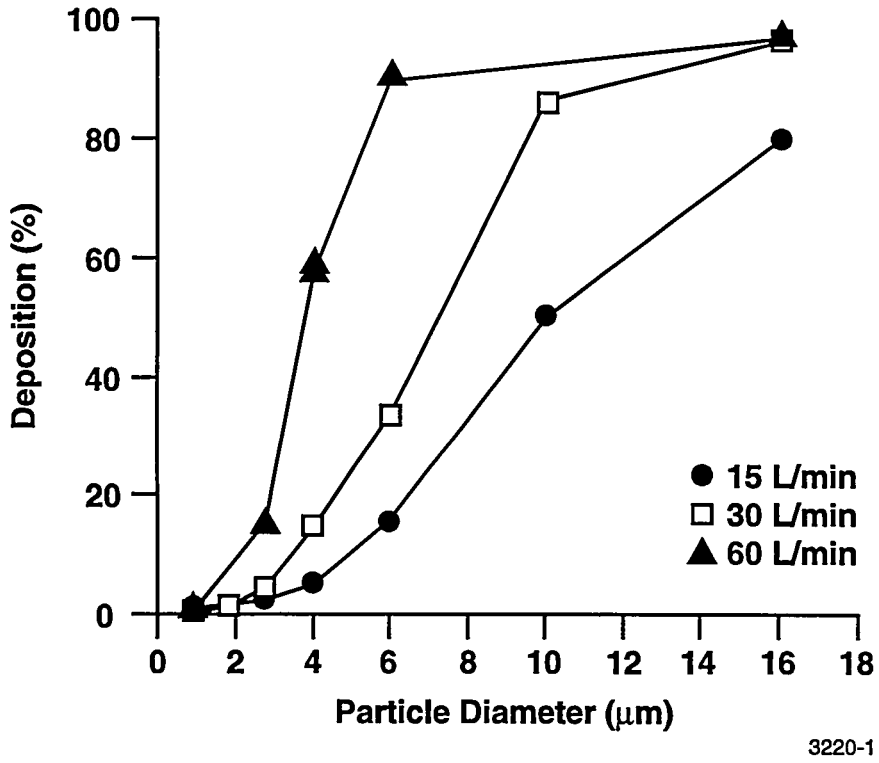

Figure 1. Percent deposition in a human oral-tracheobronchial airway cast as a function of particle size and flow rate.

Our results show a substantial deposition in the oral airway and a clear influence of particle size and flow rate for micrometer-size particles. Note that most aerosol drugs range in size between 1–5 μm and would have a maximum penetration of 70% to the tracheobronchial airway in our test system. Data will be analyzed further to relate the deposition to the impaction parameter and to compare with *in vivo* deposition data. This oral deposition model will be useful for understanding the deposition of aerosol drugs in the respiratory tract.

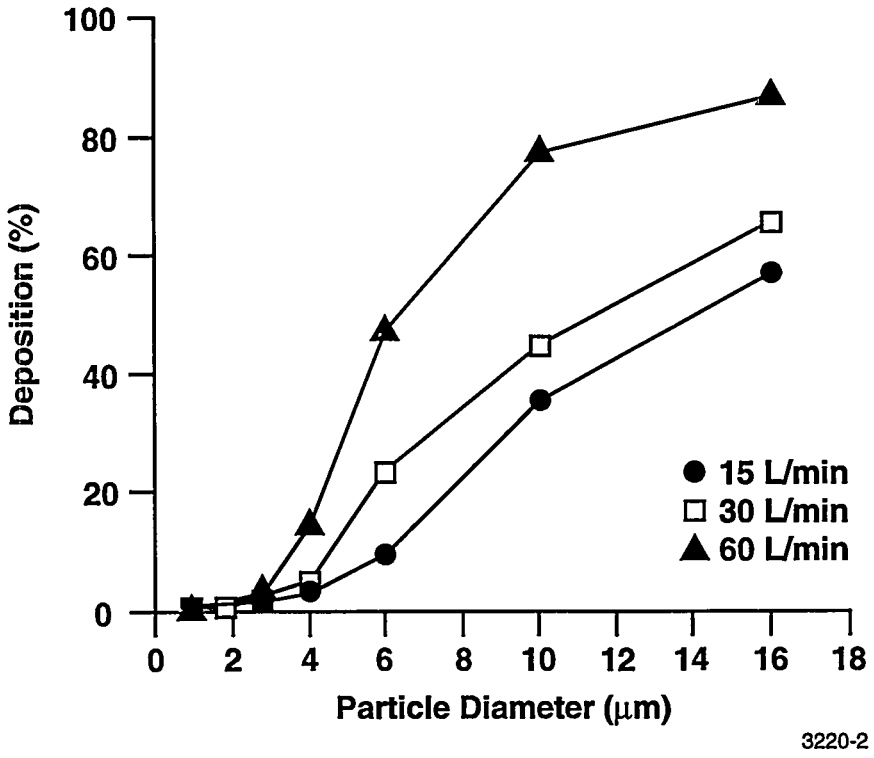

Figure 2. Percent deposition in a human oral airway cast as a function of particle size and flow rate.

(Research sponsored by the Office of Health and Environmental Research, U.S. Department of Energy, under Contract No. DE-AC04-76EV01013.)

ACCUMULATION OF BENZO(a)PYRENE IN THE EPITHELIAL CELL LAYER OF THE CANINE TRACHEA

Per Gerde and Alan R. Dahl*

While tobacco smoke has been conclusively linked to lung cancer, the smoke constituent(s) that are primarily responsible for carcinogenesis are still unidentified. Previous studies in our laboratory suggested that highly lipophilic carcinogens, such as polycyclic aromatic hydrocarbons (PAHs), are slowly absorbed in the thicker epithelium of the conducting airways, potentially allowing for substantial local metabolism. Therefore, the bioactivation of PAHs in airway epithelium may be important in tobacco smoke-induced carcinogenesis.

The hypothesis of slow absorption of highly lipophilic carcinogens in airway epithelium was tested by measuring the blood absorption of benzo(a)pyrene (BaP) deposited at very low levels in the canine trachea (1994–95 Annual Report, p. 37). A single dose of tritiated BaP dissolved in a saline/phospholipid suspension was instilled in the trachea, just anterior to the carina. Blood samples were repeatedly drawn over 3 h from the azygous vein—which drains the area around the point of instillation—and from the systemic circulation. Tissue samples were taken at the end of the experiment. Metabolite patterns were determined by solvent extraction and fractionation using high-pressure liquid chromatography. The purpose of this paper is to describe the local metabolism and microdosimetry of BaP in the tracheal mucosa.

Autoradiography was used to determine the depth distribution of BaP in the mucosa during absorption. Following similar exposures to those for measuring disposition, autoradiographs were taken of the tracheal mucosa by freezing the tissues at the approximate half time of absorption of BaP. Ten-μm sections were cut perpendicular to the tracheal length axis and apposed to the film for autoradiography. The distribution of radioactivity with depth in the mucosa was used in conjunction with data on retained total radioactivity in the trachea to determine the epithelial dose of BaP. Table 1 shows the distribution of total BaP-equivalent activity in selected tissues at 3.2 h after instillation.

Table 1

The Distribution of BaP-Equivalent Activity
in Selected Tissues of the Dog 3.2 Hours After Tracheal Instillation

Tissue	Tissue Weight (g)	BaP Conc. (pmole-eq/kg)	Fraction of Instilled
Trachea + bronchi	20	550	0.23
Tracheal epithelium	0.2	42,000	0.17
Liver	250	19	0.10
Fat	470	0.22	0.002
Muscle	4300	1.4	0.13
Blood	610	0.8	0.01

*National Institute for Working Life, Solna, Sweden

The very high concentration of BaP-eq in tracheal epithelium was based on the fact that about three-fourths of the radioactivity was retained in the epithelium, with the remaining fraction present in the superficial region of the underlying capillary bed. Adding the critical information on the distribution between metabolites and parent compound in the tracheal tissues indicated the extent of the local dosimetry. Three hours after the exposure, 23% of the BaP-equivalent activity remained in the tracheal mucosa. Of this fraction, 13% was parent compound, 28% was organic extractable metabolites, 31% was water-soluble metabolites, and 28%—7% of the instilled dose—was bound to tracheal tissues. So nearly 90% of the radioactivity retained in the tracheal mucosa at 3.2 h consisted of metabolites of BaP (Fig. 1).

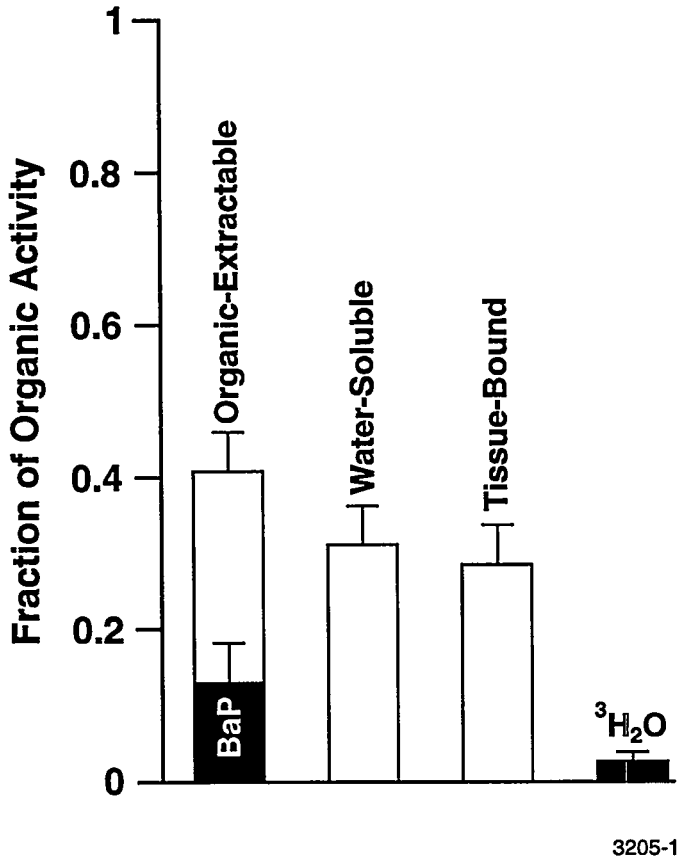

Figure 1. The metabolite pattern of BaP in tracheal tissues at 3.2 h after instillation.

Thus, the concentration of metabolites in the tracheal epithelium was on the order of 2000 times higher than in the liver, which suggests that a substantial metabolic transformation of slowly diffusing BaP takes place before this procarcinogen reaches the blood circulation in the capillaries of the subepithelium. The results explain the tendency of highly lipophilic carcinogens, such as BaP, to induce tumors at the site of entry. Highly lipophilic components of tobacco smoke and polluted air are also likely to be important contributors to lung tumors of the conducting airways.

(Research sponsored by the NIH/NIEHS under Grant R01-ES07665 from the National Institute of Environmental Health Science with the U.S. Department of Energy, under Contract No. DE-AC04-76EV01013.)

A COMPARISON OF OBSERVED PARTICLE RETENTION PATTERNS IN RAT LUNGS FIXED BY DRYING, INTRAVASCULAR PERFUSION, AND INTRA-AIRWAY INFUSION

Morris B. Snipes, Kristen J. Nikula, and Raymond A. Guilmette

Histological methods can be used in studies designed to quantify temporal retention and distribution patterns of particles in lung tissue. However, an important issue in these studies is the possible effect of tissue fixation procedures on both qualitative and quantitative results. The purpose of this study was to compare the distribution patterns of inhaled 1.5 μm fluorescent polystyrene latex (PSL) microspheres in lungs of Fischer 344 rats fixed by three different methods.

Eighteen adult female CDF® (F344)/CrlBR rats were exposed for 4 h nose-only to an aerosol of 1.5 μm diameter fluorescent PSL microspheres. Nine exposed rats were sacrificed 1 d after inhalation of the microspheres; the other nine rats were sacrificed 14 d after exposure. Lungs from three rats from each sacrifice group were tracheally intubated, inflated with air, and dried while suspended in a microwave oven. During drying, inflation was maintained at 25 cm hydrostatic pressure, and air drying was assisted with intermittent operation of the microwave oven to maintain lung tissue temperature in the range of 40–44°C. Microwave heating was discontinued after 3 h, but air flow through the inflated lungs continued for an additional 21 h. A second group of three lungs from each sacrifice group was inflated (25 cm hydrostatic pressure) with air *in situ* and intravascularly perfused with 10% neutral buffered formalin (NBF). After 4 h, the tracheas were tied off, and the lungs were removed from the rats and immersed in 10% NBF to complete the lung fixation process. Lungs from the third group of rats from each sacrifice were fixed by intra-airway infusion with 10% NBF at 25 cm hydrostatic pressure. After 4 h, the tracheas were tied off, and the lungs were immersed in 10% NBF. Systematically derived samples (Fig. 1) of fixed left lungs were embedded in methyl methacrylate, and 2.5-μm thick sections were produced. The sections were mounted on standard histological microslides, stained with toluidine blue, and evaluated at 400 or 600X magnification using epifluorescent microscopy.

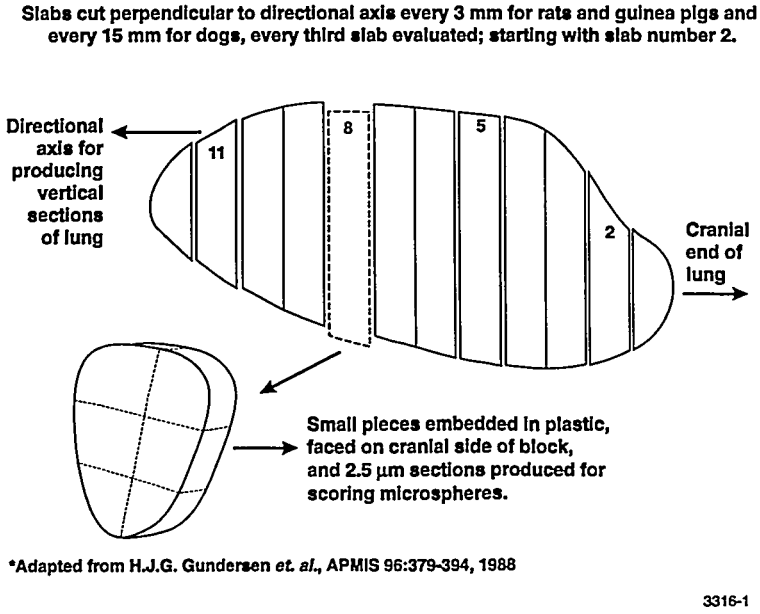

Figure 1. Generalized sampling scheme for fixed left lungs of rats exposed by inhalation to 1.5 μm fluorescent polystyrene latex microspheres.

The evaluation procedure involved identifying and scoring locations of fluorescent microspheres within the lung. Because lungs from rats sacrificed 1 d after exposure are still being evaluated, this report emphasizes results for rats sacrificed 14 d after exposure.

Lung tissues fixed by the three methods differed substantially in appearances. The air-dried lungs were severely dehydrated and did not fully rehydrate during the embedding process. Alveolar macrophages in the air-dried lungs adhered to tissue constituents of the lungs, and generally had a flattened morphological appearance, so that identifying them was sometimes difficult. In contrast, liquid-fixed lungs, especially lungs fixed by vascular perfusion, typically contained spherical alveolar macrophages that were generally dissociated from other tissue constituents and were more easily identified.

Results of the epifluorescent microscopy evaluations are summarized in Table 1 for rats sacrificed 14 d after inhalation exposure. Small percentages of the microspheres were found associated with conducting airways, pulmonary interstitium, and bronchus-associated lymphoid tissue (BALT); 95 to 99% of the microspheres were found in alveolar ducts or alveoli. Overall, fewer PSL microspheres were found in liquid-fixed versus dried lungs, suggesting that some microspheres were lost from the liquid-fixed lung tissue samples during handling and embedding. The percentages of total microspheres on the surface of tracheobronchial airways were (air drying) > (intravascular perfusion) > (intra-airway infusion). Relative to the numbers of microspheres present on the airway surfaces of the air-dried lungs, about 40% and 80% of the microspheres appeared to have been displaced from airway surfaces of the intravascularly perfused and intra-airway infused lungs, respectively. The loss of particles from airway surfaces during processing is expected to have the most impact on results for animals sacrificed at relatively early times after inhalation exposure. Several weeks or more after exposure, only a few particles would be expected on the surfaces of conducting airways, and displacement or loss of a small number of microspheres during handling and tissue-embedding procedures would not be expected to substantially influence the results of particle retention evaluations.

The overall mean $\pm$ s.d. for microsphere retention in conducting airway epithelial cells and interstitium of the nine rats evaluated after 14 d represented $0.18 \pm 0.11\%$ of the total number of microspheres scored (40,929). This represents a small, but important percentage of particles retained in the lung and provides quantitative data that helps determine the magnitude of this lung retention parameter. Particles retained in the conducting airways can result in long-term exposure of airway cells and tissues, and understanding the magnitude of long-term airway retention has important implications for respiratory tract dosimetry for all types of inhaled particles.

Lung retention patterns for the PSL microspheres inhaled by rats were qualitatively similar for lungs fixed by all three methods. More than 95% of the retained microspheres were found in alveolar ducts and alveoli, and small numbers of microspheres were found in the pulmonary interstitium. Importantly, fluorescent microspheres were also found in the epithelium and sub-epithelium of conducting airways. Our quantitative results are expected to help improve airway dosimetry modeling. To date, results are similar for the rats sacrificed 1 and 14 d after exposure, with the exception that losses of PSL microspheres from the surfaces of conducting airways was higher in liquid-fixed lungs from rats sacrificed 1 d after exposure. This would be expected because more microspheres would be predicted to be present 1 d after exposure than after 14 d. Air-dried lungs were technically more difficult to evaluate than formalin-fixed lungs, but both redistribution and loss of mobile cells from airspaces of the dried lung were minimized. Therefore, results obtained from air-dried lungs appear to be more indicative of retention patterns *in vivo*.

Table 1

Locations of Fluorescent PSL Microspheres in
Lung Tissue of F344/Crl Rats 14 Days After Inhalation Exposure

Fixation Method	Animal Number	Total Microspheres Scored	Tracheobronchial Airways			Microspheres in Macrophages in:		Microspheres in Pulmonary Interstitium	Microspheres in BALT
			Macrophage on Surface	Epithelial Cell	Interstitium	Alveolar Duct	Alveoli		
Air Drying	1	4039	110 (2.72%)[a]	0	10	1795 (44.4%)[a]	2032 (51.3%)[a]	27	14
	2	6470	57 (0.88%)	2	18	2778 (42.9%)	3357 (51.9%)	125	14
	3	5586	106 (1.90%)	0	13	2471 (44.2%)	2848 (51.0%)	63	13
	Mean	5365	91 (1.83%)	< 1	14	2348 (43.8%)	2746 (51.1%)	72	14
Intravascular Perfusion	1	4703	44 (0.94%)	0	12	2157 (45.9%)	2412 (51.3%)	30	8
	2	5002	87 (1.74%)	1	5	2085 (41.7%)	2736 (54.7%)	43	15
	3	3115	13 (0.42%)	0	0	1305 (41.9%)	1763 (56.6%)	3	4
	Mean	4273	48 (1.03%)	< 1	6	1849 (43.2%)	2304 (54.2%)	25	9
Intra-Airway Infusion	1	5196	12 (0.23%)	2	9	1981 (38.1%)	3149 (60.6%)	6	27
	2	4092	18 (0.44%)	0	1	1728 (42.2%)	2288 (55.9%)	5	26
	3	2726	11 (0.40%)	0	7	1236 (45.3%)	1424 (52.2%)	8	27
	Mean	4005	14 (0.36%)	< 1	6	1648 (41.9%)	2287 (56.3%)	6	27

[a]Percentage of total microspheres scored for the reference fixation method and animal number.

(Research sponsored by the Office of Health and Environmental Research, U.S. Department of Energy, under Contract No. DE-AC04-76EV01013.)

BIOKINETICS OF INHALED TERBIUM OXIDE ($^{160}Tb_4O_7$) IN NONHUMAN PRIMATES

Raymond A. Guilmette, Morris B. Snipes, Edward B. Barr, and Bruce A. Muggenburg

Current concepts in respiratory tract dosimetry modeling assume for the purpose of interspecies comparisons that the mechanical clearance of particles is dependent on species. This assumption has been validated by widely differing patterns of retention and clearance of poorly soluble particles by various species (Snipes, M. B. *CRC Crit. Rev. Toxicol. 20*: 175, 1989). A second assumption is that the *in vivo* dissolution of deposited particles is independent of species. This assumption, which has been incorporated into the most recent ICRP (1994) and NCRP (1996) respiratory tract dosimetry models, has not been rigorously validated by experiments, mainly because of the difficulty in conducting interspecies studies in which all subjects are exposed to the same aerosol particles. The single exception is the interspecies study conducted by the European Late Effects Project (EULEP) Task Group on Interspecies Lung Clearance, in which mice, rats, Syrian hamsters, dogs, baboons, and humans inhaled monodisperse cobalt oxide ($^{57}Co_3O_4$) particles prepared by a single scientist. Results of this study suggest that the *in vivo* dissolution of the Co particles was strongly dependent on species, contradicting the model assumption of independence (Bailey, M. R. *et al. J. Aerosol Sci. 20*: 169, 1989).

This study with Co particles was important because the results did not support the assumption of species independence. Therefore, it was considered important to perform a second interspecies inhalation study using a different aerosol in which the biochemical properties of the test particles would be different from those of Co_3O_4. Thus, one could differentiate between intrinsic interspecies differences in *in vivo* solubility and those specifically due to Co.

The present study, using inhaled monodisperse $^{160}Tb_4O_7$ (Tb oxide) particles, is one of a set of coordinated experiments being conducted by scientists participating in the EULEP Interspecies Task Group. All of the aerosol particles were prepared by a single investigator and distributed to the various participating laboratories in Germany, England, and the United States (ITRI). Each laboratory used an experimental design that allows for the assessment of the rate of *in vivo* dissolution of the inhaled deposited Tb oxide particles in rats, dogs, monkeys, and humans for comparison with earlier results from Co oxide.

The objective of this study was to determine the biokinetics of ^{160}Tb in the nonhuman primate following the deposition of inhaled Tb oxide particles. Seven male rhesus monkeys received a single pernasal inhalation exposure to monodisperse Tb oxide particles (1.28 μm MMAD; 1.16 σ), previously prepared by Dr. Wolfgang Kreyling, GSF, Oberschleissheim, Germany. Following exposure, each animal was placed in a metabolism cage for the collection of urine and feces for the duration of the experiment. The animals were serially killed and a necropsy done from 2–180 d after exposure. The tissue, urine, and feces samples were measured for ^{160}Tb activity by γ-counting. The initial body burden (IBB) was calculated by summing the ^{160}Tb activities in all tissues (except the pelt and nares, which are subject to external contamination during exposure), and in all urine and feces. The tissue and excreta data, expressed as percent IBB, were then fitted to mathematical functions to describe the organ-level biokinetics of Tb.

The retention and clearance patterns of Tb in the major tissue retention sites are shown in Figure 1, and the fitted equations are shown in Table 1. The fitted function for lung retention, a two-component exponential, accounted for 60% of the IBB, indicating that about 40% of the IBB was deposited in the head airways and the ciliated airways of the lung, and was rapidly cleared to feces. Attempts to fit a three-component exponential were unsuccessful due to the lack of adequate data during the early clearance period of 0–5 d.

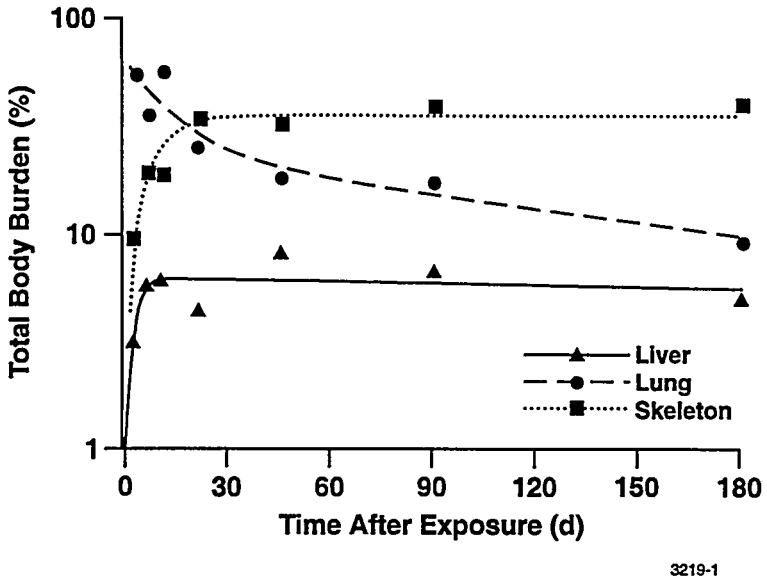

Figure 1. Retention of Tb inhaled as $^{160}Tb_4O_7$ in lung, liver, and skeleton of rhesus monkeys.

Table 1

Equations Fitted to the $^{160}Tb_4O_7$ Biokinetic Data in Monkeys

Lung	$Lu(t) = 35.6\ e^{-0.077t} + 24.5\ e^{-0.0051t}$
Liver	$Li(t) = 6.3\ e^{-0.00033t}\ (1 - e^{-0.49t})$
Skeleton	$Sk(t) = 36.1\ (1 - e^{-0.14t})$
Feces	$F(t) = 1.25\ e^{-0.24t} + 0.066\ e^{-0.0049t}$
Urine	$U(t) = 1.2\ e^{-0.36t} + 0.35\ e^{-0.046t} + 0.036$

where T is in days after exposure, and the coefficients are in units of %IBB.

The more rapidly clearing fraction of the lung burden represented about 36% IBB, and had a clearance half time of about 9 d. This clearance rate, taken together with the rapid accretion of Tb in the liver and skeleton, the major systemic deposition sites, indicated that most of the Tb leaving the lung during the 3–14-d period did so as a result of dissolution of the oxide particles *in vivo*. The accretion half times for liver and skeleton were 1.5 and 5 d, respectively. Thus, in the nonhuman primate, the solubility of the Tb oxide particles was shown to be high. Solubility guidelines of the current regulatory respiratory tract dosimetry models employed in 10CFR20 (NRC) and 10CFR835 (DOE) are based on the model in ICRP Publication 30 (1979). Using these guidelines, this material would be classified as a class D compound because the lung clearance rate was less than 10 d.

On the other hand, a significant fraction (24.5% IBB) of the Tb was retained in the lung with a half time of 136 d. The form of this longer-term retained Tb is not known. Autoradiography of histologically prepared lung slices did not indicate clearly whether the Tb existed in particulate or more distributed forms, as the amount of Tb administered to the monkeys was not large enough. Most developed silver grains were single grains and were dispersed throughout the parenchymal region of the lung, suggesting that the Tb particles had dissolved, and that some were bound to lung constituents, as was determined previously for an analogous trivalent actinide, ^{241}Am (Taya, A. *et al. Ann. Occup. Hyg. 38(Suppl. 1)*: 265, 1994). In any case, at least part of this Tb lung fraction appears to be cleared via the feces as though the material was particulate; note that the clearance half times for longer-term fractions are similar for lung and feces (136 and 141 d, respectively).

Because the fitting procedures used for data analysis are empirical, more mechanistic interpretation of the biokinetics of inhaled Tb oxide must await the results of a material-balance modeling procedure currently in progress. This approach, which accounts for the totality of the Tb at all times, provides the appropriate tool for differentiating between mechanical and solubility clearance pathways from the lung, and also can evaluate the retention characteristics in the various systemic organ compartments, as described for the observed urinary and fecal excretion patterns. The modeling approach also will provide the means to consistently evaluate the data being obtained in rat, dog, and human experiments, and thus determine whether the *in vivo* solubility of Tb oxide is species independent.

For the time being, results from this study in nonhuman primates suggest that the Tb oxide aerosol used in this study can be described as 60% class D and 40% class Y (half time $>$ 100 d).

(Research sponsored by the Office of Health and Environmental Research, U.S. Department of Energy, under Contract No. DE-AC04-76EV01013.)

FURTHER COMPARISONS OF CALCULATED RESPIRATORY TRACT DEPOSITION OF PARTICLES BASED ON NCRP AND ICRP66 MODELS

Hsu-Chi Yeh

In last year's report (1994–95 Annual Report, p. 27), we compared the calculated respiratory tract deposition of particles using the proposed NCRP respiratory tract dosimetry model and the ICRP66 model (ICRP, *Human Respiratory Tract Model for Radiological Protection*, Publication 66, Pergamon Press, New York, 1994), under two ideal conditions of normal nose breathing for two types of aerosol size distributions, namely monodisperse with the geometric standard deviation, $\sigma_g = 1.0$ and polydisperse with $\sigma_g = 2.5$. However, due to the nature of aerosol production from various mechanisms, smaller aerosols usually are associated with smaller σ_g, and larger aerosols are associated with larger σ_g. Because of this, the ICRP66 model has suggested different values of σ_g for different particle sizes, presumably closer to what would occur from aerosol releases in the workplace. It is anticipated that the ICRP66 model may be widely used by industry as a guide or for regulatory purposes, and the NCRP model may be more often used by the research community. The purpose of this report is to further compare the calculated respiratory tract deposition of particles using the NCRP model and the ICRP66 model, under the particle size distributions and breathing conditions suggested by the Task Group of the ICRP.

As described in our previous report (1994–95 Annual Report, p. 27), the respiratory tract is divided into the naso-oro-pharyngo-laryngeal (NOPL), tracheobronchial (TB), and pulmonary (P) regions for the NCRP model, and extrathoracic 1 (ET_1), extrathoracic 2 (ET_2), bronchial (BB), bronchiolar (bb), and alveolar-interstitial (AI) regions for the ICRP66 model. For comparison, the depositions within ET_1 and ET_2 were summed to compare with the NOPL, and the BB and bb were summed to compare with the TB. Table 1 lists the particle size distributions and particle properties as suggested by the ICRP66 model. Three breathing conditions as defined by the ICRP66 model are: (1) sitting (breathing frequency f = 12 breaths/min, tidal volume [TV] = 750 mL, ventilation rate [VR] = 0.54 m^3/h, 100% nose breathing); (2) light exercise (f = 20 breaths/min, TV = 1250 mL, VR = 1.5 m^3/h, 100% nose breathing), and (3) heavy exercise (f = 26 breaths/min, TV = 1923 mL, VR = 3 m^3/h, 50% nose breathing). The calculations were based on these particle size distributions, particle properties, and breathing conditions, along with the functional residual capacity = 3001 mL as suggested by ICRP66 model for a normal adult male.

Results are shown in Figures 1A–C, which compare the two models for sitting, light exercise, and heavy exercise, respectively. The discontinuity in the curves between particle sizes 0.3–0.5 μm is due to the change in particle diameter definition as used by the ICRP66 model from AMTD (activity median thermodynamic diameter) to AMAD (activity median aerodynamic diameter) associated with particle density of 3.0 g/cm^3 and a shape factor of 1.5. Sitting (Fig. 1A) is essentially equivalent to "normal" breathing. As expected, the results are similar to previous results (1994–95 Annual Report, p. 27) for regions in which particles < 0.01 μm with $\sigma_g = 1$ and > 0.5 μm with $\sigma_g = 2.5$, because for the current calculation, the particle size distributions change from $\sigma_g = 1$ for very small particles and approach $\sigma_g = 2.5$ for micrometer-sized particles. For sitting and light exercise, the ICRP66 model predicted: (1) higher NOPL deposition, (2) lower TB deposition, and (3) higher P deposition for small particles. For heavy exercise, the deposition patterns are slightly different because of the 50% mouth breathing and the different equations used for the nasal and oral depositions. The NOPL depositions are lower than for 100% nose breathing for large particles. The ICRP66 model predicted the following: (1) lower NOPL

deposition, (2) higher TB deposition for particles > 0.5 μm and lower TB deposition for 0.002 μm < particles < 0.3 μm, and (3) higher P deposition for particles < 0.02 μm. For all three breathing patterns, the NCRP model predicted higher TB deposition for ultrafine particles where deposition is dominated by diffusion. This is because the NCRP model considers the effects of branching (or entrance configuration) on diffusional deposition at a bifurcation (Yeh, H. C. *Bull. Math. Biol. 36*: 105, 1974; Cohen, B. S. *et al. Aerosol Sci. Technol. 12*: 1082, 1990). Consequently, the ICRP66 model predicted a higher P deposition for ultrafine particles; these difference were substantial for particles < 0.02 μm.

Table 1
Particle Size Distributions and Properties Suggested by ICRP Model

Particle Diameter[a] (μm)	σ_g[b]	Particle Density (g/cm^3)	Particle Shape Factor
0.001	1.00	3.0	1.5
0.002	1.01	3.0	1.5
0.005	1.05	3.0	1.5
0.01	1.14	3.0	1.5
0.02	1.33	3.0	1.5
0.05	1.79	3.0	1.5
0.1	2.14	3.0	1.5
0.2	2.35	3.0	1.5
0.5	2.43	3.0	1.5
1.0	2.47	3.0	1.5
2.0	2.49	3.0	1.5
> 3.0	2.50	3.0	1.5

[a]Particle diameter is activity median thermodynamic diameter (AMTD) = equivalent diffusion diameter for particle sizes ≤ 0.3 μm and activity median aerodynamic diameter (AMAD) for particle sizes ≥ 0.5 μm.
[b]σ_g = geometric standard deviation.

In summary, the general conclusions reached in our previous study (1994–95 Annual Report, p. 27) are also valid here, except for heavy exercise, i.e., the trend of the deposition curves for the two models is similar. Both models predict increasing NOPL and P deposition with increasing ventilation rate until mouth breathing takes over and reduces NOPL deposition. For heavy exercise during which partial mouth breathing is involved, the deposition patterns have changed from that of sitting and light exercise with decreasing NOPL deposition, but increasing P deposition. This change in deposition patterns will have significant implications on the dosimetry of inhaled radionuclides, especially for particles < 0.01 μm and > 2 μm.

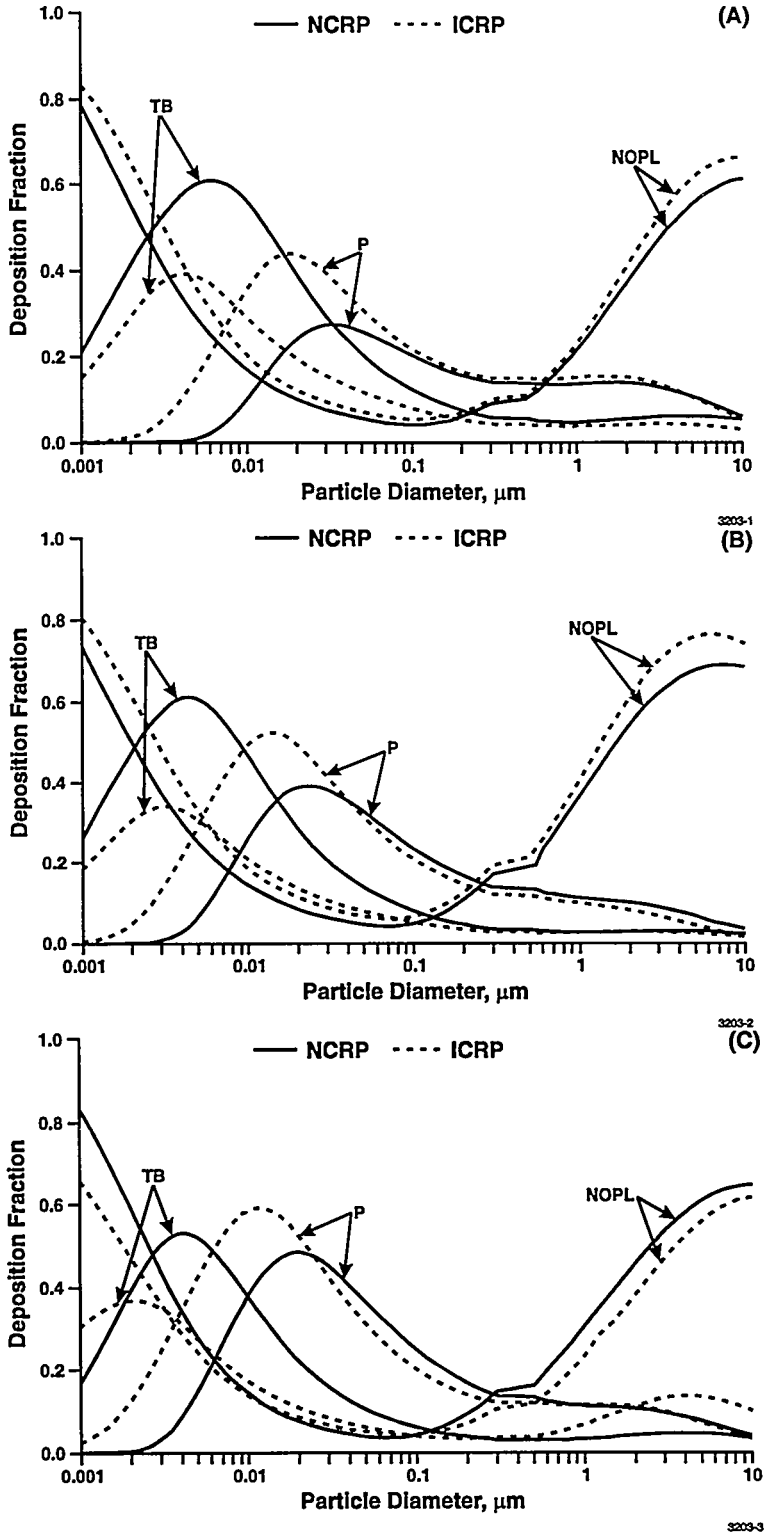

Figure 1. Comparison between the NCRP and ICRP66 models for deposition of inhaled particles during (A) sitting, (B) light exercise, and (C) heavy exercise. The particle diameter = AMTD for $d_p \leq 0.3$ μm and AMAD for $d_p \geq 0.5$ μm. Particle density = 3 g/cm^3 and particle shape factor = 1.5.

(Research sponsored by the Office of Health and Environmental Research, U.S. Department of Energy, under Contract No. DE-AC04-76EV01013.)

III. DOSIMETRY OF INHALED TOXICANTS

DEVELOPMENT OF AN S-PHENYLCYSTEINE ASSAY USING PURGE AND TRAP-GAS CHROMATOGRAPHY/MASS SPECTROMETRY

Mark J. Meyer and William E. Bechtold*

Previous studies have provided evidence for the formation of protein adducts in animals and humans exposed to benzene (Bechtold, W. E. *et al. Carcinogenesis 13*: 1217, 1992; Bechtold, W. E. and R. F. Henderson. *J. Toxicol. Environ. Health 40*: 377, 1993; Melikian, A. A. *et al. Cancer Epid. Biomarkers Prev. 1*: 307, 1993; McDonald, T. A. *et al. Carcinogenesis 14*: 1921, 1993). These adducts are formed with cysteine sulfhydryls of both serum albumin and hemoglobin and can be recovered as S-phenylcysteine (SPC). Their presence may provide a method of monitoring for exposure to very low levels of benzene over extended periods of time. These adducts are thought to result from the reaction of proteins with a primary metabolite of benzene in the liver, benzene oxide, and may quantitatively represent the presence of this metabolite in blood.

This adduct has been detected by high-performance liquid chromatography and gas chromatography/mass spectrometry (GC/MS) of digested proteins (Bechtold and Henderson, 1993). In the study described below, we evaluated a method to measure benzene released from cysteine adducts on intact proteins upon treatment with a nickel-aluminum catalyst commonly used for hydrogenation, Raney nickel (Aldrich Chemical Company, Inc., Milwaukee, WI). The catalytic cleavage of the carbon-sulfur bond between the adducting agent and cysteine generates free benzene that can be measured by GC/MS. Cleavage of these adducts in deuterium oxide (D_2O, Cambridge Isotope laboratories, Woburn, MA) generates monodeuterobenzene that can be distinguished from the ubiquitous benzene background present in most laboratory environments. The ability to recover and measure adducts of styrene oxide (Ting, D. *et al. Carcinogenesis 11*: 755, 1990) and benzoquinone (McDonald *et al.*, 1993) using Raney nickel has been demonstrated.

In this study, we carried out the reductive cleavage of SPC in the purge vials of a Tekmar 3000 Purge and Trap concentrator (Tekmar Company, Cincinnati, OH). Each vial is purged with helium for 10 min onto a Supelco Btextrap absorbent column (Supelco, Bellefonte, PA). Upon heating to 225°C, the entrapped material is desorbed and backflushed off the trap and onto a cryofocusing module developed in-house. This vapor is released and injected onto a Hewlett Packard 5890 GC/5970 Mass Selective Detector (Hewlett Packard Company, San Fernando, CA) equipped with a Restek 30 m × 0.53 mm ID Rtx-1 column (Restek Corporation, Bellefonte, PA) operated in selected ion mode.

This assay was developed in three steps. We first evaluated our ability to recover and measure benzene added to water by purge and trap-GC/MS. Early results indicated that recovery and detection of very small amounts of benzene or deuterated benzene analogs (10 pg/10 mL water, Fig. 1) were possible. Raney nickel was then added to evaluate background benzene present in this material. Despite repeated lyophilization and re-suspension of the Raney nickel prior to use, measurable levels of background benzene were consistently found. These levels were high enough to obscure added benzene standards or benzene released from SPC in later experiments.

Benzene released by Raney nickel from synthetic SPC or blood proteins from benzene-exposed animals was then measured using D_3 benzene or ^{13}C benzene as internal standards. This assay did, in fact, support our observations that background benzene in Raney nickel prevented the measurement of benzene in this manner. It was also apparent that Raney nickel caused the generation of a spectrum of deuterated compounds from background and released benzene (Fig. 2).

---

*UNM/ITRI Graduate Student

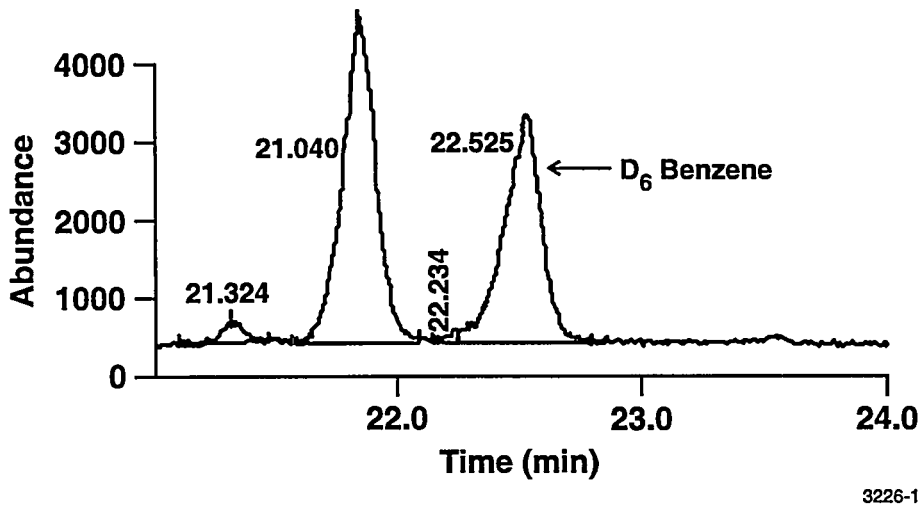

Figure 1. GC/MS chromatogram of 10 pg D_6 benzene in 10 mL water.

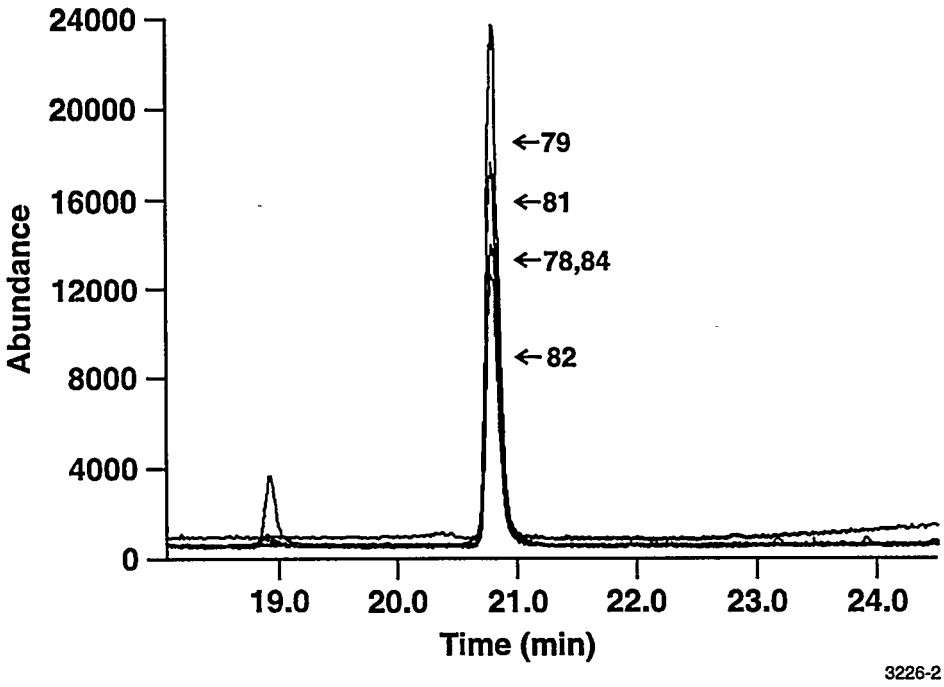

Figure 2. GC/MS chromatogram of material purged from Raney nickel in D_2O. Several deuterated analogs of benzene are generated by the catalytic activity of Raney nickel in the presence of deuterium.

The catalytic activity of Raney nickel appeared to cause the exchange of hydrogen and deuterium on benzene when these materials were mixed in D_2O. All quantitative analyses carried out for this study were based on ratios of monodeuterated benzene (parent ion at m/z = 79) released from SPC by reductive cleavage to tri-deuterated (parent ion at m/z = 81) or ^{13}C benzene (parent ion at m/z = 84) internal standards; generation of random amounts of these compounds from our analytes rendered these measurements of little value. Similar results were obtained when synthetic SPC or adducted proteins were

analyzed. We therefore determined that this method is not suitable for isotope dilution GC/MS analysis of benzene released from SPC, and the study was terminated.

Although the method developed for this project proved to be of little immediate use, the assay itself proved to be quite sensitive. It may, in fact, prove useful in the measurement of other analytes or under different conditions, such as those produced by different forms of Raney nickel, by low temperatures, or with analytes and internal standards other than those with exchangeable protons in the presence of free deuterium. Recently a new method was developed that measures SPC by treating protein with trifluoroacetic anhydride to release S-phenyl trifluoro-acetate. Alternatively, reaction with heptafluorobutyric anhydride would yield S-phenylheptafluorobutyrate. We are exploring this as a possible method of measuring SPC.

(Research sponsored by the Health Effects Institute under Funds-In-Agreement No. DE-FI04-95AL87216 with the U.S. Department of Energy, under Contract No. DE-AC04-76EV01013.)

IMPROVED DETECTOR SYSTEM FOR *IN VIVO* MEASUREMENT OF LEAD-210 IN URANIUM MINERS

Raymond A. Guilmette, Mark D. Hoover, and Morris B. Snipes

Significant uncertainties exist in estimating uranium miners' exposures to radon and its radioactive progeny during their mining careers. These uncertainties are due in part to the limited number and poor quality of measurements of radon and radon progeny concentrations made in various uranium mines. Uncertainties are particularly large for the 1945–1960 time period during which radon levels were the highest because of ineffective ventilation in mines. Uncertainties in exposure estimates directly impact the quality of risk estimates for lung-cancer induction by radon progeny, and may contribute to the large range of risk estimates determined for 11 different mining populations throughout the world (Lubin, J. H. *et al. Radon and Lung Cancer Risk: A Joint Analysis of 11 Underground Miners Studies*, NIH Publication No. 94-3644, 1994). For example, the excess relative risk per unit of exposure (in Working Level Months, WLM) for these populations currently ranges from 0.16% for Chinese tin miners to 5.06% for the Radium Hill miners in Australia, a factor of 32. A major part of the variability observed is likely due to biases in the estimates of exposures among the various miner study populations.

We have hypothesized that *in vivo* measurement of the long-lived Rn progeny ^{210}Pb (22.3 y physical half life), which accumulates and is long retained in the skeleton of uranium miners who inhale Rn progeny, is a metric of cumulative exposure to these progeny. In a previous annual report, we demonstrated our ability to measure ^{210}Pb *in vivo* in a pilot study involving 20 former uranium miners from the Grants, New Mexico mining district (1994–95 Annual Report, p. 74). Additionally, we demonstrated a statistically significant correlation between the measured ^{210}Pb and the WLM exposures from the individual miners' records.

During the course of that pilot study, we also discovered several problems that affect the limit of detection (5.2 Bq for a 90-min measurement) for the ITRI ^{210}Pb detection system as well as the precision of the measurement. The purpose of this study was therefore to modify the ITRI detection system to improve its overall performance before the full-scale study of the relationships between ^{210}Pb *in vivo* and WLM exposure estimates in Grants uranium miners and miners from other study populations in the United States and Canada.

The detection system was improved in three ways: (1) the uranium-contaminated beryllium (Be) entrance windows of the existing detectors were replaced with high-purity aluminum, (2) the ambient radon-progeny concentration within the shielded room was reduced by recirculating filtration, and (3) the counting geometry was improved by adding two phoswich detectors to the counting array.

First, the presence of ^{238}U and its radioactive progeny ^{234}Th in the Be entrance windows was confirmed by taking a room background spectrum with the ITRI phoswich detectors in a different shielded facility (Los Alamos National Laboratory In Vivo Counting Facility, courtesy of Dr. George Neuschaefer), and observing the same contamination peaks characteristic of ^{234}Th as seen in the ITRI shielded room. An example of a room spectrum taken with the U-contaminated entrance windows is shown in Figure 1. Discussions with the detector manufacturer, and gamma measurements of samples of "high-purity" Be obtained from the manufacturer indicated essentially uranium-free Be was not possible to procure. Therefore, the material for the entrance window was changed to high-purity aluminum (0.010" thickness). Although this change in window material imposes a loss of detection efficiency for gamma-ray energies < 25 keV, the resulting improvement in the room background spectrum was dramatic (Fig. 1) and due exclusively to the removal of uranium contamination from the detectors. The background count

rate in the ^{210}Pb region of interest was decreased 32% compared to that obtained with the U-contaminated detectors. This has resulted in an 8% decrease in the limit of detection for ^{210}Pb.

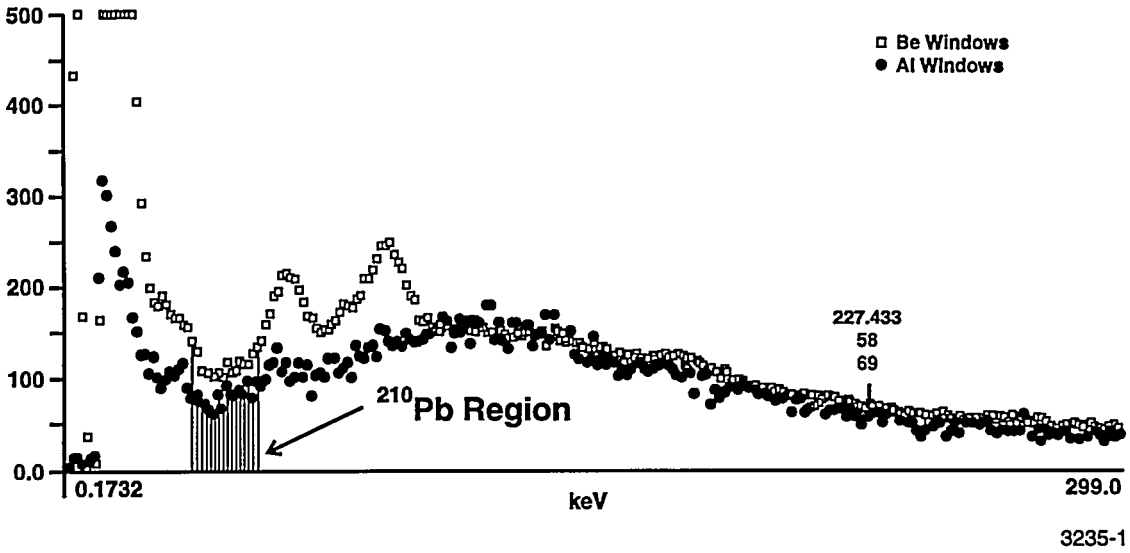

Figure 1. Energy spectrum measurement of the ITRI counting room background before (□) and after (●) replacement of the uranium-contaminated Be entrance windows with high-purity aluminum. The region of interest indicated in the spectrum is the ^{210}Pb counting region.

Second, it was recognized that fluctuating levels of Rn progeny in the shielded counting room were producing unacceptable variations in the skull phantom backgrounds that are necessary for analyzing the spectra collected from each miner. This was due principally because of spectrum distortions attributable to varying quantities of Pb K X rays emitted by one Rn progeny, ^{214}Pb. Because the intake air supply is HEPA-filtered (and therefore the incoming Rn progeny are filtered out), the source of the Rn progeny was ^{222}Rn decay and progeny ingrowth within the counting room. To mitigate this problem, a 2' × 2' window fan with attached medium efficiency filter (about 30% filtration efficiency) now runs continuously in the room. The flow rate of the fan was sufficient to filter the counting room air volume every minute. The effectiveness of the internal filtration system is illustrated in Figure 2, in which Rn progeny ^{218}Po and ^{214}Po were being monitored *in situ* with an alpha-particle continuous air monitor (Model Alpha 6A, Eberline Instrument Company, Santa Fe, NM). Within 30 min of turning on the fan, the ^{214}Po levels in the room were decreased by about 85%. Since the initial experiment, two window fans have been running in the counting room, and the average diminution of Rn progeny inside vs. outside the room has been 90%. This reduction has significantly stabilized the head phantom background measurements, such that the variability is now only slightly higher than counting statistics alone—the theoretical limit for improved performance.

The third improvement made to the detection system was the addition of two detectors to the *in vivo* measurement geometry. In addition to the original four detectors, which were placed two detectors each laterally on the right and left sides of the head perpendicular to the coronal plane, a fifth detector was placed in back of the head and a sixth detector in front of the face, centered approximately on the middle of the forehead. Using a ^{210}Pb-labeled surrogate skull phantom, the detection efficiency was increased from 11.7 cpm/nCi to 15.1 cpm/nCi, an increase of 29%.

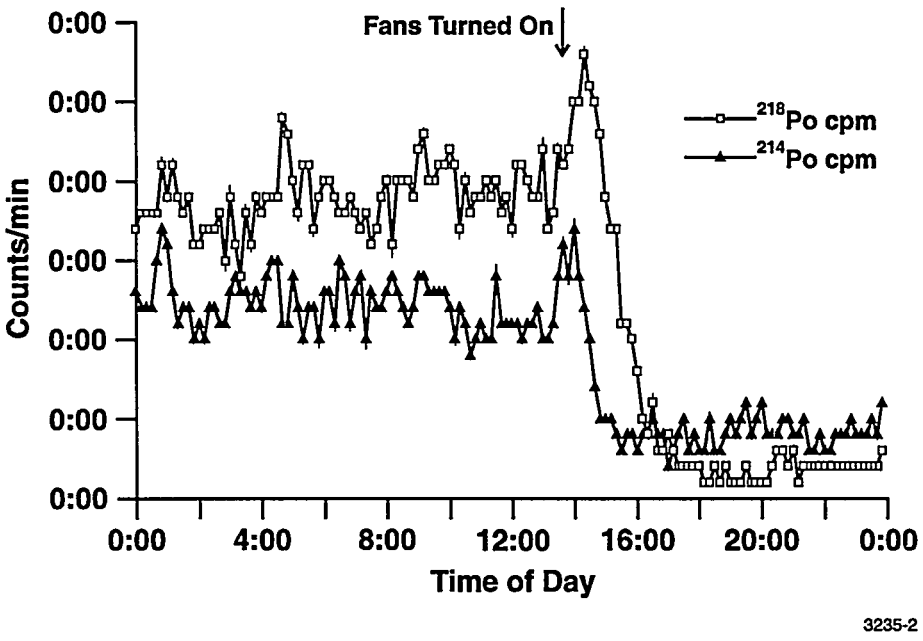

Figure 2. Count rates (in cpm) of the radon progeny radionuclides ^{218}Po (□) and ^{214}Po (▲) measured at 10-min intervals in the ITRI shielded room with an Eberline Alpha 6A continuous air monitor. Radon progeny concentrations were reduced substantially after the recirculation fan was turned on in the room (1:30 pm).

In summary, the system efficiency for measuring ^{210}Pb *in vivo* has been improved by (1) decreasing the background contribution due to uranium-contaminated detectors, (2) stabilizing the head phantom backgrounds by reducing the radon progeny interference in the counting room by 90%, and (3) increasing the detection efficiency about 30% by adding two detectors. The result is that the lower limit of detection of ^{210}Pb *in vivo* in a 90-min count has been reduced from 5.2 Bq to 3 Bq, a 42% improvement. To our knowledge, this is the lowest limit of detection for ^{210}Pb *in vivo* measurement.

(Research sponsored by the Office of Health and Environmental Research, U.S. Department of Energy, under Contract No. DE-AC04-76EV01013.)

BENZENE OXIDE: SYNTHESIS AND ANALYSIS BY GAS CHROMATOGRAPHY/MASS SPECTROMETRY

Mark J. Meyer, William E. Bechtold, and Alan R. Dahl*

Chronic benzene intoxication may result in several adverse effects, including aplastic anemia and acute myelogenous leukemia (Snyder, R. and G. F. Kalf. *Crit. Rev. Toxicol. 24*: 177, 1994). Neither the responsible mechanism nor the toxic metabolite(s), however, are known. While several models for this toxic mechanism have been proposed, most include the metabolism of benzene to benzene oxide in the liver (Snyder, R. *et al. Toxicol. Appl. Pharmacol. 122*: 172, 1993). Benzene oxide, however, has never been isolated from benzene-exposed animals; it was thought to be very short-lived (Jerina, D. M. and J. W. Daly. *Science 185*: 573, 1974). If benzene oxide is reasonably stable in blood, it could serve to carry benzene to the target tissue for these effects, the bone marrow.

There is evidence that benzene oxide exists in blood after benzene exposure. S-phenyl cysteine (SPC) is presumably formed by the reaction of benzene oxide and cysteine sulfhydryl groups in proteins. SPC has been detected as an amino acid residue in the hemoglobin and serum albumin of animals (Bechtold, W. E. *et al. Carcinogenisis 13*: 1217, 1992; Melikian, A. A. *et al. Cancer Epid. Biomarkers Prev. 1*: 307, 1993) and humans (Bechtold, W. E. *et al. J. Toxicol. Environ. Health 40*: 377, 1993) exposed to benzene. SPC has also been measured in bone marrow protein (McDonald, T. A. *et al. Carcinogenisis 14*: 1921, 1993).

This paper describes the preliminary work required to isolate and detect benzene oxide generated *in vivo* in mice exposed to benzene. Benzene oxide is highly unstable and must be synthesized in the laboratory, along with deuterated analogs as internal standards for analysis by mass spectrometry. An accurate, highly sensitive gas chromatography/mass spectrometry (GC/MS) method for analyzing this material must also be developed.

The three steps used to synthesize benzene oxide were similar to those used by Platt, K. L. and F. Oesch (*J. Labeled Compounds and Pharmaceuticals 13*: 471, 1977). 4,5-Dibromocyclohexene (van Tamelen, E. E. *J. Am. Chem. Soc. 77*: 1704, 1954) was first synthesized by 4,5-dibromination of 1,4-cyclohexadiene in dry chloroform at 0°C under anhydrous conditions. The identity of the product was verified by melting point, mass spectrometry, and proton nuclear magnetic resonance spectroscopy (^{1}H NMR).

4,5-Dibromocyclohexane-1,2-oxide (Gillard, J. R. *et al. Can. J. Chem. 69*: 1337, 1991) was synthesized from 4,5-dibromocyclohexene and dried meta-chloroperoxybenzoic acid (Aldrich Chemical, Milwaukee, WI) in chloroform heated to reflux for 16 h. Meticulous clean up (repeated precipitation, recrystallization from cold hexane) was then required. The identity of the product was verified by melting point, mass spectrometry, and ^{1}H NMR.

Generation of the final product, benzene oxide, was completed by dehydrohalogenation of 4,5-dibromocyclohexane-1,2-oxide. A molar excess of sodium methoxide in boiling ether (20 min) (Vogel, E. and E. Gunther. *Angewandte Chemie 6*: 385, 1967) or 1,8-diazobicyclo-[5.4.0]undec-7-ene in ether at room temperature (24 h) (Gillard *et al.*, 1991) produced the desired product. Benzene oxide was ultimately isolated by vacuum-line distillation at 1.0–0.5 millitorr (Dahl, A. R. *et al. Am. Ind. Hyg. Assoc. J. 45*: 193, 1984). The solution was distilled through a meta-xylene/liquid nitrogen slush. The identity of this compound was verified by its ^{1}H NMR spectrum (Fig. 1), the interpretation of which

*UNM/ITRI Graduate Student

agrees with the benzene oxide-oxepin structure as well as spectra found in the literature. The process was ultimately repeated with 1,2,4,5-d_4 cyclohexadiene (Cambridge Isotope Labs, Woburn, MA) to generate internal standard.

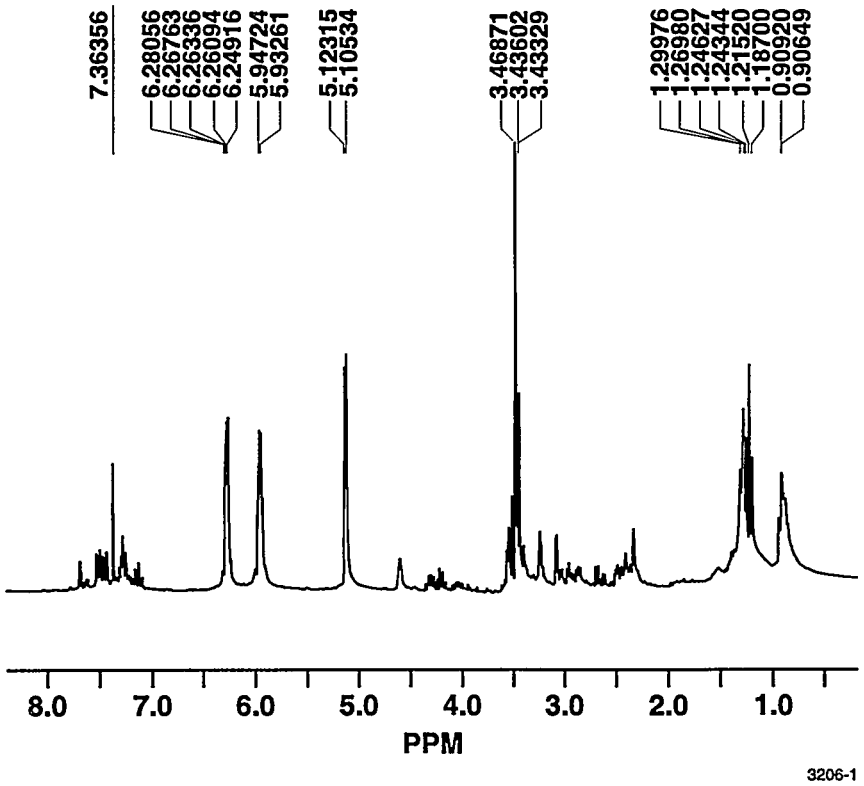

Figure 1. ^{1}H NMR spectrum of benzene oxide (singlets at 5.1, 5.9, and 6.2 ppm).

Further purification will be carried out by preparatory GC using a micropacked column. The flow from this column will be split into two fused silica columns, one flowing 10 times that of the other. The column carrying the lower flow will be routed into a flame ionization detector and will be used to identify the materials eluting from the column. The column carrying the greater flow will be used to re-direct the eluting benzene oxide into a vessel cooled to 0°C for collection. This very pure benzene oxide will be used for *in vivo* experiments.

The GC/MS method developed for analysis of this material was required to be sensitive enough to detect the anticipated small quantities generated by *in vivo* benzene exposures and capable of separating all expected contaminants. All work was carried out on a Hewlett Packard 5890 GC equipped with a 5972 Mass Selective Detector. Once a reliable mass spectrum of benzene oxide was generated, several contaminants in the synthesis product with boiling points similar to that of benzene oxide were, at least tentatively, identified by operating the GC/MS in scan mode. Primary among these contaminants was phenol, which is formed by the spontaneous rearrangement of benzene oxide, and a large amount of a compound produced as a by-product of dehydrohalogenation.

Ultimately, a 30 m × 0.25 mm ID Restek Rtx-200 column was found to produce good results, including satisfactory peak shape and adequate separation of benzene oxide from contaminants (Fig. 2). The analyte was injected at 0°C and heated at 5°C/min to the point at which benzene oxide elutes, 60°C.

The GC oven was then rapidly heated to 150°C to remove all of the higher boiling contaminants. This method will be utilized for further development of an isotope dilution GC/MS method for quantitative analysis. Using the GC/MS in selected ion mode, the ratios of deuterated internal standard to analyte will be used to develop a standard curve and to establish the limits of detection. Preliminary work indicates that the limit of detection will be in the 100 pg/μL range.

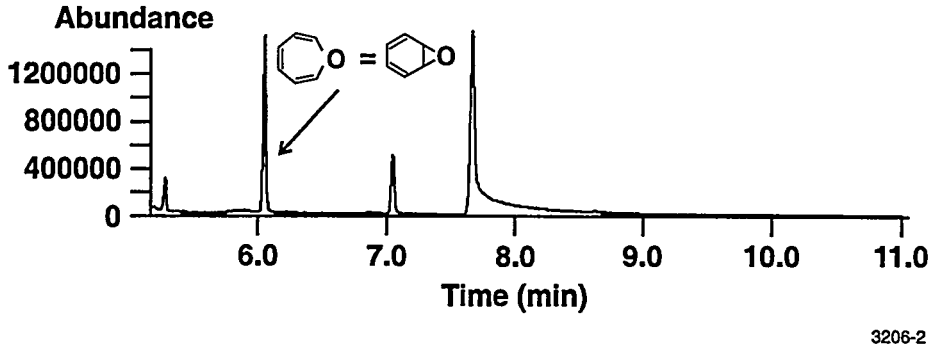

Figure 2. Gas chromatogram of benzene oxide synthesis product.

Based on the results of this preliminary work, we are hopeful that additional work will yield evidence of benzene oxide formation *in vivo*. Successful synthesis of benzene oxide at ITRI is a critical first step in the study of this material as a transported metabolite in the blood of benzene-exposed animals. With synthesized standards and a newly developed analytical method, work continues to establish our ability to isolate benzene oxide from blood and assess this compound's role in the toxic effects associated with benzene exposure.

(Research sponsored by the Office of Health and Environmental Research, U.S. Department of Energy, under Contract No. DE-AC04-76EV01013.)

CONCENTRATIONS OF BUTADIENE EPOXIDES IN RAT TISSUES FOLLOWING EXPOSURES TO 62.5 AND 8000 PPM 1,3-BUTADIENE

Janice R. Thornton-Manning, Alan R. Dahl, William E. Bechtold, and Rogene F. Henderson

1,3-Butadiene (BD) is used extensively in the production of styrene-butadiene rubber, polybutadiene elastomers, and other polymers. Occupational exposures of workers in areas with concentrations of up to 374 ppm BD have been documented in U.S. plants (Fajen J. M. *et al. Environ. Health Perspect. 86*: 11, 1990). Additionally, BD is present in cigarette smoke, gasoline vapors, and automobile exhaust resulting in exposures of this chemical to most of the U.S. population (Miller, L. M. EPA Document 560/2-78-008, 1978). Recent epidemiological studies have revealed increased incidences of mortality due to leukemia among workers in the styrene-butadiene rubber industry (Delzell, E. *et al. Toxicology*, in press). However, some uncertainty remains as to the "carcinogenic" dose of BD. The workers who developed leukemia were employed in the 1950s when occupational exposures were much greater than those presently encountered in occupational settings.

Long-term animal studies have revealed that BD is carcinogenic in both Sprague-Dawley rats and B6C3F$_1$ mice (Huff J. E. *et al. Science* 227: 548, 1985; Melnick R. L. *et al. Cancer Res. 50:* 6592, 1990; Owen P. E. *et al. Am. Ind. Hyg. Assoc. J. 48*: 407, 1987). These studies have shown profound species differences in the potency and organ-site specificity of BD carcinogenesis. In mice, hemangiosarcomas, lymphomas, and lung, forestomach, liver, ovary, and mammary gland tumors were observed. Most notable was that lung tumors resulted from exposures as low as 6.25 ppm. In rats, chronic exposures of 1000 and 8000 ppm resulted in tumors of the thyroid, testis, uterus, mammary gland, and pancreas, although the data suggested that some of the tumors may not have been treatment-related. These species differences in tumorigenic responses to BD have made extrapolation of these data to humans difficult.

Our laboratory (Bechtold, W. E. *et al. Chem. Res. Toxicol. 8*: 182, 1995; Thornton-Manning J. R. *et al. Carcinogenesis 16*: 1723, 1995) and others (Himmelstein, M. W. *et al. Carcinogenesis 15*: 1479, 1994; *Toxicol. Appl. Pharmacol. 132:* 282, 1995) have shown that differences in metabolism also exist between rats and mice. The initial product of cytochrome P450-mediated metabolism of BD, butadiene monoepoxide (BDO), is present in tissues of mice at concentrations that exceed those of rats by 3- to 8-fold following inhalation exposures to BD. Butadiene diepoxide (BDO_2) is present in mouse tissues at concentrations about 40- to 120-fold greater than those of rat tissues. While both epoxides are genotoxic, BDO_2 is more genotoxic than BDO (Cochrane, J. E. and T. R. Skopek. *Carcinogenesis 15*: 13, 1994) and hence, may be the primary determinant of BD carcinogenicity. The purpose of the present investigation was to examine the production and disposition of BDO and BDO_2 in several tissues in rats following 6-h exposures to a low level (62.5 ppm) and a high level (8000 ppm) of BD.

Eleven- to 14-wk-old female Sprague-Dawley rats were exposed to 8000 ppm BD by nose-only inhalation for 6 h/d for 10 d (Monday-Friday on 2 consecutive wk). Controls were exposed simultaneously to house air on a separate exposure plenum. At the end of the 6 h exposure on day 10, the animals were sacrificed, and tissues, including lungs, mammary glands, femurs, and fat were removed and immediately frozen in liquid nitrogen. The tissues were stored in liquid nitrogen until they were analyzed. Metabolites were separated from the tissues by cryogenic vacuum distillation and then analyzed by multidimensional gas chromatography/mass spectrometry as previously described (Thornton-Manning *et al.*, 1995).

Concentrations of the BDO in tissues of rats following exposures to 62.5 and 8000 ppm are shown in Figure 1. This epoxide was present in femurs and mammary and fat tissues of rats exposed to 8000 ppm BD at concentrations approximately 10- to 22-fold greater than those in tissues of rats exposed to 62.5 ppm BD. BDO was not detected in the lungs of rats exposed to 62.5 ppm BD, but was present at a concentration of 1237 ± 207 pmol/g (mean ± SE) in the lungs of rats exposed to 8000 ppm BD.

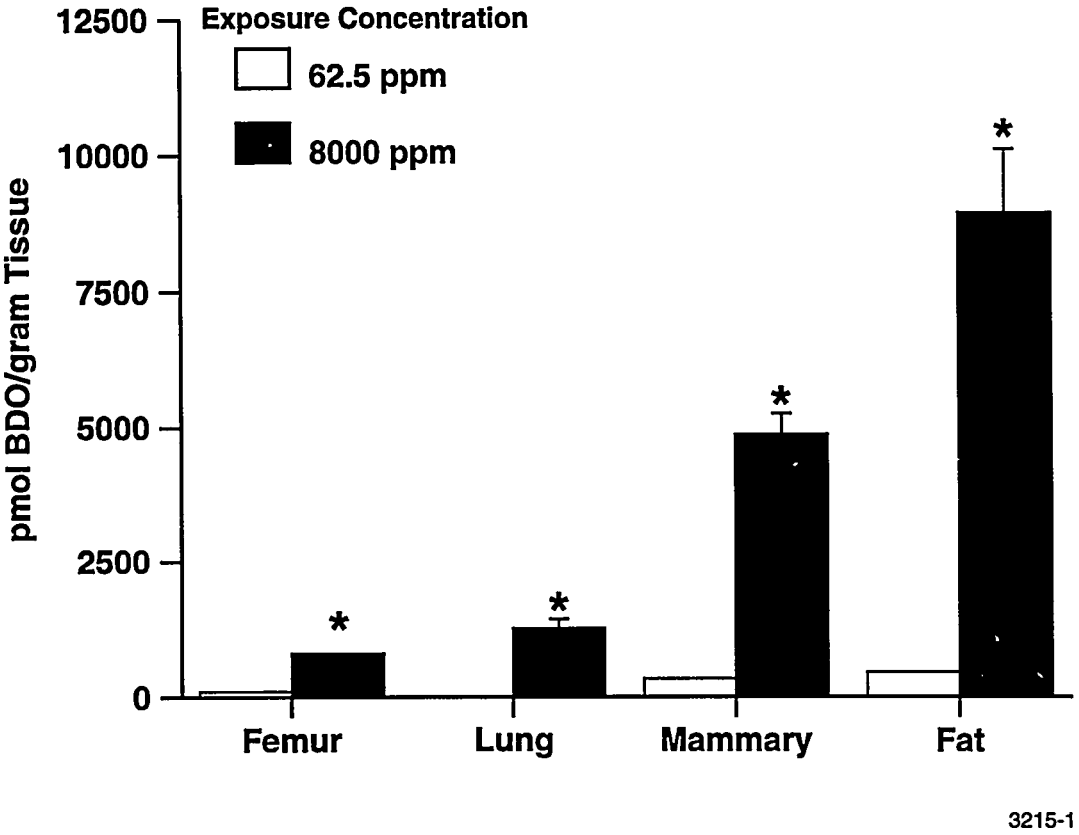

Figure 1. Concentrations of BDO present in rat tissues (n = 3–4) following exposures to either 8000 ppm BD or 62.5 ppm BD. Data are shown as mean with standard error bars. (*significantly different from 62.5 ppm data, $p \leq 0.05$).

BDO_2 concentrations were very similar in tissues of rats from the two exposure groups (Fig. 2). Concentrations of this metabolite were lower in the femur and mammary tissues of rats exposed to 62.5 ppm BD as compared to those of rats exposed to 8000 ppm BD. It appears that pathways responsible for the accumulation of BDO_2 in rats are saturated following exposures to 62.5 ppm BD. This may be due to competition of BD and BDO for cytochrome P450 2E1, the primary enzyme involved in the metabolism of BD to BDO (Csanady G. A. *et al. Carcinogenesis 13*: 1143, 1992; Duescher, R. J. and A. A. Elfarra. *Arch. Biochem. Biophys. 311*: 342, 1993) and BDO to BDO_2 (Seaton, M. J. *et al. Carcinogenesis 16:* 2287, 1995).

This lack of a dose-related accumulation of BDO_2 dose not occur in mice following exposures up to 1250 ppm (Himmelstein *et al.*, 1995). This inability to accumulate the highly mutagenic BDO_2 may explain the relative resistance of rats to BD-induced carcinogenicity.

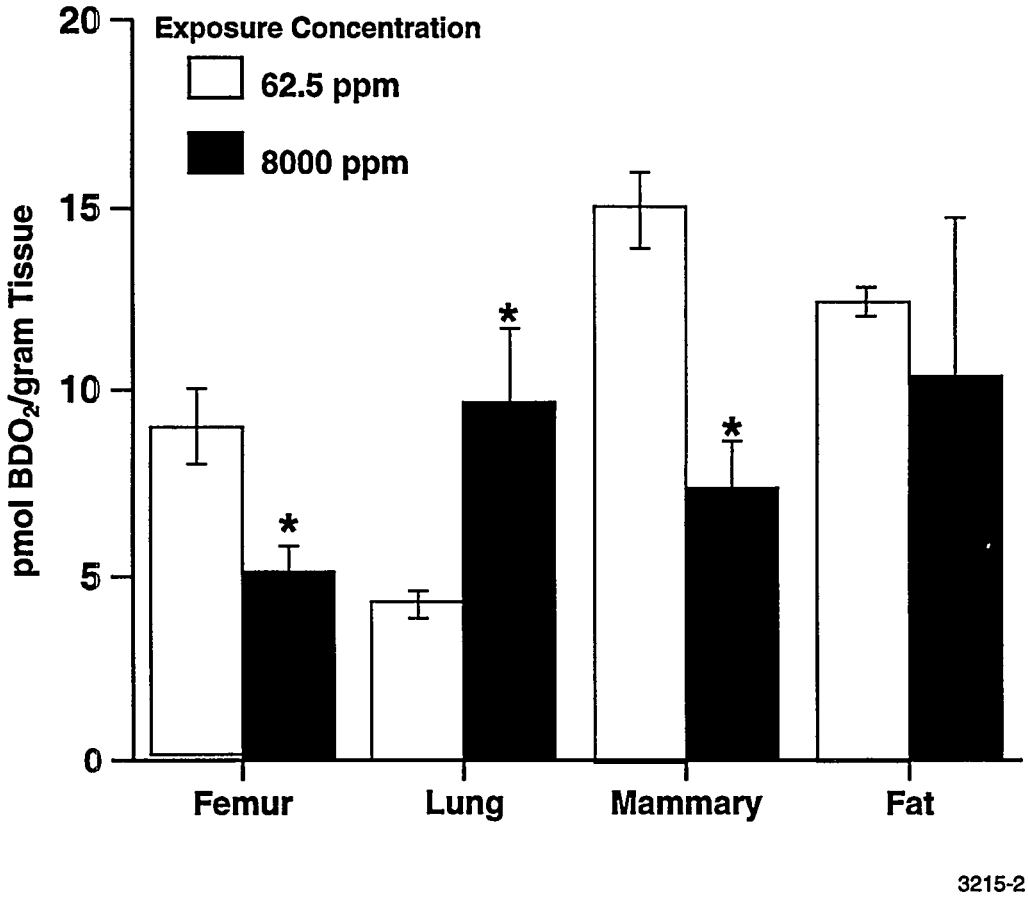

Figure 2. Concentrations of BDO_2 present in rat tissues (n = 3–4) following exposures to either 8000 ppm BD or 62.5 ppm BD. Data are shown as mean with standard error bars. (*significantly different from 62.5 ppm data, $p \leq 0.05$).

(Research supported by the Chemical Manufacturers' Association under Funds-In-Agreement No. DE-FI04-91AL66351 and DE-FI04-93AL94550 with the U.S. Department of Energy under Contract No. DE-AC04-76EV01013).

LOCALIZATION OF XYLENE AND ITS METABOLITES IN THE CELL LAYERS OF RAT OLFACTORY BULB FOLLOWING THRESHOLD LIMIT VALUE EXPOSURE

Kee H. Pyon, Alan R. Dahl, and Johnnye L. Lewis*

Evidence that many nasally introduced materials accumulate in the olfactory bulbs and deeper brain regions has been reported but is not consistent across all animals tested (McLean, J. H. *et al. Brain Res. Bull. 22*: 867-881, 1989). It is obvious that not everything we inhale accumulates in the brain; thus some barrier mechanisms must exist between the olfactory mucosa and the brain. A nose-brain barrier that protects the central nervous system (CNS) from inhaled toxicants has been suggested (Lewis, J. L. *et al.* In *The Vulnerable Brain and Environmental Risks, Vol. 3: Toxins in Air and Water* [R. L. Isaacson and K. F. Jenson, eds.], Plenum Press, New York, p. 77, 1994). The nose-brain barrier may be composed of many components. For example, in the olfactory epithelium, tight junctions exist between the olfactory receptor cells and the sustentacular cells (Costanzo, R. M. and E. E. Morrison. *J. Neurocytol. 18(3)*: 391, 1989), and high xenobiotic metabolizing capacity exists within the sustentacular cells (Dahl, A. R. and W. M. Hadley. *CRC Rev. Toxicol. 21*: 372, 1991). It is likely that, in the intact epithelium, these two characteristics function as components of a barrier between the external environment and the brain.

In studies of inhaled xylene, mainly nonvolatile metabolites of ^{14}C-labeled xylene accumulated in mouse olfactory bulbs following a 1-h exposure to 2900 ppm xylene (Ghantous, H. *et al. Pharmacol. Toxicol. 66*: 92, 1990). They could not determine with their methods the regional localization of those metabolites within the olfactory bulbs nor the site of metabolism of the parent compound. Results from our laboratory have shown that xylene metabolism occurs at high levels in the rat nasal mucosa but is not detectable in the olfactory bulb. The nonvolatile metabolites of xylene, along with a small quantity of volatiles, representing either parent xylene or volatile metabolites, are found in the glomeruli within the olfactory bulbs of rats exposed to ^{14}C-xylene at Threshold Limit Value (TLV; 123 ppm) (1993–94 Annual Report, p. 47). The occurrence of metabolites in the bulb and the discrete localization in the glomeruli suggest that metabolism occurs in the nasal mucosa and the metabolites then migrate to the bulb rather than enter the bulb through the systemic circulation.

Based on the results of these previous acute ^{14}C-xylene inhalation studies, the purpose of this study was to determine the effects of prolonged exposure duration at TLV and induced loss of olfactory epithelium on the entry of inhaled xylene and its metabolites into the olfactory bulb of F344 rats. Understanding the components of the nose-brain barrier and under what conditions this barrier may be disrupted can give much insight into the olfactory transport of inhalants into the CNS.

Male and female F344 rats were pre-exposed either to 6 h of filtered air or a single 6-h exposure to 190 ppm methyl bromide (MeBr; male rats only). An acute exposure to MeBr, a gas found in some pesticides, is known to cause total destruction of the rat olfactory epithelium. The olfactory receptor cells regenerate and begin to establish functional connections to the olfactory bulb within 8 d (Hurtt, M. E. *et al. Toxicol. Appl. Pharmacol. 94*: 328, 1988). The rats were then exposed to 0, 2 (air pre-exposed only), or 9 d of unlabeled xylene (6 h/d at TLV), followed by a 2-h exposure to ^{14}C-xylene (TLV; specific activity of 0.45 mCi/mmole).

Following the exposures, the rats were sacrificed and the brains removed with the olfactory bulbs attached. The right and left brain hemispheres were cryosectioned (8 μm slices). Multiple serial sections,

---

*UNM/ITRI Pulmonary Epidemiology and Toxicology Training Program Participant

along with standards containing known amounts of radiolabel embedded in plastic, were processed as follows: (1) one set was apposed to Fuji MI-NC, blue-base medical imaging film in autoradiography cassettes (detection of volatile and nonvolatile radioactivity), and (2) the second set was evaporated overnight on a heat block at 60°C to remove volatiles, then apposed to film and placed in cassettes. Due to the level of specific activity, films were exposed at -20°C for 12 mo. After exposure, the film was developed, fixed, rinsed, and dried. The film was cut into 2 × 6 cm strips along the outline of the slides and mounted onto clean microscope slides with Permount. Serial tissue sections to the autoradiographs were stained with hematoxylin and eosin and used to localize the radioactivity. The autoradiographs were examined with a light microscope for exposed silver grains and the intensity of the radioactivity was quantitated by visually comparing them to the known radiolabel standards that were exposed with the serial tissue sections.

Inhaled xylene gave rise to bilateral radioactivity in the olfactory bulbs under all the exposure conditions. No radioactivity was observed in the rest of the brain. Figure 1 shows the localization of volatile and nonvolatile radioactivity in the cell layers of the olfactory bulbs. Figure 2 shows the average (average $\pm$ SE) total (T) and nonvolatile (NV) radioactivity in the right and left olfactory bulbs under all the exposure conditions (n = 8, 6, 12, 3, 4, for exposure conditions Air/0 d-xyl, Air/2 d-xyl, Air/9 d-xyl, MeBr/0 d-xyl, and MeBr/9 d-xyl, respectively). Radioactivity was observed in the olfactory bulb glomerular and external plexiform layers of 50% of rats following a 2-h exposure to ^{14}C-xylene. In rats first exposed for 2 d to unlabeled xylene, radioactivity varied bilaterally in the olfactory nerve, glomerular, and external plexiform layers after the ^{14}C-xylene exposures. Higher total radioactivity was observed with an increase in the volatile fraction accounting for the increased radioactivity. Following 9-d exposure to xylene, autoradiographs showed more intense radioactive labeling of olfactory bulbs. Nonvolatile radioactivity accounted for most of the total activity. With MeBr treatment, staining density after ^{14}C-xylene exposure was less intense than without MeBr treatment.

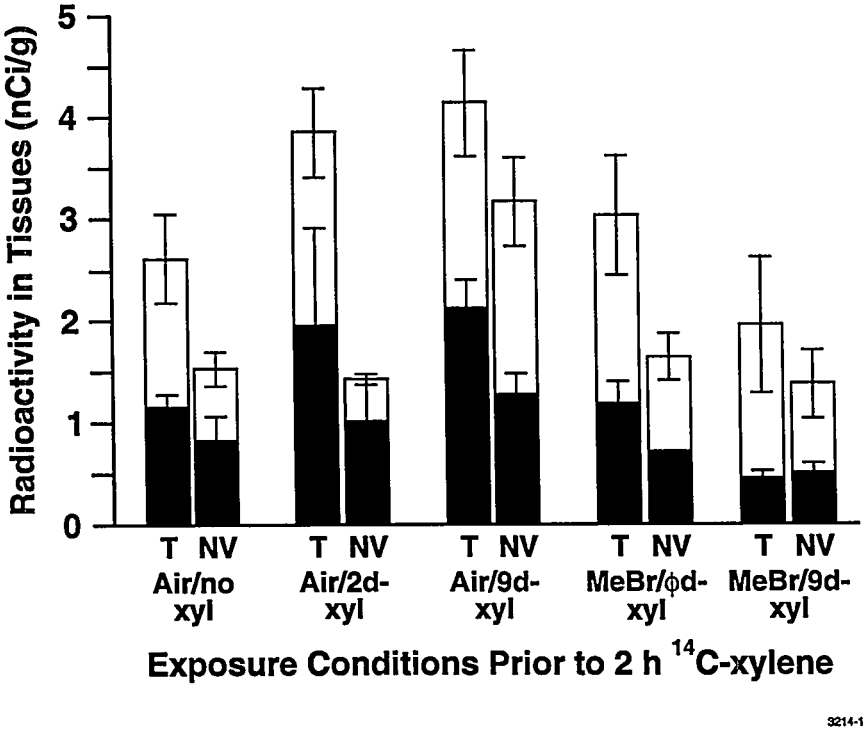

Figure 1. Localization of total and nonvolatile radioactivity in the cell layers of the right and left olfactory bulbs.

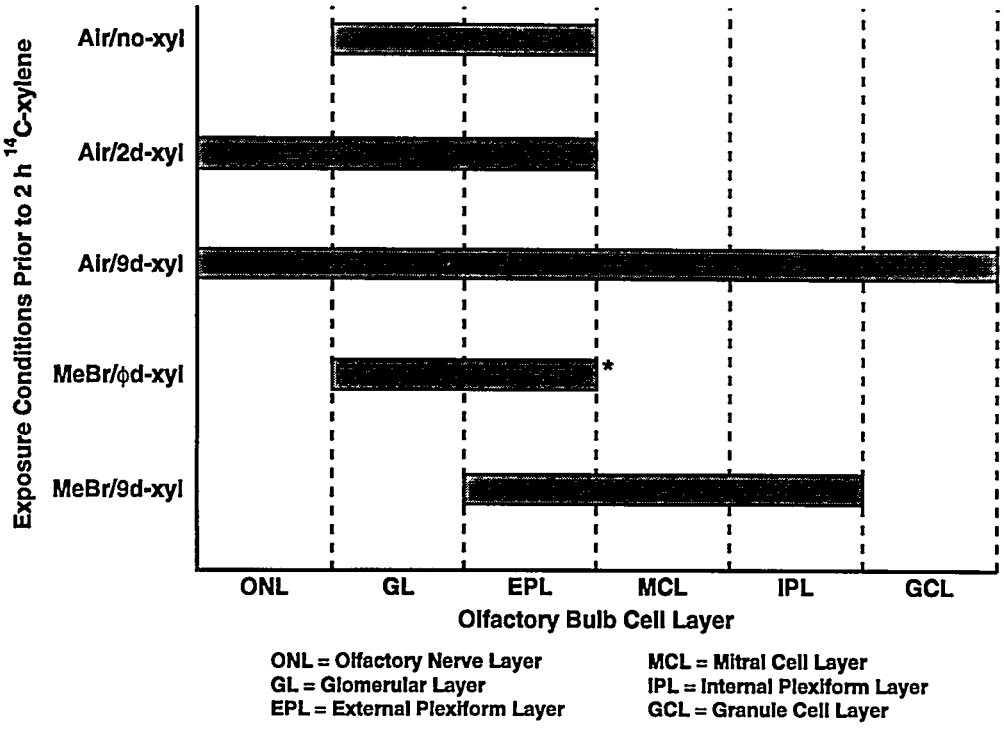

Figure 2. Average total (T) and nonvolatile (NV) radioactivity in the right and left olfactory bulbs (average $\pm$ SE, n = 8, 6, 12, 3, 4, for exposure conditions Air/0 d-xyl, Air/2 d-xyl, Air/9 d-xyl, MeBr/0 d-xyl, and MeBr/9 d-xyl, respectively). This is a semi-quantitative analysis based on visual comparison of the radioactivity staining to the known standards that were exposed with the serial tissue sections.

These results are consistent with results in preparation from a companion study (unpublished) which show that, in rats exposed only to air and xylene, a continued exposure to xylene (air/2d-xylene) produces an inhibition of nasal metabolism which recovers by 9-d xylene exposure. In the current study, the increase in the volatile fraction of radioactivity in the olfactory bulbs of rats exposed to 2 d of xylene can be attributed to a decrease in xylene metabolism. However, following a 9-d exposure to xylene, the presence of higher nonvolatile radioactivity indicates the recovery of the nasal metabolism. These results show that metabolism is an important factor in determining the form of the parent compound that may enter the olfactory bulb through the olfactory epithelium. Furthermore, the decreased staining intensity following MeBr pre-treatment suggests that intact neurons are necessary for significant uptake of xylene and its metabolites.

(Research sponsored by the PHS/NIH under Grant R01-DC01714 from the National Institute on Deafness and Other Communication Disorders and National Institute on Aging with the U.S. Department of Energy, under Contract No. DE-AC04-76EV01013.)

SITES OF PARTICLE RETENTION AND LUNG TISSUE RESPONSES DIFFER BETWEEN RATS AND CYNOMOLGUS MONKEYS EXPOSED CHRONICALLY TO DIESEL EXHAUST AND COAL DUST

Kristen J. Nikula, William C. Griffith, Kelly J. Avila, and Joe L. Mauderly

The usefulness of pulmonary carcinogenicity data from rats exposed to high concentrations of particles for quantitatively predicting lung cancer risk in humans exposed to much lower environmental or occupational concentrations has been questioned. The results of several chronic inhalation bioassays of poorly soluble, nonfibrous particles have suggested that rats may be more prone than other rodent species to develop persistent pulmonary epithelial hyperplasia, metaplasia, and tumors in response to the accumulation of inhaled particles (Mauderly, J. L., unpublished). In addition, rats and primates differ in pulmonary anatomy and their rate of particle clearance from the lung. The purpose of this investigation was to directly compare the patterns of particle retention and the lung tissue responses of rats and monkeys exposed chronically to diesel exhaust (DE), coal dust (CD), or diesel exhaust combined with coal dust (DECD) at exposure concentrations equivalent to the current permissible airborne concentration in underground coal mines in the U.S. (2 mg respirable particulate/m^3). The hypothesis was that particles would be retained differently in lungs of chronically exposed rats and monkeys, and that the tissue responses would also differ.

Lung sections from male cynomolgus monkeys and F344 rats exposed 7 h/d, 5 d/wk for 24 mo to filtered ambient air (FA), DE (2 mg soot/m^3), CD (2 mg respirable particulate material/m^3), or DECD (1 mg soot and 1 mg respirable coal dust/m^3) were obtained from a study (Lewis, T. R. *et al. J. Am. Coll. Toxicol. 8*: 345, 1989) conducted at the U.S. National Institute of Occupational Safety and Health (NIOSH). Hematoxylin and eosin-stained lung sections from 14 FA-, 14 CD-, 15 DE-, and 15 DECD-exposed monkeys and from 15 rats in each group were examined histopathologically, and the severity of lesions was scored. Lungs that had been inflated with fixative at a constant pressure of 20–25 cm hydrostatic pressure from eight animals per exposure group from each species were used for morphometry. Digitized images of the lung were captured and projected onto a computer monitor screen at a final magnification of 1280X. A 64-point grid (Stereology Toolbox, Davis, CA) was superimposed over each image, and the number of points hitting particulate material and the location of each point were recorded. The volume percentage of the total particulate material in the lumens of alveoli and alveolar ducts and in interstitial compartments was calculated for each animal from the number of points hitting particulate material in these compartments divided by the total number of points hitting particulate material $\times$ 100%.

The criterion for statistical significance was set at $p < 0.05$ for all analyses. The pathology severity scores were analyzed using polychotomous logistic regression (McCullagh, P. and J. A. Nelder. *Generalized Linear Models*, Chapman and Hall, London, 1983). The estimates of the volume percentages of the total particulate material in the lumens of alveoli and alveolar ducts and in interstitial compartments were assumed to be binomially distributed, and logistic regression was used for the statistical analysis. Extra binomial variation among animals was accounted for in the analysis by using a scaling factor, greater than one, to multiply the sampling variance (McCullagh and Nelder, 1983).

The lungs of DE-, CD-, and DECD-exposed rats exhibited the same histopathology. Overall, the particles were observed mainly within multifocal collections of alveolar macrophages. Most commonly, these macrophage aggregates were located within centriacinar alveoli, but the alveoli immediately adjacent to the pleura was another common location. A lesser portion of the retained particles was located in the interstitium. The characteristic tissue response to densely aggregated alveolar macrophages was alveolar epithelial hyperplasia. Other responses were particle-associated inflammation and a local septal fibrotic reaction.

The predominant sites of particle retention and the characteristic tissue responses were the same in DE-, CD-, and DECD-exposed monkeys. The retained particles had a multifocal distribution in the monkey lungs, but, in contrast to the rat, more of the particulate material was located in the interstitium than in the alveoli. Most commonly, interstitial particle-laden macrophages were (1) within the alveolar septa, (2) within interstitium of respiratory bronchioles, (3) within the adventitia and lymphatic capillaries surrounding arterioles and veins within the pulmonary parenchyma, and (4) in the pleura. The interstitial particulate material did not seem to elicit a tissue response. The portion of the particulate material within intralumenal collections of alveolar macrophages was smaller than in rats, and the aggregates of particle-laden macrophages elicited much less of a tissue response in the monkeys than in the rats.

Alveolar epithelial hyperplasia was significantly greater in particle-exposed rats than monkeys ($p < 0.001$). Alveolar epithelial hyperplasia was significantly greater in particle-exposed than control rats ($p < 0.001$), but there was no difference in the hyperplastic response due to type of particle exposure ($p = 0.3$). The monkeys did not have a significant alveolar epithelial hyperplastic response to particle exposure ($p = 0.4$).

Rats had a significantly greater inflammatory response to particles than monkeys ($p = 0.02$). Particle-exposed rats had significantly greater inflammation than control rats ($p < 0.001$). There was no significant difference in the inflammatory response due to the type of particle exposure in rats ($p = 0.5$). In monkeys, there was no significant effect of particle exposure ($p = 0.1$).

Rats had a significantly greater septal fibrotic reaction to particles than monkeys ($p = 0.006$). In rats, this reaction was significantly greater in particle-exposed than control rats ($p = 0.001$). There was no significant difference in the septal fibrotic reaction due to the type of particle exposure in rats ($p = 0.15$). There was less septal fibrotic reaction in particle-exposed than control monkeys ($p = 0.02$).

The morphometry showed clear differences between the rats and monkeys in the predominant sites of particle retention (Fig. 1). In rats, almost three-fourths of the particulate material was retained in lumens of alveoli and alveolar ducts. In monkeys, the particulate material was almost equally divided between these lumenal compartments and the interstitium, but more material tended to be in the intersitium. As shown in the figure, particles in the pleural lymphatics and connective tissue were grouped with the interstitial particles for this analysis. Interspecies comparison showed a significantly greater volume percentage of the total particulate material in the lumens of alveoli and alveolar ducts in the exposed rats than in the exposed monkeys ($p < 0.001$). Conversely, a significantly greater volume percentage of the total particulate material was in the interstitium of exposed monkeys than in exposed rats ($p < 0.001$). Within each species, there were no statistical differences between DE, CD, and DECD animals for the volume percentage of the total particulate material in lumens of alveoli and alveolar ducts or in the interstitium.

The present findings, combined with the known anatomical differences and data showing that primates clear deposited particles more slowly than rats (Snipes, M. B. *Crit. Rev. Toxicol. 20*: 175, 1989), suggest that a greater proportion of particles or particle-laden macrophages penetrates the airway epithelium and enters the interstitium in primates than in rats and that the particles in the interstitium may be cleared more slowly than those cleared via mucociliary action. If the presence of respiratory bronchioles, the amount of interstitial and pleural tissue, and the thickness of the alveolar septa are important determinants of the sites of particle retention, the differences between rats and humans might be even greater than the differences between rats and monkeys because human lungs have more extensive interlobular septa, thicker pleura, and wider interstitial spaces in the alveolar septa than monkeys (Weibel, E. R. In *The Evolution of Respiratory Processes* [S. C. Wood and C. Lenfant, eds.], Vol. 13, Marcel Dekker, New York, p. 289, 1979; Tyler, W. S. and M. D. Julian. In *Comparative Biology of the Normal Lung, Vol. I.* [R. A. Parent, ed.], CRC Press, Inc., Boca Raton, p. 37, 1992).

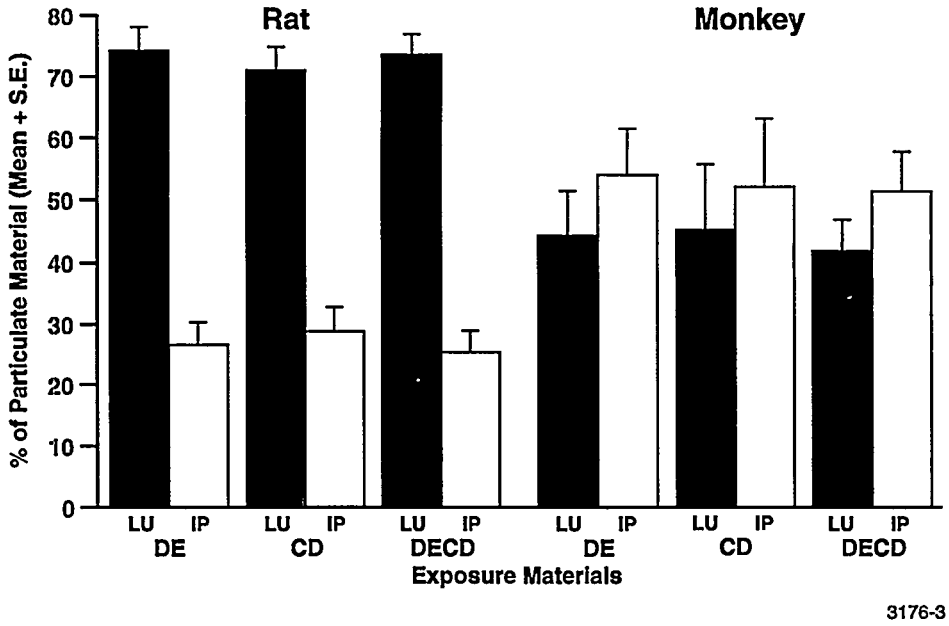

Figure 1. Volume percentages of particulate material in alveolar and alveolar duct lumens (LU) versus interstitium and pleura (IP) as the mean percentages of the total particulate material (+ S.E.) for animals exposed to DE, CD, or DECD.

The response to particles, including alveolar epithelial hyperplasia, inflammation, and focal septal fibrosis was significantly greater in rats than monkeys. Epithelial hyperplasia concomitant with the aggregation of particle-laden macrophages in alveolar lumens is a characteristic response to many poorly soluble particles in the rat lung (Nikula, K. J. *et al. Fundam. Appl. Toxicol.* 25: 80, 1995; *Toxicology and Carcinogenesis Studies of Talc in F344/N Rats and B6C3F$_1$ Mice (Inhalation Studies)*, National Toxicology Program, Technical Report 421, NIH Publication No. 92-3152, National Institutes of Health, Bethesda, MD, 1983; *Studies of Nickel Subsulfide*, NTP Technical Report 453, NIH Publication No. 94-3369, 1994; *Studies of Nickel Oxide*, NTP Technical Report 451, NIH Publication No. 94-3363, 1994). Hyperplasia of the surrounding epithelium in response to accumulation of particulate material in focal aggregates of alveolar macrophages was not characteristic of the response to diesel soot or coal dust in monkeys in this investigation, nor is it characteristic of coal workers' pneumoconiosis (Green, F. H. Y. and W. A. Laqueur. *Pathol. Annu. 1980 Part 2 15*: 333, 1980), silicosis (Peters, J. M. Silicosis. In *Occupational Respiratory Disease* [J. A. Merchant *et al.*, eds.], Department of Health and Human Services Publication, Centers for Disease Control, NIOSH, DHHS (NIOSH) Publication No. 86-102, Washington, DC, p. 219, 1986), or talc pneumoconiosis (Gamble, J. F. In *Occupational Respiratory Disease*, p. 243, 1986) in humans.

If human lungs respond to particles more like monkey lungs than rat lungs, this investigation suggests that the pulmonary response of rats to particles may not be predictive of the response in human lungs at concentrations representing high occupational exposures. Furthermore, these findings support the argument against using carcinogenicity data from rats exposed heavily to diesel exhaust to quantitatively predict carcinogenicity in humans exposed at lower rates because inflammatory and epithelial proliferative responses that seem critical to the carcinogenicity in rats exposed to high concentrations of particles may not occur in primate lungs exposed at environmental or occupational concentrations.

(Research sponsored by Volkswagen, under Funds-In-Agreement No. DE-FI04-95AL89515 with the U.S. Department of Energy, under Contract No. DE-AC04-76EV01013.)

EFFECT OF CIGARETTE SMOKE ON XENOBIOTIC-METABOLIZING ENZYMES OF RAT NASAL MUCOSAE

Sarah A. Wardlaw, Dean A. Kracko, Kristen J. Nikula, Gregory L. Finch, Alan R. Dahl, and Janice R. Thornton-Manning*

Tobacco smoke, a primary cause of respiratory disease, alters the levels of multiple xenobiotic-metabolizing enzymes in the lung. In the early 1980s nasal tissue was reported to contain xenobiotic-metabolizing enzymes at mass-normalized levels exceeding those in the liver for many substrates. Knowledge of the effects of cigarette smoke on the level and function of these enzymes in a tissue that first contacts inhaled toxicants and can concentrate environmental pollutants 1000–10,000-fold may contribute to investigations into the effects of other toxicants on nasal tissue and the tissue-specific regulation of these enzymes.

To investigate the effects of cigarette smoke on xenobiotic-metabolizing enzymes of the nasal mucosae, groups of 30 male CDF®(F-344)/CrlBR rats (Charles River Laboratories, Raleigh, NC) were exposed to 100 mg/m^3 mainstream cigarette smoke or filtered air for 2- and 8-wk time periods as described previously (1991–92 Annual Report, p. 110). Following sacrifice, liver, lung, and kidneys were collected, as well as respiratory and olfactory mucosae of the nasal cavity. Representative tissues were fixed and processed for immunohistochemical analysis, while the remaining tissues were homogenized and fractionated by centrifugation. The resulting S-9 fractions were stored at -80°C until enzyme levels and activity could be analyzed.

Xenobiotic-metabolizing enzyme levels were compared in the tissues of smoke-exposed and control rats by Western analysis of microsomes isolated from the S-9 fractions (example shown in Fig. 1; results summarized in Table 1). Results indicated an induction of CYP1A1 after both 2 and 8 wk of smoke exposure in respiratory and olfactory mucosae, with a level of induction in nasal respiratory mucosa similar to that seen in the lung. CYP1A2 increased slightly in 8-wk exposed olfactory mucosa, as well as 2-wk exposed respiratory mucosa, but remained relatively constant in 2-wk exposed olfactory tissue and was present only at very low levels in the respiratory mucosa of 8-wk control and exposed animals. CYP2B1 protein levels in the olfactory mucosa were relatively unaffected by 2 wk and 8 wk of smoke exposure, while CYP2B1 in the respiratory mucosa decreased. Glutathione S-transferase levels remained unchanged in the respiratory mucosa following 8 wk of smoke exposure, but declined in the olfactory mucosa (2 wk control and exposed samples not yet tested).

Changes in the activities associated with these enzymes as a result of smoke exposure often did not correlate with changes in protein levels (see Table 1). Activities were measured by spectrophotometric quantitation of the reaction products produced by microsomes in the presence of test substrate. Ethoxyresorufin O-deethylase (EROD) activity, associated with CYP1A1 (and to a lesser extent CYP1A2), increased significantly in the lung as a result of smoke exposure. This was also true of CYP1A1 protein levels in the lung as determined by Western analysis. However, EROD activity in the olfactory mucosa decreased significantly, while CYP1A1 protein levels increased and CYP1A2 increased or remained the same. EROD activity in the respiratory mucosa responded erratically to smoke exposure (no change overall), making comparisons to protein levels difficult. Methoxyresorufin O-deethylase (MROD) activity, associated with CYP1A2, was virtually undetectable in the lung where CYP1A2 protein was also not detected. However, in both the respiratory and olfactory mucosae, MROD activity decreased in the smoke-exposed samples, while CYP1A2 protein levels remained the same or increased. Pentoxyresorufin O-deethylase (PROD) activity, associated with CYP2B1, was affected in a manner more

---

*Postdoctoral Fellow

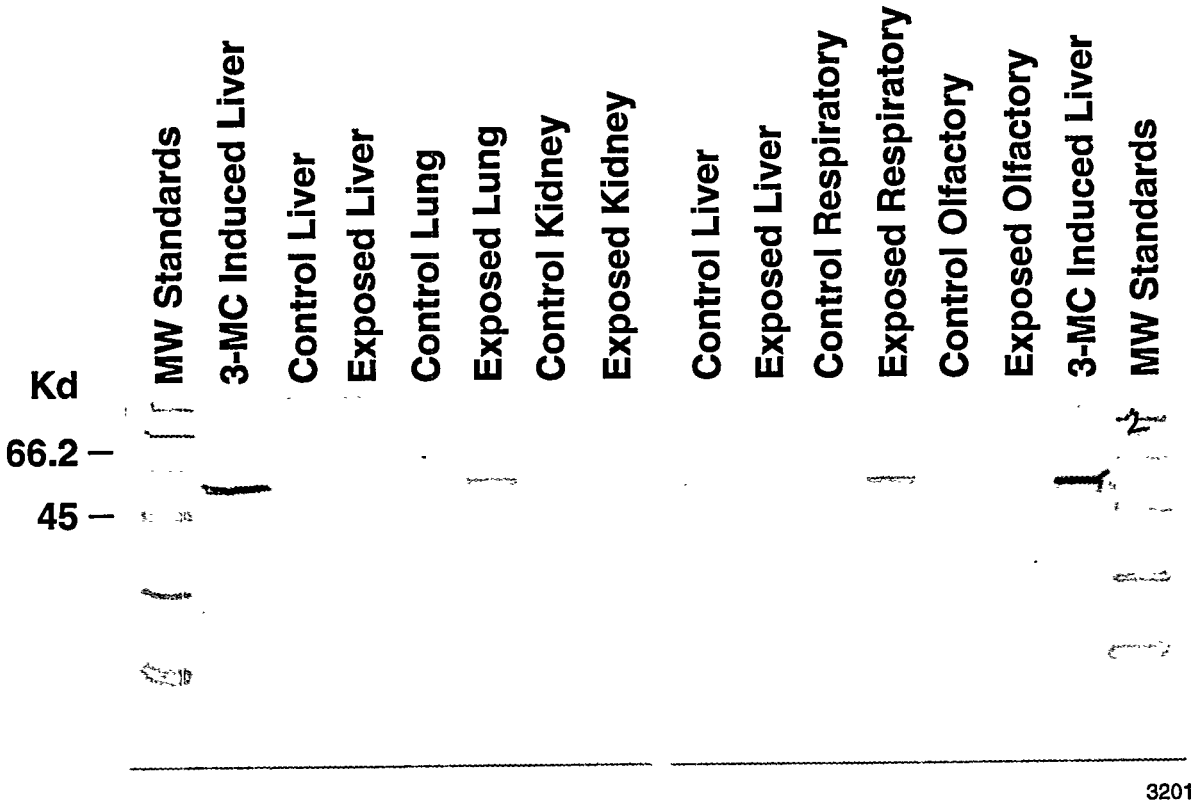

Figure 1. Immunoblot analysis of CYP1A1 in liver, lung, kidney, nasal respiratory, and olfactory microsomes from rats exposed to mainstream cigarette smoke or filtered air for 8 wk. Liver and lung microsomes represent individual animals; kidney, respiratory, and olfactory microsomes were prepared from pooled tissues from five animals.

Table 1

Effect of Smoke Exposure on Antigenic P450 Protein and Corresponding Enzyme Activity

Microsomes	CYP1A1[a] Activity/Protein	CYP1A2 Activity/Protein	CYP2B1 Activity/Protein
Liver	↑ / ↑[b]	↑ / ↑	↑ / ↑
Lung	↑ / ↑	ND / ND[c]	↓ / ↓
Kidney	↑ / ↑	→ / ND	ND / ND
Respiratory Mucosa	→ / ↑	↓ / ↑,→	↓ / ↓
Olfactory Mucosa	↓ / ↑	↓ / ↑,→	↓ / →

[a]Activity was measured using ethoxyresorufin (CYP1A1), methoxyresorufin (CYP1A2), or pentoxyresorufin (CYP2B1) as substrate.

[b]↑, ↓, → = increased, decreased, remained relatively constant following smoke exposure.

[c]ND = not detectable.

like that of the protein with which it is associated. PROD activity decreased to undetectable levels in the nasal mucosae of smoke-exposed rats, and CYP2B1 protein levels remained unchanged (olfactory) or decreased (respiratory). The conflicting effects of smoke exposure on CYP1A1 and CYP1A2 protein levels and enzymatic activity suggest a competing activity or interfering process in nasal tissue which is not present in other tissues examined. Other P450 enzymes that use ethoxyresorufin or methoxyresorufin as substrates may be present in the nasal tissues. On the other hand, a supporting process such as heme synthesis may be affected by smoke exposure, thereby altering enzymatic activities in ways unrelated to changes in protein level.

The results of preliminary immunohistochemical analysis of fixed ethmoturbinate sections for CYP1A1 support the altered expression of this enzyme in nasal tissue as a result of smoke exposure as suggested by Western analysis. CYP1A1 immunoreactivity in respiratory epithelium increased slightly in the smoke-exposed animals. This was also true of the olfactory epithelium where smoke exposure appeared to induce immunoreactivity in multifocal, neuroepithelial sustentacular cells. The most dramatic effect of smoke exposure, however, appeared in areas of mucocilliary metaplasia of the neuroepithelium occurring only in smoke-exposed animals. Intense CYP1A1 staining of ciliated cells was observed in these areas of respiratory-like epithelium in the olfactory region of the nasal cavity.

Altered levels, activity, and expression patterns of xenobiotic-metabolizing enzymes in nasal tissue may be a factor in the increased incidence of nasal cancer observed in smokers due to the ability of such enzymes to "bioactivate" inhaled toxicants by producing metabolites of greater carcinogenicity than the parent compound. In addition, these enzymes are postulated to play a role in olfaction, possibly producing odorants from nonodorants, or metabolizing odorants to nonodorants, thereby regenerating free olfactory receptors. Therefore, altered expression in response to cigarette smoke may be a factor in the olfactory deficits experienced by smokers. These dual roles of olfaction and defense carried out by the xenobiotic-metabolizing enzymes of nasal tissue may explain the less responsive nature of these enzymes to induction in comparison to enzymes found in other tissues due to the possible requirement for stable metabolism rates for odorants. Knowledge of the regulation of these enzymes will not only be predictive of the effects of other toxicants on nasal tissues, but may also increase understanding of the action of xenobiotic-metabolizing enzymes in other tissues.

(Research sponsored by the Office of Health and Environmental Research and Assistant Secretary for Defense Programs, U.S. Department of Energy, under Contract. No. DE-AC04-76EV01013.)

IV. NONCARCINOGENIC RESPONSES TO INHALED TOXICANTS

ROLE OF THE HISTOCOMPATIBILITY II COMPLEX IN MEDIATING BERYLLIUM-INDUCED GRANULOMATOUS LUNG DISEASE

Janet M. Benson, Edward B. Barr, and Kristen J. Nikula

Beryllium (Be) metal, oxides, and alloys are used extensively in the electronics, aerospace, and nuclear industries. Use of Be-containing materials has been significant in the past and continues to occur within DOE facilities, and the potential for future worker exposure exists during decontamination and decommissioning of some of these facilities. Some individuals inhaling low concentrations of Be may develop chronic Be disease (CBD), a debilitating and potentially fatal disease characterized by decreased respiratory function and by progressive granulomatous lung lesions. Be-specific immune responses in Be-exposed individuals are generally accepted as mediating CBD, but the mechanisms are poorly understood. Basic unanswered questions regarding CBD include the relative potential of various forms of Be-containing materials to induce the disease, dose-response relationships for Be metal, oxides, and alloys, and the underlying mechanism(s) for induction of this granulomatous disease. Answers to these questions may provide insight into why certain Be-exposed individuals within the DOE complex have developed CBD and may help to reduce the potential for workers to develop the disease. Questions regarding the relative toxicities of the Be-containing materials and their dose-response relationships can only be answered through animal studies using an adequate model for human CBD.

The overall purpose of this research is to better define the health risks associated with inhalation of Be-containing materials relevant to the Department of Energy. The underlying hypotheses are: (1) that the ability of Be-containing materials to produce granulomatous lung disease is dependent on their solubility within the respiratory tract and, where applicable, on the toxicities of other component metals and (2) that cell-mediated immune responses mediate Be-induced pulmonary lesions in the C3H mouse. The magnitude and nature of the Be-induced response obtained in the mouse depend on its MHC Class II gene haplotype and the functional adequacy of the MHC molecules expressed by the IA and IE loci.

Two loci of the MHC II complex in mice, designated IA and IE, produce MHC II proteins that are necessary for antigen presentation and for development of functional CD4+ T helper cells. Ishii, N. and coworkers (*J. Invest. Dermatol. 94*: 673, 1990; *Lab. Invest. 67*: 138, 1992) have presented evidence that Ni- and Cr-mediated delayed hypersensitivities are controlled by alleles at the IA rather than the IE loci. Further evidence exists that H-2^k and H-2^b MHC haplotype mice respond to a greater extent to Ni and Cr than mice with H-2^f, H-2^s, and H-2^d haplotypes and that the magnitude of response depends on the metal as well as the mouse haplotype.

Be-exposed C3H and A/J mice, but not C57BL/6 mice, develop pulmonary lesions with a strong lymphocytic component and other histological characteristics consistent with pulmonary lesions associated with CBD. The former strains are H-2^k haplotype (k alleles at both the IA and IE loci; k/k), while the C57BL/6 mouse has an H-2^b haplotype, but no functional MHC II molecule is produced by the IE locus (b/–). We believe the C3H mouse develops a strong immunopathological response in the lung, similar to human CBD, because its HMC haplotype is H-2^k, and both the IA and IE loci produce functioning MHC II molecules for antigen presentation.

Carefully selected congenic and knockout mouse strains are being used to confirm that the pulmonary and systemic responses in Be-exposed C3H mice are indeed immune mediated and MHC Class II restricted, and to determine the importance of haplotype and MHC II molecule production by IA and IE loci in regulating the magnitude of cell-mediated immune response obtained. The wild-type, congenic, and knockout mouse strains being used are listed in Table 1.

Table 1

Mouse Strains Used

Mouse	H-2 Alleles IA	H-2 Alleles IE
C3H/HeJ	k	k
C57BL/6	b	–
$A^b\beta$ Knockout (CD4+ lymphocyte-depleted)	–	–
B10.A (4R)	k	–
B10.A (5R)	b	b

Lack of pulmonary lesions with a strong lymphocytic component in the CD4+ lymphocyte-depleted knockout mice will indicate that pulmonary responses in the C3H mouse are immune mediated rather than nonspecific toxic responses to the inhaled Be. An enhanced influx of lymphocytes and severity of granulomatous inflammation, enhanced Be-specific IgG titres, and delayed-hypersensitivity reactions to $BeSO_4$ challenge in the B10.A(5R) strain (b/b) over that observed in C57BL/6 mice (b/–; no functioning MHC II molecule from the IE locus) would be expected if the MHC II protein from the MHC II IE locus is important for Be presentation to CD4+ cells. Similarly, a diminution in these responses in the B10.A(4R) mice (k/–; no functional MHC II molecule from the IE locus) compared to the C3H mouse would also suggest the importance of Be presentation by this MHC II molecule. Greater responses in the C3H compared to the B10.A(5R) strain would suggest that H-2^k haplotype mice may serve as more sensitive models for predicting the abilities of Be-containing materials to produce CBD in humans.

Female mice of each wild-type (C3H, C57BL/6), knockout (A^b, CD4+ lymphocyte depleted), congenic (B10.A[4R], and B10.A [5R]) strain were sham exposed to filtered air or exposed nose-only to ~30 mg Be metal/m^3 to provide lung burdens of 20 and 40 μg Be/lung. Subgroups of six mice/strain/Be exposure level were sacrificed 7 d after the nose-only exposure for quantitation of Be initial lung burdens and concentration of Be in whole blood. Additional groups of 12 mice/strain/Be level will be sacrificed 6 and 9 mo after the exposures for evaluation of gross and histopathological changes, lymphocyte proliferation in lung lesions, lymphocyte proliferation *in situ*, titres of Be-specific IgG antibodies in serum, and delayed hypersensitivity responses to intradermal $BeSO_4$ challenge. Groups of six mice per Be exposure level will be sacrificed 9 mo after the exposures for quantitation of final Be lung burdens and concentrations of Be in whole blood. Groups of 10 mice will be sacrificed 9 mo after exposures for evaluation of lymphocyte proliferation in response to $BeSO_4$ challenge *in vitro*. Pulmonary histopathological changes, lymphocyte proliferation *in situ*, and humoral and delayed-hypersensitivity responses to the inhaled Be in each mouse strain will be compared qualitatively and quantitatively (where possible) to responses obtained in the C3H mouse.

Lung burdens of Be metal achieved in this study are close to the target values of 20 and 40 μg. The lung burden data are summarized in Table 2. Because of the low availability of B10.A(5R) mice, it was only possible to expose a total of five mice of this strain. We chose to expose these few mice to 40 μg Be. The 6- and 9-mo sacrifices will be conducted during the second and third quarters of FY-1997, respectively.

Table 2

Summary of Initial Lung Burdens of Be Metal Achieved in this Study[a]

Mouse Strain	20 μg/Lung Target	40 μg/Lung Target $\pm$ SEM
C3H	15.3 $\pm$ 0.92	34.5 $\pm$ 2.6
C57BL/6	19.3 $\pm$ 1.1	25.4 $\pm$ 3.0
B10.A(4R)	19.8 $\pm$ 2.2	37.8 $\pm$ 3.2
B10.A(5R)	not done	43.5 $\pm$ 0.81
A^bB	18.5 $\pm$ 3.8	38.9 $\pm$ 0.93

[a]Results represent the mean $\pm$ SEM of six values except for the B10.A(5R) mice where n = 2.

(Research sponsored by the Office of Health and Environmental Research, U.S. Department of Energy, under Contract No. DE-AC04-76EV01013.)

EFFECT OF INHIBITOR OF ALKALINE PHOSPHATASE ON UPTAKE OF CHOLINE INTO PULMONARY TYPE II CELLS

Rogene F. Henderson and James J. Waide

Alkaline phosphatase (AP) is a marker enzyme for type II cells in the lung, but the function of the enzyme in the type II cell is unknown. AP appears in type II cells at the same time as the lamellar bodies which are characteristic of the surfactant synthesized and stored in those cells (Edelson, J. D. *et al. Am. Rev. Respir. Dis. 138*: 1268, 1988). Some of the AP in type II cells is associated with the lamellar bodies and appears to be secreted along with the surfactant. In the gut, AP is associated with lamellar-like bodies that are required for the transepithelial transport of lipids (Eliakim, R. *et al. J. Biol. Chem. 264*: 20614, 1989). Pulmonary type II cells are known to recycle secreted surfactant by uptake of degraded surfactant lipids from the alveoli (Wright, J. O. *Am. J. Physiol. 29*: L-1, 1990). Based on this background information, we hypothesized that AP in type II cells was necessary for the uptake of lipids for surfactant synthesis. The purpose of the current study was to test that hypothesis.

We measured the uptake of ^{14}C-choline in freshly isolated rat type II cells and pulmonary macrophages in the presence and absence of an AP inhibitor. The macrophages were used as control cells which do not synthesize, but phagocytize, surfactant. Choline is a component of dipalmitoyl phosphatidylcholine, a major surfactant lipid, and was used as a marker for surfactant lipid. The inhibitor was (–)-p-bromotetramisole (BT), a potent inhibitor of AP.

The freshly isolated type II cells and pulmonary macrophages were obtained from Fischer 344 rats, 26 wk old, by standard methods. Briefly, isolated perfused lungs were incubated with elastase for 35 min; the reaction was stopped by addition of serum, and the lungs were minced and filtered through nylon mesh. The resultant cell suspension was plated on IgG-coated dishes to remove cells with Fc membrane receptors. Macrophages were also removed by treating the cells with barium sulphate and separating the cells with high burdens of barium by density gradient centrifugation. Cell viability was determined by trypan blue exclusion, and the purity of the enriched type II cell population was measured using the modified Papanicolaou stain. Alveolar macrophages were obtained by centrifugation of bronchoalveolar lavage fluid from the same rats.

Type II cells and macrophages were cultured on Transwell membranes in essential minimal Eagle's media containing 10% fetal bovine serum. Cell numbers per well for both macrophages and type II cells were 4.4×10^6 with 78% purity (major contaminant cell was the macrophage) for the type II cells. The macrophage cell suspensions were 95% macrophages.

The uptake of ^{14}C-choline was measured in triplicate in both macrophage cell cultures and type II cell cultures in the presence and absence of the AP inhibitor, BT. Each well received 0.5 μCi ^{14}C-choline and 0, 0.25, 0.5, or 1.0 mM final concentration of BT. Cells were incubated overnight (16 h) at 37°C in a 5% CO_2, humidified atmosphere. The cells were washed 3 times with fresh media and lysed in 1 mL water. An aliquot was counted in a liquid scintillation counter.

The results are shown in Figures 1 (type II cells) and 2 (macrophages). Uptake of ^{14}C-choline was higher in the type II cells than in the macrophages, and the degree of inhibition of the uptake by BT was greater in the type II cells.

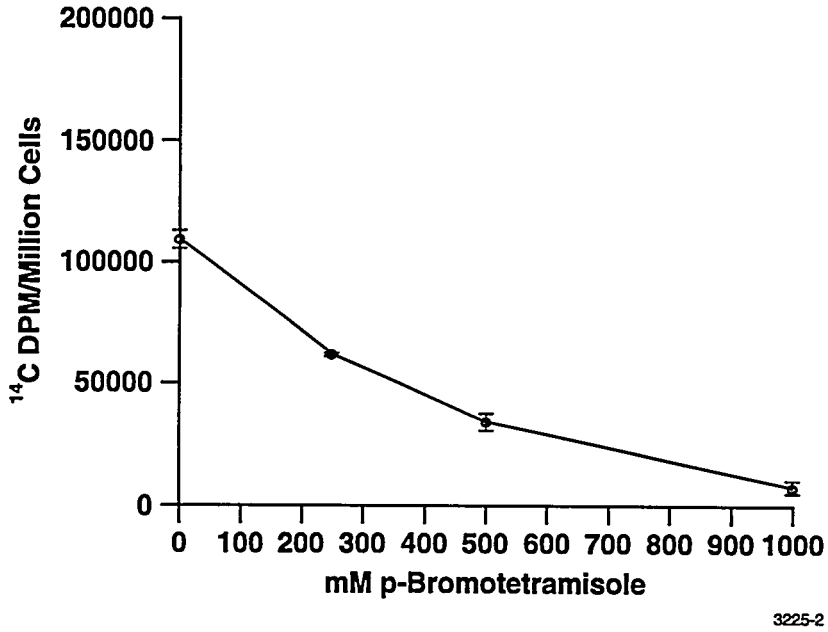

Figure 1. Inhibition of ^{14}C-choline chloride uptake into type II cells by p-bromotetramisole.

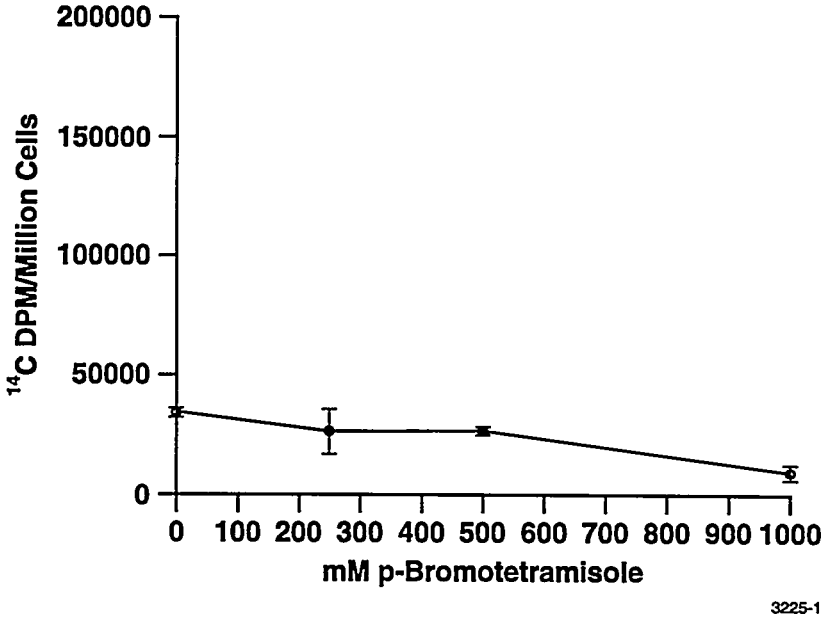

Figure 2. Inhibition of ^{14}C-choline chloride uptake into pulmonary macrophages by p-bromotetramisole.

Data suggest that AP plays a role in the uptake of surfactant precursors into type II cells. The study provides a basis for developing hypotheses for further studies to determine the specific role played by AP in the recycling of surfactant in the lung.

(Research sponsored by the Office of Health and Environmental Research, U.S. Department of Energy, under Contract No. DE-AC04-76EV01013.)

EFFECTS OF INHALED CIGARETTE SMOKE ON AIRWAY REACTIVITY

David E. Bice, David D. S. Collie, Julie A. Wilder**, Kristen J. Nikula, and Gregory L. Finch*

Although a genetic susceptibility is accepted for allergic asthma, not all genetically susceptible individuals develop atopic disease (Godfrey, S. *Agents Actions Suppl. 40*: 109, 1993). Therefore, additional risk factors must determine if pulmonary immune responses produced to inhaled allergens will or will not cause asthma. Epidemiologic studies have identified potential risk factors for the development of asthma including (1) exposure to high levels of allergens or pollutants, (2) being raised in a damp home where gas is used for cooking, and (3) pulmonary viral infections (Duff, A. L. *et al. Pediatrics 92*: 535, 1993). Young age at the time of pulmonary infection or exposure to pollutants also appears to be an important risk factor in the development of asthma (Sporik, R. *et al. N. Engl. J. Med. 323*: 502, 1990). Regardless of what triggering factors are responsible, a major concern is that the establishment of allergic immune responses in the lungs of children could result in a permanent asthmatic status.

Because children raised in homes of cigarette smokers have a significantly higher incidence of asthma than children raised in homes of nonsmokers, we hypothesize that the inhalation of mainstream cigarette smoke by pregnant women and/or sidestream smoke by genetically susceptible children increases the incidence of asthma by altering pulmonary immune responses to inhaled antigens. This report presents preliminary data on how cigarette smoke exposures affect the development of allergic pulmonary immunity and airway hyperreactivity (AHR) in mice.

Twenty-two male and 34 female Balb/c mice were exposed to clean air or to cigarette smoke for 3 mo. Exposures to cigarette smoke during the first week were to 100 mg total particulate material (TPM)/m^3 to acclimatize the mice to inhaled cigarette smoke. The exposure was then increased to 250 mg TPM/m^3 for the remainder of the exposure. Exposures were 6 h/d, 5 d/wk. One-half of the exposed and one-half of the control mice were removed from the chambers and immunized to ovalbumin (OVA) by three nose-only inhalation exposures. These three exposures, which were once a week for the last 3 wk of cigarette smoke exposure, were to a nebulized solution of 5% OVA in saline for 1 h. The remaining one-half of the mice from cigarette smoke chambers and control chambers were sham exposed 3 times to saline. Airway hyperreactivity to intravenous methacholine was measured at 24 h after the last OVA or saline exposure. Mice were then sacrificed, and serum was taken for measurement of antibody to OVA. The lungs were fixed in 10% formalin for histopathology.

Increased airway reactivity to methacholine was observed in mice exposed to cigarette smoke compared with controls (Fig. 1). We also showed that the airways in exposed and control female mice were significantly more reactive ($p < 0.05$) than in male mice (Fig. 2). Women also have more reactive airways than men, suggesting that the differences in airway reactivity in male and female mice may be representative of human responses (Peat, J. K. *et al. Eur. Respir. J. 5*: 921, 1992).

Mild perivenular and peribronchiolar infiltrates of lymphocytes with lesser numbers of neutrophils, plasma cells, and eosinophils were observed in mice exposed to air and OVA. The main lesion in mice exposed to tobacco smoke and saline was a centriacinar alveolitis characterized by pigment (smoke tar)-containing macrophages and neutrophils in the alveoli. Macrophages and neutrophils were frequently observed along the lumenal surface of the bronchiolar epithelium, probably as a result of mucocilliary clearance from the alveoli. However, neutrophils and pigment-containing macrophages were also observed in the walls of bronchioles, and transepithelial migration of neutrophils was rare.

---

*Postdoctoral Fellow

**UNM/ITRI Pulmonary Epidemiology and Toxicology Training Program Participant

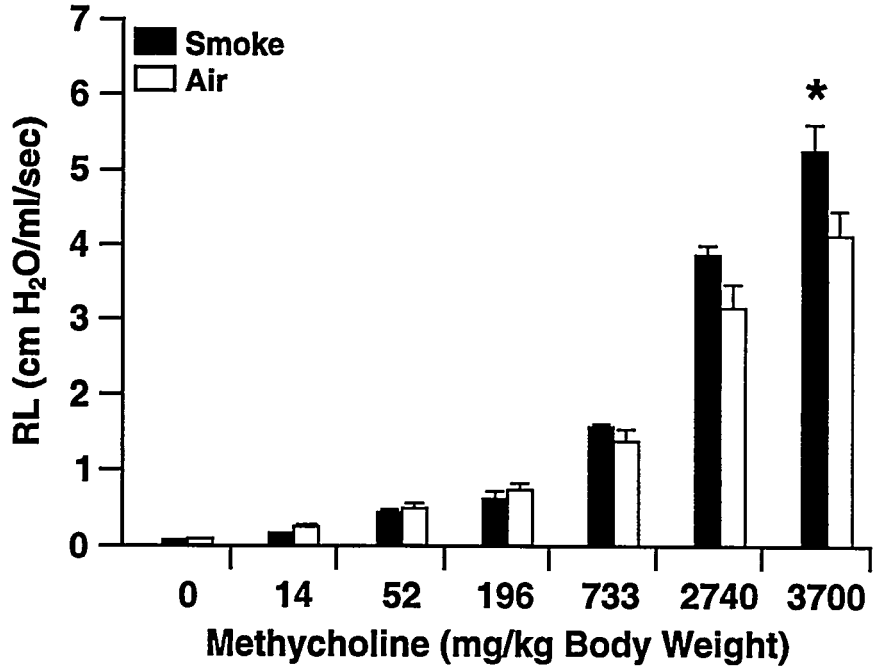

Figure 1. Airway reactivity of control mice and mice exposed to cigarette smoke. RL = difference in pulmonary resistance (cm H_2O/mL/sec) between the baseline measurement and that following the injection of methylcholine, MCh = methylcholine (mg/kg). * = $p < 0.05$. Data are presented as means $\pm$ S.E.

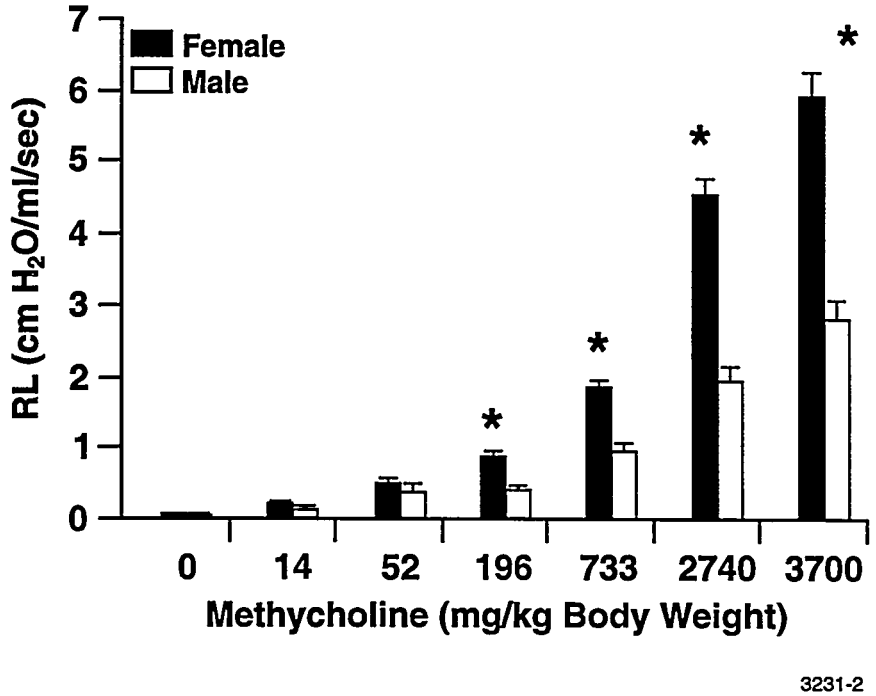

Figure 2. Comparison of airway reactivity in male and female mice. RL = difference in pulmonary resistance (cm H_2O/mL/sec) between the baseline measurement and that following the injection of methylchloine, MCh = methylcholine (mg/kg). * = $p < 0.05$. Data are presented as means $\pm$ S.E.

The mice exposed to tobacco smoke and OVA had a combination of the alterations in the smoke/saline and air/OVA groups, suggesting an additive effect of tobacco-smoke and OVA exposures. Although histopathology suggested immune responses were produced in the lungs to OVA, anti-OVA antibody was observed in the serum of only some of these mice. Apparently, the three single nose-only inhalation exposures to OVA were not adequate to induce significant levels of immunity to OVA.

Large numbers of infants and young children who are genetically susceptible for the development of asthma are exposed to cigarette smoke. To evaluate the effects of inhaled cigarette smoke on the development of asthma in children, pregnant mice and their offspring will be exposed to OVA in either cigarette smoke or clean air. However, because the level of antibody observed in mice from this study was low, the offspring in our future studies will be exposed to OVA in chronic, whole-body exposures rather than in three nose-only exposures as used in these preliminary studies. The effects of cigarette smoke exposure on the development of airway inflammation, allergic pulmonary immunity, and AHR in the offspring will be evaluated. Data from these studies will help identify the changes in pulmonary immunity induced by inhaled cigarette smoke that might cause a susceptible individual to develop asthma. Identifying how the risk factors of inhaled cigarette smoke and age interact to produce allergic immunity to inhaled allergens could help establish the basis for increased educational activities to curtail cigarette smoking in the presence of high-risk groups. In addition, identifying mechanisms responsible for the production of asthma by inhaled cigarette smoke could provide information about how other risk factors (e.g., pulmonary viral infections) might increase the incidence of asthma.

(Research sponsored by the Office of Health and Environmental Research and Assistant Secretary for Defense Programs, U.S. Department of Energy, under Contract No. DE-AC04-76EV01013.)

LOCALIZATION OF ASTHMATIC RESPONSES TO SINGLE AIRWAYS IN THE LUNG: A MODEL TO DETERMINE THE ROLE OF PULMONARY IMMUNITY IN ASTHMA

David E. Bice, David D. S. Collie, Bruce A. Muggenburg, and Fletcher F. Hahn*

All allergic individuals are systemically immune to sensitizing allergens as indicated by allergen-specific antibody and positive skin tests. The presence of systemic antibody to allergens suggests that all tissues and organs in allergic individuals should be equally responsive to allergen exposures. However, this is not true. Allergic diseases are usually isolated to certain "target organs" such as the lung, nose, eyes, and skin (von Mutius, E. and T. Nicolai. *Am. J. Respir. Crit. Care Med. 153*: 1266, 1996). In individuals with allergic asthma, the lung is the most responsive organ to allergen exposures, and clinical allergic disease is usually found only in their lungs. In contrast, the nasal airways of other individuals are highly responsive to allergens, and they have hay fever (rhinitis). We propose that the localization of anti-allergen immunity to a specific organ is responsible for the development of allergic disease in that "target organ." If this is true, the level of anti-allergen antibody in the serum of asthmatics and individuals with rhinitis would be the same, but the level of immunity localized to their lungs or nose could be quite different.

Clinical studies support the possibility that the immune responses that cause allergic asthma are localized to the lungs. For example, asthmatic recipients of lungs from nonatopic donors no longer have asthma. In addition, the recipients of lung transplants can become asthmatic if they receive donor lungs from asthmatics (Corris, P. A. and J. H. Dark. *Lancet 341*: 1369, 1993). The maintenance of sensitivity in the lung allograft to inhaled allergens indicates that the mechanisms responsible for asthma are localized in the lungs, with a minimal systemic immune component. Pulmonary immunity to inhaled allergens in the donor lung from an asthmatic could cause allergic asthma in the transplant recipient. In support of this possibility, we have shown that that pulmonary immune cells continue to produce antibody in an allograft lung for over 300 d after transplantation (Bice, D. E. *et al. Am. J. Respir. Cell Mol. Biol. 14*: 341, 1996). Although these data suggest that pulmonary immunity to allergens is pivotal in the cause of asthma, studies have not been done to determine if immune cells and products found in the lungs of asthmatics are a result of immunity localized to the lung. We present here the development of a model of asthma that will allow us to determine the roles of pulmonary immunity in the induction of eosinophil inflammation, mucin production, airway resistance, and airway hyperreactivity.

To develop an airway model of asthma, we used a litter of six Beagle dogs (three males and three females) from breeders who produce offspring with elevated serum IgE and pulmonary eosinophilia (Collie, D. D. S. *et al. Am. J. Vet. Res.*, in press). Elevated serum IgE and blood eosinophilia are markers of susceptibility for asthma (Gleich, G. J. *Clin. Exp. Allergy 20*: 245, 1990). Therefore, the identification of dogs in the ITRI dog colony that recruit large numbers of eosinophils into their lungs in response to instilled antigens suggests that these dogs could be used in the development of an asthma model. The dogs were immunized within 24 h of birth by intraperitoneal injection of 500 μg ragweed pollen extract and aluminum hydroxide. Systemic anti-ragweed antibody and positive skin tests indicated that these dogs were systemically immune. When the dogs were young adults, they were anesthetized by inhalation of isoflurane, and selected airways in the left and right cardiac and in the left and right diaphragmatic lung lobes were instilled using a fiberoptic bronchoscope with either 200 μg ragweed extract in 3 mL saline or with 3 mL of saline as controls. The left cardiac and left diaphragmatic lung lobes in three dogs were instilled with ragweed, and saline was instilled into the right cardiac and the right

*Postdoctoral Fellow

V. CARCINOGENIC RESPONSES TO TOXICANTS

EFFECTS OF COMBINED EXPOSURE OF F344 RATS TO RADIATION AND CHRONICALLY INHALED CIGARETTE SMOKE

Gregory L. Finch, Kristen J. Nikula, Edward B. Barr, William E. Bechtold, William C. Griffith, Fletcher F. Hahn, Charles H. Hobbs, Mark D. Hoover, David L. Lundgren, and Joe L. Mauderly

Nuclear workers may be exposed to radiation in various forms, such as low-LET γ-irradiation or high-LET α-irradiation from inhaled $^{239}PuO_2$ particles. These workers may then have increased risk for lung cancer compared to the general population. Of additional concern is the possibility that interactions between radiation and other carcinogens may increase the risk of cancer induction, compared to the risks from either type of agent alone. An important and common lung carcinogen is cigarette smoke. The purpose of this project is to determine the combined effects of chronically inhaled cigarette smoke and either inhaled $^{239}PuO_2$ or external, thoracic x-irradiation on the induction of lung cancer in rats and mice.

For our initial study of combined cigarette smoke and $^{239}PuO_2$, male and female CDF®(344)/CrlBR rats (4 ± 1 wk old; Charles River Laboratories, Raleigh, NC) were placed on study in 1991–92. Beginning at 6 wk of age, groups of rats were exposed by the whole-body mode for 6 h/d, 5 d/wk, to either filtered air (FA) or mainstream cigarette smoke (CS) diluted to concentrations of either 100 or 250 mg total particulate matter (TPM)/m^3 (LCS or HCS groups, respectively). At 12 wk of age, rats were removed from the chambers, exposed nose-only to either FA or a $^{239}PuO_2$ aerosol, then returned to the chambers 1 wk later for a 30 mo continued exposure to FA or CS. This study included six exposure groups: FA alone, $^{239}PuO_2$ alone, LCS alone, LCS + $^{239}PuO_2$, HCS alone, and HCS + $^{239}PuO_2$. Exposures and terminal sacrifices were completed in 1994. Additional details have been given in previous reports (1991–92 Annual Report, p. 110; 1992–93 Annual Report, p. 53; 1993–94 Annual Report, p. 71; 1994–95 Annual Report, p. 77).

Initial lung burdens of $^{239}PuO_2$, and the effects of CS exposure on body weights, survival, and lung clearance of ^{239}Pu have been reported (1994–95 Annual Report, p. 77). Histological evaluation of lungs and other selected tissues continues. For animals on study for at least 1 y, a significant influence of CS exposure on the induction of lung tumors was found in female rats, but not males. Incidences of benign and/or malignant lung tumors in female rats remain similar to those reported previously (1994–95 Annual Report, p. 77). Figure 1 illustrates the prevalence (number of rats with lung tumors divided by the total number of rats examined at necropsy) of lung tumors observed in male and female rats exposed to smoke for 12 to 30 mo, 12 mo being the approximate time at which the first tumor was observed. The most prevalent malignant neoplasms were adenocarcinomas, followed by squamous cell carcinomas and adenosquamous carcinomas. Interestingly, in groups exposed to both agents, there were increased tumor multiplicity, an increased proportion of neoplasms of the squamous phenotype, and several animals with airway-associated lung neoplasms. These results demonstrated that cigarette smoke and ^{239}Pu interacted synergistically in producing lung cancer in rats.

Analysis of this study is continuing. During FY-1996 we began a new study involving combined exposures to CS + X rays. This research is important because of (1) the prevalence of cigarette smoking; (2) concerns for workers exposed to low-LET radiation in ongoing DOE nuclear operations and in decontaminating, decommissioning, and environmental restoration activities; and (3) conflicting epidemiologic data regarding possible CS/X-ray interactions. In addition, the issue of CS-induced decreased lung clearance of radioactive particles and associated dose increase will be avoided using X-ray exposures.

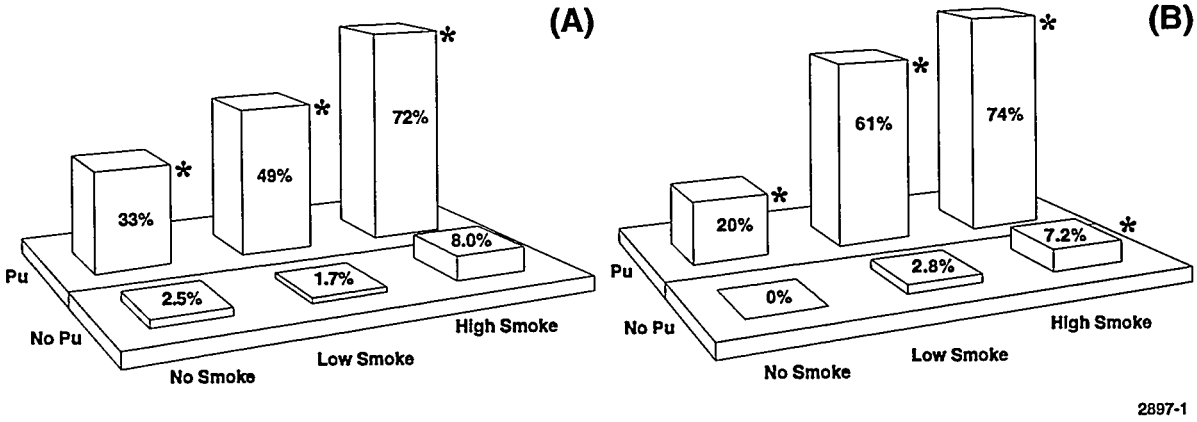

Figure 1. Prevalence of (A) male or (B) female rats with benign or malignant lung tumors as a function of exposure group for animals on study for at least 12 mo. Asterisk (*) denotes a statistically significant difference (one-sided Yates test, $p \leq 0.05$) compared to unexposed controls.

The experimental design for the study of interactions between CS and X-irradiation is shown in Table 1. Significant design features include the following: (1) only one level of CS exposure is being used (HCS; 250 mg TPM/m^3), because this level showed the greatest carcinogenic and interactive effects in our first study, yet did not have a major effect on life span; (2) fractionated, thoracic x-irradiation is being used to partially mitigate the significant effect of whole-body X-irradiation on life span (see 1992–93 Annual Report, p. 61); (3) levels of X-ray exposure are based on our previous work with rats and literature reports on effects in mice; and (4) both F344/Crl rats and B6C3F$_1$ mice are being studied, because the use of more than one animal species is an important toxicological strategy that often provides help in extrapolating results to humans.

Table 1

Experimental Design for Study of Combined Effects of Cigarette Smoke with Either X rays or $^{239}PuO_2$[a] on Rats and Mice

Radiation:		None		X rays		$^{239}PuO_2$	
Animal:		Rats	Mice	Rats	Mice	FBNF$_1$ Hybrid Rat	Mice
Cigarette Smoke (mg TPM/m^3)	0	300 (270/30)	372 (342/30)	252 (222/30)	192 (162/30)	54 (48/6)	198 (156/42)
	250	300 (270/30)	372 (342/30)	252 (222/30)	192 (162/30)	54 (48/6)	198 (156/42)

TOTALS: CDF®(F344)/CrlBR rats 1104 (984/120)
B6C3F$_1$ mice 1524 (1320/204)
FBNF$_1$ rats..... 108 (96/12)

[a]Total number of animals with the number of life span/number of serial sacrifice animals given in parentheses.

Additional limited exposures were done with $^{239}PuO_2$ with or without CS exposure in B6C3F$_1$ mice, to provide comparable data to those obtained previously in rats. We also exposed a hybrid strain of rat

($FBNF_1$) to $^{239}PuO_2$ alone or CS + $^{239}PuO_2$ to perform a microsatellite assay on lung tumors. This technique may reveal mutations characteristic of specific agents and mutations in as yet unidentified tumor suppressor genes in rats (Davis, L. M. *et al. Carcinogenesis 15*: 1637, 1994).

The experimental approach is similar to that used in the first CS + $^{239}PuO_2$ study. Exposures to CS began at 6 wk of age for both rats and mice, and radiation exposure occurred at either 12 wk of age (for $^{239}PuO_2$) or during the 12th and 13th wk of age (for the x-irradiation). Exposures to CS or FA will then continue through 30 mo. Approximately 10% of the animals will be serially sacrificed for dosimetric and histological evaluations, and the remainder will be held and exposed for their life spans.

All animals were entered into the study in five blocks between October 1995 and September 1996. As of October 1, 1996, 92% of the study animals were alive, 7% had been serially sacrificed, and 1% had either died or been euthanized as moribund. For FY-1996, CS exposures were 96% of target averaged over all CS exposure chambers. Through 140 d on study, body weights of CS-exposed mice were approximately 81% those of FA-exposed mice, and within CS- or FA-exposure groups, there were no effects of radiation treatment on body weight. These effects in mice are nearly identical to those previously observed in rats (1992–93 Annual Report, p. 53).

As in previous ITRI studies with inhaled $^{239}PuO_2$, the particles were labeled with the gamma emitter ^{169}Yb for external weekly whole-body counting between 7 and 42 d after exposure for clearance modeling using a single-component negative exponential function. Clearance half times of $^{239}PuO_2$ were 27 or 200 d for mice also receiving FA or CS, respectively. These data compare with half times of 29 or 67 d for female rats receiving FA or CS, respectively. Thus, we conclude that (1) clearance of particles is similar between control mice and rats, (2) CS significantly impairs the clearance of particles in both species, and (3) this impairment appears greater in mice than in rats.

In conclusion, histologic and dosimetric evaluations of rats in the CS + $^{239}PuO_2$ study continue, and the study of CS + X rays is continuing with exposures, in-life procedures, serial sacrifices, and endpoint analyses. This research will generate significant new information regarding the induction of cigarette smoke-induced lung cancer in rats, and the potential for interaction between cigarette smoke and lung irradiation in the induction of lung cancer.

(Research sponsored by the Assistant Secretary for Defense Programs, U.S. Department of Energy, under Contract No. DE-AC04-76EV01013.)

CARCINOGENIC EFFECTS OF INHALED BERYLLIUM AND PLUTONIUM-239 DIOXIDE IN RATS AND MICE

Gregory L. Finch, Fletcher F. Hahn, Mark D. Hoover, William C. Griffith, Steven A. Belinsky, John F. Lechner, and Charles H. Hobbs

Nuclear weapons industry workers have the potential for inhalation exposures to plutonium (Pu) and other agents, such as beryllium (Be) metal. Inhaled Pu deposited in the lung delivers high linear energy transfer alpha particle radiation and is known to induce pulmonary cancer in laboratory animals (*Biological Effects of Ionizing Radiation-IV*, National Academy of Sciences, Washington, DC, 1988). Beryllium is a metal which is classified as a suspect human carcinogen in the United States (*Health Assessment Document for Beryllium*, U.S. EPA/600/8-84/026F, 1987) and as a demonstrated human carcinogen by the International Agency for Research on Cancer (IARC, *Beryllium, Cadmium, Mercury, and Exposures in the Glass Manufacturing Industry*, Vol. 58, Lyon, France, 1993).

Work within this project is oriented toward understanding the effects in rodents of inhaling aerosols of $^{239}PuO_2$ and Be metal. The purpose of this ongoing study is two-fold: (1) to investigate the potential interactions between Pu and Be in the production of lung tumors in rats, and (2) to explore the use of a transgenic murine system as a potential alternative to standard life-span carcinogenesis bioassays.

The study of potential carcinogenic interactions between Pu and Be in rats is being conducted in two phases. In Phase I, F344/N rats (ITRI bred; both male and female; 12 $\pm$ 1 wk old at exposure) were exposed once nose-only to respirable aerosols of $^{239}PuO_2$ and/or Be metal from 1987–1989. Groups of rats received $^{239}PuO_2$ followed immediately by exposure to Be metal, or the appropriate air control. Rats received one of two target initial lung burdens (ILBs) of $^{239}PuO_2$ (56 or 170 Bq), and/or one of three target ILBs of Be metal (50, 150, or 450 μg). Rats were either serially sacrificed or held for life-span observation; moribund rats were euthanized. At death, a complete necropsy was performed, and lungs, other selected tissues, and all lesions were fixed in formalin for histological analysis. Lungs of exposed rats were analyzed for Be and/or ^{239}Pu as appropriate. All Phase I rats were dead as of March 1991.

Significant findings from Phase I were that (1) exposure to Be significantly retarded the clearance of ^{239}Pu (1989–90 Annual Report, p. 125), (2) survival was decreased by Be metal in a dose-dependent manner (1990–91 Annual Report, p. 99), and (3) inhaled Be metal induced significant tumorigenicity in the lungs of rats (approximately 66% crude tumor incidence in the lowest dose group; 1993–94 Annual Report, p. 77). The observed incidences of Be metal-induced lung tumors were significantly higher than expected. To obtain dose-response information for lung carcinogenesis from lower lung burdens of Be metal, and because interactions between two carcinogens are best analyzed when lung tumor incidences from the individual agents are relatively low, Phase II of this study was initiated.

In Phase II of the carcinogenic interaction study, CDF®(F344)/CrlBR rats (Charles River Laboratories, Raleigh, NC) are being used. Compared to Phase I, we are using a lower range of ILBs of Be metal (sham-exposed controls and five target levels of Be; 0.3, 1, 3, 10, and 50 μg) and two ILBs for $^{239}PuO_2$ (sham-exposed controls and two target ILBs; 230 and 450 Bq). Two groups of rats receiving combined exposure were included within the experimental design; these animals received 230 Bq of $^{239}PuO_2$ combined with Be ILBs of either 1 or 10 μg. The 450 Bq ILB of $^{239}PuO_2$ alone was included to mimic the increased radiation dose caused by Be-induced reductions in lung ^{239}Pu clearance.

Phase-II exposures were conducted in 1993 and 1994. As of September 30, 1996, 10% of the rats remain alive, 30% have been sacrificed for Be and/or ^{239}Pu dosimetry and histologic lung changes, and

60% have died or been euthanized as moribund. Lung burdens of 1 and 10 μg Be were sufficient to decrease $^{239}PuO_2$ clearance compared to rats receiving $^{239}PuO_2$ alone (1994–95 Annual Report, p. 84).

Although histological evaluation of lung in this continuing study has not begun, a crude tumor prevalence in rats on study for 12 to 30 mo can be estimated by examining lungs at necropsy for evidence of masses and/or nodules (Fig. 1). Preliminary analysis indicates (1) the presence of a dose-response relationship for the individual agents alone, (2) an apparent no-effect level for lung carcinogenesis from Be metal in the 0.3 to 1 μg ILB range, (3) an incidence of masses and/or nodules in the 50 μg ILB group that is similar between the two phases of the study, and (4) the presence of a carcinogenic interaction between $^{239}PuO_2$ and Be metal that is approximately additive (for $^{239}PuO_2$ and the 10 μg ILB of Be metal) to superadditive (for $^{239}PuO_2$ and the 1 μg ILB of Be metal).

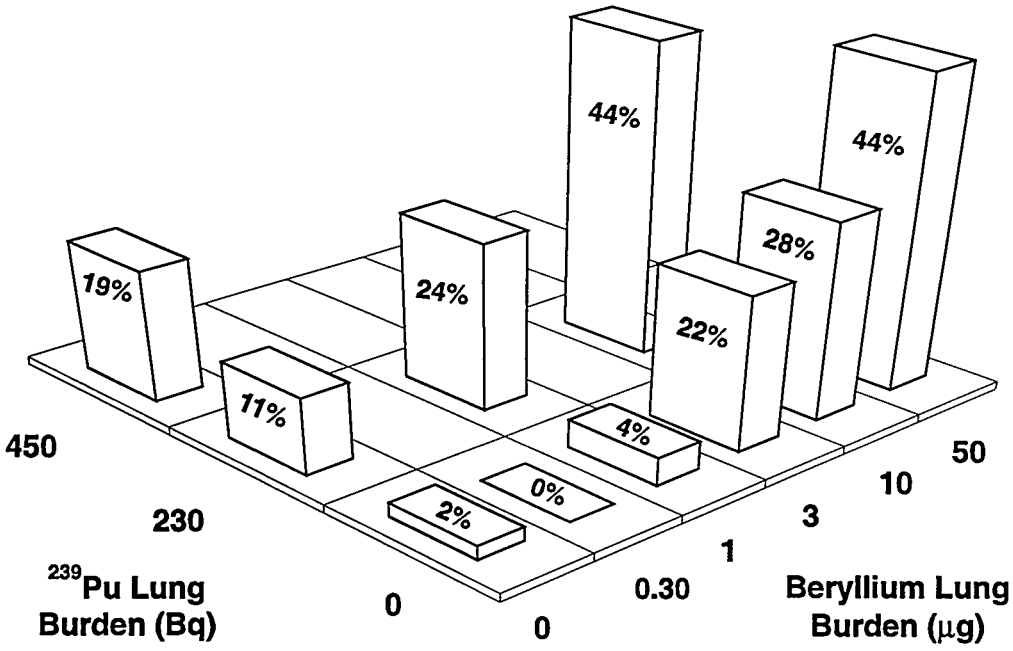

Figure 1. Bars indicate the crude estimated prevalence of lung tumors in rats between 12 and 30 mo following inhalation exposure to $^{239}PuO_2$, Be metal, or these materials in combination. Note that within this 3 × 6 matrix experimental design, only two possible combinations of Be and Pu are being examined (230 Bq Pu combined with either 1 or 10 μg Be).

As a possible alternative to the standard life-span carcinogenesis bioassay in rodents, we are studying mice heterozygous for a wild-type p53 allele. These animals are reported to have a low spontaneous tumor incidence and a shorter latency time for cancer induction (Harvey, M. *et al. Nature Genet. 5*: 225, 1993). To evaluate the utility of this model for inhaled inorganic carcinogens, we exposed groups of 30 (15 males, 15 females) heterozygous ($p53^{+/-}$) TSG-p53® mice (GenPharm International; 8–10 wk of age at exposure) to either $^{239}PuO_2$ or Be metal aerosols. Target ILBs for $^{239}PuO_2$ were 100 or 500 Bq, and for Be metal were 15 or 60 μg. Thirty $p53^{+/-}$ mice were sham-exposed as controls, and groups of wild-type mice ($p53^{+/+}$) were exposed to achieve ILBs of 500 Bq $^{239}PuO_2$ or 60 μg Be metal for comparative purposes.

Exposures were conducted in July 1995. In a portion of the mice (4–6 per group) sacrificed 6-mo post-exposure, few lung tumors were observed. At 12 mo post-exposure, survival was approximately 63% in the $p53^{+/-}$ mice and 82% in the $p53^{+/+}$ mice. Some lung tumors have been observed in the $p53^{+/-}$ mice (Table 1); however, the distribution does not indicate the presence of a dose-response relationship between exposure and lung tumorigenicity for either ^{239}Pu or Be metal. Thus, our preliminary conclusion is that the $p53^{+/-}$ mouse model does not have either a marked sensitivity or a decreased latent period for the induction of lung tumors caused by either ^{239}Pu or Be metal. Recent data, however, suggest that this $p53^{+/-}$ mouse strain might be a good model for lung tumors produced by benzo[a]pyrene and related compounds (Denissenko, M. *et al. Science 274*: 430, 1996).

Table 1

Estimated Lung Tumor Prevalence in Mice Receiving Inhalation Exposures to Either $^{239}PuO_2$ or Beryllium Metal

Type of Mouse	Exposure Material	Level	Est. Lung Tumor Prevalence[a]
$p53^{+/+}$ (wild-type)	Be metal	60 μg	1/13
	$^{239}PuO_2$	500 Bq	0/12
$p53^{+/-}$ (heterozygous)	Control		0/15
	Be metal	15 μg	0/15
		60 μg	3/22
	$^{239}PuO_2$	100 Bq	3/21
		500 Bq	0/16

[a]Males and females pooled. Incidences estimated from observations (presence of masses and/or nodules) at necropsy. Prevalence is across the time interval from 5 mo (when the first animal was euthanized as moribund) to 12 mo.

The studies described above are in progress. As additional data are obtained and analyzed, this work will define dose-response relationships for Be-induced lung cancer in rats, and will confirm the preliminary indications that (1) Be and Pu interact in an additive to slightly greater than additive manner in producing lung cancer, and (2) $p53^{+/-}$ transgenic mice do not constitute a useful, relative short-term model carcinogenesis bioassay system for inhaled materials such as Be and Pu.

(Research sponsored by the Assistant Secretary for Defense Programs, U.S. Department of Energy, under Contract No. DE-AC04-76EV01013).

ACUTE INHALATION TOXICITY OF CARBONYL SULFIDE

Janet M. Benson, Fletcher F. Hahn, Edward B. Barr, Alfred W. Nutt, and Alan R. Dahl*

Carbonyl sulfide (COS), a colorless gas, is a side product of industrial procedures such as coal hydrogenation and gasification. It is structurally related to and is a metabolite of carbon disulfide (CS_2). COS is metabolized in the body by carbonic anhydrase to hydrogen sulfide (H_2S), which is thought to be responsible for COS toxicity (Chengelis, C. P. P. and R. A. Neal. *Toxicol. Appl. Pharmacol. 55*: 198, 1980). No workplace or environmental standards have been set for exposure to COS.

Reported incidences of humans poisoned by COS have been rare. A construction worker was poisoned recently when a pipe containing ash-like corrosion deposits was cut with a welding torch (Martin, H. L. *et al.*, MS-94-0180, Westinghouse Savannah River Co., 1994). The victim breathed the gases released from the end of the pipe only briefly and subsequently became ill. He was transported to a local hospital where he responded immediately to the H_2S antidotes of amyl nitrite (inhalation) and sodium nitrite (intravenous). Post-incident investigation revealed that burning of the materials in the pipe under a reducing atmosphere generated COS, CS_2, and sulfur dioxide. It was initially estimated that the victim may have been exposed to over 1000 ppm of each gas. We hypothesize that the poisoning was a result of metabolism of the acutely inhaled COS to H_2S.

As a result of the above incident, we began an in-depth investigation of the acute toxicity of inhaled COS. We determined that the median lethal concentration for inhaled COS in rats is 590 ppm, indicating that the toxicity was somewhat less than that of H_2S. We also determined that a major target organ for COS toxicity is the brain, particularly the cerebellum (1994–1995 Annual Report, p. 151). One hypothesis we are pursuing is that the lesions observed in brain are secondary to inhibition of cardiac cytochrome oxidase, which results in cardiac insufficiency, in decreased blood flow to the brain, and relative anoxia at the periphery of cerebellar arteries.

The overall purpose of this study was to further our investigations on COS toxicity by focusing on high exposure concentrations that may be encountered during industrial accidents. Specific purposes included: (1) comparison of survival times, toxic effects, and histopathological changes in rats exposed to $>$ 1000 ppm compared to $<$ 1000 ppm; (2) determination of the synergistic or additive effects, if any, associated with co-exposure to CS_2; and (3) comparison of the effects of high levels of COS and H_2S, including the effectiveness of antidote administration.

Two groups of eight female rats, approximately 12 wk-old, (Harlan Sprague-Dawley, Indianapolis, IN) were exposed to 1000 or 5000 ppm COS. Two additional groups of eight female rats each were exposed to 2500 ppm CS_2 or a 1:1 mixture of COS:CS_2 (1250 ppm of each compound, for a total of 2500 ppm) to determine the antagonistic, additive, or synergistic effects of co-inhalation of CS_2 with COS. Five rats per exposure group were designated for histopathological evaluation, and three were surgically equipped with physiotel implants for monitoring of heart rate and core body temperature during the exposures. Two groups of six female rats each were exposed by inhalation to either 2500 ppm H_2S or COS to: (1) compare the effects of inhalation of high levels of H_2S and COS, (2) determine the effects of administration of an antidote for H_2S, sodium nitrite, and (3) compare the effects of COS and H_2S exposure on cardiac cytochrome oxidase activity. Three rats exposed to each compound were administered sodium nitrite (30 mg/kg in sterile saline) by intraperitoneal injection 30 min before exposure. Six rats served as sham controls. The hearts were removed from the rats immediately after death, and mitochondria were isolated for quantitation of cytochrome oxidase activity.

---

*Westinghouse Savannah River, Company, Aiken, South Carolina

Animal exposures were conducted in a 96-port nose-only chamber. The COS and H_2S were metered from the lecture bottles, and desired exposure concentrations were maintained through the use of a calibrated rotameter. The CS_2 vapors were generated using a heated J tube located within the glove box. The liquid CS_2 was supplied to the J tube using a syringe pump. Nitrogen was used to carry the vapors from the tube after which they were mixed with air and delivered to the exposure chamber. The concentrations of COS and CS_2 in the exposure chamber were quantitated using a Miran portable infrared analyzer (Foxboro Co, Foxboro, CT). The concentration of H_2S was quantitated using a photoionization detector (Rae Corporation, Sunnyvale, CA), calibrated using certified standards of H_2S. The concentrations of test gases/vapors in the exposure chamber were verified at least once per exposure by taking a "grab" sample in a gas sampling bottle and quantitating the concentration using gas chromatography. The gas chromatograph (Varian Model 3700 with a flame ionization detector) was calibrated using certified COS and H_2S standards on each exposure day. Known dilutions of neat CS_2 were used to calibrate the GC for CS_2 exposures.

Inhalation exposures were for a maximum of 4 h. Rats dying during the exposure were removed from the chamber for necropsy. Surviving rats were sacrificed immediately after the exposure, necropsied, and tissues taken for evaluation of histopathological changes.

No animals exposed to 1000–5000 ppm COS survived the targeted 4-h exposure; survival times were inversely related to COS exposure concentration (Table 1). Rats inhaling CS_2 survived the 4-h exposure period. Inhalation of CS_2 in combination with COS did not appear to affect the lethal effects of COS. Rats inhaling 2500 ppm COS survived significantly longer than those inhaling 2500 ppm H_2S (18 ± 6 min versus 43 ± 10 sec). Pre-administration of the antidote sodium nitrite increased survival time of COS and H_2S-exposed rats to 24 ± 1 min and 6 ± 3 min, respectively.

Table 1

Relationship between COS Exposure Concentration, Survival Time, and Concentration x Time Product

COS Concentration (ppm)	Survival Time (min)	Concentration × Time × 1000
590	240	142
625	224	140
700	197	138
750	208	156
1000	150	300
1000[a]	97	194
1250[a,b]	47	59
2500[a]	18	45
5000[a]	3	30

[a]Only female rats were used in these experiments.
[b]COS was inhaled in combination with 1250 ppm CS_2.

Rats inhaling COS experienced an initial period of agitation during which respiratory rate was increased. This was followed by a period during which the rats became increasingly less active, their respiration and heart rate slowed, and core body temperature decreased. The time of onset of agitation decreased with increasing COS exposure concentration. This pattern of agitation followed by sedation

was not observed in the H_2S or CS_2-exposed rats. An example of the effects of COS inhalation on heart rate is shown in Figure 1.

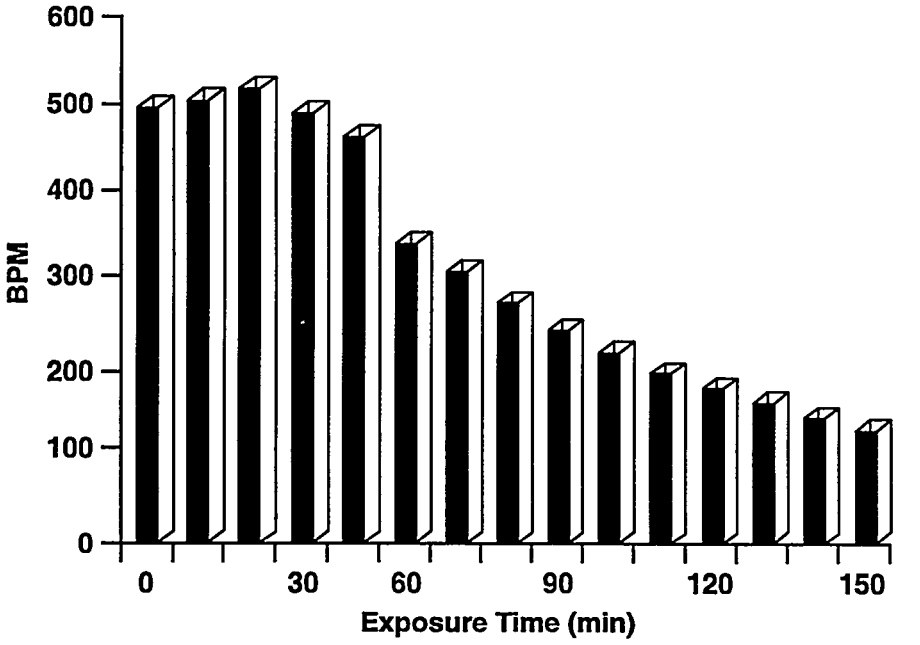

Figure 1. Progressive decrease in heart rate observed among a rat inhaling 1000 ppm COS.

Cardiac cytochrome oxidase activity in rats dying following inhalation of 2500 ppm H_2S or COS was not different from activity in hearts from control rats. No histopathological changes were identified in brains of the exposed rats.

The results of this study provide useful information regarding the toxic effects resulting from acute inhalation of high concentrations of COS. First, it does not appear that saturation of COS transport mechanism(s) or metabolism occurs at high COS exposure concentrations because the survival time continues to decrease rather than plateau with increasing COS concentration. CS_2 inhaled in combination with 1250 ppm COS does not significantly shorten survival time nor enhance the toxic effects (depression of heart rate, body temperature, or histopathological changes) resulting from inhalation of COS alone. This is consistent with the fact that toxic effects of CS_2 generally are associated with prolonged low-level exposures rather than acute, high-level exposures. Useful information regarding possible interactions between these COS and CS_2 are more likely to be identified using repeated low-level exposures. Longer survival times seen in rats exposed to 2500 ppm COS over survival time in rats inhaling 2500 ppm H_2S suggest that metabolism of COS to H_2S may be required for lethality or that COS may be acting directly but may be a less potent toxin than H_2S. Increased survival following administration of sodium nitrite in both COS- and H_2S-exposed rats strongly suggest they act by similar mechanisms. Lack of histopathological changes in any of the rats exposed to high levels of COS or H_2S suggests that rapid death may be due to direct inhibition of the respiratory center, while lesions observed in rats surviving lower concentrations of COS are produced by a different mechanism. Further studies are needed to determine the mechanisms of COS-induced toxicity and clarify whether COS acts directly and/or through metabolism to H_2S.

(Research sponsored by the Westinghouse Savannah River Corporation, U.S. Department of Energy, under Contract No. DE-AC04-76EV01013).

ASSESSMENT OF SPATIAL LEARNING IN DOGS IN THE MORRIS WATER TASK

Bruce A. Muggenburg, Gina E. Adam, Rob J. Sutherland*, Carl W. Cotman**, and William Milgram****

Alzheimer's disease is a debilitating disease characterized by a progressive loss of memory and mental functions that leads to severely impairing dementia. This dementia is attributed to characteristic changes in the brain that do not occur to the same extent with other forms of dementia (Sinto, L. F. M. *et al. Science 266*: 1051, 1994). These changes include the development of neuritic plaques, neurofibrillary tangles, and substantial loss of neurons. Little is known about the causes of this pathology, and even less is known about how, if at all, the lesions affect behavior.

The relationship between cognitive dysfunction and neuropathology is not well understood due to the lack of an appropriate animal model. To date, many animal models have been proposed, yet only a few animal species are known to naturally develop beta-amyloid protein deposits similar to those seen in the brains of patients with dementia. Selkoe, D. *et al.* (*Science 235*: 873, 1987) reported that the brains of aged nonhuman primates, dogs, and a polar bear displayed the characteristic plaques and suggested that due to its shorter life span, the dog might provide a suitable model for studying dementia. In addition to noting the presence of plaques in canine brain tissue, Cummings, B. *et al.* (*Neurobiol. Aging 14*: 547, 1993) observed that these plaques were diffuse and may be an earlier stage of plaque development. These plaques are often seen in and around the hippocampus. Canine brain tissue appears to be free of neurofibrillary tangles (Cummings *et al.*, 1993). These findings suggest that the canine model may be appropriate for studying the course of plaque development.

Amyloid plaque development in the dog appears to increase with age, with significant numbers of plaques appearing after the dog has reached middle age. Thus, dogs of a range of ages could be used to assess cognitive function on a variety of tasks to examine the relationship between dysfunction and diffuse plaque development. Cummings *et al.* (unpublished data) have obtained preliminary evidence of a correlation between plaque density and what they have termed a *global index* of cognitive dysfunction.

The ITRI dog colony is a unique resource in which to study the development of brain lesions and changes in cognitive function in Beagles. All of the dogs were born into the colony and were raised with similar environment and nutrition. The dogs enrolled into this study were from 3 to 15 y old. This range of ages provided the opportunity to compare cognitive function and brain lesions and relate any changes found to age.

A part of the effort to characterize the pattern of behavioral deficits in aged dogs was the development of a variant of the Morris water task, a spatial task which has been repeatedly shown to rely on normal hippocampal function. Previous work with aged rats has shown impaired performance in some spatial memory tasks, especially hippocampal-dependent tasks. We placed two identical cue configurations in a large swimming pool. Only one of these cue configurations marked the location of an escape platform which required that the dogs learn the location of the platform by associating it with cues outside of the pool. This hidden platform and cue set remained in the same location for every trial. The other cue set was placed in different locations in the pool and was never a reliable indicator of the hidden

*Department of Psychology, University of New Mexico, Albuquerque, New Mexico
**Institute for Brain Aging and Dementia, University of California, Irvine, California
***Scarborough College, University of Toronto, Toronto, Canada

platform location. By testing dogs ranging in ages from very young to very old, we hypothesized that performance on the task would decrease with increasing age.

Eighteen dogs (3 to 15 y) participated in this study (Table 1). The 24-ft diameter round, outdoor swimming pool had a number of poles and distant building around it that provided cues. There were two cues inside the pool: two black plastic barrels 24 inches tall and 15 inches in diameter. One cue remained in the same location for all trials, and the other cue was moved to different locations in the pool every day. Each dog received two trials per day. Four different release points were used with two different points used randomly each day. After the dog was released in the pool, it had 60 sec to find the platform. If it did not, a person got into the pool and placed the dog on the platform where it remained for 10 sec. Dogs that found the platform were also left on the platform for 10 sec. A meatball reward and verbal praise were given on the platform to all dogs. Each dog was tested on nonconsecutive days. On the final day each dog was given one standard trial (two cue sets, one platform), one trial with both cues missing (the platform was still in the pool in the hidden location), and a final trial with the cues and platform removed.

Table 1

Age and Sex of Dogs in the Three Age Categories

Young			Middle			Old		
Tattoo	Age (y)	Sex	Tattoo	Age (y)	Sex	Tattoo	Age (y)	Sex
1565S	6.3	F	1467S	11.0	F	B1994	15.4	M
1567S	6.0	F	1498U	9.3	F	1338U	15.3	F
1584A	5.2	M	1474B	10.5	M	1408C	13.4	M
1584C	5.2	M	1507B	8.7	M	1409T	13.3	F
1588A	4.5	M	1509T	8.6	F	1438U	12.3	F
1588S	4.5	F	1511U	8.5	F			
			1538U	7.4	M			

We used three dependent measurements to analyze this task. First, for each trial, we recorded the amount of time to find the platform. Dogs were given a score of 60 sec if they did not find the platform. Second, for the trial with the cue sets removed from the pool, our dependent measure was the time taken to find the platform. For the final trial with no cue sets or platform in the pool, the dogs' swim paths were recorded for 60 sec, and the proportion of swim path spent in the correct quadrant of the pool was calculated. Of the 17 dogs tested, one showed striking impairment on this task. This dog found the platform only 3 times out the 15 trials when both cue sets were in the pool. In fact, he rarely oriented to the cues but swam around the periphery of the pool. In rats, this swimming pattern has been observed following damage to the striatum (McDonald, R. and N. White. *Behav. Neural Biol. 61*: 260, 1994). Little is known about the incidence of plaques in and around the striatum of dogs.

Figure 1 shows the average proportion of swim paths in the correct quadrant. For this analysis, the dogs were divided into three age groups: young, 3 to 6 y; middle aged, 6.5 to 11 y; and old, 12+ y (Table 1). When examining the proportion of swim path in the quadrant with the platform for each age group, an interesting pattern emerged. The proportion was decreased in the middle-aged group but not in the very old dogs. The old dogs swam an average of about 50% in the correct quadrant, similar to the young dogs.

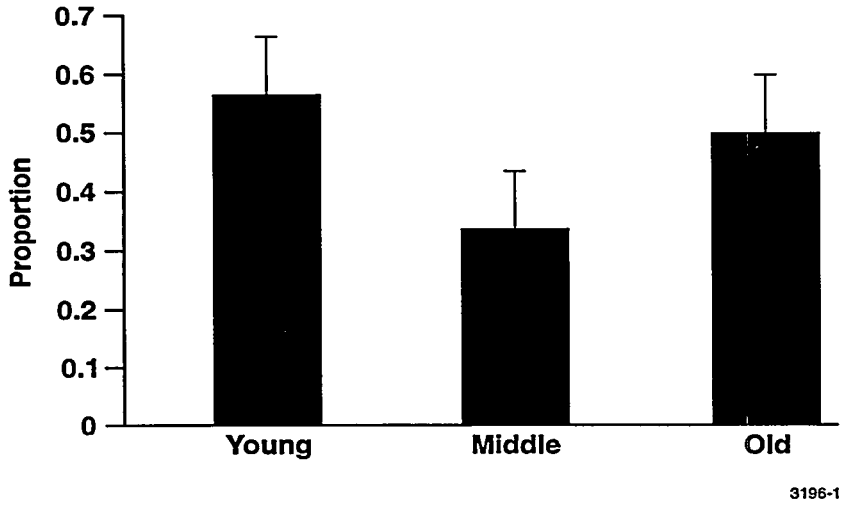

Figure 1. The dogs were grouped by age into young (3 to 6 y), middle (6.5 to 11 y), and old (12+ y). The bars for each age show the proportion of swim paths in the quadrant with the platform. Error bars represent standard error.

The results of this study showed that the Morris water task is a useful test of place learning in dogs. Within a small number of trials, dogs of all ages displayed that they had learned the location of the platform. Age was not significantly correlated with performance on this task, although the data showed an interesting trend. Performance tended to decrease with age, but the performance of the oldest dogs was much better than expected. Thus, performance of dogs in the middle of the age profile (7 to 11 y) was the worst. It is important to note that the five dogs in the oldest group were 12 y or older. These dogs may represent a subpopulation of animals that is less susceptible to age-related cognitive deficits. Because previous work indicated a correlation between plaque density and cognitive dysfunction, we would predict that these aged dogs have lower plaque densities than the middle-aged dogs.

This hypothesis will be tested with magnetic resonance images and examination of the brain tissues after sacrifice. Once these measures are obtained, further correlation and regression analyses will be done to relate any observed pathology with the results of the Morris water task and with other tests of cognitive function. The immediate goal of this study was to demonstrate that the dog is a useful model of human brain aging.

(Research sponsored by the National Institute for Aging, Grant AG 12694 to the University of California, Irvine and ITRI, with the U.S. Department of Energy, under Contract DE-AC04-76EV01013.)

ACUTE TOXICITY OF BUTADIENE DIEPOXIDE IN RATS AND MICE

Rogene F. Henderson, Janet M. Benson, Fletcher F. Hahn,
Edward B. Barr, William E. Bechtold, David G. Burt, and Alan R. Dahl

Butadiene diepoxide (BDO_2), a metabolite of 1,3-butadiene (BD), and a potent mutagen, is suspected to be a proximate carcinogen in the multisite tumorigenesis observed in $B6C3F_1$ mice exposed to BD. BD is only a weak carcinogen in Sprague-Dawley rats; a possible reason for the species differences in response to BD is the fact that rats metabolize very little of the BD to BDO_2, while mice readily metabolize BD to BDO_2. The current study was designed to determine if rats would get multisite tumors if exposed to similar amounts of BDO_2 as mice. The study consists of exposure of mice and rats for 6 wk by inhalation to BDO_2, observation of any acute toxicity at the end of the exposure, and retention of the remainder of the animals for observation of tumor development. The route of exposure to BDO_2 chosen was inhalation because the lung is the most sensitive target organ for carcinogenesis in the mouse. The current report is of the acute toxicity observed in the rats and mice at the end of the 6-wk exposure.

Fifty-six female $B6C3F_1$ mice and 56 female Sprague-Dawley rats, 11 wk of age, were exposed 5 d/wk for 6 wk to 0, 2.5, or 5 ppm BDO_2 in Hazleton 2000 chambers. Chamber atmospheres were monitored for stability by a Miran IR spectrometer and were quantitated by GC analysis of impinger samples. Overall average exposure concentrations were 2.48 ± 0.42 and 5.07 ± 0.65 ppm BDO_2 for the low and high exposure chambers, respectively.

Eight animals per group were sacrificed at the end of the exposure and examined for acute toxicity. Rats exposed to 5 ppm BDO_2 for 6 wk had a 10% decrease in body weight compared to controls; there was no effect on body weight in the low exposure group. Mice exposed to 2.5 and 5.0 ppm had an 8% and 28% decrease in body weight, respectively. Complete blood cell counts indicated no effects in rats; mice had a 60% decrease in peripheral, circulating lymphocytes at the high dose. During the last exposure week, most mice in the high exposure group showed signs of labored breathing, which disappeared within a month after the exposure. Four mice died during the last week of exposure.

In both rats and mice exposed to the high concentration, the only significant lesions were concentrated around the main airflow pathway through the nose. Necrosis, inflammation, and squamous metaplasia of the nasal mucosa were present as well as atrophy of the turbinate bones in the nose. High-dose rats also had a focal acute inflammation with ulceration of the mucosa lining the nasopharyngeal duct. Lesions were less severe in the low exposure groups for both species.

In contrast to the mice, the rats held for long-term observation developed labored breathing post exposure and 13 died (12 in high- and 1 in low-dose group) within 6 mo after the end of the exposure. Cause of death was occlusion of the nasopharyngeal duct by squamous metaplasia, leading to suffocation.

Previous studies indicate that the dose per kg received by mice is about twice that in rats under the inhalation exposure conditions used. Despite this, higher mortality was observed in rats than in mice, due to persistent squamous metaplasia in the rats.

The acute toxicity of BDO_2 to the upper respiratory tract is not surprising, because the compound is known to be highly reactive as well as water-soluble. Water-soluble, reactive vapors have high deposition in the upper respiratory tract. The significance of the findings for this study is that the amount of BDO_2 that reaches the lung for distribution via blood to the rest of the body is limited in inhalation exposures by the high deposition in the upper respiratory tract. The exposure concentrations used appear to be the

maximal ones that can be used for inhalation studies. Prior studies indicate that some of the BDO_2 does reach the lung and the blood. It remains to be seen if the rest of the animals on this study develop tumors.

(Research sponsored by the Health Effects Institute under Funds-In-Agreement No. DE-FI04-95AL86988 with the U. S. Department of Energy, Under Contract No. DE-AC04-76EV01013.)

DISSOLUTION AND EARLY EFFECTS OF IMPLANTED DEPLETED URANIUM FOILS IN RATS AND MICE: A PILOT STUDY

David L. Lundgren, Fletcher F. Hahn, Raymond A. Guilmette, and Mark D. Hoover

Several soldiers who participated in Operation Desert Storm were wounded while in Bradley armored personnel carriers that were hit directly by armor-penetrating projectiles containing depleted uranium (DU) alloyed with 0.75% titanium [DU(Ti)]. Bioassay measurements in two of these soldiers confirmed elevated levels of uranium (U) in the urine at least 1 y after exposure. The presence of shrapnel fragments was confirmed radiographically in at least one subject, and documented that measurable U is present *in vivo*. These data indicate that humans are being chronically exposed to U in insoluble forms as DU(Ti) fragments and soluble forms as dissolving U.

Quantitation of the long-term risk from exposure to U, particularly in the form of embedded fragments, is complex and involves chemical and radiological components, as well as possible foreign-body effects. Because of the unique features of these exposures, it is not currently possible to reasonably predict carcinogenic risks to these soldiers from their U-bearing wounds. Such predictions are necessary, however, to guide the medical management of soldiers with U-bearing wounds.

To assess more confidently the carcinogenic risks associated with long-term exposure to DU-containing shrapnel in wounds, we will conduct studies in rodents to determine the carcinogenicity of radioactive DU(Ti) fragments in tissues relative to nonradioactive metallic foreign-body fragments. Once a relative carcinogenicity factor is determined in rodent model systems, it can be used to compare the carcinogenicity of DU(Ti) with the known carcinogenicity of metal fragments in humans. Information from this pilot study will be used in designing the carcinogenesis study.

One rodent test system that has been considered for the carcinogenesis study is the initiation and promotion model of induction of foreign body tumors in the subcutis of rats or mice. The development of sarcomas near the site of subcutaneous implantation of metal foils, glass slides, or polymer films is well characterized (Brand, K. G. *et al. Cancer Res. 35*: 279, 1975). A number of physical characteristics of the implanted materials are important in foreign body carcinogenesis in rodents (Brand *et al.*, 1975). Smooth surfaces with a relatively large area appear to be essential for a foreign body to be carcinogenic. Therefore, if the surface of the DU(Ti) foil to be used is altered when in the subcutis or if the foils are reduced in size through dissolution, this approach would not be appropriate for carcinogenesis studies on DU.

The purpose of this work was to conduct a confirmatory study in rats and mice to determine the following: (1) the *in vivo* solubility of DU during the first 60 d after its implantation in rats and mice, (2) any changes in the surface characteristics of the DU foil after implantation, and (3) histological responses of rats and mice to the implanted DU during this time. This information is critical to planning relative carcinogenesis studies in these rodents.

Two types of foils containing DU were used. One contained only DU, while the other was the DU alloyed with 0.75% Ti. DU is a byproduct of the uranium enrichment process for nuclear power and nuclear weapons and typically contains 0.001% ^{234}U and 0.2% ^{235}U by mass (Loewenstein, P. In *Metals Handbook. Properties and Selection: Stainless Steels. Tool Materials and Special Purpose Metals.* Vol. 3 [D. Benjamin, ed.], 9th Edition, American Society for Metals, Metals Park, OH, p. 773, 1980). The specific activity of DU is 0.4 μCi (15 kBq) g^{-1}, whereas the specific activity of natural U is 0.7 μCi (26 kBq) g^{-1}. The difference is mainly due to the depletion of ^{234}U in the DU. The DU and DU(Ti) foils (0.18 mm × 15 mm × 22 mm) were obtained from Manufacturing Sciences Corporation (Oak Ridge, TN).

Tantalum (Ta) foils (Goodfellow Corp., Berwyn, PA) of similar size were used as the control implant in this study.

The experimental design for the *in vitro* portion of this study is summarized in Table 1. Twenty-eight 12-wk-old male F344 rats (Charles River Laboratories, Wilmington, MA) and 28 12-wk-old male CBA/J mice (Harlan Sprague-Dawley) were used (Table 1). Animals (three or four per cage) were housed in filter-topped polycarbonate cages (rats: 20 cm high × 25 cm wide × 48 cm long and mice: 16 cm high × 21 cm wide × 27 cm long) on hardwood chip bedding or in metabolism cages. Animal rooms were maintained at 20–22°C with a 40–60% relative humidity on a uniform 12-h light cycle. Food (Lab-Blox, Allied Mills, Chicago, IL) and water were available *ad libitum*.

Table 1

Experimental Design for the Study of Dissolution and Excretion of Uranium and Early Biological Effects of Subcutaneously Implanted DU, DU(Ti), and Ta Metal Foils in Male Rats and Mice

	Foil Type and Number Sacrificed at 30 d			Foil Type and Number Sacrificed at 60 d[a]			
Rodent	DU	DU(Ti)	Ta	DU	DU(Ti)	Ta	Total
F344 Rats[b]	5	5	4	5	5	4	28
CBA/J Mice[b]	5	5	4	5	5	4	28
Total	10	10	8	10	10	8	56

[a]Twenty-four hour urine samples were collected from three rats and three mice on days –2, –1, 1, 2, 3, 4, 7, 14, 21, 28, 35, 42, 49, 56, and 60 after DU and DU(Ti) foils were implanted and on days –2, 7, 14, 28, and 35 after Ta foils were implanted.
[b]Deaths of animals prior to the scheduled sacrifice time are discussed in the text.

Metal foils (0.18 mm × 15 mm × 22 mm) were weighed (mean foil weights ± SD; DU 8.4 ± 0.3 g, DU(Ti) 7.4 ± 0.3 g, and Ta 5.6 ± 0.1 g) and surgically inserted in the subcutis of the upper part of the back region of rats and mice while under inhalation anesthesia (halothane). A sterile field was prepared over the anterior dorsum, and a surgical incision about 2.5 cm long in the skin was made to place sterile foils into the subcutis. The surgical site was closed with surgical wound clips which were removed about 7 d after surgery. Twenty-four-hour urine samples were collected from rats and mice housed in metabolism cages.

Rats and mice were sacrificed (Table 1) using an overdose of pentobarbital given by intraperitoneal injection, and necropsied. The tissue capsules around the metal foils were removed, along with the heart-lung block, liver, kidney, femur, urinary bladder, epididymis, testes, and lesions, and were fixed with 10% neutral buffered formalin. Tissues were sectioned at 5 μm, and sections were stained with hematoxylin and eosin. The left kidney, tissue capsule, and lesions were examined histopathologically.

The excretion of U (μg) per each day's collection was measured for individual rats and is summarized in Figure 1. The urinary excretion of U appeared to increase throughout the study in rats with implanted DU foils. In contrast, the excretion of U by rats with implanted DU(Ti) increased rapidly until about 15–20 d after which the daily excretion seemed relatively constant. Similar excretion pattern was seen in mice (data not presented), except that the rate of excretion of U in the mice implanted with

DU(Ti) was not constant after 15–20 d as in the rats, but continued to increase. The dissolution of U in the mice with the implanted DU(Ti) resulted in the accumulation of toxic levels in the kidneys resulting in the death of all but one mouse within 30 d compared with the death of only one mouse with implanted DU. In contrast, only one rat with a DU(Ti) implant died, but not until day 33. The DU(Ti) foils were more soluble in both rodents than the DU foils in either species. The translocation of U to the kidney and skeleton also indicated that the DU(Ti) foils were more soluble that the DU foils.

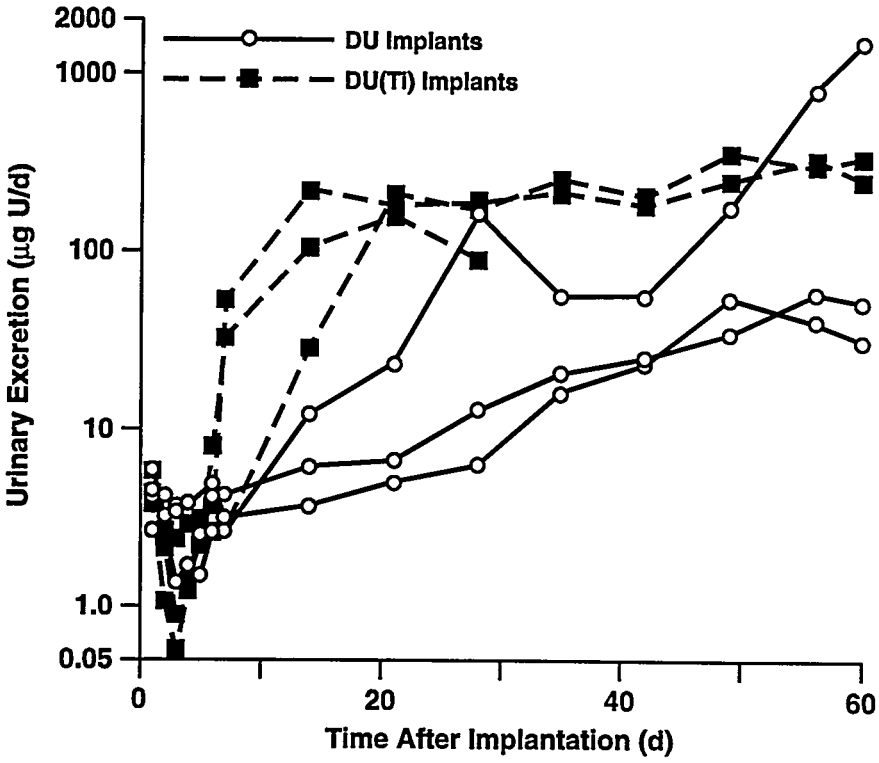

Figure 1. Urinary excretion of uranium in $\mu g\ day^{-1}$ in individual rats with DU or DU(Ti) implants.

Thirty days after implantation in the subcutis, the physical appearance of both the DU and the DU(Ti) foils were markedly altered. The surfaces were roughened and friable, with flaking of small black particles from the foils. The flaked particles blackened the lining of the connective tissue capsule surrounding the foils. Histopathological evaluations of the kidneys and tissues surrounding the foils are in progress.

This work indicates that DU and DU(Ti) foils dissolve more rapidly in mice and rats than expected and that DU(Ti) dissolves more rapidly than DU. With these results in both species it is evident that the subcutaneous foreign-body carcinogenesis system described by Brand *et al.* (1975) cannot be applied to a study of the carcinogenesis of implanted foils containing DU. Therefore, a bioassay carcinogenesis study in rats will involve primarily intramuscular implants of DU(Ti) in the form of small pellets (1.0 mm in diameter × 2 mm in length) and fragments (2.5 mm × 2.5 mm × 1.5 mm and 5.0 mm × 5.0 mm × 1.5 mm) in dimensions similar in size to some of the wide range of fragments seen in wounded veterans. Thorotrast® will be used as a positive control material, and surgical stainless steel (type 316LVM) pellets will be used as the negative control.

(Research sponsored by the U.S. Medical Research Development Command under MIPR No. KVFM5529 with the U.S. Department of Energy, under Contract No. DE-AC04-76EV01013.)

THE TOXICITY OF CERIUM-144 INHALED IN AN INSOLUBLE FORM BY DOGS

Fletcher F. Hahn, Bruce B. Boecker, Bruce A. Muggenburg, and William C. Griffith

Understanding the toxicity of cerium-144 (^{144}Ce) is important in assessing the health risks associated with uranium-fueled nuclear reactors because of cerium's prominence as a fission product in irradiated fuel elements after sustained reactor operation. An accidental release of ^{144}Ce into the environment and subsequent inhalation exposure of people are possible consequences. Inhaled, insoluble forms of ^{144}Ce would be retained in the body for some time and could result in early or late health effects, depending on the absorbed doses received by the target organs. To better understand the toxicity of ^{144}Ce, we studied the effects of ^{144}Ce in fused aluminosilicate particles inhaled by Beagle dogs. The purpose of the study was to document the health effects of inhaled ^{144}Ce and relate the effects to radiation dose.

The study was conducted in 126 Beagle dogs from the ITRI colony, 66 males and 60 females, 12–14 mo old. Dogs were exposed, nose only, to aerosols of ^{144}Ce incorporated into heat-fused aluminosilicate particles or to stable cerium in fused aluminosilicate particles. Different combinations of exposure time (from 2–48 min) and aerosol concentration (from 0.008–320 μCi/L air) were used to achieve a range of initial lung burdens (ILBs) of radioactivity among the exposed dogs. The radioactivity in each dog was measured by a whole-body counter at different intervals after exposure to determine the initial content of the radionuclide in the lung and its subsequent whole-body retention as a function of time after exposure. The ILB was considered that portion of the body burden associated with the ^{144}Ce in the deep lung. Radiation doses to lung were calculated for each dog based on the pulmonary content of ^{144}Ce as a function of time.

The concentration of ^{144}Ce in the lung decreased with time after exposure because of radionuclide decay and the clearance of ^{144}Ce from the lung both by particle-clearance processes and by dissolution *in vivo*. The distribution of ^{144}Ce in other organs and tissues was determined from a separate group of similarly exposed dogs that were sacrificed at predetermined times. The concentration in the tracheobronchial lymph nodes (TBLNs) steadily increased as particles were translocated from the lung to these nodes. The concentration of ^{144}Ce in the TBLNs exceeded that in the lung at about 100 d after exposure and remained higher for the remainder of the life span. In long-term survivors, the calculated doses to the TBLNs were about 6–7 times those of the lung (Hahn, F. F. *et al.* In *Low Dose Radiation: Biological Bases of Risk Assessment* [K. F. Baverstock and J. W. Stather, eds.], Taylor and Francis, London, p. 216, 1989).

These dogs were observed for health effects for their entire life span. Routine clinical examinations were made yearly and at any indications of illness. At death or euthanasia, dogs were given detailed post-mortem examinations that included histopathological examination of all organ systems. The primary cause of death, major contributing diseases, and incidental lesions were determined by review of all clinical and pathology data.

The experimental design and summary of dosimetry and survival times for groups of exposed dogs are shown in Table 1. The five highest exposure groups had significantly reduced survival times. The median ILBs for these groups were 0.28 MBq/kg or greater, and the median lung doses were 110 Gy or greater. The primary cause of death could be related to the radiation dose to the lung (Table 2). In the highest two exposure groups (8 and 9), most of the dogs died of radiation pneumonitis or pulmonary vascular disease before 2 y after exposure. These early deaths were related to high radiation doses to the lung (280 Gy or greater). In exposure groups 7 and 8, 60% of the dogs that

Table 1

Experimental Design and Summary of Dosimetry and Survival Times for Dogs that Inhaled ^{144}Ce Fused Aluminosilicate Particles and Associated Controls[a] (Median and Range)

Exposure Level[a]	Number of Dogs M	Number of Dogs F	Number Surviving 2 y	ILB (MBq/kg)	Lung Initial Dose[b] Rates (Gy/day)	Lung Dose to Death[b] (Gy)	Survival Times (DPE)[c]
9	4	2	0	6.8 (3.5–7.8)	10 (5.5–13)	1,300 (700–1400)	177* (143–189)
8	6	6	2	2.0 (1.5–2.5)	3.1 (2.3–3.8)	520 (280–610)	274* (185–790)
7	8	6	13	1.0 (0.85–1.4)	1.7 (1.3–2.2)	330 (240–460)	1240* (193–3001)
6	8	7	15	0.56 (0.44–0.70)	0.89 (0.68–1.2)	190 (150–260)	2501* (1749–3961)
5	8	8	16	0.28 (0.18–0.41)	0.45 (0.30–0.68)	110 (60–150)	3610* (1527–5746)
4	5	5	10	0.057 (0.04–0.089)	0.088 (0.066–0.14)	23 (15–32)	4126 (2479–5735)
3	5	6	11	0.016 (0.0093–0.026)	0.024 (0.014–0.041	5.5 (3.6–10)	4679 (2682–5547)
2	5	7	12	0.0030 (0.0019–0.0067)	0.0048 (0.0030–0.011)	1.2 (0.74–3.1)	4429 (3366–6137)
1	9	6	15	0.00067 (0.000088–0.0016)	0.0011 (0.00014–0.0026)	0.26 (0.035–0.64)	5380 (2612–6205)
Control	8	7	15	0	0	0	4652 (4151–5454)

[a]Dogs were regrouped into exposure levels based on initial lung burden (ILB) so that groups were not overlapping.
[b]Radiation doses and dose rates calculated using mass of the whole lung.
[c]DPE = Days post exposure.
*Significantly different from mean of control survival ($p = < 0.001$) using t test.

Table 2

Primary Cause of Death in Dogs that Inhaled ^{144}Ce Fused Aluminosilicate Particles and in Associated Controls

Exposure Level	Number of Dogs	Number Surviving 2 y	Radiation Pneumonitis/ Pulmonary Vasc. Disease	Other Respiratory Disease	Other Non-neoplastic Disease	Neoplasia			
						Lung	Tracheo-bronchial Lymph Node	Heart	Other[a]
9	6	0	6	0	0	0	0	0	0
8	12	2	10	0	0	2	0	0	0
7	14	13	3	0	1	7	1	1	1
6	15	15	0	2	2	1	7	1	1
5	16	16	0	2	3	2	7	1	1
4	10	10	0	0	5	1	1	0	3
3	11	11	0	1	3	0	0	0	7
2	12	12	0	2	5	0	0	0	5
1	15	15	0	1	9	1	0	0	4
0	15	15	0	0	9	0	0	0	6

[a]Other includes neoplasia (in exposed) of mammary glands (5), brain (3), spleen (3), bladder (2), lymphosarcoma (2), liver (1), kidney (1), prostate (1), nasal (1), soft tissue (1), thyroid (1) and tonsil (1). Neoplasia in controls includes brain (1), lymphosarcoma (1), mammary gland (1), spleen (1), stomach (1) and tonsil (1).

survived past 2 y after exposure died of a lung neoplasm. Many of these lung neoplasms were hemangiosarcomas, unusual neoplasms of the lung that appear to be related to the high radiation doses to the lung in these groups, > 240 Gy. In the two lower exposure groups (5 and 6), over 45% of the dogs died of neoplasms primary in the tracheobronchial lymph nodes. These neoplasms were also hemangiosarcomas, a type of primary neoplasm not reported in the lymph nodes of unexposed dogs. The next lower exposure group, group 4, did not have a significantly reduced survival time. However, one dog each had a lung and a tracheobronchial neoplasm, an indication that a radiation effect was expressed at this exposure level. The lower three exposure groups, (< 0.026 MBq/kg ILB and < 10 Gy to the lung) did not have survival times significantly less than that of controls and did not have lesions different from controls.

The neoplasms of lung and tracheobronchial lymph nodes were considered to be induced by radiation because of their relation to high radiation doses and the fact that many of them were hemangiosarcomas, unusual spontaneous primary neoplasms of the lung or lymph nodes. In addition, hemangiosarcomas of the heart were the cause of death in three dogs in the high exposure groups. Although hemangiosarcomas are not unusual heart neoplasms in dogs, the site within the heart was unusual, at the base of the heart adjacent to the tracheobronchial lymph nodes. The high concentration of ^{144}Ce in the TBLNs served as a focal source for irradiation of the heart. Based on this information, we considered the lung, tracheobronchial lymph nodes, and heart to be target organs for inhaled, insoluble ^{144}Ce in the dog. The results of this study show that pulmonary irradiation from ^{144}Ce will result in neoplasms of the lung, but that the radiation doses required are rather high, >10 Gy. Neoplasms of the TBLNs also appear to be significant at exposure levels lower than those for lung neoplasms because of the concentration and retention of insoluble ^{144}Ce particles in the nodes. These findings indicate that, for radiation protection purposes, the TBLN may need to be considered with separate risk factors and not combined with risk factors of the lung, as is the approach used in current U.S. radiation protection standards (10 CRF 20 and 10 CRF 835).

(Research supported by Office of Health and Environmental Research, U.S. Department of Energy, under contract DE-AC04-76EV01013.)

EFFECTS OF ALPHA-PARTICLE DOSE NONHOMOGENEITY FROM INHALED MONODISPERSE PLUTONIUM-239 DIOXIDE AEROSOLS IN THE LUNGS OF F344 RATS

David L. Lundgren, Raymond A. Guilmette, William C. Griffith, Fletcher F. Hahn, Joseph H. Diel, Bruce A. Muggenburg, and Bruce B. Boecker

Plutonium-239 is a by-product of nuclear reactors used for energy generation and has uses in civilian as well as military applications. Relatively large quantities of plutonium have been handled over the past several decades during which time humans have been exposed by inhalation to aerosols containing this radionuclide (Voelz, G. L. and J. N. P. Lawrence. *Health Phys. 61*: 181, 1991). Although the potential for additional human exposure to ^{239}Pu continues, the potential human health effects of such exposures are not well understood (Wiggs, L. D. *et al. Health Phys. 67:* 577, 1994). Lacking information on the responses of humans to inhaled ^{239}Pu, studies of the toxicity of inhaled $^{239}PuO_2$ in laboratory animals have been used to aid in prediction of the potential effects of accidentally inhaled ^{239}Pu (Bair, W. J. *et al. Radiat. Prot. Dosim. 26*: 125, 1989; BEIR V. National Academy of Science, National Academy Press, Washington, DC, 1990; Volez, G. L. In *Occupational Medicine: State of the Art Reviews 6*: 681, 1991). An important question not addressed by most of the previous work noted above has been the relative effectiveness of uniform versus nonuniform alpha-particle dose to the lung, what has been referred to by some as the "hot particle" effect (Ad Hoc Committee on Hot Particles, *Health Effects of Alpha-Emitting Particles in the Respiratory Tract* [R. E. Albert, ed.], National Academy of Sciences, Washington, DC, p. 1, 1976).

Some studies of the relative effectiveness of uniform compared with nonuniform irradiation of the lung have been conducted. Preliminary results from a study in progress in dogs that inhaled one of three different sizes of monodisperse $^{239}PuO_2$ particles indicated that relatively uniform alpha-particle irradiation of the lung had the same relative risk of causing lung cancer as did less uniform radiation (Muggenburg, B. A. *et al.* In *Low Dose Radiation: Biological Basis of Risk Assessment* [K. E. Baverstock and J. W. Stather, eds.], Taylor and Francis, London, p. 305, 1989).

The purpose of this study was to compare the biological responses to inhaled $^{239}PuO_2$ of two different particle sizes that resulted in different patterns in the alpha-particle radiation dose to the lungs in female and male F344 rats. This study will provide data in a rodent species to be compared with parallel studies on the effects of alpha-particle dose homogeneity in the lungs of dogs exposed to monodisperse aerosols of $^{239}PuO_2$ (McClellan, R. O. *et al.* In: *Life-Span Radiation Effects Studies in Animals: What Can They Tell Us?* [R. C. Thompson and J. A. Mahaffey, eds.], National Technical Information Service, Springfield, VA, p. 74, 1986). The hypotheses being tested is that the heterogeneous distribution of alpha-particle dose in the lung from "hot particles" is no more effective in producing lung neoplasms than is a uniform distribution of alpha-particle dose.

The experimental design for this study has been previously described in detail (1980–81 Annual Report, p. 178). Briefly, a total of 649 (approximately equal numbers of males and females) F344/Crl rats 11–12 wk of age at exposure and reared at this Institute in barrier-type rodent housing were used. The breeding colony for these rats was rederived by cesarean section from pregnant female rats (CDF®(F344)/CrlBR; Charles River Laboratories, Wilmington, MA). Two monodisperse aerosols of $^{239}PuO_2$, one having an activity median aerodynamic diameter (AMAD) of 1.08 μm and the other AMAD of 2.41 μm were prepared and the rats exposed as previously described (Raabe, O. G. *et al. Toxicol. Appl. Pharmacol. 26*: 264, 1973). Of the 639 rats exposed to $^{239}PuO_2$, 243 were serially sacrificed for dosimetry, and 396 were held for their life span and examined histologically. Diagnostic criteria for

classifying lung neoplasms have been described (Hahn, F. F. and D. L. Lundgren. *Toxicol. Pathol. 20*: 169, 1992).

The fraction of the lung irradiated is a stochastic variable depending on the particle size, lung burden, particle distribution in lung, and the time after exposure (Diel, J. H. and J. A. Mewhinney. *Radiat. Environ. Biophys. 22: 251,* 1983). For purposes of comparison in this study, the fraction of the lung irradiated was approximated by using the lung burden at exposure and calculated assuming that each PuO_2 particle irradiated a spherical region equal in radius to the penetration distance of a 5.15 MeV alpha particle in lung tissue having a density of 0.21 g cm^{-1}, the average density of an inflated rat lung.

Because of the distribution of the ILBs in the exposed rats relative to the experimental design, we regrouped the rats within ranges of doses to the lungs that would facilitate the comparison of effects in rats exposed to the two $^{239}PuO_2$ particle sizes. Accordingly, the rats were grouped in the following alpha-particle doses to the lungs: Controls, <0.32, >0.32 to 1.0, >1.0 to 3.2, >3.2 to 7.9, and > 7.9 Gy to lungs (Table 1). From the mean ILBs for the rats in each group, the fraction of the lung initially irradiated in each group of rats was calculated (Table 1).

Neither the crude incidences (Fisher's two-tailed exact test; $p > 0.05$) (Fig. 1) nor the cumulative distribution (Mantel-Cox statistic; $p > 0.05$) of lung neoplasms were different when groups of rats exposed to the two particle sizes of aerosols but with similar doses to the lungs were compared. The crude incidence of primary lung tumors was well described by Weibull cumulative distribution functions fitted to the data points (Fig. 1). The similarities in the crude incidences of lung tumors in the rats exposed to either sized $^{239}PuO_2$ aerosol are readily apparent. Based on the 95% confidence intervals of the parameters (data not presented), there were no significant differences in the parameters fit to the two data sets.

The most frequently occurring morphological types of lung neoplasms in rats exposed to either the 1.08 μm or 2.41 μm AMAD aerosol were adenocarcinomas followed by squamous cell carcinomas, adenomas, and adenosquamous carcinomas with decreasing frequency. Large granular cell (mononuclear cell) leukemia (MCL) infiltration of the lungs was a common finding. Among the exposed rats, the incidence of MCL infiltration of the lung (range: 27 to 38%) was not radiation-dose or particle-size related, nor was it significantly different (Fischer's exact test; $p > 0.05$) from the incidence in controls (32%).

The fraction of the lungs irradiated was different among some groups of rats (Table 1), although the initial alpha-particle dose rates and cumulative doses to the lungs were similar. The fractions of the lung irradiated ranged from 0.08 to 1.0 among the rats exposed to 2.41 μm AMAD particles, whereas the entire lungs of all rats exposed to the 1.08 μm AMAD particles were theoretically irradiated (Table 1).

There were no consistent differences in the neoplastic lesions in the rats exposed to either the 1.08 μm or 2.41 μm AMAD $^{239}PuO_2$ aerosols. Within the limits of this study, the occurrence of pulmonary neoplasms was related to the total dose to the lung rather than the fraction of the lung initially irradiated. This study adds additional support to the hypothesis that inhalation of "hot particles" resulting in a more heterogeneous distribution of the radiation dose to the lungs are not more carcinogenic than similar average doses distributed more homogeneously.

Table 1

Numbers of Rats per Dose Group, Initial Lung Burdens (ILBs), and Fraction of the Lung Irradiated in Rats Exposed to Monodisperse Aerosols of $^{239}PuO_2$

Ranges of Lifetime Doses (Gy) to Lungs	Aerosol AMAD[a] and Number of Rats[b]		ILBs (kBq kg^{-1} ± SD)		Initial Fraction of Lungs Irradiated[c]	
	1.08 μm	2.41 μm	1.08 μm	2.41 μm	1.08 μm[d]	2.41 μm[e]
<0.32	0	15	-	0.27 ± 0.13	-	0.08
>0.32–1.0	10	30	0.67 ± 0.18	0.85 ± 0.28	1.0	0.27
>1.0–3.2	84	78	1.8 ± 0.52	2.7 ± 0.78	1.0	0.86
>3.2–7.9	74	77	5.2 ± 1.2	6.5 ± 1.7	1.0	1.0
>7.9	17	11	9.2 ± 2.0	13 ± 2.7	1.0	1.0

[a]AMAD = activity median aerodynamic diameter of exposure aerosol.
[b]Male and female rats combined (excluding rats that were serially sacrificed for dosimetry purposes).
[c]Based on the mean ILBs of the rats per dose range and assuming: Volume irradiated per particle of 0.024 mm^3 based on lung density of 0.21 g cm^{-3} resulting in average track length of 180 μm; lung weight of 0.96 g; and body weight of 206 g.
[d]Real diameter was 0.28 μm with activity per particle of 200 μBq.
[e]Real diameter was 0.72 μm with activity per particle of 3.4 mBq.

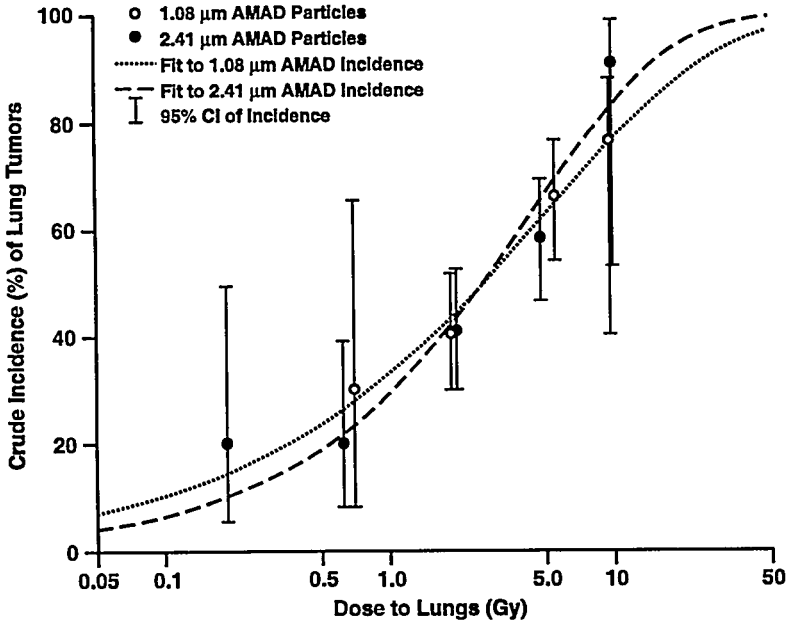

Figure 1. Crude incidence (%) of rats with primary pulmonary tumors (benign and malignant) in groups of rats exposed to either 1.08 μm (●) or 2.41 μm (O) AMAD monodisperse aerosols of $^{239}PuO_2$. Weibull cumulative distribution functions were fitted to the data. Parameters (± SE) for the rats exposed to the 1.08 μm AMAD particles = $(1.0-e^{(-0.40 \pm 0.031X-0.56 \pm 0.048X)}) \times 100$ and for the rats exposed to the 2.41 μm AMAD particles = $(1.0-e^{(-0.34 \pm 0.078X-0.71 \pm 0.15X)}) \times 100$; where X = average alpha-particle dose to lung.

(Research sponsored by the Office of Health and Environmental Research, U.S. Department of Energy, under Contract No. DE-AC04-76EV01013.)

VI. MECHANISMS OF CARCINOGENIC RESPONSE TO TOXICANTS

COMPARISON OF K-ras GENE TRANSCRIPTION AND EXPRESSION IN TWO INBRED MOUSE STRAINS

Susan E. Jones, Jonathon S. Wiest, Elisabeth Johanson*, William A. Palmisano, Marshall W. Anderson*, and Steven A. Belinsky*

The C3H mouse (lung tumor resistant) and the A/J mouse (lung tumor sensitive) differ significantly in their rates of spontaneous and carcinogen-induced lung tumors. The C3H mouse has decreased size, longer latency, and lower multiplicity of 4-(methylnitrosamino)-1-(3-pyridyl)-1-butanone (NNK)-induced lung tumors compared to the A/J mouse (Devereux, T. R. *et al. Carcinogenesis 12*: 299, 1991). Differences in sensitivity between the two strains have been linked to a repetitive element polymorphism within the second intron of the K-ras gene (You, M. *et al. Proc. Natl. Acad. Sci. USA 89*: 5804, 1992). Lung tumor resistant strains have a 37 base pair repetitive element within the second intron of the K-ras gene, whereas lung tumor sensitive strains have a 37 base pair deletion (i.e., lack one repetitive element). This deletion was then used to determine if the K-ras allele from the A/J parent would predominate in NNK-induced lung tumors from the C3A mouse (F1 hybrid cross of the C3H and A/J mice). Ninety percent of the lung tumors from the C3A mouse contained an activated K-ras allele derived from the A/J mouse (You *et al.*, 1992).

One hypothesis to explain the F1 hybrid data is that the transcription rate and expression of the mutated K-ras allele from the A/J strain is greater than the C3H strain. Sequence differences within the promoter region of the K-ras gene and/or the second intron (37 base pair deletion) could alter gene expression through interaction with the K-ras promoter. Previous studies by Hoffman, E. K. *et al.* (*Mol. Cell. Biol. 7*: 2592, 1987) have characterized the 5′ region of the K-ras gene from the Y1 mouse. A functional promoter was localized to a 688 base pair fragment which included exon 0 (Hoffman *et al.*, 1987). Stepwise deletion of 5′ promoter sequences resulted in a gradual decrease in transcription of the reporter gene, suggesting that the promoter is composed of multiple cis-acting elements. Potential binding sites for only one transcription factor, Sp1, were identified. In addition, fine mapping of this region identified a 166 base pair regulatory domain that contained several recognition sites for DNA-protein binding (Hoffman, E. K. *et al. Proc. Natl. Acad. Sci. USA 87*: 2705, 1990). One site was found to exist as a homopurine/homopyrimidine motif that exhibited S1 nuclease sensitivity and bound at least one unidentified nuclear protein *in vitro*. Deletions within this motif were found to result in marked loss of promoter activity. Thus, differences within the promoter region with or without influence of the second intron polymorphism between A/J and C3H mice could affect transcription of the K-ras gene.

The purpose of this study was to determine whether differences exist in the transcription rate and expression of the K-ras allele between the A/J strain and the C3H strain. The promoter regions of the K-ras gene from the A/J and C3H mice were cloned in order to compare the sequence between the two strains, and determine whether differences in the promoter region along with the repetitive element in the second intron affect the transcription rate of the K-ras gene. Levels of K-ras gene expression in target cells (alveolar type II) and in lung tumors from the A/J and C3H mice were also quantified.

An 838 base pair fragment of the K-ras gene promoter region was amplified by PCR and cloned from each mouse strain. Five different clones from each mouse were sequenced using an ABI systems automated sequencer. Single-strand phage recapture was performed on each of the five clones to obtain single-stranded template for confirmation of sequence differences.

---

*University of Cincinnati, Department of Environmental Health, Cincinnati, Ohio

Sequence homology between the K-ras gene promoter regions from the A/J and C3H mouse was 99% with only minor base pair differences. Two of these differences created a binding site for the CAP-BOX transcription factor and an additional Sp1 transcription binding site for the C3H mouse. Figure 1 delineates the base pair differences and their effect on transcription factor binding sites.

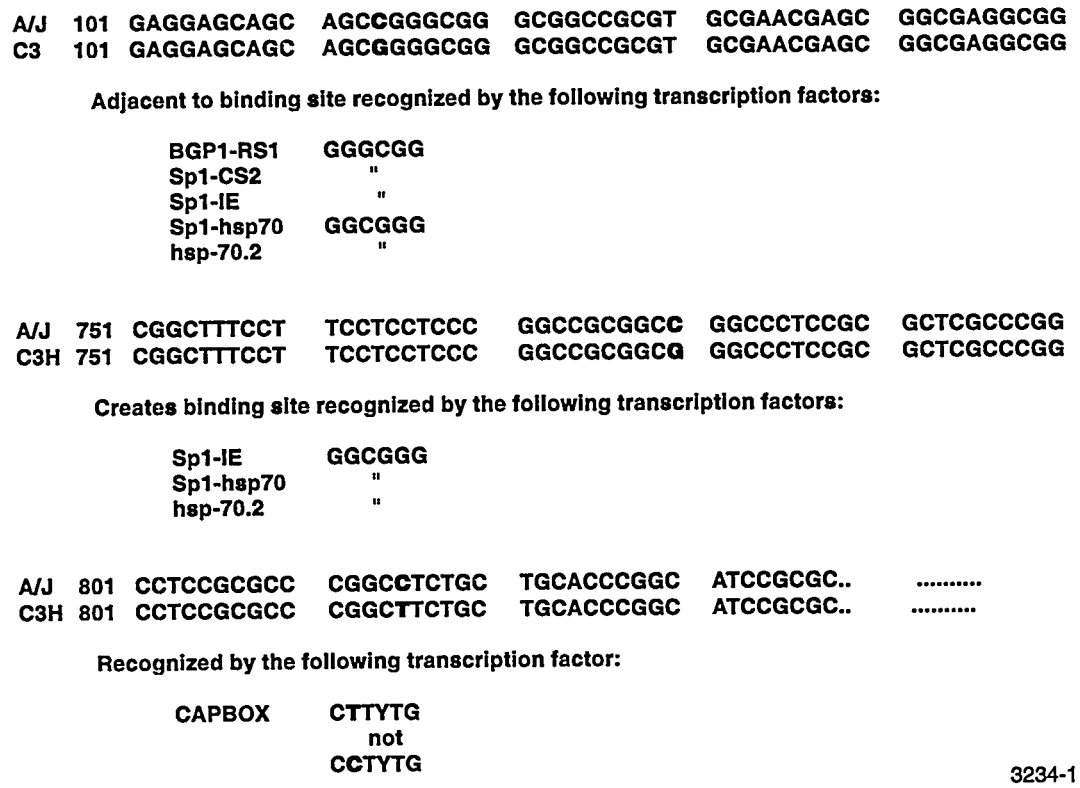

Figure 1. Transcription factor binding sites associated with base pair sequence differences found within the promoter region of the K-ras gene from the A/J and C3H mouse.

Promoter regions from both mice were attached to a pGL3-Basic vector (Promega, Madison, WI), then transfected into sensitive, intermediate and resistant murine lung tumor cell lines. Following transfection with the luciferase reporter gene constructs, the cells were lysed and the luciferase activity was measured by a scintillation counter. These counts were then standardized against β-galactosidase activity.

Promoter construct reporter gene assays were performed following transfection into the three different lung tumor cell lines derived from sensitive, intermediate, and resistant mouse strains. No difference in activity between the promoter regions of the A/J and C3H mouse were seen in any of the cell lines (see Fig. 2). Promoter construct assays with and without the second intron insertion are pending.

K-ras gene expression in the two mouse strains was determined by RNase protection. RNA derived from alveolar type II cells isolated from A/J and C3H mice before and 7 d following NNK treatment (50 mg/kg, intraperitoneal, every other day for three treatments) were hybridized to specific cDNA probes for the murine K-ras and the murine actin genes. Type II cell isolations from 20 mice in each group were pooled, and the type II cell purity was 68% ± 2%.

Preliminary results reveal no significant differences between the mice when comparing K-ras messenger RNA (mRNA) levels in type II cells either endogenously or following NNK-exposure.

Comparison of K-ras mRNA levels from nine different NNK-induced lung tumors in these two mouse strains also show no significant difference.

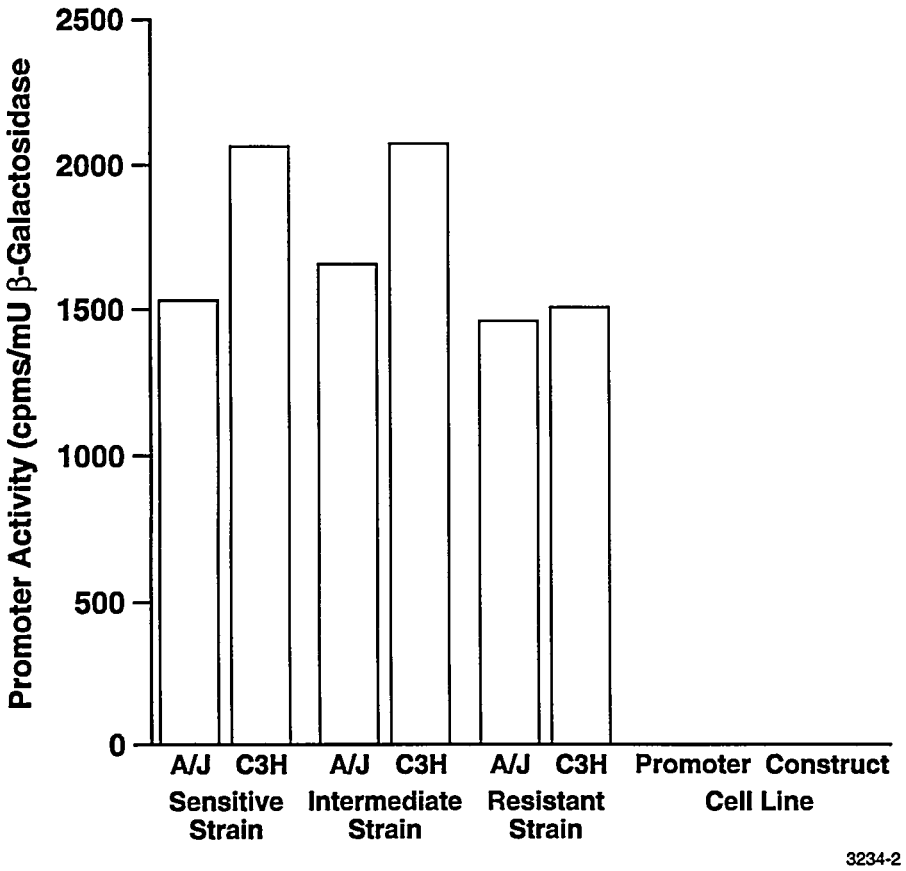

Figure 2. Comparison of luciferase reporter gene activity in the two mouse strains. The K-ras gene promoter region from the A/J mouse or the C3H mouse was attached to PGL3-Basic Vector and co-transfected with a β-galactosidase reporter gene into three tumor cell lines. Values were normalized against β-galactosidase activity.

Results of this investigation indicate that only minor differences exist in the sequence of the promoter region between the lung tumor sensitive A/J strain and the lung tumor resistant C3H strain. These base pair differences are unlikely to have any influence on K-ras gene expression because the luciferase activity for A/J and C3H promoters were identical. The K-ras second intron polymorphism, which segregates with lung tumor susceptibility, could influence the transcription rate of the K-ras gene. Studies are in progress to determine the effect of the repetitive element on promoter activity using a human growth hormone reporter gene (Selden, R. F. *et al. Mol. Cell. Biol. 6*: 3173, 1986). Alternatively, K-ras gene mRNA stability may differ in the two strains of mice and, therefore, lead to altered expression of the K-ras gene. The half-life of the K-ras gene mRNA will be assessed using cell lines from lung tumor resistant, sensitive, and intermediate strains of mice.

Information from this study will further characterize differences in lung tumor susceptibility between these two mouse strains.

(Research sponsored by the Office of Health and Environmental Research, U.S. Department of Energy, under Contract No. DE-AC04-76EV01013).

FREQUENT ABERRANT METHYLATION OF $p16^{INK4A}$ IN PRIMARY RAT LUNG TUMORS

Steven A. Belinsky, Susan K. Middleton, William A. Palmisano, Kristen J. Nikula, Johannes Tesfaigzi, Stephen B. Baylin, James G. Herman*, and Deborah S. Swafford*

Inactivation of the *p16* tumor suppressor gene on chromosome 9p21 has been detected in > 70% of cell lines derived from human non-small cell lung cancers (NSCLCs [Kamb, A. *et al. Science 264*: 436 1994; Otterson, G. A. *et al. Oncogene 11*: 1211, 1995]). The predominant mechanisms for inactivation of the *p16* gene in human tumors include homozygous deletion (Kamb *et al.*, 1994) and aberrant methylation of a CpG island which extends from the promoter region into exon 1 (Merlo, A. *et al. Nature Med. 1*: 686, 1995). Despite the strong evidence for the tumor suppressing function and frequent inactivation of *p16* in cell lines derived from NSCLCs, a role for the *p16* gene in the genesis of primary NSCLCs has not been clearly substantiated due to a significantly lower frequency for dysfunction in primary tumors (Merlo *et al.*, 1995; Cairns, P. *et al. Nature Genet. 11*: 210, 1995). The discordance in frequency for inactivation between cell lines and primary tumors could result from the occurrence or selection of *p16* dysfunction in cell culture. Alternatively, this difference in frequency may stem from a lack of sensitivity by the assays used to detect homozygous deletion (microsatellite markers) and methylation (Southern analysis), within tumors that may have heterogeneous cell populations for *p16* dysfunction and may also include normal tissue.

The question of whether *p16* inactivation arises within primary or cultured tumors is particularly important in light of the involvement of CpG island methylation in the development and progression of many human cancers (Jones, P. A. *Cancer Res. 56*: 2463, 1996). CpG island hypermethylation has been identified within specific chromosome loci prior to allelic loss (Makos, M. *et al. Cancer Res. 53*: 2719, 1993), and the expression of several tumor suppressor genes including *p16*, is silenced in tumors with aberrant methylation within the CpG island of the gene (Herman, J. G. *et al. Proc. Natl. Acad. Sci. 91*: 9700, 1994; Merlo *et al.*, 1995). However, aberrant CpG island methylation of tumor suppressor genes, including *p16*, is especially common in cultures of transformed cells (Herman *et al.*, 1994; Merlo *et al.*, 1995; Yoshiura, K. *et al. Proc. Natl. Acad. Sci. 92*: 7416, 1995). Therefore, it is critical to define the dynamics underlying the evolution of *p16* gene hypermethylation during tumorigenesis and its contribution to establishing cultures from primary cancers. The purpose of this investigation was to address these issues by using a rat model for lung cancer in which the frequency and mechanism for inactivation of *p16* could be determined in matched primary lung tumors and derived cell lines.

Eighteen primary rat lung tumors (T1–T18) and corresponding cell lines (CL1–CL18) were analyzed. Lung tumors were induced in F344/N rats exposed to either X-rays (Belinsky, S. A. *et al. Radiat. Res. 145*: 449, 1996), beryllium metal (Nickell-Brady, C. *et al. Carcinogenesis 15*: 257, 1994), cigarette smoke (Finch, G. *et al. 1994–95 Annual Report*, p. 77, 1995), plutonium-239 oxide, or to cigarette smoke and plutonium-239 oxide. Two spontaneously derived cell lines were used in this study. They were derived from type II lung epithelial cells isolated from a F344/N rat (CL19 [Li, A. P. *et al. Toxicology 27*: 257, 1983]) and a Sprague-Dawley rat (CL20 [Lehup, B. P. *et al. Lab. Invest. 60:* 791, 1989]).

Expression of *p16* transcript was determined by polymerase chain reaction (PCR) of cDNA synthesized from total RNA isolated from all cell lines and normal lung. *p16* mRNA was not detected in 11 of 20 tumor-derived cell lines, and the expression varied significantly in the nine lines for which a transcript was observed (Table 1). Only three cell lines (CL 10, 15, 19) had expression levels similar to

*Johns Hopkins University, Baltimore, Maryland

that of normal lung (Table 1), while only a trace amount of *p16* transcript was evident in three other cell lines (CL 2, 6, 9). Expression of *p16* in the remaining three cell lines (CL 4, 7, 14) was higher than found in normal lung and was readily detected by northern analysis (data not shown).

Table 1

p16 Expression and Mechanism of Inactivation
in Primary Lung Tumors and Derived Cell Lines

Cell Line				*p16* Transcript[a]	*p16* Gene Dysfunction	
Number	Designation	Exposure	Histology[b]	Cell Line	Cell Line	Primary Tumor
1	C006	Pu	AdSCC	–	Deleted[c]	Methylated
2	X404	X-ray	AdC	trace	Methylated	Methylated
3	U635	X-ray	AdC	–	Methylated	Methylated
4	R623	Pu/Sm	SCC[b]	+++	Unmethylated	Methylated
5	L173	Pu/Sm	SCC	–	Methylated	Methylated
6	J429	Pu/Sm	SCC[b]	trace	Methylated	Methylated
7	D434	Be	SCC	+++	Methylated[d]	Methylated
8	D391	Sm	SCC[b]	–	Deleted	Unmethylated
9	U640	X-ray	AdC	trace	Deleted[c]	Methylated
10	W173	X-ray	AdC	+	Deleted[c]	Unmethylated
11	J546	Pu/Sm	SCC[b]	–	Deleted	Methylated
12	N204	Pu	AdC	–	Deleted[c]	Unmethylated
13	H177	Pu	AdC	–	Methylated	Methylated
14	B444	Pu	Os	+++	Unmethylated	Unmethylated
15	U649	X-ray	SCC[b]	+	Methylated	Methylated
16	V304	X-ray	SCC	–	Deleted	Methylated
17	I149	X-ray	SCC	–	Methylated	Methylated
18	V309	X-ray	SCC	–	Deleted	Unmethylated
19	LEC	Spont.	AdC	+	Methylated	NA
20	FRLE	Spont.	AdC	–	Methylated	NA
lung	NA	NA	NA	+	NA	Unmethylated

[a]+, expression approximates that seen in normal lung; +++, expressed at levels detectable by Northern analysis.

[b]The histology indicated is that observed in the nude mouse tumor produced from each cell line. The resulting tumor generally recapitulated those seen in primary tumors, except the indicated squamous cell carcinomas which showed an adenosquamous phenotype in the primary tumor.

[c]These cell lines had reduced *p16*E1 amplification product as compared to the *p53* control amplimer.

[d]Both methylated and unmethylated alleles were present in this cell line.

Abbreviations: Pu, plutonium; Sm, smoke; Be, beryllium; Spont., spontaneous; NA, not applicable.

The lack of *p16* expression seen in 11 of 20 cell lines and only trace expressions in three others could stem from gene deletion in some cells or from transcriptional silencing associated with methylation of the CpG island located within exon 1 (E1). Tumor cell lines were first analyzed by PCR for deletion of the E1. Amplification of genomic DNA by PCR primers specific for E1 was used to assess gene status. Homozygous deletion of *p16*E1 was detected in four cell lines (Table 1) that showed loss of *p16* expression (CL 8, 11, 16, 18). Four additional cell lines which had absent-to-trace *p16* expression (CL 1, 9, 10, 12) showed markedly reduced amplification products, suggestive of gene deletion. The weak *p16* amplification products in these cell lines were not due to DNA degradation, because the *p53* control fragments were present at similar levels among all cell lines (not shown). Because these cell lines are not clonal and were examined at early passage (< 10 passages), the weak *p16* amplification products may reflect heterogeneity of cell populations in these cultures.

To determine whether the reduced or absent *p16* expression in cultures retaining a *p16* gene might be due to gene methylation, eight cell lines (CL 2, 3, 5, 6, 13, 15, 17, 20) were grown in the presence of 2-deoxy-5-azacytidine to achieve widespread demethylation of genomic DNA. RT-PCR analysis of treated cultures showed that the *p16* expression relative to *GAPDH* was induced, as compared to untreated samples examined at the same passage (not shown).

A new method (Herman, J. G. *et al. Proc. Natl. Acad. Sci. 93*: 9821, 1996), methylation-specific PCR (MSP) in which site-specific methylation can be determined for CpG sites, was then used to analyze the methylation status of the 12 cell lines having no evidence for *p16* gene deletion. Only three lines (CL 4, 7, 14) produced strong amplification product using the primers specific for unmethylated DNA; these same cell lines had abundant expression of the *p16* transcript. The remaining nine cell lines with absent to low levels of *p16* expression produced amplification product only with the methylation-specific primers, suggesting that the majority of the *p16*E1 alleles in these samples were methylated.

Eighteen primary rat lung tumors from which the tumor cell lines were established were analyzed by PCR for presence of *p16*E1. *p16*E1 was amplified from all primary tumor samples (data not shown). Primary lung tumors were then analyzed for methylation of *p16*E1 by the MSP assay. Seventeen of 18 tumors produced amplimers from the unmethylated primer pairs, consistent with the presence of either nonneoplastic tissue and/or neoplastic cells with unmethylated alleles. However, 13 tumors also clearly produced amplimers using the methylation-specific primers indicating substantial levels of methylated CpG sites within *p16*E1 (Table 1). All cell lines in which the *p16* gene was extensively methylated were derived from tumors that also had methylation of this gene (Table 1). Interestingly, of the eight cell lines with homozygous deletion of the *p16* gene, four were derived from primary tumors that contained methylated *p16* alleles (Table 1). Hypermethylation within CpG islands has been hypothesized to lead to changes in chromatin structure which may predispose the islands to genetic instability. For example, a previous study (Makos *et al.*, 1993) in renal tumors demonstrated that regional hypermethylation on chromosome 17p, in an area subsequently shown to harbor a candidate tumor suppressor gene (Makos, M. *et al. Nature Med. 1*: 570, 1995), preceded allelic loss. Our results may indicate such a relationship between methylation and homozygous deletion of the *p16* locus. Methylation was detected in one tumor (T4) but not in its derived cell line. The phenotype of this tumor was adenosquamous, and the derived cell line was asquamous cell carcinoma, suggesting that the methylation detected in the primary tumor may have been localized to the adenomatous portion which was not propagated in culture.

Results of this investigation clearly demonstrate that aberrant *p16* CpG island methylation leading to the loss of *p16* expression originates in primary tumors. Moreover, *de novo* methylation of the *p16* exon 1 CpG island occurs frequently in primary lung tumors induced in rats. The mechanisms for *p16* dysfunction in the rat lung tumor cell lines examined in this study parallel those seen in human cell lines, validating the rat as a model for studying the role of *p16* in lung cancer.

The presence of aberrant *p16* methylation in cell lines was strongly correlated with absent or low expression of the gene. Only CL7 which expressed *p16* at high levels showed evidence for both methylated and unmethylated alleles, indicating heterogeneity within this cell line. The fact that trace-to-low levels of expression were detected in some cell lines with apparent complete methylation of exon 1 may indicate a lack of methylation at sites within the promoter region, leading to minimal levels of transcription. Although the methylated phenotype showed an absolute correlation between cell cultures and parent tumors, both methylated and unmethylated alleles were detected by the MSP procedure in most primary tumors. Estimating the extent to which this heterogeneity of methylation reflects contamination of the tumor by normal tissue or heterogeneity within the tumor cell population is difficult. In tumor 15, no unmethylated alleles were observed, and contamination of this tumor with normal cells was estimated to be only 2%. The fact that methylation was detected in tumors contaminated by up to 50% with normal tissue indicates that methylation must be extensive within many of these tumors.

The frequency of *p16* methylation observed in primary rat lung tumors (72%) surpasses the frequency of 26% reported using Southern analysis in human lung tumors (Merlo *et al.*, 1995). A similar frequency has also been observed in primary rat lung tumors induced by plutonium from which cell lines were not established (S. Belinsky, unpublished), indicating that the high frequency for aberrant methylation of *p16* was not a function of selecting tumors for analysis from which cell lines were established in culture. This difference may be due in part to the greater capability for MSP analysis to detect methlyation, but could also reflect the fact that the majority of rat lung tumors examined were induced by radiation exposure. A recent study by Issa, J. P. J. *et al.* (*Cancer Res. 56*: 3655, 1996) revealed a carcinogen-specific effect on methylation of the estrogen receptor gene in rat and human lung tumors. Alternatively, factors involved in initiating the spread of methylation through the *p16* CpG island may differ between humans and rodents. Vertino, P. *et al.* (*Mol. Cell Biol. 16*: 4555, 1996) demonstrated that CpG island loci differ in their inherent susceptibility to undergo *de novo* methylation.

The potential contributions of species and exposure differences to the frequency of CpG island methylation will remain elusive until events that lead to *de novo* methylation and the targeting of specific genes are clearly defined. Our rat model may be an excellent setting for such studies. Affects on locus-specific factors such as Sp1 (Macleod, D. *et al. Genes Develop. 8*: 2282, 1994) may protect CpG islands from *de novo* methylation and could be required for initiating aberrant methylation within the *p16* gene. Studies of *p16* throughout tumor evolution in rodent carcinogenesis models should help identify factors important to aberrant methylation of this gene and define its role in the progression of neoplasia.

(Research sponsored by the Office of Health and Environmental Research and the Assistant Secretary for Defense Programs, U.S. Department of Energy, under Contract No. DE-AC04-76EV01013 and by the NIH Grant 5P50CA58184.)

EXPRESSION OF SPR1 AND p16^{INK4A} IS INDUCED IN HYPERPLASTIC TYPE II CELLS FROM RATS EXPOSED TO PLUTONIUM-239 DIOXIDE

Johannes Tesfaigzi, Teresa A. Liberati, Fletcher F. Hahn, David L. Lundgren, and Steven A. Belinsky*

Identifying genetic and epigenetic alterations that initiate neoplasias is crucial for the early detection of premalignant disease and for the development of anticancer therapies. Studies using immunohistochemistry and transmission electron microscopy show the alveolar type II pneumocytes to be the cellular origin of $^{239}PuO_2$-induced pulmonary preneoplastic epithelial lesions in F344/N rats (Herbert, R. A. *et al. Vet. Pathol. 31*: 366, 1994). The purpose of this investigation was to isolate normal and hyperplastic alveolar type II pneumocytes from control and $^{239}PuO_2$-exposed rats in order to identify molecular changes that occur during the evolution of neoplasias.

Male F344/N rats, 10–12 wk old (Taconic Laboratories, Germantown, NY) were randomized by body weight. Housing conditions and methods used to expose rats to aerosols of $^{239}PuO_2$ leading to a 100 nCi (3.7 kBq) initial lung burden have been described previously (Herbert *et al.*, 1994). The time when the precursor lesions (i.e., alveolar type II hyperplasia) from which adenocarcinomas develop has been determined in previous studies (Herbert, R. A. *et al. Radiat. Res. 134*: 29, 1993). Sixty rats were exposed to $^{239}PuO_2$, and 15 rats were exposed to air only as control. At 8 and 10 mo after exposure, five $^{239}PuO_2$-exposed rats were sacrificed to assess the development of preneoplastic lesions in the lungs. Because these lesions were very small at the time, hyperplastic type II cells were not isolated until 15 mo post exposure when some rats began to die of various cancers. Whenever a lung tumor was encountered, it was removed before cell isolation. Type II cells were isolated from groups of seven rats. The rats were anesthetized and the blood removed from the pulmonary vasculature by perfusing with saline through the portal vein and allowing the blood to escape through a cut of the descending vena cava. Lungs were removed and lavaged three times via the trachea with 5 mL Dulbecco's phophate-buffered saline (DPBS). Lavaged cells were centrifuged at 1000 *g* for 5 min and stored at –80°C for further analysis. Lungs were digested by instilling with elastase (Worthington Biochem. Corp., Freehold, NJ) via the trachea at a specific activity of 4.3 units/mL in JMEM supplemented with 1 mg DNase (Sigma Chemical Co., St. Louis, MO) and were incubated at 37°C for 15 min. Lungs were minced with scissors; the suspension was agitated on ice and sequentially filtered through nylon mesh with pore sizes of 150 μm, then 70 μm. Cells were separated from red blood cells by centrifugation on a percoll gradient for 20 min at 2500 *g*. After washing cells twice, type II cells were separated from macrophages by panning on rat IgG-coated petri dishes. Panned type II cells as determined by a modified Papanicolaou staining (Tesfaigzi, J. *et al. Int. J. Exp. Pathol. 77*: 143, 1996) were between 55 and 65% pure. The rest of the cells were inflammatory cells (lymphocytes, neutrophils, and macrophages). Total RNA was isolated from lavaged alveolar macrophages and enriched type II cells, and was analyzed by northern blotting as described previously (Tesfaigzi, J. and D. M. Carlson. *J. Cell. Physiol. 166*: 480, 1996). p16 levels were quantified by polymerase chain reaction, as described elsewhere (Belinsky, S. A. *et al. Carcinogenesis*, in press, 1996).

Hybridization to the ^{32}P-labeled GAPDH probe, which shows the expression levels of the housekeeping gene, glyceraldehyde phosphate dehydrogenase, showed that similar amounts of type II and lavaged cell RNA (10 μg) from control and $^{239}PuO_2$-exposed rats were fractionated and transferred onto the blot. A cDNA probe for the surfactant protein SPC8 hybridized to RNAs from type II cells but not to RNAs from lavaged cells, thus confirming the identity of the type II cells and the presence of similar amounts of RNA from normal and hyperplastic type II cells. SPR1 mRNA, which has been shown to be

---

*Postdoctoral Fellow

induced early during the squamous differentiation process (Tesfaigzi, J. *et al. Am. J. Respir. Cell Mol. Biol. 14*: 478, 1996), could only be detected in RNAs from $^{239}PuO_2$-exposed rats.

GAPDH and p16 mRNAs were amplified by PCR from RNAs isolated from the lavaged and type II cells of control and $^{239}PuO_2$-exposed rats. The amplified products were electrophoresed through an agarose gel and viewed with UV light after staining with ethidium bromide. The intensity of the DNA bands was quantified by laser densitometry using the Collage image analysis software (Fotodyne Inc., Hartland, WI). When normalized for the GAPDH, the actual increase of p16 mRNA in $^{239}PuO_2$-exposed rats over control rats was determined to be 2.6-fold.

The presence of SPR1 in isolated preneoplastic type II cells indicates that the cells may be undergoing squamous differentiation. This suggestion is supported by previous studies that found a high number of squamous cell carcinomas and adenosquamous carcinomas in rats exposed to 100 nCi $^{239}PuO_2$ (Herbert, R. A. *et al.*, 1993).

p16 contributes to the maintenance of the retinoblastoma protein in the unphosphorylated state and thereby inhibits cell cycle progression. Therefore, increase of p16 levels in the preneoplastic type II cells indicates that p16 attempts to control the proliferation of these cells. These findings correlate with recent data that p16 mRNA is induced in rat lung tumors and the derived cell lines (Swafford, D. S. *et al. Mol. Cell. Biol.*, in press). These results show that expression of SPR1 and p16 are induced in hyperplastic type II cells isolated from preneoplastic lesions of rat lungs. These changes could, therefore, be used as molecular markers to identify preneoplastic cells.

(Research sponsored by the Office of Health and Environmental Research, U.S. Department of Energy, under Contract No. DE-AC04-76EV01013.)

EXPRESSION OF DNA DAMAGE-INDUCIBLE GENES p53, Cip1 AND Gadd153 FOLLOWING TREATMENT OF A549 CELLS WITH CROCIDOLITE OR JM CODE 100 FIBERS

Neil F. Johnson and Richard J. Jaramillo

Asbestos has been shown to induce the early response genes c-*fos*, c-*jun*, NF_kB, and c-*myc* in a variety of pulmonary cells (Heintz, N. H. *et al. Proc. Natl. Acad. Sci. USA 90*: 3299, 1993). These early response genes are part of a more general cascade of genes induced by exposure to toxicants. This work was conducted to determine whether crocidolite, a known human carcinogen, could induce DNA damage-inducible genes. A glass microfiber (JM Code 100), which has been shown to be free of carcinogenic potential in a number of inhalation studies in rats (Johnson, N. F. *Reg. Toxicol. Pharmacol. 20*: S22, 1994), was also used for comparison.

A549 cells were obtained from American Type Culture Collection (Rockville, MD). Cells within passages 7-8 and in log-phase growth were used in all experiments. The colony-forming efficiency of A549 cells treated with UICC crocidolite or JM Code 100 was determined; 5×10^5 cells were plated per 25-cm diameter culture flask. After 24 h at 37°C in a humid atmosphere of 5% carbon dioxide and 95% oxygen, the medium was replaced with RPMI containing five different concentrations of test material (0, 5, 10, 15, 25, and 50 μg/mL). Cultures were incubated as above for 20 h, after which the cells were washed in buffered saline. The cultured cells were replaced at a density of 1.25×10^4 cells per well of a six-well plate. After 8 d, the number of colonies that formed in each well was determined. Relative colony-forming efficiency was calculated as the ratio of the number of colonies formed in treated versus control cultures.

The temporal patterns of the expression of p53, Cip1, and Gadd153 were determined in A549 cells in log-phase growth. Cells were plated and cultured for 20 h before exposure to 2.0 $\mu g/cm^2$ of UICC crocidolite (MRC Toxicology Unit, Leicester, UK) or JM Code 100 (Manville, Denver, CO) for an additional 20 h. Media were then changed, and the cells were harvested by trypsinization at various time periods. The temporal pattern of protein expression was determined in a single experiment, and the results were used to determine the appropriate period post exposure for delineating the dose-response relationships. For the dose-response studies, triplicate cultures of cells were treated in a similar fashion, exposed to graded doses of crocidolite or JM Code 100 (0.0, 0.1, 0.5, 1.0, 2.0, and 3.0 $\mu g/cm^2$), and harvested 18 h after the fiber-exposure period.

The harvested cells were rinsed in Dulbecco's phosphate buffered saline (DPBS), fixed, and stored in 70% methanol at -20°C. Cells were immunostained for p53 using Clone DO-7 (Ab-6, Oncogene Sciences, Uniondale, NY), Cip1 using Clone EA10 (Oncogene Sciences), or Gadd153 (R20, Santa Cruz Biotechnology, Santa Cruz, CA). These antibodies were labeled with the appropriate biotinylated secondary antibodies and streptavidin fluorescein conjugates (Vector Laboratories, Burlingame, CA). Cell-cycle status was determined by staining with 25 μg/mL propidium iodide in DPBS containing 100 μg/mL RNAase A and was analyzed by using the MacCycle program (Phoenix Flow Systems, San Diego, CA). The percentages of positively stained cells were determined by flow cytometry on a FACStar Plus (Becton Dickinson, San Jose, CA) using the channel subtraction method of the CellQuest program. These analyses were conducted in files containing 10,000 events.

Crocidolite and JM Code 100 samples displayed a dose-dependent toxicity toward A549 cells. The cytotoxicity was more marked in the JM Code 100 sample than in the crocidolite sample. Temporal changes in the cell cycle were evident in the crocidolite-exposed cells. There were a persistent elevation

of the number of cells in the G_2 and a persistent decrease in the number of cells in G_1 phase of the cell cycle (data not shown). The increase in the number of cells in the G_2 phase of the cell cycle 18 h following crocidolite exposure was dose-dependent. The expression of p53, Cip1, and Gadd153 proteins increased with time after exposure in cells treated with crocidolite (data not shown). The protein response of cells exposed to JM Code 100 was much less marked (data not shown). There was a dose-dependent increase in the expression of p53, Cip1 (Fig. 1), and Gadd153 (Fig. 2) in crocidolite-exposed cells, but not in those cells treated with JM Code 100.

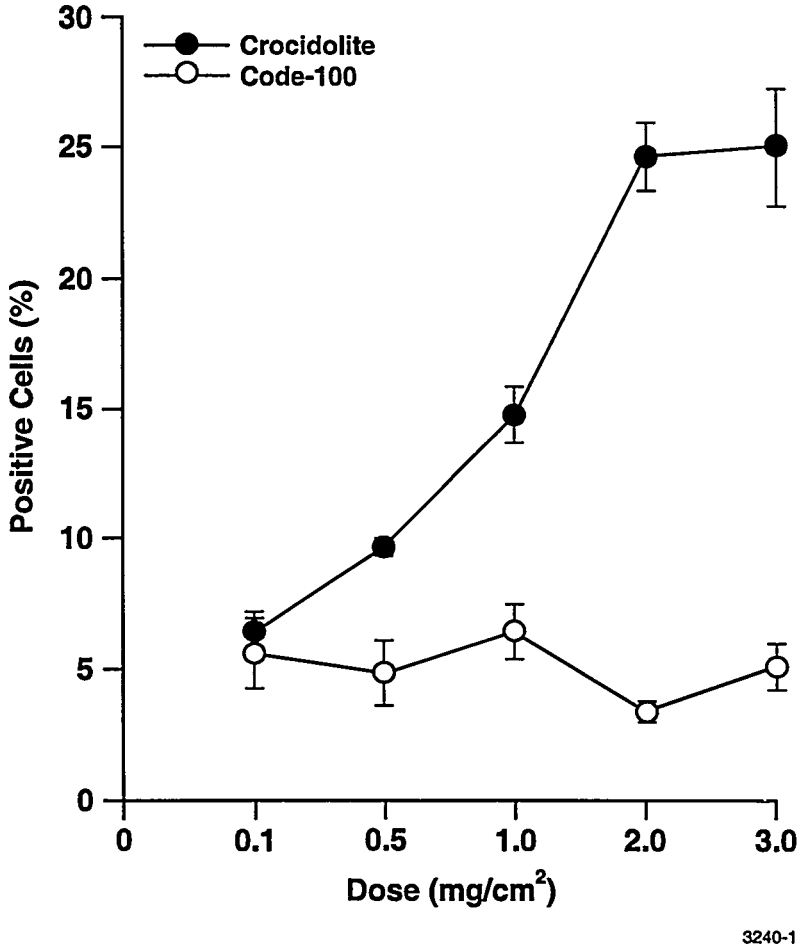

Figure 1. Dose-response relationship between concentration of crocidolite and JM Code 100 and the percentage of cells expressing elevated amounts of Cip1 protein. Error bars represent standard error of the mean of three experiments.

Crocidolite asbestos can induce genes associated with DNA damage and cell-cycle arrest. In this respect, crocidolite behaves in a similar fashion as other carcinogens such as UV, ionizing radiation, 4-nitroquinoline-1-oxide, and methyl methanesulfonate. p53 protein has been shown to be induced by the presence of DNA strand breaks; however, p53 protein can also be induced by other factors such as low-oxygen conditions and elevated temperatures. In a similar fashion, p21 can be induced by DNA damage via a p53-mediated pathway and by a p53-independent pathway unrelated to DNA damage. These p53-independent inducers of p21 include cellular senescence, TGFβ, and oxidative stress. The mechanism by which crocidolite induces the expression of p53, Cip1, and Gadd153 proteins is unknown, but it may be as a result of DNA damage. Crocidolite induced a noticeable cell-cycle arrest in the G_2 phase of the cell

cycle with no apparent disturbance of the G_1 phase of the cell cycle. This pattern of cell-cycle arrest would not have been predicted from the protein expression where p53 and Cip1 proteins are closely associated with arrest of cells in G_1. However, recent studies have indicated a role for p53 in G_2 arrest.

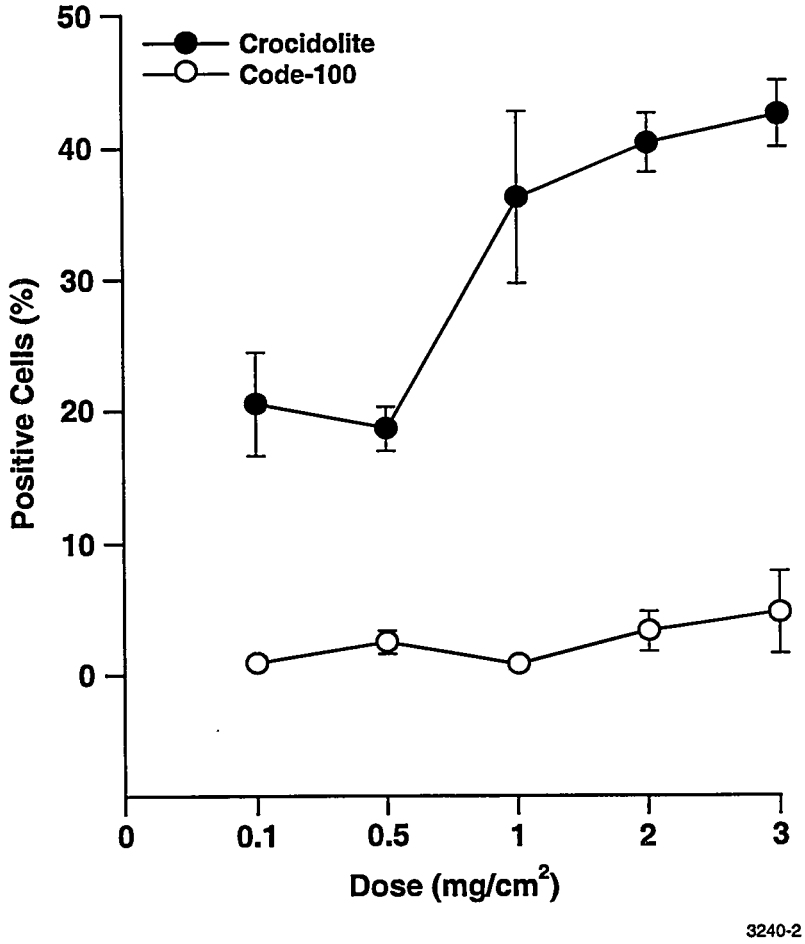

Figure 2. Dose-response relationship between concentration of crocidolite and JM Code 100 and the percentage of cells expressing elevated amounts of Gadd153 protein. Error bars represent standard error of the mean of three experiments.

The markedly reduced ability of JM Code 100 glass microfiber to induce p53, Cip1, and Gadd153 proteins is of interest because JM Code 100 was shown to be more toxic to cultured A549 cells than crocidolite on an equal mass/unit area basis. The expression of these proteins appears to be independent of cytotoxicity. Crocidolite is a known human carcinogen, while results of JM Code 100 inhalation exposures in rats have not produced an elevated risk of lung or pleural tumors. This protein response may also be independent of fiber size. The crocidolite and JM Code 100 samples had approximately equal numbers of fibers per μg, while the JM Code 100 sample had approximately 33% more fibers longer than 15 μm. These fibers are thought to be the most pathogenic for inducing pulmonary and pleural neoplasia. The durability of crocidolite in the lung is much higher than that of JM Code 100; however, biopersistence is an unlikely factor to explain the differences in protein response because the duration of the culture is only a small fraction of the half-life of these materials.

Crocidolite has a high iron content compared to JM Code 100, and this may be a factor in the expression of p53, Cip1, and Gadd153 proteins. Crocidolite fibers can induce hydroxyl radicals via the Fenton reaction, which has been postulated as the mechanism of induction of DNA damage detected *in vitro*. Changes in the redox potential of cells have been shown to alter the expression of p53 protein. The possibility that the iron content of the fiber is a major factor in the induction of these proteins is being tested *in vitro* using amosite, which contains iron, and erionite, which contains little iron. Amosite and erionite have been shown to induce pulmonary neoplasia in rats exposed to these materials by inhalation; studying the inducible proteins using iron-rich and iron-poor fibers will delineate the potential role of iron in these responses.

These results show that asbestos behaves like genotoxic chemicals and ionizing radiation by inducing proteins associated with DNA damage and cell-cycle arrest. The clear difference in response between crocidolite and JM Code 100 may help elucidate the mechanisms of action of toxic and nontoxic fibers.

(Research sponsored by NIH/NIEHS under grant R01-ES07665 from the National Institute of Environmental Health Science with the U.S. Department of Energy, under Contract No. DE-AC04-76EV01013.)

THE ROLES OF CYCLIN B1, Cdc2, Wee1, AND Cdc25 IN G_2/M ARREST FOLLOWING IONIZING RADIATION

Kenneth A. Schafer, Neil F. Johnson, and Fletcher F. Hahn*

Ionizing radiation is known to arrest cells in various stages of the cell cycle depending on the stage at which the cells are exposed (Datta, R. *et al. Cell Growth Differ. 3*: 637, 1992). Cell cycle arrest is thought to be a mechanism that allows repair of damaged DNA before the cell continues through division, thereby preventing transmission of the damage to progeny cells. G_1 cell cycle arrest allows the repair of mutations produced by processes such as dimerization and adduct formation. G_2 arrest is thought to allow repair of DNA damage that would result in gross chromosomal aberrations, such as nondisjunctions and translocations (Hong, J. H. *et al. Radiat. Res. 140*: 17, 1994). G_2 arrest may be one response of respiratory cells to radon exposure. In addition, the regulation of G_2 arrest after ionizing radiation has not been thoroughly investigated.

The normal cell cycle transition through G_2/M is regulated and primarily catalyzed by the serine/ threonine protein kinase cdc2 (Fig. 1) which is expressed constitutively throughout the cell cycle (Draetta, G. *et al. Nature 336*: 738, 1988). The kinase activity of cdc2 can be regulated by at least three mechanisms. The first is by noncovalently binding to Cyclin B1, which is required for cdc2 kinase activity (Gautier, J. *et al. Cell 60*: 487, 1990). The second is translocation into the nucleus, where the putative targets of cdc2 reside. This translocation is mediated by Cyclin B1, which contains a nuclear localization signal. The third mechanism is phosphorylation. Cdc2 is phosphorylated on multiple sites that affect its substrate binding ability and its kinase activity (Morla, A. O. *et al. Cell 58*: 193, 1989).

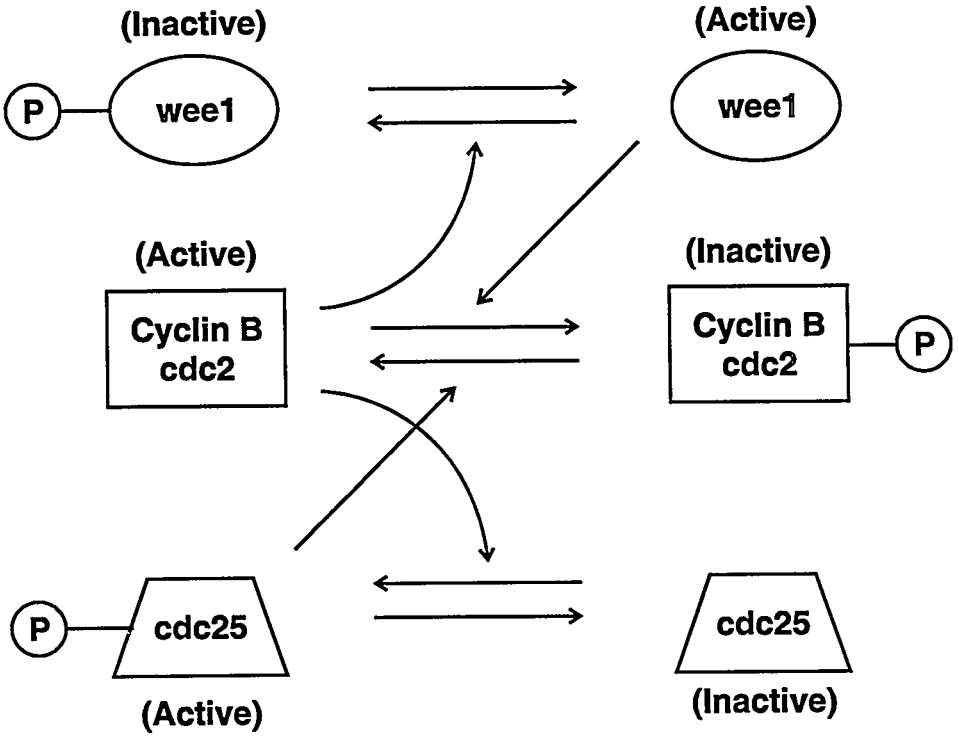

Figure 1. Interactions of cdc2/Cyclin B, wee1, and cdc25 at G2-M transition.

*Experimental Pathology Program Graduate Student

Cyclin B1 regulates the progression through G_2/M via its binding with cdc2 as described above. In addition, this G_2/M transition is regulated by the expression levels of Cyclin B1. Cyclin B1 is expressed cyclically during the cell cycle; it slowly accumulates through the early stages of the cycle with the greatest expression in G_2 and M phases. Cyclin B1 is rapidly and completely degraded at the end of mitosis (Marcote, M. J. *et al. Mol. Cell. Biol. 13*: 5122, 1993).

Cdc25 and wee1 regulate the cdc2 kinase activity (Fig. 1). Cdc25 promotes the cell cycle by dephosphorylating the active site of cdc2, thereby activating the cdc2 kinase (Sadhu, K. *et al. Proc. Natl. Acad. Sci. USA 87*: 5139, 1990). Cdc25 has multiple isotypes. Cdc25B and cdc25C are expressed in the G_2 stage of the cell cycle. wee1 inhibits the cell cycle by phosphorylating cdc2 in its active site, thereby inactivating the cdc2 kinase (Parker, L. L. *et al. Science 257*: 1955, 1992).

Because ionizing radiation induces G_2/M cell cycle arrest, the purpose of these studies was to determine how the cell cycle is regulated in response to ionizing radiation. We suspect, based on models of cell cycle regulation, that Cyclin B1 and cdc25 protein concentrations would decrease following ionizing radiation, and wee1 concentrations would increase (Fig. 1).

A549 cells were cultured using standard methods in RPMI 1640 medium supplemented with 10% fetal bovine serum and 2 mM l-glutamine (Wu, F. *et al. Am. J. Respir. Cell Mol. Biol. 10*: 437, 1994). Cells were exposed to X rays at levels including 0.01, 0.05, 0.10, 0.25, 0.50, 1.0, 2.0, 4.0, 6.0, and 10.0 Gy with a Philips RT 250 Radiotherapy Unit (Philips Medical Systems, Shelton, CT). Cells were harvested 6 h post exposure, fixed in 70% methanol, and stored at -20°C.

Cells were also exposed in time-course experiments to 2.0 and 6.0 Gy of X rays. Cells were harvested at time points of 0, 1, 2, 4, 6, 8, 10, 12, 15, 18, 21, 24, 36, and 48 h post exposure. Cells were harvested and stored as before.

The cell cycle regulatory proteins in these cells were detected with antibodies against the proteins of interest, secondary biotinylated antibodies, and streptavidin-conjugated fluorescein isothiocyanate (FITC) (Hickman, A. W. *et al. Cancer Res. 54*: 5797, 1994). Cells were simultaneously stained with propidium iodide (PI) for determining cell cycle distributions of cells. Fluorescence of FITC and PI were measured by flow cytometry on a Becton-Dickinson FACStar Plus. Flow cytometric data were analyzed using MacCycle (Phoenix Flow Systems, San Diego, CA) and Cell Quest (Becton-Dickinson, San Jose, CA) software for cell cycle fractions and protein levels, respectively.

Dose response curves demonstrated induction of G_2/M arrest starting at approximately 0.5 Gy. The percent of cells arrested in G_2 rose rapidly at 2 Gy, then gradually from 2 to 10 Gy. Cyclin B levels were induced starting at approximately 0.5 Gy and peaked at 8 Gy with approximately a 25% increase in cellular Cyclin B1 expression. wee1 had a similar induction, but was first detectable at 1 Gy. Cdc25B had increased expression above 1 Gy, while cdc25C had decreased expression first observable at the lowest doses. These data indicate that Cyclin B1 levels continued to increase despite cell cycle arrest and increasing doses. This suggests that, in A549 cells, Cyclin B1 is not a key regulator of the arrest. Also, wee1 increased with increasing dose, which is compatible with an inhibitory role of wee1. At the same time, cdc25C, which is thought to be the key cdc25 isoenzyme, decreased, compatible with its cell cycle promoting role.

Time-course experiments with A549 cells irradiated with 2 Gy X rays demonstrated a short-lived G_2/M arrest that started at approximately 2 h post exposure, peaked between 6 and 8 h, and disappeared around 12 to 15 h. This peak coincided with a rapid decline in the number of cells in G_1 and shortly followed a rapid drop in S-phase fractions. Following 2 Gy X-ray exposure, Cyclin B1 peaked simultaneously with the peak of the G_2/M arrest, then rapidly declined to below baseline by 15 h. wee1

followed a similar pattern. Both cdc25B and cdc25C largely declined post exposure with, at its nadir, $< 40\%$ of expression compared to controls. These results basically followed those of the dose-response curves, in that Cyclin B1 accumulated with arrest, wee1 levels peaked simultaneously with G_2/M arrest, and cdc25 levels dropped. These wee1 and cdc25 responses are compatible with their putative regulatory roles.

Time-course experiments with 6 Gy X rays had similar, but more exaggerated responses. The G_2/M arrest started at 4 h post exposure, peaked between 10 and 12 h post exposure, and did not return to control levels until after 20 h. The peak during arrest was approximately a 65% increase over controls. Cyclin B1 rapidly rose at 10 h, and its peak coincided with the G_2/M arrest. Wee1 and cdc25 analyses have not been completed.

The studies completed thus far indicate that wee1 and cdc25 enzymes regulate the G_2/M arrest in concert. Wee1, an inhibitor of cell cycle progression, accumulates, while cdc25C, a promoter of cell cycle progression, decreases in concentration. Cyclin B1, via its expression level, does not appear to affect the cell cycle progression of A549 cells after X-ray exposure.

These studies are preliminary. Regulatory methods yet to be examined include phosphorylation patterns of cdc2, wee1, and cdc25, subcellular localization of cdc2-Cyclin B1 complexes, and comparison of X-ray exposure to alpha-particle exposure results. Furthermore, protein levels determined by flow cytometry will be confirmed with western blot analyses. The results of these studies will further clarify how the G_2 stage of the cell cycle is regulated after ionizing radiation.

(Research sponsored by the Office of Health and Environmental Research, U.S. Department of Energy, under Contract No. DE-AC04-76EV01013.)

UNCOUPLING OF S AND M PHASES IN CHINESE HAMSTER OVARY CELLS IS INDUCED BY cAMP BUT NOT DIBUTURYL cAMP

Johannes Tesfaigzi and Leslie Watrin

As an activator of protein kinase A (PKA), cyclic 3′, 5′ AMP (cAMP) has long been recognized to inhibit the growth of certain cells (Boynton, A. L. and J. F. Whitfield. *Adv. Cycl. Nucl. Res. 15*: 193, 1983). Treatment of bone marrow-derived macrophages with analogues of cAMP arrests the cells in the G_1 phase of the cell cycle (Rock, C. O. *et al. Mol. Cell. Biol. 12*: 2351, 1992). In these cells, cAMP blocks the mitogenic effects of colony-stimulating factor -1, by increasing the cyclin-dependent kinase inhibitor, p27KIP1, which prevents the cdk-activating kinase (CAK) from phosphorylating the Cyclin D/cdk4 complex (Kato, J. *et al. Cell 79*: 487, 1994). In the presence of dibutyryl cAMP, the normally compact, randomly oriented Chinese hamster ovary (CHO) cells grow into a monolayer of elongated fibroblast-like cells which grow parallel to one another (Hsie, A. W. and T. T. Puck. *Proc. Natl. Acad. Sci. USA 68*: 358, 1971). The ability of CHO cells treated with dibutyryl cAMP to grow in a monolayer and their ability to synthesize collagen, a differentiation protein, renders this system of particular interest for the problem of cancer. Ryan, W. L. and M. L. Hedrick (*Science 162*: 1484, 1968) reported that the growth of HeLa and Strain L cells in culture is inhibited by cAMP, but to a lesser degree by dibutyryl cAMP. However, the mechanism by which cAMP induces cell cycle arrest in CHO cells remains unknown. The purpose of the present study was to compare the effects of dibutyryl cAMP and cAMP on the growth of CHO cells and to determine the mechanism of the cell cycle arrest.

CHO cells (ATCC, Rockville, MD) were cultured in Ham's F12 supplemented with 10% FBS. Logarithmically growing cells were treated with dibutyryl cAMP or cAMP (Boehringer Mannheim Co., Indianapolis, IN), and medium was changed every other day. To determine the number of cells synthesizing DNA, BrdU was added either 2 h or 18 h before harvest. CHO cells were synchronized by treating with nocodazole (66 ng/mL) for 15 h to enrich cells in M phase. Mitotic cells were prepared by shaking off the plates, and 1.8×10^6 cells were plated on T225 flasks for each time point. Cells were harvested using Trypsin/EDTA (Life Technologies, Grand Island, NY), washed in HEPES, suspended, and stored in ice-cold methanol for analysis of DNA content and BrdU incorporation. The mitotic index was determined by preparing cytospins and fixing cells in a solution containing 2 mg/mL malachite green in 100% methanol, staining the nuclei with 0.1% (w/v) eosin Y in formaldehyde, and finally counterstaining the cytoplasm with 0.04% (w/v) methylene blue and 0.04% (w/v) Azure A. Preparations and analyses with the flow cytometer were carried out as described previously (Tesfaigzi, J. and R. Jaramillo. *BioTechniques 21*: 800, 1996). For western blot analysis, 10^6 cells were frozen in -80°C as a pellet and processed as described elsewhere (Tesfaigzi, J. and D. M. Carlson. *J. Cell. Physiol. 166*: 480, 1996).

In preliminary experiments, CHO cells were treated with increasing concentrations of dibutyryl cAMP and cAMP (0.01-1 mM) for 48 h. cAMP inhibited CHO cell proliferation to a greater degree than dibutyryl cAMP. Therefore, the growth of CHO cells was investigated over a time course of 24, 48, 72, and 96 h. After 24 h, dibutyryl cAMP had reduced the cell numbers by 40%, while cAMP completely stopped CHO cell proliferation within the first 24 h (Fig. 1). Significant differences were also observed in the morphology of these cells. While dibutyryl cAMP treatment caused cells to elongate to the characteristic fibroblast-like form, the cAMP-treated cells looked larger, spread out, and contained 3- to 4-fold larger nuclei than control cells.

To determine the phase of the cell cycle in which growth arrest occurred, the DNA content was analyzed by flow cytometry. Interestingly, the control and dibutyryl cAMP-treated cells showed a normal

DNA distribution for G_1, S, and G_2 cells, and cAMP-treated cells contained a higher amount of DNA than 2C. Cells exposed to cAMP for 4 d had a 16 C DNA content, suggesting that cAMP had blocked the entry of cells into M phase and had redirected cells to undergo multiple rounds of DNA replication. To further test whether cells were blocked from entering G_2, M, or G_1 phases, control cells and cells treated with cAMP for 2 d were maintained in BrdU-containing medium (3 μM) for 18 h. Cells were double stained with propidium iodide and fluorescently labeled anti-BrdU antibody and analyzed by flow cytometry. While control cells showed the characteristic histogram of G_1, S, and G_2 cells, the cAMP-treated cells had completely incorporated the BrdU into their DNA and showed no G_1 or G_2 cells, confirming that these cells are actively and continuously synthesizing DNA.

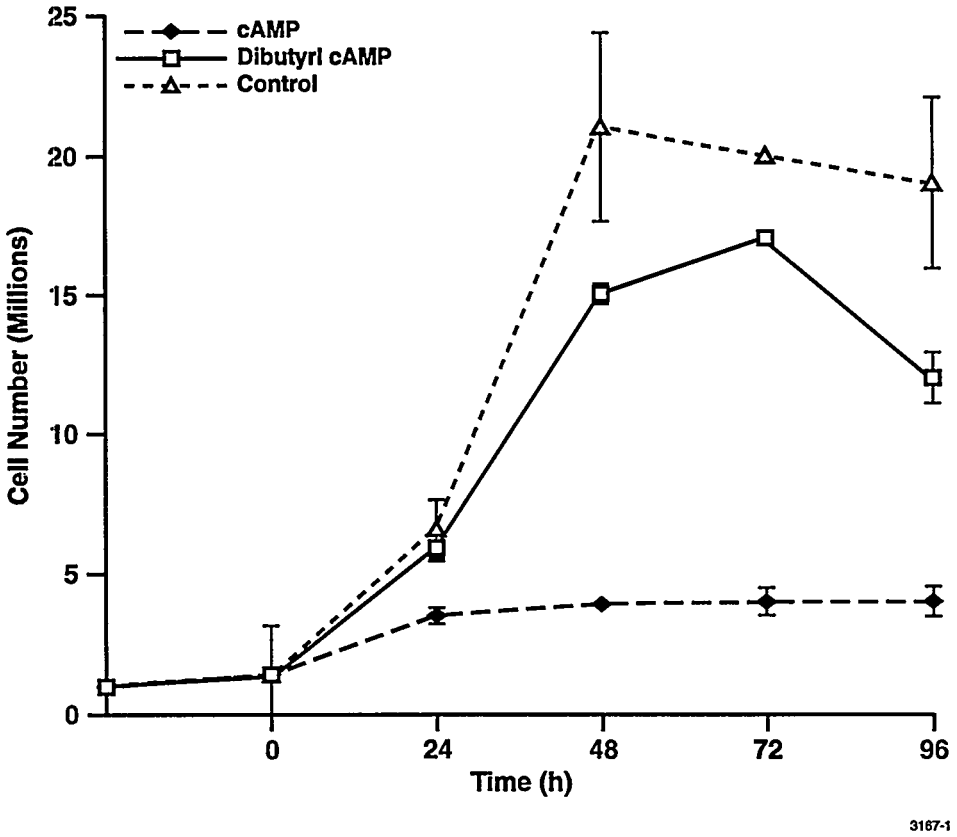

Figure 1. Growth curve of control CHO cells and cells treated with dibutyryl cAMP and cAMP. T225 flasks were seeded with 1×10^6 cells and treated after 24 h of culture. Cells were harvested at 0, 24, 48, 72, and 96 h and counted. Each data point represents data from at least three flasks; error bars denote the standard deviation; where no error bars are shown, the values were smaller than the size of the symbol.

The levels of the proteins responsible for entry into M phase, Cyclin B and cdc2, were analyzed, to determine whether this mechanism was at least partly responsible for the block to enter M phase. The cdc2 protein was detected in both proliferating control and cAMP-treated cells; however, as cells reached confluence and stopped proliferation after 72 and 96 h, cdc2 was absent in control cells. That cdc2 expression is downregulated in growth-arrested cells has been reported previously (Draetta, F. *Trends Biol. Sci. 15*: 378, 1990). Cyclin B levels were completely downregulated in cAMP-treated cells although cdc2 was still being expressed in these cells; the lack of Cyclin B expression may have been responsible for the inhibition of cells to enter mitosis. To investigate which phase of the cell cycle was inhibited by

cAMP treatment, cells synchronized in M phase were released into the cell cycle, and samples were taken at 0, 4, 17, and 24 h from control and cAMP-treated cells. Interestingly, the number of cells in control populations had doubled after 24 h, while the numbers remained the same for cAMP-treated cells (Table 1). Furthermore, the number of cells with condensed chromatin was significantly lower in cells exposed to cAMP, suggesting that the chromatin condensation was inhibited in these cells (Table 1). This possibility is supported by the finding that the Cyclin B/cdc2 complex, which is known to be involved in the initiation of chromatin condensation, is downregulated by cAMP in these cells. It remains to be investigated whether cAMP downregulates Cyclin B expression directly or indirectly in CHO cells. These results clearly show that dibutyryl cAMP, although a close relative of cAMP, does not inhibit growth of CHO cells as effectively and does not cause cells to become polyploid by inhibiting chromatin condensation. The uncoupling of M and S phases by cAMP could be significant for elucidation of the control mechanisms that ensure the correct sequence in the cell cycle to prevent occurrence of polyploidy.

Table 1

Effect of cAMP Treatment on the Progression of CHO Cells that were Enriched in M Phase. Increase in the Cell Number and the Change of Percentage of Cells with Mitotic Figures at 4, 17 and 24 h after Release from M Phase were Determined. Data for the Mitotic Figures Represent the Mean from Three Counts; the Standard Error of the Mean is Shown.

	0	4		17		24	
Treatment		Contr.	cAMP	Contr.	cAMP	Contr.	cAMP
Cell Number (in millions)	1.8	2.1	2.12	3.6	3.6	5.0	3.3
Mitotic Figures (%)	78 ± 2.1	0.2	0.4	0.5	1.5 ± 0.8	5.4 ± 1.1	0.9 ± 0.2

(Research sponsored by the Office of Health and Environmental Research, U.S. Department of Energy, under Contract No. DE-AC04-76EV01013.)

INVESTIGATION OF THE EFFECTS OF ALTERED IQGAP1 EXPRESSIONS ON THE REGULATION OF GENE EXPRESSION IN THE Cdc42 AND c-Jun PATHWAYS

Charles E. Mitchell, William A. Palmisano, Johannes Tesfaigzi, Steven A. Belinsky, John F. Lechner, Andre Benards, and Lawerence Weissbach**

IQGAP1 is a calmodulin-binding protein with a ras GAP-related domain. IQGAP1 binds to Cdc42, a member of the Rho family of small GTPases which regulate a variety of morphological events leading to changes in the actin cytoskeleton, cell motility, and c-Jun signaling pathway (Ridley, A. J. *Curr. Opin. Genet. Dev. 5*: 24, 1995). Alteration in cytoskeletal function may be involved in events that regulate cell proliferation, differentiation, and cancer. We have reported that the expression of IQGAP1 was altered in some human lung cancer cell lines (1994–95 Annual Report, p. 141). In the present report, we hypothesized that altered expression of IQGAP1 in human lung cancer cell lines is reflected by a subsequent change in the expression of the Cdc42 and c-Jun.

SW900, Calu-1, Calu-3, Calu-6, A549, and A427 (human lung cancer cell lines) were obtained from ATCC (Rockville, MD), while 3-90t, 54-t, 76-t, 114-87-t, and 253-t (human lung cancer cell lines) were obtained from Dr. Jill Siegfried (University of Pittsburgh, Pittsburgh, PA). Normal human bronchial epithelial cells were obtained from Clonetics (San Diego, CA). Each cell line was grown to 70% confluency, harvested, and subjected to total cellular RNA isolation using Tri Reagent (Molecular Research Center, Inc., Cincinnati, OH) according to the manufacturer's recommendations. Twenty μg of RNA from each cell line was size fractionated on a denaturing formaldehyde agarose (1.0%) gel and transferred onto Zetaprobe GT membrane (BioRad Laboratories, Inc., Hercules, CA) by capillary action. The IQGAP1 and the c-Jun cDNA probes were radiolabeled with [a-^{32}P]dCTP using randomly primed synthesis. The Cdc42 probe was generated by the polymerase chain reaction (PCR) using specific Cdc42 primers. The generated fragment (429 bp) was cloned, rescued, and labeled with [a-^{32}P]dCTP. The cDNA probes were hybridized overnight at 65°C in 7.0% SDS/0.25 M Na_2HPO_4, pH 7.2. The membrane was washed twice at room temperature for 30 min each time in 5.0% SDS/20 mM Na_2HPO_4 and once at 65°C for 1 h in 1.0% SDS/20 mM Na_2HPO_4 before exposure to X-ray film at –70°C. Following autoradiography, the membrane was stripped and rehybridized with a glyceraldehyde-3-phosphate dehydrogenase (GAPDH) radiolabeled cDNA probe as a control for gel loading and transfer. Autoradiographs were analyzed by densitometry. A change in expression was considered present when different from normal cells by at least 50% or more.

It has been reported that the expression of IQGAP in several cell lines was altered (Mitchell C. E. *et al. Proc. Am. Assoc. Cancer Res. 37*: 521, 1996). This observation was confirmed using reverse transcription (RT)-PCR. In addition, an antibody prepared against IQGAP1 protein showed differential expression in the same cell lines. These cell lines were used in the present study. Figure 1A shows that a transcript of ~2.1 kb in size was observed for Cdc42. Expression of Cdc42 was found in all cell lines examined. The expression of Cdc42 was higher in 4/12 lung cancer cell lines. However, altered expression of Cdc42 did not correlate with the altered expression of IQGAP1. A transcript of ~2.6 kb was found for the c-Jun protein (Fig. 1B). c-Jun was heterogeneously expressed in the cell lines examined. Approximately 33% of the lung cancer cell lines expressed c-Jun at the same level as normal lung cells, 33% expressed levels higher than normal cells, and 33% expressed levels lower than normal lung cells.

Several Rho GTPases have now been shown to play a role in cell transformation. Cdc42 regulates multiple pathways, which include control of reorganization of the actin cytoskeleton, and signal

*Massachusetts General Hospital, Boston, Massachusetts

transduction of the c-Jun pathway. Approximately 17% of the human lung cancer cell lines examined showed altered expression of IQGAP1. Thus, the frequency of alterations is not high; in addition, it is not known if the altered expression is due to changes that occurred during the establishment of cell culture. To determine whether altered expression of IQGAP1 affected Cdc42 and c-Jun, expression of these genes were quantitated in human lung cancer cell lines. c-Jun was differentially expressed in human lung cancer cell lines, but there was no apparent correlation with the expression of IQGAP1. Previous studies have shown that c-Jun is expressed as an early event in human lung carcinogenesis and that c-Jun may function as a mediator of growth factor signals in non-small cell lung cancer (Szabo, E. *et al. Cancer Res. 56*: 305, 1996). Similarly, the altered expression of Cdc42 did not correlate with the expression of IQGAP1 in the cell lines investigated. Future studies will focus on defining the frequency of the altered expression of these genes, particularly IQGAP1, in primary lung tumors, and on development of specific models aimed at determining if and to what extent IQGAP1 plays a role in the regulation of other growth-control pathways in human lung carcinogenesis. These investigations will contribute to an understanding of the role(s) the IQGAP1 gene plays in the initiation and/or progression of lung cancer.

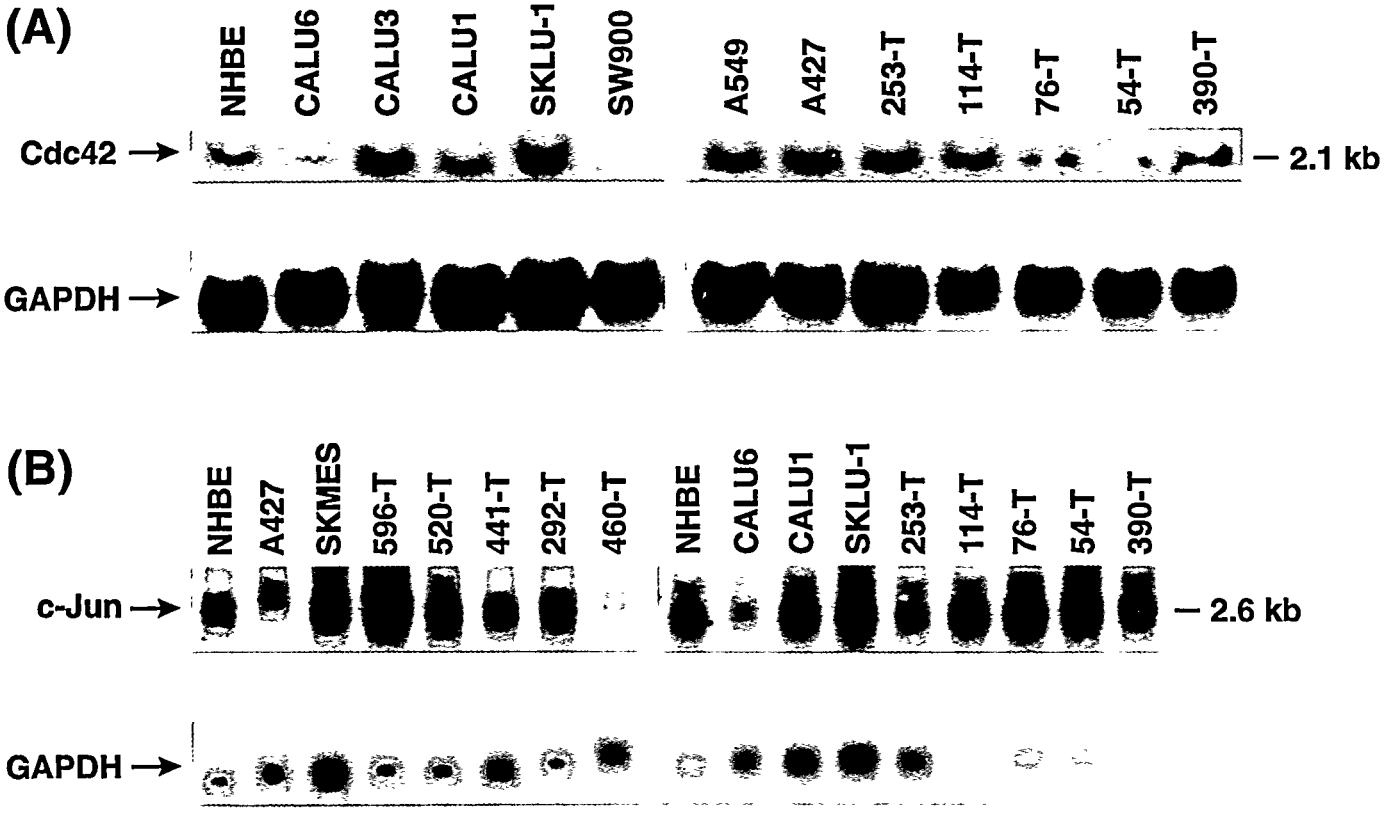

Figure 1. Representative Northern analysis of Cdc42 (A) and c-Jun (B) expression in normal and cancer cell lines. Each lane was loaded with 20 μg of total RNA from each cell line. All cell lines express a 2.1 and a 2.3 kb transcript of Cdc42 and c-Jun, respectively. A glyceraldehyde-3-phosphate dehydrogenase (GAPDH) cDNA was used as a control for RNA integrity.

(Research sponsored by the Office of Health and Environmental Research, U.S. Department of Energy, under Contract No. DE-AC04-76EV01013.)

ROLE OF Mad-RELATED GENES IN THE RESPONSE OF HUMAN AIRWAY EPITHELIAL CELLS TO TGF-β_1

Lauren A. Tierney, Gerald Curley, Jr., Charles E. Mitchell, William A. Palmisano, and John F. Lechner*

Normal human bronchial epithelial (NHBE) cells undergo terminal squamous differentiation if exposed to stress conditions (Lechner, J. F. *et al. Differentiation 25*: 229, 1984). However, lung tumor cells fail to differentiate; thus, a major difference between lung tumor cells and their normal counterparts is the loss of control of squamous differentiation processes. Subsequently, Masui, T. *et al.* (*Proc. Natl. Acad. Sci. USA 83*: 2438, 1986) showed that transforming growth factor type beta (TGF-β_1) is the principal endogenous signal that induces normal airway epithelial cells to differentiate. In contrast, lung tumor cells do not undergo terminal squamous differentiation, although the binding of TGF-β_1 to the cellular receptors of tumor and normal cells is identical. Therefore, the molecular pathway through which TGF-β_1 induces squamous differentiation in NHBE cells has remained enigmatic. Recently, however, Massagué, J. (*Cell 85*: 947, 1996) and Niehrs, C. (*Nature 381*: 561, 1996) suggested that the binding of the various TGF-β proteins to their receptor activates a latent kinase activity that phosphorylates a Mad-related protein (MADR). The phosphorylated MADR protein then translocates into the nucleus where it serves as a transcription factor. The complexity of this proposed pathway is underscored by the fact that the human MADR protein family consists of (at least) six different genes (Madr1/Smad-1, DPC-4, JV4-1, JV15-1, JV15-2, and JV18-1/Madr2) that share homology in the carboxy terminal region of the proteins. Although these members have been identified within the last year, one member, DPC-4, is implicated as a putative tumor suppressor gene for pancreatic carcinoma (Riggins, G. J. *et al. Nat. Genet. 13*: 347, 1996). The TGF-β gene family also has multiple members, and it is the association of each member with a particular MADR species that provides for the cell-specific effects of TGF-β family proteins (Riggins *et al.*, 1996; Schutte, M. *et al. Cancer Res. 56*: 2527, 1996). The purpose of this investigation was to determine if any of these seven Mad-related genes are associated with TGF-β_1-induced growth arrest and squamous differentiation of cultured NHBE cells.

The Mad family of proteins differs from one another primarily in the N-terminal sequence of amino acids (Riggins *et al.*, 1996). Accordingly, primers were designed to specifically amplify that region of the cDNA using the standard polymerase chain reaction (PCR) technique (Table 1). These primers were first used to amplify cDNA produced by the standard reverse transcription procedure of RNA extracted from lung tumor cell lines. Subsequently, the primers were used to amplify the cDNA of NHBE cells grown in the presence or absence of TGF-β_1.

The initial supposition was that some tumor cells would be refractory to TGF-β-induced squamous differentiation because the gene was lost, or at least not transcribed. Accordingly, cDNA from 16 lung tumor cell lines and NHBE cells were amplified using the primer sets for the six MADR genes. Examination of 16 lung tumor cell line cDNA by PCR revealed that all cell lines expressed the MADR gene products (data not shown).

A second series of experiments determined if TGF-β_1 affected the transcription of any Mad-family gene. Accordingly, mRNA was extracted from NHBE cells 0, 4, and 12 h after incubation with 100 pmoles of the factor. Semiquantitative PCR demonstrated (Fig. 1; and data not shown) that the levels of JV15-1 and JV18/Madr2 mRNAs were induced by TGF-β_1 at 4 h and 12 h post-treatment, respectively. Transcription of the other family members was unaffected by TGF-β_1 treatment.

---

*UNM/ITRI Graduate Student

Table 1

Mad-Related Gene PCR Primers

Name	Primer Pair	PCR Product Size
DPC-4	F-GTAATGATGCCTGTCTGAGC-3′ R-AAGCCTCCCATCCAATGTTC-3′	210 bp
JV4-1	F-TCAATCGTGTCTGACTCATCC-3′ R-GAGCAGAATACCACCGCC-3′	215 bp
Smad-1/Madr1	F-TAAACATTGGTGTTCAATAGTC-3′ R-TGTTTTCAATTGTCGAATTACG-3′	174 bp
JV15-1	F-TGGACAAAACAAGAAAGACGC-3′ R-CAAAAACCATACACCAAACCC-3′	161 bp
JV15-2	F-TGGGCTCCCCAAGCATCCG-3′ R-TTCCTTGACAACAATGGGTTG-3′	136 bp
JV18-1/Madr2	F-GTCCATCTTGCCATTCACG-3′ R-TGGTGATGGCTTTCTCAAGC-3′	194 bp

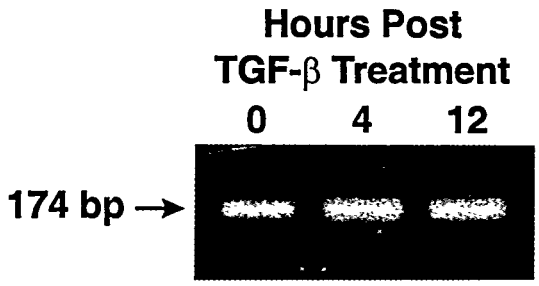

Figure 1. Expression of JV-15 in NHBE cells following treatment with TGF-β_1. Maximal induction of the genes was observed at 4 h.

These results suggest that at least two MADR genes (JV15-1 and JV18/Madr2) are intermediate factors in the TGF-β_1 signaling pathway that leads to growth arrest and squamous differentiation on NHBE cells in culture. Future efforts can now be directed toward ascertaining if either the JV15-1 or JV18/Madr2 gene products or the transcriptional regulation mechanism is altered in lung tumor cells following exposure to TGF-β_1.

(Research sponsored by the Office of Health and Environmental Research, U.S. Department of Energy, under Contract No. DE-AC04-76EV01013.)

IDENTIFICATION OF TGF-β-INDUCIBLE TRANSCRIPTS IN NORMAL HUMAN EPITHELIAL CELLS USING A NOVEL PCR-cDNA-SUBTRACTION APPROACH

William A. Palmisano, Lauren A. Tierney, and John F. Lechner*

Understanding the mechanisms that regulate growth and differentiation of normal human epithelial cells is critical to our understanding of carcinogenesis because most human cancers are of epithelial origin and are often resistant to factors that regulate growth and differentiation of normal cells. The archetype of a family of growth factors that acts as a negative growth factor for epithelial cells is transforming growth factor-β (TGF-β). TGF-β inhibits cell proliferation by arresting growth in the G_1-phase of the cell cycle, and escape from the growth-inhibitory effects of TGF-β is thought to be a key step in the process of oncogenic transformation (Mausi, T. *et al. Proc. Natl. Acad. Sci. USA 83*: 2438, 1986). TGF-β-induced G_1 cell cycle arrest is known to be mediated through activation of TGF-β receptors type-I and -II by ligand binding at the cell surface. The signaling cascade is then transduced through a series of yet unknown events that lead to the phosphorylation and activation of a family of proteins known as Mad-related proteins (Niehrs, C. *Nature 381:* 561, 1996; Massagué, J. *Cell 85:* 947, 1996). These proteins have been shown to have transcriptional activity (Fang, L. *et al. Nature 381*: 620, 1996), and are believed to be the transcription factors responsible for the activation of several low molecular weight proteins known as cyclin-dependent kinase inhibitors (CdkIs). These CdkIs, which include $p15^{INK4B}$, $p21^{Waf1/Cip1}$, and $p27^{Kip1}$, physically associate with specific target cyclin-dependent kinases and prohibit cell cycle progression (Hannon, G. J. and D. Beach. *Nature 371*: 257, 1994; Datto, M. B. *et al. Proc. Natl. Acad. Sci. USA 92*: 5545, 1995; Reynisdóttir, I. *et al. Genes Dev. 9*: 1831, 1995).

The purpose of this study was to identify the unknown genes that are involved in the TGF-β-mediated signal transduction pathway following receptor activation. To investigate this pathway, an innovative method known as PCR-Select™ (Clonetech, Palo Alto, CA) was used to selectively amplify genes that are differentially expressed. In contrast to traditional subtraction hybridization methods, this procedure requires only a small amount of poly A^+ RNA as starting material, involves no physical separation of single-strand or double-strand cDNA fractions and uses suppression PCR (Siebert, P. D. *et al. Nucleic Acids Res. 23*: 1087, 1995) to enrich for differentially expressed sequences.

To study the TGF-β signaling pathway, primary human keratinocyte cultures were grown to 70% confluence in Keratinocyte Serum-Free Media (Life Technologies, Inc., Gaithersburg, MD), and treated with 50 pM TGF-β for 8 h. Poly A^+ RNA was isolated from control and treated cells using the Fast Track® mRNA Isolation Kit (Invitrogen, San Diego, CA), and each sample was treated with DNase I to eliminate any contaminating DNA. cDNA synthesis was performed using 2.0 μg of poly A^+ RNA from each cell type and was digested with *Rsa I*, a four-base-cutting restriction enzyme that yields blunt ends. The resulting exposed cDNA was divided into two portions, and each was ligated with a different cDNA adaptor supplied with the PCR-Select™ kit. After an initial hybridization with excess control cDNA, a second hybridization was performed by combining the two primary exposed samples together without denaturing. An additional sample of denatured control cDNA was added to further enrich for differentially expressed genes, then the entire population of molecules was subjected to PCR amplification using primers that anneal to the cDNA adaptor ends. A second PCR amplification was then performed using nested primers to further reduce any background produced during the initial PCR amplification, and to enrich for differentially expressed sequences.

---

*UNM/ITRI Graduate Student

The results of the secondary PCR amplification using subtracted exposed cDNA (Lane 1) and unsubtracted exposed cDNA (Lane 2) are shown in Figure 1, and clearly show an enrichment of differentially expressed products following subtraction. The resulting enriched products were excised from the gel, electroeluted, and ligated into the pCR™ II cloning vector using the TA Cloning® Kit (Invitrogen, San Diego, CA). Following bacterial transformation and blue/white screening, 15 unique gene fragments were identified based upon restriction fragment patterns and preliminary DNA sequence information.

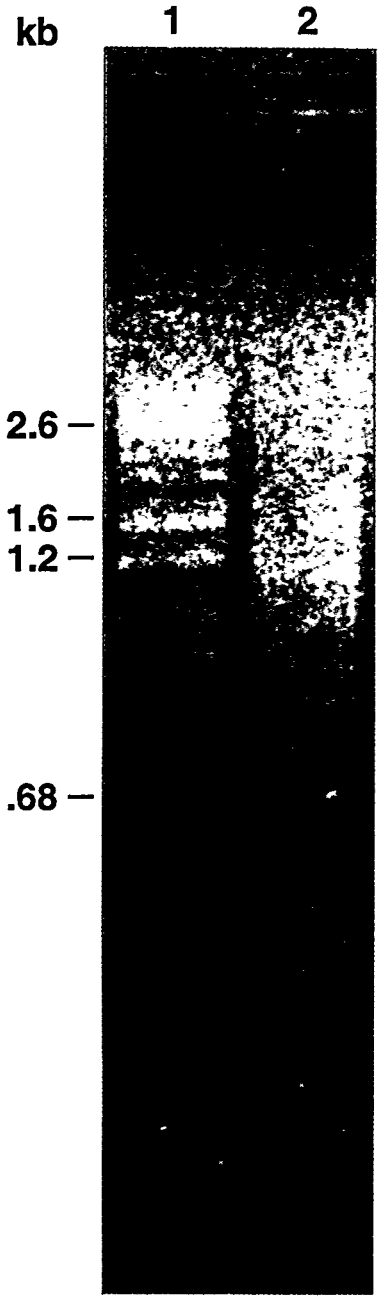

Figure 1. Amplification of TGF-β inducible transcripts in normal human keratinocytes using the PCR-Select™ subtraction hybridization technique. Lane 1: Secondary PCR products produced from subtracted, exposed cDNA. Lane 2: Secondary PCR products produced from unsubtracted, exposed cDNA. 2.0% agarose/EtBr gel.

PCR primers have now been designed for each clone and will be used in a Reverse Transcriptase-PCR assay to confirm that these transcripts are induced by TGF-β. Further efforts will focus on obtaining full-length cDNAs and sequence information of up-regulated genes and determining their function.

Information from this study will further characterize the process by which TGF-β mediates its effects on growth and differentiation of normal epithelial cells, and may provide insight into how these controlling mechanisms differ in human cancers.

(Research sponsored by the Office of Health and Environmental Research, U.S. Department of Energy, under Contract No. DE-AC04-76EV01013.)

LOSS OF DIFFERENTIATION IN THE PHENOTYPICALLY ALTERED PROGENY OF ALPHA-PARTICLE-EXPOSED NORMAL HUMAN BRONCHIAL EPITHELIAL CELLS

Christopher H. Kennedy, Johannes Tesfaigzi, and John F. Lechner

Pulmonary deposition of α-particle-emitting radon daughters is estimated to account for 10% of all lung cancer deaths in the United States (Lubin, J. H. *et al. J. Natl. Cancer Inst. 87*: 817, 1995). However, the nature and timing of early (preneoplastic) genetic alterations in radon-associated lung cancer are still relatively uncertain. Exposure of normal human bronchial epithelial (NHBE) cells to fractionated low doses (0.33–0.67 Gy) of ^{238}Pu α-particles (total dose = 2–4 Gy) results in the formation of foci of phenotypically altered cells (PACs) (Kennedy, C. H. *et al. Carcinogenesis 17*: 1671, 1996). Although these PAC cultures are not immortalized, they do exhibit an extended population-doubling potential relative to unexposed NHBE cells. Lechner, J. F. *et al.* (*Carcinogenesis 5*: 1697, 1984) first observed this phenomenon in NHBE cells exposed to nickel sulfate. Further, they found that PACs show reduced responsiveness to agents (*i.e.*, fetal bovine serum and 12-O-tetradecanoylphorbal-13-acetate [TPA]) that induce squamous terminal differentiation in NHBE cells. The purpose of this investigation was to determine if altered responsiveness to differentiation-inducing signals is also a feature of radiation-induced PACs. To this end, we have cultured NHBE cells and PACs and examined the expression of three different genes involved in differentiation.

Expression of small proline-rich protein (SPR1), a 20 kD protein recognized as a molecular marker of squamous terminal differentiation in tracheobronchial cells (Tesfaigzi, J. *et al. Biochem. Biophys. Res. Comm. 172*: 1304, 1990), is induced by TPA (An, G. *et al. J. Biol. Chem. 268*: 10977, 1993) and down-regulated by retinol (An, G. *et al. J. Cell. Physiol. 157*: 562, 1993). The protein p21 (WAF1/CIP1), a downstream effector of p53 that mediates growth arrest in the G_1 phase of the cell cycle, is also upregulated by differentiation-inducing agents and is tightly coupled to early markers of differentiation (Steinman, R. A. *et al. Oncogene 9*: 3389, 1994). The protein product of the bcl-2 oncogene inhibits apoptosis and is believed to prolong the life span of terminally differentiated epithelial cells (Lu, Q. L. *et al. Hum. Pathol. 27*: 102, 1996). Further, the bcl-2 protein may play a role in the early stages of tumorigenesis. Because retinoic acid-deficiency induces squamous terminal differentiation in bronchial epithelial cells (Love, J. M. and L. J. Gudas. *Curr. Opin. Cell Biol. 6*: 825, 1994), we examined the effect of retinol on the following: (1) expression of SPR1 and p21 in NHBE cells and PACs at the mRNA level by northern analysis; and (2) expression of SPR1 and bcl-2 in NHBE cells and PACs at the protein level by western analysis.

NHBE cells from a nonsmoking, 15 y-old male were purchased (Clonetics, San Diego, CA), cultured, and exposed to fractionated doses of ^{238}Pu α-particles (total dose = 0 Gy for sham-exposed, 2 Gy for low dose group, and 4 Gy for high dose group) as described previously (Kennedy *et al.*, 1996). One unexposed control (NHBE [passage 3, cultured only on FNC-coated plastic petri dishes]), two sham-exposed controls (U11 [passage 5] and U14 [passage 8]), two PAC cultures from the low dose group (L6 [passage 6] and L41 [passage 7]), and two PAC cultures from the high dose group (H6 [passage 6] and H9 [passage 8]) were cultured in the absence of retinoic acid for 6 d prior to harvesting.

Tri Reagent™ (Molecular Research Center, Inc., Cincinnati, OH) was used (2 mL per 100 mm dish of cells) to prepare cell lysates. Total RNA was prepared by extracting the lysate with chloroform (Chomczynski, P. *BioTechniques 15*: 532, 1993). RNA was precipitated from the aqueous layer with isopropanol and resuspended in RNase-free H_2O. The concentration and purity were calculated by absorption at 260 and 280 nm, respectively, and only preparations with a ratio of greater than 1.7 were

used. Total cellular RNA (10 μg) was electrophoresed on a denaturing formaldehyde agarose gel, blotted onto a Zeta-Probe GT membrane (Bio-Rad, Hercules, CA), and hybridized under the conditions described by Church, G. M. and W. Gilbert (*Proc. Natl. Acad. Sci. 81*: 1991, 1984) with cDNA probes labeled with [^{32}P]dCTP (Amersham, Arlington Heights, IL). The membranes were then subjected to autoradiography using Biomax MR film (Kodak, Rochester, NY). The intensity of autoradiographic bands was quantitated by densitometry using the Collage™ image analysis software (Fotodyne Inc., Hartland, WI).

For protein preparation, cells were harvested by the method of Elliget, K. A. and J. F. Lechner (In *Culture of Epithelial Cells* [R. I. Freshney, ed.], Wiley-Liss, New York, p. 181, 1992). Cells (5×10^5) were washed twice with PBS, then lysed with 10 mM Tris/HCl (pH 7.8), 150 mM NaCl, 1.5 mM MgCl2, and 1% NP-40 by vortexing for 3 min. Cytosolic proteins were separated from membrane and nuclei by centrifugation at 2,000 *g* for 5 min. The whole volume of supernatant was mixed with sample buffer, boiled for 5 min and fractionated on a 12.5% SDS-PAGE. Western blot analysis was performed as described previously (Tesfaigzi, J. *et al. BioTechniques 17*: 268, 1994). Staining the blot with Ponceau S (Sigma, St. Louis, MO) verified that all lanes contained the same amounts of protein. The preparation and specificity of antibodies to SPR1 have been described (Tesfaigzi J. *et al. J. Cell. Physiol. 164*: 571, 1995).

Figure 1 shows the mRNA levels of Waf1, GAPDH, and SPR1 detected by Northern analysis in unexposed NHBE cells and PACs. The ratio of Waf1 mRNA to GAPDH mRNA was calculated as follows based on densitometry measurements: NHBE, 0.50; H9, 0.81; H6, 0.62; and U14, 0.84. Thus, Waf1 mRNA levels are similar for both unexposed controls and the two PACs analyzed, suggesting that Waf1 expression is not affected in PACs. However, Figure 1 does show a significant difference in SPR1 mRNA expression between unexposed NHBE cells and the PACs. The ratio of SPR1 mRNA to GAPDH mRNA was calculated as follows based on densitometry measurements: NHBE, 0.64; H9, 0.19; H6, 0.0; and U14, 0.33. These data indicate that SPR1 mRNA levels are increased in unexposed NHBE cells (NHBE and U14), while the PACs are either unaffected (H6) or only mildly induced (H9) when these cells are cultured in retinoic acid-free medium. This phenomenon was also detected at the protein level by western analysis (Fig. 2). However, SPR1 protein levels were only detected in one sham-exposed control (U14). No SPR1 protein was detected in any other unexposed or PAC samples. Because U14 was at a higher passage number than the other two controls, this difference in SPR1 protein expression may indicate increased sensitivity of this particular culture to the induction of differentiation in the absence of retinoic acid.

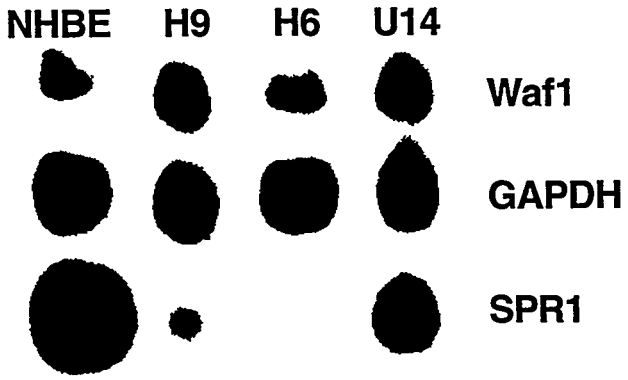

Figure 1. Waf1, GAPDH, and SPR1 mRNA levels in unexposed NHBE cells and PACs cultured in the absence of retinoic acid.

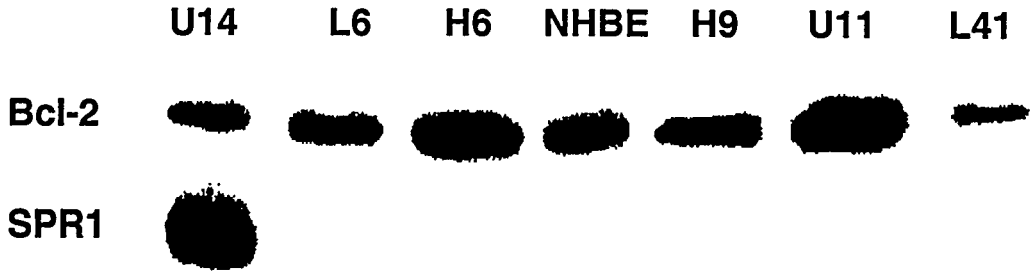

Figure 2. Bcl-2 and SPR1 protein levels in unexposed NHBE cells and PACs cultured in the absence of retinoic acid.

Figure 2 also shows the levels of bcl-2 protein expression in unexposed NHBE cells and PACs. The levels of bcl-2 are similar for both the unexposed controls and the four PACs analyzed. These data suggest that bcl-2 expression is not elevated in α-radiation-induced PACs.

Together, the data presented herein indicate that PACs do not respond in the same manner as NHBE cells with regard to differentiation-inducing signals. Expression of SPR1 mRNA is upregulated in NHBE cells and sham-exposed controls in the absence of retinoic acid, whereas no increase in expression is detected in PACs. Further, the data suggest that the uncoupling of SPR1 expression from retinoic acid regulation in PACs occurs via a mechanism that is independent of both Waf1 and bcl-2 expression. Because altered control of differentiation is a hallmark of transformed cells, elucidation of the mechanism by which PACs fail to induce SPR1 following retinoic acid deprivation should provide insight into the early genetic changes during the development of radon-associated lung cancer.

(Research sponsored by the Office of Health and Environmental Research, U.S. Department of Energy, under Contract No. DE-AC04-76EV01013.)

CONCURRENT FLUORESCENCE *IN SITU* HYBRIDIZATION AND IMMUNOCYTOCHEMISTRY FOR THE DETECTION OF CHROMOSOME ABERRATIONS IN EXFOLIATED BRONCHIAL EPITHELIAL CELLS

Robin E. Neft, Minerva M. Murphy, Lauren A. Tierney, Steven A. Belinsky, Marshall Anderson**, Geno Saccomanno**, Frank D. Gilliland***, Richard E. Crowell****, and John F. Lechner*

Lung cancer is the leading cause of cancer-related deaths in the U.S. for both men and women (Boring, C. *et al. CA Cancer J. Clin. 43*: 7, 1993). The prognosis for these patients is dependent on the stage of the tumor at the time of clinical diagnosis. It has been shown that several years before clinical development of lung cancer, high-risk individuals exfoliate cells exhibiting moderate to marked atypia in their sputum (Saccomanno, G. *et al. Cancer 33:* 256, 1974). However, the diagnostic sensitivity and specificity of this procedure vary due to sample preparation and cytologic interpretation that is based on subjective morphological changes. Molecular cytogenetic and immunological techniques, such as fluorescence *in situ* hybridization (FISH) and immunocytochemistry, may improve the value of sputum cytology as a screening tool for the early detection of lung cancer.

In this study, the presence of trisomy 7 in cells from sputum was assayed by FISH. Trisomy 7 was chosen as a molecular cytogenetic marker because it is common in lung tumors (Matturri, L. and Lavezzi, A. M. *Eur. J. Histochem. 38*: 53, 1994) and has been detected in the tumor-free margins of some resected lung tumors (Crowell, R. E. *et al. Cancer Epidemiol. Biomarkers Prev. 5*: 631, 1996) and in the bronchial epithelial cells of smokers with and without lung cancer (Lee, J. S. *et al. Cancer Res. 47*: 6349, 1987). Therefore, trisomy 7 may serve not only as a molecular marker of lung cancer, but as a prognostic marker as well.

Cytokeratin staining of exfoliated bronchial epithelial cells identifies upper and lower airway epithelial cells. In addition, lack of cytokeratin aids in the identification of nonepithelial cells such as macrophages and neutrophils and allows the rapid identification of cells to examine for chromosome aberrations.

The purpose of this study was to develop a method to detect chromosome aberrations relevant to lung cancer in exfoliated bronchial epithelial cells in sputum using FISH and immunocytochemistry.

Five consecutive deep lung sputum samples were collected from a patient with known primary bronchogenic adenocarcinoma. Approximately 30 mL of sputum were expectorated into a specimen container filled with Saccomanno Fixative™ (Shandon Lipsaw, Inc., Pittsburgh, PA).

The five samples were processed using the accepted Saccomanno method for processing and evaluation of pulmonary specimens (Saccomanno, G. *et al. Acta Cytol. 7*: 305, 1963). Once adequacy was assessed, the five specimens were pooled into one aliquot. Slides were prepared for FISH/ immunocytochemistry by using a modified cytocentrifuge Megafunnel™ slide procedure for the processing of pulmonary samples (Shandon Lipshaw, Inc.).

---

*UNM/ITRI Graduate Student

**St. Mary's Hospital and Medical Center, Cancer Research Institute, Grand Junction, Colorado

***New Mexico Tumor Registry and Department of Medicine, University of New Mexico, Albuquerque, New Mexico

****Pulmonary Department, University of New Mexico, and Veterans Administration Medical Center, Albuquerque, New Mexico

Microscope slides were denatured at 75°C in 70% formamide for 5 min according to manufacturer's instructions (Vysis, Downers Grove, IL). Slides were then dehydrated, successively, in 70, 85, and 100% ethanol for 1 min each. The cells were hybridized with 2 μL of SpectrumOrange™-labeled alpha satellite probe for the centromere of chromosome 7 (CEP® 7, Vysis) overnight, in a humidified chamber, at 37°C. Following hybridization, the slides were washed successively 3 times in 50% formamide, 2X saline sodium citrate (SSC), and once in 2X SSC/0.1% NP-40 (Vysis) for 10 min each at 45°C and allowed to air dry in the dark.

Hybridized slides were rinsed twice for 5 min each in 2X Dulbecco's phosphate-buffered saline (DPBS) with 0.1% Brij (Sigma), then washed for 30 min in the same buffer. The slides were incubated with a 1:400 dilution of anti-human pancytokeratin monoclonal antibody (Sigma, clones C-11, PCK-26, CY-90, Ks-1A3, M20, A53-B/A2) in 1X DPBS/0.2% bovine serum albumin (BSA) (Sigma) for 1 h at 37°C (Tierney, L. A. *et al. J Histotechnol.,* in press). The slides were then incubated with a 1:128 dilution of FITC-conjugated sheep anti-mouse IgG (Sigma) in 1X DPBS/0.2% BSA for 30 min at 37°C. Finally, the slides were counterstained with 10 μL of DAPI (1000 ng/mL, Vysis).

The slides were viewed with an Olympus BX60 fluorescence microscope equipped with a DAPI/FITC/TRITC triple bandpass filter (Chroma Technology, Brattleboro, VT). Use of this filter allows the simultaneous viewing of red, green, and blue fluorophores.

Airway epithelial cells from a lung cancer patient exhibiting trisomy 7 showed bright green cytoplasm, three fluorescent FISH signals, and a DAPI counterstained nucleus. Using this technique, polyploid neoplastic cells with high nucleus/cytoplasm ratios were easily detected in this sputum sample. Oral squamous epithelial cells were identified and could be distinguished from airway epithelial cells by characteristic morphology and amount of FITC-labeled cytokeratin in the cytoplasm. Neutrophils were identified by the lack of FITC staining and segmented nuclei.

The results of this study indicate that concurrent use of FISH and immunocytochemistry on sputum samples will facilitate the identification of epithelial cells with numerical chromosome aberrations. Although immunocytochemistry has been performed on sputum, to our knowledge this is the first study to combine immunocytochemistry and FISH. This procedure is simple and rapid, involving hybridization with a commercially available FISH probe on day 1, post-hybridization washes, and FITC staining on day 2. A fluorescence microscope with a triple bandpass filter readily identifies epithelial cells containing FISH signals. In addition, using this procedure, other molecular cytogenetic and immunologic markers present in malignant cells might be detected in sputum. Molecular and immunologic markers may provide a more objective means of identifying malignant or pre-malignant cells and may help to reduce the problems associated with sputum cytology as a diagnostic and predictive tool.

(Research sponsored by the U.S. Department of Energy under Contract Nos. DE-AC04-76EV01013 and DE-FG02-90ER60939, and NIH SPORE Grant, Contract No. 1-P50-CA8184, Johns Hopkins University.)

VII. THE APPLICATION OF MATHEMATICAL MODELING TO RISK ESTIMATES

A GENOMIC-INSTABILITY-STATE MODEL FOR NEOPLASTIC TRANSFORMATION OF CELLS BY HIGH-LET RADIATION

Bobby R. Scott

A current trend in cancer risk assessment is the use of mechanistic models. The purpose of the present research was to develop a mechanistic model for neoplastic transformation of cells by high-LET ionizing radiations, such as fission neutrons and alpha particles, applicable to low doses and dose rates.

Unlike alpha particles, which produce biological effects mainly via highly clustered secondary electrons arising through ionization, neutrons, through their atomic interactions, produce gamma photons, secondary electrons, protons, and can produce heavier charged particles depending on their energy. Thus, to study neutron radiobiological effects is to study effects of combined exposure.

Neoplastic transformation studies conducted *in vitro* have demonstrated that exposure of cells to low doses of high-LET radiations, such as fission neutrons, at a low rate, can lead to more transformants per survivor than the same dose delivered at a high rate (i.e., an inverse dose-rate effect). An inverse dose-rate effect has also been observed for lung cancer induction in miners by alpha radiation from inhaled radon daughters. It has been assumed by some that the mechanism responsible for the inverse dose-rate effect for neoplastic transformation is the same mechanism responsible for the inverse dose-rate effect for lung cancer induction in miners (Elkind, M. M. *Int. J. Radiat. Biol. 66*: 649, 1994). A new mechanistic model called NEOTRANS1 (pronounced "neotrans one") was developed to explain the inverse dose-rate effect for neoplastic transformation *in vitro*, and results of its application to high-LET data are used to examine whether inverse dose-rate effects for cell transformation and lung cancer induction are due to the same mechanism. NEOTRANS1 is a genomic-instability-state (GIST) model.

GIST models can be developed on the premise that differing states of genomic instability arise in mammalian cells from radiation-induced DNA damage, and states of instability can lead to various outcomes, including gene-regulated arrest at cell-cycle checkpoints (to facilitate repair of damage); apoptosis (programmed cell death which selectively eliminates cells with problematic genomic instability); and neoplastic transformation (which arises spontaneously because of persistent, problematic, genomic instability).

Like GIST models in general, NEOTRANS1 is kinetic and includes effects of genomic damage accumulation (dose-rate dependent), DNA repair during cell-cycle arrest (i.e., repair of subtransformation damage), DNA misrepair (nonlethal repair errors), and spontaneous transformation of daughter cells with persistent-problematic genomic instability. Cell killing and neoplastic transformation are assumed to be statistically independent. Thus, it is unnecessary to model cell killing when data for neoplastic transformants per surviving cell are available. The model presented here therefore does not have any cell-killing pathways.

With NEOTRANS1, two broad classes of cellular radiosensitivity have been considered: (1) hypersensitive cells and (2) resistant cells. In addition to a stable genome, four types of genomic instabilities have been considered. Normal-minor instability, which is associated with normal cell function and normal genome status, is presumed to be responsible for the experimentally demonstrated (Miller, R. C. *et al. Radiat. Res. 130*: 129, 1992) and theorized (Brenner, D. J. *et al. Radiat. Res. 133:* 365, 1993) sensitive stages of the cell cycle for transformation. Transient-minor instability is associated with toxicant-induced genomic damage that is fully repairable (without any significant errors). Transient-problematic instability is associated with genomic damage (subtransformation damage) that may sometimes be misrepaired (repair errors). The misrepair leads to persistent-problematic instability (e.g.,

point mutation, deletion, loss of a tumor suppresser gene, etc.) that can be passed to progeny, and thereby significantly increase their potential for spontaneous neoplastic transformation.

Genomic instability states associated with NEOTRANS1 and state transitions related to damage accumulation, repair (i.e., correct repair), and misrepair are presented in Figure 1. Products αc account for accumulation of subtransformation damage, where c is the instantaneous dose rate (assumed constant during exposure), and the αs are positive parameters that depend on the type of radiation and type of cell. Parameters μ (which are positive) account for correct repair of subtransformation damage. Parameters η (which are positive) account for misrepair of subtransformation damage that leads to persistent-problematic genomic instability. Cells with transient genomic instability are assumed to be arrested at cell cycle checkpoints until subtransformation damage is fully and correctly repaired or until after persistent-problematic genomic instability arises from misrepair. Progeny of cells with persistent-problematic genomic instability are assumed to have a relatively high, follow-up time-dependent probability of undergoing spontaneous neoplastic transformation. Progeny of other cells are presumed to have negligible probability of undergoing spontaneous neoplastic transformation.

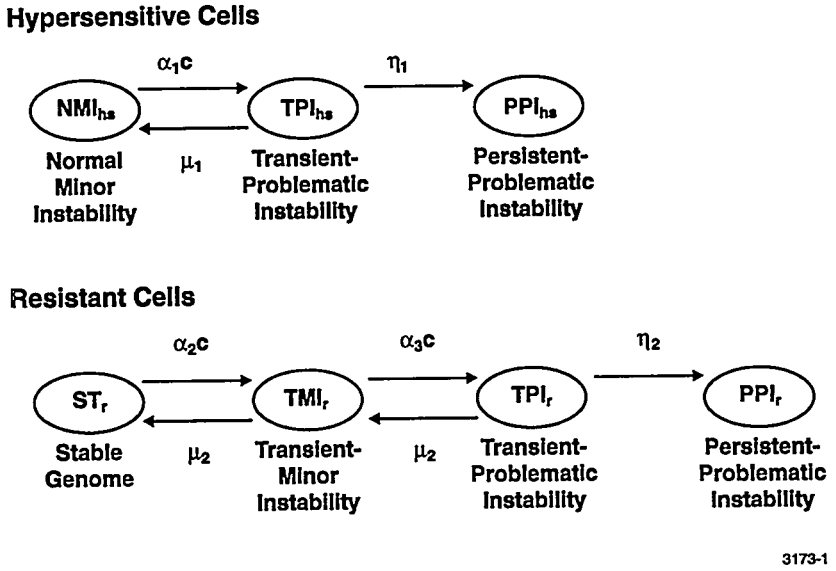

Figure 1. NEOTRANS1 model genomic instability states and transitions for hypersensitive and resistant cells. Model parameters are explained in the text. For hypersensitive cells, a single damage step is required for the production of transient-problematic instability, while for resistant cells, two damage steps are required.

NEOTRANS1 was applied to data for neoplastic transformation of C3H 10T1/2 cells by fission neutrons (Balcer Kubiczek, E. L. *et al. Int. J. Radiat. Biol. 54*: 531, 1988; Hill, C. K. *et al. Nature 298*: 67, 1982) and by alpha particles (Bettega, D. *et al. Radiat. Res. 131:* 66, 1992). Implication of the model for other high-LET radiations (e.g., heavy ions used in studies related to radiation hazards in space) were considered. Key results obtained are summarized below.

NEOTRANS1 was found to account for key experimental observations obtained *in vitro* following exposure of C3H 10T1/2 cells to high-LET radiations (fission neutrons and alpha particles), including the neutron inverse dose-rate effect and the complex dose-response curve shape observed after exposure to alpha radiation when delivered at a high rate (see Fig. 2). With NEOTRANS1, the inverse dose-rate effect for neoplastic transformation is attributed to DNA-repair errors associated with a postulated fast (repair half-time of about 3.5 min), error-prone; repair process operating in a hypersensitive subset of

cells (1.4% of C3H 10T1/2 cells). The fast repair process appears to be inactivated by very high-LET (> 130 keV/μm) radiation and by the fission neutron source used by Balcer-Kubiczek *et al.* (1988).

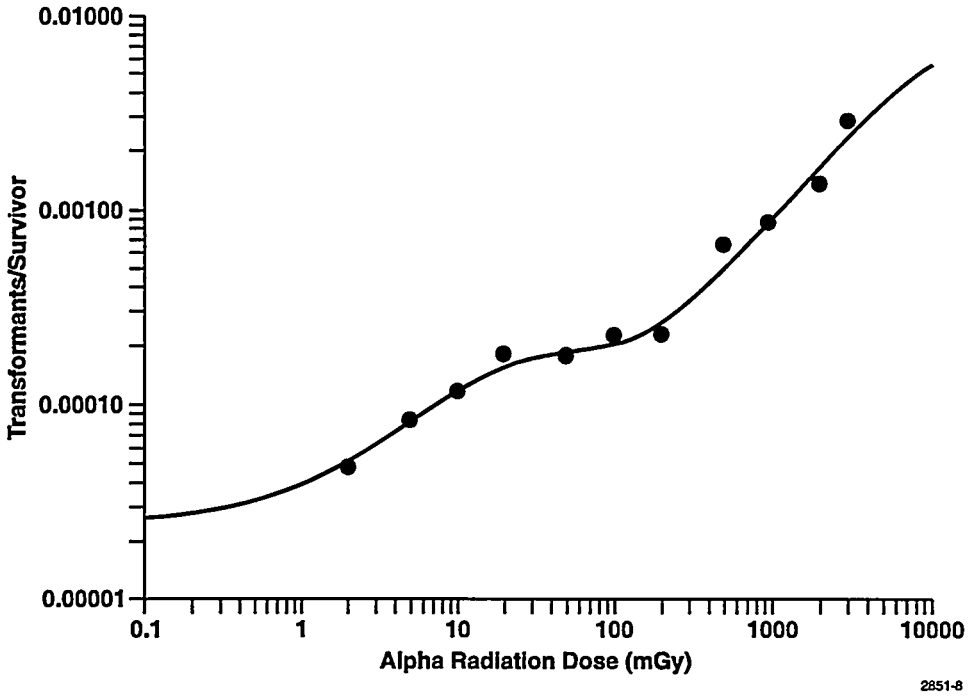

Figure 2. Use of NEOTRANS1 to simulate transformants/survivor for neoplastic transformation of C3H 10T1/2 cells by 4.3 MeV alpha particles from ^{244}Cm, based on data from Bettega *et al.* (1992). The plateau at about 100 mGy is modeled as being due to hypersensitive cells (1.4%) and to a competition between correct repair and misrepair of subtransformation damage associated with transient-problematic genomic instability.

Just what repair process is operating in hypersensitive C3H 10T1/2 cells with a repair half-time of about 3.5 min is unclear. However, a component of DNA double-strand break repair has been reported to have the same half-time (Cerdervall, B. *et al. Radiat. Res. 41*: 23, 1995). Thus, a double-strand break in a key gene may be the initial lesion responsible for the transient-problematic genomic instability. Nonlethal misrepair of the double-strand break would then be responsible for the persistent-problematic genomic instability. Transcription-coupled repair is a relatively fast process, and a form of this type of repair may be operating in hypersensitive cells. The corresponding repair process in resistant C3H 10T1/2 cells appears to be a relatively slow process (repair half-time estimated to be 2.3 h) with misrepair being about 25-fold less likely than for the fast repair process for hypersensitive cells.

The inverse dose-rate effect for *in vitro* neoplastic transformation of C3H 10T1/2 cells by high-LET radiation is explained based on errors associated with a fast repair process (which appears to be carried out in much less than an hour). Therefore, the inverse dose rate effect observed *in vitro* at relatively high dose rates (0.1–100 mGy/min) after exposure of cells to high-LET radiation is likely not the same mechanism responsible for the induction of lung cancer in miners exposed via inhalation, over years, to alpha radiation from radon daughters at very low average dose rates. It is suggested that age-related changes in the lung (e.g., reduced DNA repair efficiency with age) are more likely responsible for the inverse dose-rate effect seen in miners exposed to radon daughters.

(Research sponsored by the Assistant Secretary for Defense Programs, U.S. Department of Energy, under Contract No. DE-AC04-76EV01013.)

INTAKE DISTRIBUTION FOR INHALED PLUTONIUM-238 DIOXIDE FOR VARIOUS CUMULATIVE EXPOSURE SCENARIOS

Bobby R. Scott, Mark D. Hoover, and George J. Newton

At some nuclear facilities around the world, workers routinely encounter airborne high-specific-activity (HSA) alpha-emitting (αE) particles. Such particles have specific activities greater than that of ^{239}Pu (i.e., $> 2.26 \times 10^3$ MBq/g) (Scott, B. R. *et al. Radiat. Prot. Dosim.*, in press). An example is $^{238}PuO_2$ particles. The current exposure limitation system of the International Commission on Radiological Protection (ICRP) assigns intake via the respiratory tract based on the expected amount of radioactivity deposited there. The expected intake is calculated based on the average in-air concentration of radioactivity and the amount of air expected to have been inhaled during an exposure episode. Thus, for any amount of measured airborne radioactivity during an exposure episode, expected intake will be greater than zero when no respiratory protection is used. However, using expected intake as a measure of exposure to HSA-αE particles can unnecessarily and greatly overestimate cancer risk (by wrongly assigning worker's radioactivity intake) when HSA-αE particles are in very low concentrations ($<< 1$ particles per m^3 of air). In such circumstances, it is possible that no airborne HSA-αE particle will be inhaled during a brief stay in a work area where the particles are present. For such cases, a probabilistic characterization of radioactivity intake is needed. With probabilistic intake, the focus is on the distribution of possible intake of radioactivity rather than on the expected intake. The purpose of the research conducted in this study was (1) to develop mathematical tools for evaluating probabilistic intake via inhalation of HSA-αE particles for brief stays in contaminated workplace air; and (2) to use the tools to evaluate the distribution of possible intake of radioactivity for specific exposure scenarios involving $^{238}PuO_2$ particles.

Details on the mathematical tools are presented elsewhere (Scott *et al.*, in press). Presented here are results of applying the mathematical tools to four hypothetical exposure scenarios where 10,000 adult male workers, engaged in light exercise, were at risk for inhaling airborne $^{238}PuO_2$ particles due to unrecognized accidental releases into the workplace atmosphere (i.e., exposure occurred before a continuous air monitor alarm sounded). The four scenarios considered were 1, 2, 4, and 8 derived air concentration hours (DAC-h) of cumulative exposure (for inhalation of Class Y material for which the DAC is 0.3 Bq/m^3), and results are summarized in Table 1. A DAC is obtained by dividing the Annual Limit on Intake (ALI, in Bq) for a radionuclide by the volume of air inhaled by a reference man (2,400 m^3) during a 2,000-h working year. A DAC-h is an exposure at a concentration of 1 DAC for 1 h. Similarly, exposure at a concentration of 0.1 DAC for 10 h also represents 1 DAC-h of cumulative exposure.

A lognormal particle-size distribution (activity median aerodynamic diameter of 5 μm and geometric standard deviation of 2.5), which is recommended for workplace exposures, was used (Bailey, M. R. *Radiat. Prot. Dosim. 53*: 107, 1994). Because of the lognormal size distribution and constraints on the in-air radioactivity concentration, there were more small particles available for inhalation than large particles. The 1, 2, 4, and 8 DAC-h cumulative exposures considered here apply to brief accidental exposures of nuclear workers to in-air radioactivity concentrations of $^{238}PuO_2$ near the DAC. The cumulative exposures would also apply to nuclear workers who were chronically exposed for years at concentrations very much less than the DAC.

In evaluating the distribution of possible intake of radioactivity via inhaled $^{238}PuO_2$, particle *availability* (probability that a particle of interest is contained in a tidal volume of air presented for inhalation) was characterized using the Poisson distribution (Scott *et al.*, in press). Particle

inhalability (probability that a particle presented for inhalation will be inhaled) and particle *deposition probability* (same as deposition efficiency) are based on the Lung Dose Evaluation Program (Jarvis, N. S. *et al. LUDEP 1.0*, NRPB-SR264, National Radiological Protection Board, Chilton, Didcot, 1993). A particle density of 10 g/cm^3 was assumed for PuO_2 (Kotrappa, P. *et al. Health Phys. 22:* 837, 1972).

Table 1

Calculated Distribution of Intake (in Bq) via Inhalation of $^{238}PuO_2$ for 10,000 Adult Males Engaged in Light, Work-related Exercise for Different DAC-h Exposure Scenarios (Scott *et al.*, in press)[a]

Intake (Bq)	Cases of Intake Among 10,000 Hypothetical Workers by Exposure Scenario			
	1 DAC-h	2 DAC-h	4 DAC-h	8 DAC-h
0	9,982	9,957	9,911	9,831
> 0–0.1	12	33	68	132
> 0.1–1	2	3	4	6
> 1–10	1	2	3	7
> 10–100	3	4	9	14
> 100–1,000	0	0	4	8
> 1,000	0	1	1	2
Overall total	10,000	10,000	10,000	10,000
Total with intake	18	43	89	169
Cases < expected[b]	9,995	9,993	9,983	9,972
Cases > expected[b]	5	7	17	28
Cases < ALI	10,000	9,999	9,998	9,996
IOF[c]	555	232	111	59

[a]Population size equals the number of trials used in the Monte Carlo calculations of the intake distribution.

[b]Expected intake based on ICRP method for which the intake for 1, 2, 4, and 8 DAC-h exposures are 0.45, 0.9, 1.8, and 3.6 Bq, respectively.

[c]IOF = intake overestimation factor = (no-intake cases)/(intake cases).

The distribution of possible radioactivity intake was evaluated by the Monte Carlo approach using Crystal Ball software (*Crystal Ball Users Manual*, Version 4, Decisioneering, Inc., Aurora, CO, 1988–1996); 10,000 trials were used, which are the bases for the 10,000 hypothetical workers. The intake overestimation factor (IOF), which represents the number of no-intake cases divided by the number of intake cases (Scott *et al.*, in press), was evaluated. Intake cases differing from those obtained with the ICRP methodology of using expected intake based on DAC-h of exposure and intake cases less than or greater than the ALI were also evaluated.

For the 8 DAC-h simulated cumulative exposure, the ALI was exceeded in 4/10,000 workers (due to intake of only a single particle by each of the four workers). For such exposures, intake of more than one particle would be expected to occur with a probability of essentially zero. The results obtained indicate that, with very low probability ($p = 4/10{,}000$ or 4×10^{-4}), an 8 DAC-h cumulative exposure of adult males undergoing light, work-related exercise could lead to intake exceeding the ALI (i.e., > 600 Bq for inhalation class Y), even though the expected intake, when calculated with the ICRP method, is only 3.6 Bq. Of the four $^{238}PuO_2$ exposure scenarios considered, the 99th percentile value for the intake distribution exceeded zero only for the simulated 8 DAC-h cumulative exposure. Also, for the same scenario, with use of the ICRP method of evaluating intake, one would assign 3.6 Bq of radioactivity intake to each of the 10,000 workers when 9,831 of the workers had no intake of radioactivity. Thus, when the ICRP approach to evaluating intake is used, these 9,831 workers would be unnecessarily assigned added cancer risk that did not occur.

The results indicate that for a brief exposure at or near the DAC, respiratory tract intake, evaluated based on DAC-h of exposure, can be considerably overestimated (with high probability) or underestimated (with low probability) for HSA-αE aerosols such as $^{238}PuO_2$ in circumstances of probabilistic intake. For such cases, with very high probability, no HSA-αE particle intake would be expected to occur, and with very low probability, particle intake (most likely a singe particle) would be expected to occur. Thus, for probabilistic intake of HSA-αE particles, it is preferable to evaluate the probability distribution of possible intake of radioactivity, rather than the expected intake.

A major outcome of this research is that the distribution of possible intake of radioactivity could be used in characterizing occupational exposure in circumstances where the cumulative exposure to airborne HSA-αE particles is on the order of a few DAC-h or less. A specified percentile of the distribution of possible radioactivity intake could be assigned to a worker as though it were actual intake, then compared to the ALI when limiting exposure. The 99th percentile value of the intake distribution is recommended for radiation protection and exposure limitation considerations. In this case, if the 99th percentile value is found to be zero, then no intake would be assigned even though the expected intake based on the ICRP methodology would exceed zero. Thus, with the use of assigned intake, cancer risks for workers would not be unnecessarily overestimated. In cases where the 99th percentile value exceeded zero, then it is recommended that workers be closely monitored for possible intake of significant radioactivity. In rare cases where bioassay data indicated a significant intake of radioactivity by a given individual and the assigned intake was found to be zero when calculated based on the in-air concentration of radioactivity, then an intake estimate based on the bioassay data should have precedence over the assigned intake.

(Research sponsored by the Albuquerque Operations Office, U.S. Department of Energy, the Carlsbad Area Office, the Secretary for Defense Programs, and the Assistant Secretary for Environment, Safety and Health, under Contract No. DE-AC04-76EV01013.)

VIII. APPENDICES

APPENDIX A

STATUS OF LONGEVITY AND SACRIFICE EXPERIMENTS IN BEAGLE DOGS

Each annual report of the Inhalation Toxicology Research Institute from 1967 (LF-38) through 1987–1988 (LMF-121) included an appendix containing detailed tabular information on all dogs in the life-span studies of inhaled radionuclides and many sacrifice series associated with these studies. In LMF-121, similar kinds of summary tables were also included for dogs in long-term and life-span studies of injected actinides that were conducted at the University of Utah. All dogs remaining alive in the Utah studies were transferred to ITRI on September 15, 1987, where they were maintained and studied for the remainder of their life spans. Responsibility for managing the completion of the Utah life-span studies has been assigned to ITRI. A small team of investigators at the University of Utah and investigators at ITRI are working together to complete the observations and summaries.

Along with other changes made in the regular ITRI Annual Report beginning with Report LMF-126, *Inhalation Toxicology Research Institute Annual Report, 1988–1989*, it was decided that the growing body of detailed information on these studies in dogs would no longer be included. Instead, separate periodic reports are being prepared that contain specific updated information on all ITRI and University of Utah long-term and life-span studies in Beagle dogs. The first three of these reports, entitled *Annual Report on Long-Term Dose-Response Studies of Inhaled or Injected Radionuclides*, were published as Report LMF-128 for 1988–1989, as Report LMF-130 for 1989–1990, and as Report LMF-135 for 1990–1991. These reports described the studies, updated experimental design charts, survival plots, pathology summaries and detailed tabular information on all dogs in a manner consistent with past practices. The most recent report, ITRI-139, was published as the *Biennial Report on Long-Term Dose-Response Studies of Inhaled or Injected Radionuclides*, 1991–1993.

Recognizing that these data are of interest to a limited number of individuals, these reports are provided without charge to individuals requesting them. To obtain these reports, please send a request to:

Director
Inhalation Toxicology Research Institute
P. O. Box 5890
Albuquerque, NM 87185-5890

APPENDIX B

ORGANIZATION OF PERSONNEL AS OF SEPTEMBER 30, 1996

LOVELACE BIOMEDICAL AND ENVIRONMENTAL RESEARCH INSTITUTE
Directors and Officers

R. W. Rubin, PhD, Chairman
J. L. Mauderly, DVM, President
C. H. Hobbs, DVM, Vice President
R. F. Henderson, PhD, Asst. Secretary/Treasurer (non-director)
J. F. Lechner, PhD, Asst. Secretary/Treasurer (non-director)
J. A. Lopez, BSChE, Asst. Secretary/Treasurer (non-director)
R. Conn, MD
N. Corzine
J. Lovelace Johnson
J. Woodard, PhD

INHALATION TOXICOLOGY RESEARCH INSTITUTE

J. L. Mauderly, DVM, Director
C. H. Hobbs, DVM, Associate Director
B. B. Boecker, PhD, Assistant Director for Research
J. F. Lechner, PhD, Assistant Director for Research
J. A. Lopez, BSChE, Assistant Director for Administration

Scientific Groups

- Aerosol Science
  Y. S. Cheng, PhD
- Chemistry and Biochemical Toxicology
  W. E. Bechtold, PhD
- Molecular and Cellular Toxicology
  N. F. Johnson, PhD
- Pathology
  F. F. Hahn, DVM, PhD
- Pathophysiology
  J. M. Benson, PhD

Scientific Programs

- Aerosols
  Y. S. Cheng, PhD
- Applied Toxicology
  C. H. Hobbs, DVM
- Cancer Mechanisms
  J. F. Lechner, PhD
- Chemical Toxicology
  A. R. Dahl, PhD
- Pathogenesis
  J. F. Lechner, PhD
- Radiation Toxicology
  R. A. Guilmette, PhD

Research Support Sections and Units

- Analytical Chemistry
  W. E. Bechtold, PhD
- Animal Care
  D. G. Burt, DVM
- Biomathematics
  B. B. Boecker, PhD
- Chronic Studies
  J. M. Benson, PhD
- Clinic
  B. A. Muggenburg, DVM, PhD
- Clinical Pathology
  F. F. Hahn, DVM, PhD
- Exposure
  E. B. Barr, MSEE
- Histopathology
  F. F. Hahn, DVM, PhD
- Necropsy
  K. J. Nikula, DVM, PhD

RESEARCH STAFF OF THE INHALATION TOXICOLOGY RESEARCH INSTITUTE AS OF SEPTEMBER 30, 1996

Employee	Research Group/Research Support Section
T. A. Ahlert, BS	Chemistry and Biochemical Toxicology
K. R. Ahlert	Chemistry and Biochemical Toxicology
M. L. Allen	Chemistry and Biochemical Toxicology
K. J. Avila, BS	Pathology
S. C. Barnett	Pathology
E. B. Barr, MSEE	Aerosol Science
S. L. Batson, BS	Animal Care
W. E. Bechtold, PhD	Chemistry and Biochemical Toxicology
S. A. Belinsky, PhD	Molecular and Cellular Toxicology
J. M. Benson, PhD	Pathophysiology
M. A. Berry, DVM*	Pathophysiology
D. E. Bice, PhD	Pathology
M. A. Billau, AS	Pathophysiology
L. F. Blair	Pathophysiology
B. B. Boecker, PhD	Biomathematics Section
D. M. Bolton	Animal Care
D. G. Burt, DVM	Animal Care
X. Chen, BS	Aerosol Science
Y. S. Cheng, PhD	Aerosol Science
D. T. Cordaro	Animal Care
P. Y. Cossey, BS	Pathology
G. Curley, Jr.	Molecular and Cellular Biology
A. R. Dahl, PhD	Chemistry and Biochemical Toxicology
F. E. Delgado	Animal Care
J. H. Diel, PhD	Task Force on Life-Span Radiation Toxicity Studies
C. A. Dison	Pathophysiology
K. K. Divine, PhD	Chemistry and Biochemical Toxicology
J. L. DuBoise	Pathology
J. M. Duran	Animal Care
D. C. Esparza, BS	Pathophysiology
B. Fan, PhD	Aerosol Science
G. A. Feather, BS	Aerosol Science
A. F. Fencl, BS	Aerosol Science
G. L. Finch, PhD	Pathophysiology
K. M. Garcia, BA	Pathology
R. B. Garlick	Pathology

Employee	Research Group/Research Support Section
K. G. Gillett, BS	Pathophysiology
W. C. Griffith, Jr., PhD	Biomathematics Section
R. A. Guilmette, PhD	Pathophysiology
D. M. Gurule*	Molecular and Cellular Biology
F. F. Hahn, DVM, PhD	Pathology
H. J. Harms, BS*	Molecular and Cellular Biology
A. M. Holmes	Pathophysiology
T. D. Holmes, BS	Aerosol Science
M. D. Hoover, PhD	Aerosol Science
R. J. Jaramillo, BS	Molecular and Cellular Biology
N. F. Johnson, PhD	Molecular and Cellular Biology
S. E. Jones, DVM	Molecular and Cellular Biology
C. H. Kennedy, PhD	Molecular and Cellular Biology
F. B. Kleinschnitz	Aerosol Science
D. M. Klinge, BS	Molecular and Cellular Biology
Y. N. Knighton	Pathology
D. A. Kracko, BS	Pathology
J. L. Lane, BS	Molecular and Cellular Biology
J. L. Lewis, PhD*	Pathology
S. N. Lucas	Aerosol Science
D. L. Lundgren, PhD	Pathophysiology
A. M. Maestas	Chemistry and Biochemical Toxicology
M. J. Meyer, BS	Chemistry and Biochemical Toxicology
P. A. Mikkelson	Aerosol Science
C. E. Mitchell, PhD	Molecular and Cellular Biology
B. A. Muggenburg, DVM, PhD	Pathophysiology
M. M. Murphy, BS	Molecular and Cellular Biology
A. D. Murrin	Animal Care
R. E. Neft, PhD	Molecular and Cellular Biology
G. J. Newton, BS	Aerosol Science
K. J. Nikula, DVM, PhD	Pathology
M. V. Nysus*	Animal Care
B. Pacheco	Pathology
W. A. Palmisano, PhD	Molecular and Cellular Biology
E. R. Perez*	Animal Care
C. H. Pertab, AS	Pathology
S. E. Phillips, BS	Molecular and Cellular Biology
K. H. Pyon, PhD*	Pathology
J. F. Quintana*	Animal Care

Employee	Research Group/Research Support Section
D. A. Rodgers, PhD*	Pathology
C. G. Romero	Animal Care
E. J. Salas	Pathophysiology
K. A. Schafer, DVM	Pathology
B. R. Scott, PhD	Biomathematics Section
G. G. Scott, MS	Chemistry and Biochemical Toxicology
M. B. Snipes, PhD	Pathophysiology
P. R. Stagg	Chemistry and Biochemical Toxicology
J. A. Stephens	Chemistry and Biochemical Toxicology
D. M. Sugino	Chemistry and Biochemical Toxicology
C. S. Tellez	Molecular and Cellular Biology
J. Tesfaigzi, PhD	Molecular and Cellular Biology
J. R. Thornton-Manning, PhD	Chemistry and Biochemical Toxicology
B. M. Tibbetts, BA	Pathophysiology
L. A. Tierney, DVM	Molecular and Cellular Biology
J. J. Waide, MS	Chemistry and Biochemical Toxicology
Y. Wang, BS	Aerosol Science
S. A. Wardlaw, PhD	Chemistry and Biochemical Toxicology
L. M. Watrin, BS	Molecular and Cellular Biology
R. A. Westhouse, DVM	Pathology
R. K. White, BS	Aerosol Science
J. A. Wilder, PhD	Pathology
D. Yazzie	Aerosol Science
C. C. Ynostroza, AS	Animal Care
H. C. Yeh, PhD	Aerosol Science
T. L. Zimmerman	Aerosol Science
G. J. Zwartz, PhD	Pathophysiology

*Part-time employee

EDUCATIONAL PARTICIPANTS

Name	School/University	ITRI Group/Unit/Section
Summer Student Research Participants		
Anna A. Bogomolets	Albertson College of Idaho, ID	Biomathematics Section
Michelle M. Busch	Colorado School of Mines, CO	Molecular and Cellular Toxicology Group
Kristina Dam	Mount St. Mary's College, CA	Chemical and Biochemical Toxicology Group
Debbie M. Gurule	University of New Mexico, NM	Molecular and Cellular Toxicology Group
Kimberly A. Koller	University of California, San Diego, CA	Molecular and Cellular Toxicology Group
Stephanie R. Konecek	University of Kansas, KS	Molecular and Cellular Toxicology Group
Scott M. Lindquist	University of Minnesota, MN	Aerosol Science Group
Kristine M. Wright	Metropolitan State College, CO	Molecular and Cellular Toxicology Group
Minority Student Research Participant		
Debbie M. Gurule	University of New Mexico, NM	Molecular and Cellular Toxicology Group
Minority High School Student and Teacher Summer Research Program Participants		
Jessica M. Chavez	Rio Grande High School, NM	Molecular and Cellular Toxicology Group
Adrian Guzman	Belen High School, NM	Pathophysiology Group, Clinic Section
Rebecca A. Rae	Manzano High School, NM	Pathophysiology Group
Ruben R. Rostro	Bernalillo High School, NM	Molecular and Cellular Toxicology Group
Francesca D. Sisneros	Manzano High School, NM	Aerosol Science Group
Judith A. Velarde	Rio Grande High School, NM	Aerosol Science Group
Student Research Participants		
Gina Adams	University of New Mexico, NM	Pathophysiology Group
Kuo-Hsi Cheng	Johns Hopkins University, MD	Aerosol Science Group
Jenny Hettema	University of New Mexico, NM	Pathophysiology Group
Vijay Kakumanu	University of New Mexico, NM	Pathophysiology Group
David T. Killough	Texas A&M University, TX	Aerosol Science Group
Alice Kramm	Sandia Preparatory High School, NM	Pathology Group
Rebecca Lee	University of New Mexico, NM	Pathophysiology Group
Jill Lent	University of New Mexico, NM	Pathophysiology Group
John Moore	University of New Mexico, NM	Pathophysiology Group
Tammy Nut	University of New Mexico, NM	Pathophysiology Group
Dan Oakley	University of New Mexico, NM	Pathophysiology Group
Deani Ohman	University of New Mexico, NM	Pathophysiology Group
Jenny Schlife	University of New Mexico, NM	Pathophysiology Group
Nancy Stafford	University of New Mexico, NM	Pathophysiology Group

Name	School/University	ITRI Group/Unit/Section
Student Employees - 1996		
Christopher C. Duran	University of New Mexico	Property Management Unit
Monique V. Nysus	University of New Mexico	Animal Care Unit
Elma R. Perez	University of New Mexico	Animal Care Unit
J. Fred Quintana	University of New Mexico	Animal Care Unit
Andrew D. Szydlowski	University of New Mexico	Facility Operations and Maintenance Section
UNM/ITRI Graduate Students		
Xuemang Chen		
Mark J. Meyer		
Shawna M. Smith		
Deborah S. Swafford		
Lauren A. Tierney, DVM		
Yansheng Wang		
Purdue/ITRI Experimental Pathology ProgramGraduate Students		
Susan E. Jones, DVM		
Kenneth A. Schafer, DVM		
Richard A. Westhouse, DVM		
Postdoctoral Fellows		
D. David S. Collie, BVM&S, PhD		
Kevin K. Divine, PhD		
Bijian Fan, PhD		
Teresa A. Liberati, DVM		
Kee H. Pyon, PhD		
Sarah A. Wardlaw, PhD		
Gordon J. Zwartz, PhD		
UNM/ITRI Pulmonary Epidemiology and Toxicology Training Program Participants		
Kee H. Pyon, PhD		
Darrell A. Rodgers, PhD		
Julie A. Wilder, PhD		

PROGRAM AND PROJECT TITLES	SPONSOR*	COORDINATOR
BRUCE B. BOECKER, ASSISTANT DIRECTOR		
Radiation Toxicology – R. A. Guilmette, Program Manager		
INSRP/BEES Panel	DOE/BNL	M. D. Hoover
Effective Dose from Inhaled Nuclear Energy Materials	DOE/OHER	R. A. Guilmette
Dose-Response Relationships for Inhaled Radionuclides	DOE/OHER	B. A. Muggenburg
Radiation Dose and Injury to Critical Cells from Radon	DOE/OHER	N. F. Johnson
Toxicity of Injected Radionuclides – Utah Effort	DOE/OHER	S. C. Miller
Statistical Analysis of Data from Radiobiologic Animal Studies	DOE/OHER	W. C. Griffith
Improved Exposure Assessment Using ^{210}Pb Measurements for Epidemiologic Studies	DOE/OHER	R. A. Guilmette
Joint USNRC/Commission of the European Communities	DOE/SNL	B. R. Scott
Determination of the Effects of Occupational Exposure to Radiation	DOE/UP	B. B. Boecker
p53 Protein Expression as a Dosimeter for Genotoxicity	NIH/NIEHS	N. F. Johnson
The Canine as a Model of Human Aging and Dementia	UCI	B. A. Muggenburg
Carcinogenicty of Depleted Uranium	USAMRDC	F. F. Hahn
CHARLES H. HOBBS, ASSOCIATE DIRECTOR		
Aerosols – Y. S. Cheng, Program Manager		
Underground Aerosol Characterization at the WIPP Site	DOE/AL	G. J. Newton
HQ Health Physics Study	DOE/HQ	M. D. Hoover
Biologically Relevant Properties of Energy Related Aerosols	DOE/OHER	Y. S. Cheng
Dosimetry of Aerosol Drug Delivery	DOE/OHER	Y. S. Cheng
Use of Radon Progeny for In-Place HEPA Filter Testing	DOE/OHER	G. J. Newton
Calibration Hardware Design/Modification of Beryllium Air Monitor	DOE/LLNL	M. D. Hoover
Consulting on the Realtime Beryllium Air Monitoring System	DOE/LLNL	M. D. Hoover
Dissolution of Metal Tritides in Biological Systems	DOE/SNL	Y. S. Cheng
Radiochem Analytical Support	DOE/SNL	G. J. Newton
Design Modifications for BLI Biological Materials	DOE/SNL	Y. S. Cheng
Aerosol Characterization Services on Ultraviolet Lidar Systems	DOE/SNL	Y. S. Cheng
Fluorescent Particle Preparation	DOE/SNL	Y. S. Cheng
Support of the Thermoionics Evaluation Facility	DOE/SNL	M. D. Hoover
Independent Testing and Evaluation of CAM	DOE/WSRC	M. D. Hoover
Y-12 Radiological Protection Program	DOE/Y-12	M. D. Hoover
Study for the Determination of Respirable Particulates in Bulk Polyacrylates	IPA	E. B. Barr
Aerosol Therapy for Mycobacterium Tuberculosis Infection	UNM	Y. S. Cheng

PROGRAM AND PROJECT TITLES	SPONSOR*	COORDINATOR
Characterization of Emissions from Heaters Burning Leaded Diesel in Unvented Tents	USAMRDC	H. C. Yeh
Penetration Test for Millipore AW19 Filter	WHC	M. D. Hoover
Applied Toxicology – C. H. Hobbs, Program Manager		
Determination of the Toxicity of Inhaled Chlorine, Ammonia, and Hydrogen Sulfide	API	J. M. Benson
Determination of *In Vitro* Fiber Solubility	Dr. David Bernstein	N. F. Johnson
Combined Exposure, Plutonium – Cigarette Smoke	DOE/DP	G. L. Finch
Combined Exposure, Plutonium – Beryllium	DOE/DP	G. L. Finch
Combined Exposure, Plutonium – X Ray	DOE/DP	D. L. Lundgren
Combined Exposure, Plutonium – Chemical Carcinogen	DOE/DP	D. L. Lundgren
Combined Exposure, Radiation – Radiation/Fiber	DOE/DP	J. M. Benson
Chronic Beryllium Disease Among Beryllium-Exposed Workers	DOE/HQ	M. D. Hoover
ER Projects Assessment Council	DOE/LANL	C. H. Hobbs
Evaluation of Bioavailability of Nickel Compounds	EPRI	J. M. Benson
Effects of Physical/Chemical HMs on Inflammatory and Proliferative Response Induced in the Lung	IPA	R. F. Henderson
Two-Year Repeated Inhalation	IPA	J. M. Benson
Evaluation of Dust Monitors	IPA	E. B. Barr
Effects of Ozone on Airway Mucous Cells	MSU	C. H. Hobbs
Pharmacokinetics of Mikasome	NXP	M. B. Snipes
Production of Size-Selected Fibers from Bulk Insulation Materials	OC	N. F. Johnson
Establishment and Validation of a Flow Through *In Vitro* System	OC	N. F. Johnson
Aerosolized Cyclosporine	UP	B. A. Muggenburg
Comparison of Particle Retention	VW	K. J. Nikula
Combined Effects of Radiation and Chemotherapeutic Agents in Mice	WAR	G. L. Finch
JOHN F. LECHNER, ASSISTANT DIRECTOR		
Cancer Mechanisms – J. F. Lechner, Program Manager		
Pre-Malignant Events in Radiation-Induced Lung Cancer	DOE/OHER	J. Tesfaigzi
Lung Cancer in Uranium Miners – Gene Dysfunction	DOE/OHER	J. F. Lechner
Cellular Models of Radiation-Induced Lung Cancer	DOE/OHER	J. F. Lechner
Molecular Mechanisms of Radiation-Induced Cancer	DOE/OHER	J. F. Lechner
Gene Dysfunction in Chemical Induced Carcinogenicity	DOE/OHER	S. A. Belinsky
Identification of Intrinsic Human Genes that Govern Susceptibility to Rn-Induced Cancer	DOE/OHER	W. A. Palmisano
Detection of Molecular Markers to Lung Cancer in Uranium Miners	JHU	J. F. Lechner

PROGRAM AND PROJECT TITLES	SPONSOR*	COORDINATOR
Effect of Modulating DNA Methylation on Lung Cancer	JHU	S. A. Belinsky
RNA Preparations	NCI	J. F. Lechner
Chemical Toxicology – A. R. Dahl, Program Manager		
Dosimetry of Benzene in Bone Marrow	API	W. E. Bechtold
Metabolism of 1,3-Butadiene, Butadiene Monoepoxide and Butadiene Diepoxide by Human and Mouse Liver and Lung Tissue Homogenates	CMA	J. R. Thornton-Manning
Influence of Respiratory Tract Metabolism on Effective Dose	DOE/OHER	J. R. Thornton-Manning
Biological Markers of Human Exposure to Organic Compounds	DOE/OHER	W. E. Bechtold
Mechanisms of Granulomatous Disease from Inhaled Beryllium	DOE/OHER	J. M. Benson
Toxicity and Toxicokinetics of Inhaled Carbonyl Sulfide	DOE/WSRC	A. R. Dahl
Carcinogenicity of Butadiene Diepoxide in Mice and Rats	HEI	R. F. Henderson
S-Phenylcysteine in Albumin as a Benzene Biomarker	HEI	W. E. Bechtold
Disposition of Inhaled Toxicants in the Olfactory System	NIH/NIDCD	J. L. Lewis
Fate of Inhaled Vapors in Rats and Dogs	NIH/NIEHS	A. R. Dahl
Carcinogenicity of Inhalants: A Dosimetric Approach	NIH/NIEHS	A. R. Dahl
Acrylate Nasal Uptake	Rohm Haas	A. R. Dahl
Human Sensitivity to Genotoxic Effects of Butadiene	UTMB	W. E. Bechtold
Measurement of Muconic Acid in Urines of Workers Occupationally Exposed to Benzene	UTMB	W. E. Bechtold
Nitrogen Heterocycles: Metabolic Effect and Toxicity	WSU	J. L. Lewis
Pathogenesis – J. F. Lechner, Program Manager		
Cellular & Biochemical Mediators of Respiratory Tract Disease	DOE/OHER	J. F. Lechner
Role of Immune Responses in Respiratory Diseases	DOE/OHER	D. E. Bice
Evaluation of Pulmonary Immune Responses to Viral Agents	UA	D. E. Bice

* API – American Petroleum Institute
CMA – Chemical Manufacturers Association
DOE/AL – Department of Energy Operations Office, Albuquerque
DOE/BNL – Department of Energy, Brookhaven National Laboratory
DOE/DP – Department of Energy, Defense Programs
DOE/HQ – Department of Energy, Headquarters
DOE/LANL – Department of Energy, Los Alamos National Laboratory
DOE/LLNL – Department of Energy, Lawrence Livermore National Laboratory
DOE/OHER – Department of Energy, Office of Health and Environmental Research
DOE/SNL – Department of Energy, Sandia National Laboratories
DOE/UP – Department of Energy/University of Pittsburgh
DOE/WSRC – Department of Energy, Westinghouse Savannah River Co.
DOE/Y-12 – Department of Energy, Y-12 Plant
EPRI – Electric Power Research Institute
HEI – Health Effects Institute
IPA – Institute of Polyacrylic Absorbents
JHU – Johns Hopkins University
MSU – Michigan State University
NCI – National Cancer Institute
NIDCD – National Institute on Deafness and Communicable Diseases
NIH/NIEHS – National Institutes of Health/National Institute of Environmental Health Sciences
NXP – NeXstar Pharmaceuticals
OC – Owens Corning
UA – University of Arizona
UCI – University of California-Irvine
UNM – University of New Mexico
UP – University of Pittsburgh
USAMRDC – US Army Medical and Research Development Command
UTMB – University of Texas Medical Branch at Galveston
VW – Volkswagen
WAR – Wyeth-Ayerst Research
WHC – Westinghouse Hanford Corporation
WSU – Wayne State University

APPENDIX D

PUBLICATION OF TECHNICAL REPORTS

OCTOBER 1, 1995 – SEPTEMBER 30, 1996

Belinsky, S. A., C. E. Mitchell, K. J. Nikula and D. S. Swafford: Examination of Target Genes Involved in Induction of Lung Cancer by Carbon Black and Diesel Exhaust. *Pulmonary Toxicity of Inhaled Diesel Exhaust and Carbon Black in Chronically Exposed Rats. Part III: Examination of Possible Target Genes*, Research Report No. 68, Health Effects Institute, Cambridge, MA, 1995.

Bechtold, W. E. and J. A. Hotchkiss: Immunoaffinity Chromatography in the Analysis of Toxic Effects Complex Chemical Mixtures. In *HEI Communications-Theoretical Approaches to Analyzing Complex Mixtures*, Vol. 4, pp. 7-16, Health Effects Institute, Cambridge, MA, 1996.

Scott, B. R.: Biology and Radiation Response of the Respiratory System. *Effects of Hot Particles on Selected Organs and Tissues with Recommended Limits*, National Council on Radiation Protection and Measurement Report (submitted).

Task Group of Committee 2, International Commission on Radiological Protection (Members: J. W. Stather, Chairman, M. R. Bailey, A. Bouville, F. T. Cross, K. F. Eckerman, R. A. Guilmette, J. D. Harrison, J. Inaba, R. W. Leggett, H. Metivier, D. Nobke, M. Roy, and D. M. Taylor): Age-dependent Doses to Members of the Public from Intake of Radionuclides: Part 4 Inhalation Dose Coefficients. *Ann. ICRP 25(3-4)*, 1995.

APPENDIX E

ITRI PUBLICATIONS IN THE OPEN LITERATURE PUBLISHED, IN PRESS, OR SUBMITTED BETWEEN OCTOBER 1, 1995 - SEPTEMBER 30, 1996

Anderson, M., S. Sladon, R. Michels, L. Davidson, K. Crowell, II, J. Lechner, W. Franklin and G. Saccomanno: Examination of p53 Alterations and Cytokeratin Expression in Sputa Collected from Patients Prior to Histological Diagnosis of Squamous Cell Carcinoma. *J. Cell Biochem.* (in press).

Bechtold, W. E., N. Rothman, S. N. Yin, M. Dosemici, G. L. Li, Y. Z. Wang, W. C. Griffith, M. T. Smith and R. B. Hayes: Urinary Excretion of Phenol, Cathecol, Hydroquinone, and Muconic Acid by Workers Occupationally Exposed to Benzene. *Occup. Ind. Hyg.* (submitted).

Bechtold, W. E. and M. R. Strunk: S-Phenylcysteine in Albumin as a Benzene Biomarker. *Environ. Health Perspect.* (in press).

Belinsky, S. A., S. K. Middleton, S. M. Picksley, F. F. Hahn and K. J. Nikula: Analysis of the K-ras and p53 Pathways in X-ray-Induced Lung Tumors in the Rat. *Radiat. Res. 145*: 449-456, 1996.

Belinsky, S. A., K. J. Nikula, S. B. Baylin and J-P J. Issa: Increased Cytosine DNA-Methyltransferase Activity is Target Cell Specific and an Early Event in Lung Cancer. *Proc. Natl. Acad. Sci. USA 93*: 4045-4050, 1996.

Belinsky, S. A., K. J. Nikula, S. B. Baylin and J-P Issa: A Microassay for Measuring Cytosine DNA-Methyltransferase Activity During Tumor Progression. *Toxicol. Lett. 82/83*: 335-340, 1995.

Belinsky, S. A., D. S. Swafford, G. L. Finch, C. E. Mitchell, G. Kelly, F. F. Hahn, M. W. Anderson and K. J. Nikula: Alterations in the K-ras and p53 Genes in Rat Lung Tumor. *Environ. Health Perspect.* (in press).

Belinsky, S. A., D. S. Swafford, S. K. Middleton, C. H. Kennedy and J. Tesfaigzi: Deletion and Differential Expression of $p16^{INK4a}$ in Mouse Lung Tumors. *Carcinogenesis* (in press).

Benson, J. M., I. Y. Chang, Y. S. Cheng, F. F. Hahn, C. H. Kennedy, E. B. Barr, K. R. Maples and M. B. Snipes: Particle Clearance and Histopathology in Lungs of F344/N Rats and $B6C3F_1$ Mice Inhaling Nickel Oxide or Nickel Sulfate. *Fundam. Appl. Toxicol. 28*: 232-244, 1995.

Benson, J. M., Y. S. Cheng, B. A. Muggenburg, W. E. Bechtold and F. F. Hahn: Fate of Inhaled Nickel Oxide, Nickel Sulfate, and Nickel Subsulfide in Cynomolgus Monkeys. *Inhal. Toxicol.* (submitted).

Benson, J. M., Y. S. Cheng, A. F. Eidson, F. F. Hahn, R. F. Henderson and J. A. Pickrell: Pulmonary Toxicity of Nickel Subsulfide in F344/N Rats Exposed for 1-22 Days. *Toxicology 103:* 9-22, 1995.

Benson, J. M. and J. T. Zelikoff: Respiratory Toxicology of Metals. In *Toxicology of Metals*, Vol. 1 (L. W. Chang, ed.), pp. 929-938, CRC Press, Lewis Publishers, 1996.

Bice, D. E.: Pulmonary Immunology. In *Immune System Toxicology*, Vol. 5, Comprehensive Toxicology Series (D. A. Lawrence, ed.), Elsevier Scientific Publications/Pergamon Press, New York, NY (in press).

Bice, D. E. and B. A. Muggenburg: Pulmonary Immune Memory: Localized Production of Antibody in the Lung after Antigen Challenge. *Immunology 88*: 191-197, 1996.

Bice, D. E., A. J. Williams and B. A. Muggenburg: Long-Term Antibody Production in Canine Lung Allografts: Implications in Pulmonary Immunity and Asthma. *Am. J. Respir. Cell Mol. Biol. 14*: 341-347, 1996.

Boecker, B. B. and W. C. Griffith: Cancer from Internal Emitters. In *Radiation Research 1895-1995, Vol. 2: Congress Lectures* (U. Hagen *et al.*, eds.), p. 1122-1125, 10th ICRR Society, Wurzburg, 1995.

Boecker, B. B., W. C. Griffith, F. F. Hahn, K. J. Nikula, D. L. Lundgren and B. A. Muggenburg: Lifetime Health Risks from Internally Deposited, Beta-Emitting Radionuclides. To be published in *Proceedings of the 27th Annual Meeting of the European Society for Radiation Biology*, held in Montpellier, France, September 2-6, 1996 (in press).

Butler, C. R., C. B. Radu and J. P. Samora: ITRI Hot Ponds Environmental Restoration Project: Lessons Learned. To be published in *Proceedings of the ER '95 Meeting*, held in Denver, CO, August 13-18, 1995 (in press).

Carpenter, T. R., R. J. Jaramillo and N. F. Johnson: Cell Cycle Arrests and p53, Mdm2, Gadd45, and Cyclin G Protein Expression Following Alpha-Particle Exposure. *Radiat. Res.* (submitted).

Chen, B. T., W. E. Bechtold, G. L. Finch, J. A. Lopez, J. J. Thompson and C. H. Hobbs: Thermal Oxidation of Cigarette Smoke Exhaust. *Aerosol Sci. Technol.* (in press).

Chen, B. T., H. C. Yeh and N. F. Johnson: Design and Use of a Virtual Impactor and an Electrical Classifier for Generation of Test Fiber Aerosols with Narrow Size Distributions. *J. Aerosol Sci. 27(1)*: 83-94, 1996.

Chen, B. T., H. C. Yeh and B. J. Fan: Evaluation of the TSI Small-Scale Powder Disperser. *J. Aerosol Sci. 26(8)*: 1303-1313, 1995.

Chen, T. R., Y. S. Cheng, P. K. Hopke and M. Pourprix: Electrical Mobility and Size Distribution of Aged ^{212}Pb Clusters in Nitrogen Gas. *J. Aerosol Sci.*(submitted).

Cheng, K. H., Y. S. Cheng, H. C. Yeh and D. L. Swift: Calculation of Mass Transfer Coefficients in the Human Oral Passage. *J. Biomech. Eng.* (in press).

Cheng, K. H., Y. S. Cheng, H. C. Yeh and D. L. Swift: An Experimental Method for Measuring Deposition Efficiency of Inhaled Aerosols in Human Oral Airway. *Am. Ind. Hyg. Assoc. J.* (in press).

Cheng, K. H., Y. S. Cheng, H. C. Yeh, R. A. Guilmette, S. Q. Simpson, Y-H Yang and D. L. Swift: *In Vivo* Measurements of Nasal Airway Dimensions and Ultrafine Aerosol Deposition in the Human Nasal and Oral Airways. *J. Aerosol Sci. 27(5)*: 785-801, 1996.

Cheng, Y. S.: Denuder Systems and Diffusion Batteries. In *Air Sampling Instruments, 8th Edition* (B. S. Cohen and S. V. Herring, eds.), pp. 511-525, American Conference of Government Industrial Hygienists, Cincinnati, OH, 1995.

Cheng, Y. S.: Wall Deposition of Radon Progeny and Particles in a Spherical Chamber. *Aerosol Sci. Technol.* (submitted).

Cheng, Y. S. and B. T. Chen: Aerosol Sampler Calibration. In *Air Sampling Instruments, 8th Edition* (B. S. Cohen and S. V. Herring, eds.), pp. 165-186, American Conference of Government Industrial Hygienists, Cincinnati, OH, 1995.

Cheng, Y. S., T. R. Chen, P. T. Wasiolek and A. Van Engen: Radon and Radon Progeny in the Carlsbad Caverns. *Aerosol Sci. Technol.* (in press).

Cheng, Y. S., A. R. Dahl and H. N. Jow: Dissolution of Metal Tritides in a Simulated Body Fluid. *Health Phys.* (submitted).

Cheng, Y. S., S. M. Smith, H. C. Yeh, D. B. Kim, K. H. Cheng and D. L. Swift: Deposition of Ultrafine Aerosols and Thoron Progeny in Replicas of Nasal Airways of Young Children. *Aerosol Sci. Technol. 23*: 541-552, 1995.

Cheng, Y. S., S. M. Smith and H. C. Yeh: Deposition of Ultrafine Particles in Human Tracheobronchial Airways. To be published in *Proceedings of Inhaled Particles VIII*, Cambridge, UK, August 26-30, 1996 (submitted).

Cheng, Y. S., H. C. Yeh, R. A. Guilmette, S. Q. Simpson, K. H. Cheng and D. L. Swift: Nasal Deposition of Ultrafine Particles in Human Volunteers and its Relationship to Airway Geometry. *Aerosol Sci. Technol. 25*: 274-291, 1996.

Collie, D. D. S., D. J. DeBoer, B. A. Muggenburg and D. E. Bice: Evaluation and Association of Blood and Bronchoalveolar Eosinophil Numbers and Serum Total IgE Concentration with Expression of Nonspecific Airway Reactivity in Dogs. *Am. J. Vet. Med.* (in press).

Crowell, R. E., F. D. Gilliland, R. T. Temes, H. J. Harms, R. E. Neft, E. Heaphy, D. H. Auckley, L. A. Crooks, S. W. Jordan, J. M. Samet, J. F. Lechner and S. A. Belinsky: Detection of Trisomy 7 in Nonmalignant Bronchial Epithelium from Lung Cancer Patients and Individuals at Risk for Lung Cancer. *Cancer Epidemiol. Biomarkers Prev. 5*: 631-637, 1996.

Dahl, A. R.: Metabolism of Isoprene *In Vivo*. *Toxicology* (in press).

Dahl, A. R.: Toxicokinetics: Concepts of Dose. To be published in *Vol. 1: General Principles/ Comprehensive Toxicology* (J. A. Bond *et al.*, eds.), Elsevier Science Ltd./Pergamon (in press).

De Silva, R., E. L. May, J. F. Lechner and R. R. Reddel: Immortalization of Human Bronchial Epithelial Cells. To be published in *Culture of Immortalized Cells* (R. I. Freshney, ed.), John Wiley & Sons, Inc. (submitted).

Drent, M., N. A. M. Cobben, R. F. Henderson, E. F. M. Wouters and M. van Dieijen-Visser: Usefulness of Lactate Dehydrogenase and its Isoenzymes as Indicators of Lung Damage. *Eur. Respir. J. 9*: 1736-1742, 1996.

Drent, M., N. A. M. Cobben, R. F. Henderson, J. A. Jacobs, E. F. M. Wouters and M. van Dieijen-Visser: BAL Fluid LDH Activity and LDH Isoenzyme Pattern in Lipoid Pneumonia Caused by an Intravenous Injection of Lamp Oil. *Eur. Respir. J. 9*: 2416-2418, 1996.

Duncan, E. L., R. De Silva, J. F. Lechner and R. R. Reddel: Immortalization of Human Mesothelial Cells. To be published in *Culture of Immortalized Cells* (R. I. Freshney, ed.), John Wiley & Sons, Inc. (submitted).

Fan, B. J., Y. S. Cheng and H. C. Yeh: Air Flow Pattern in a Conducting Airway of Five-Generation Tracheobronchial Tree. *Aerosol Sci Technol.* (submitted).

Fan, B. J., Y. S. Cheng and H. C. Yeh: Gas Collection Efficiency and Entrance Flow Effect of an Annular Diffusion Denuder. *Aerosol Sci Technol. 25*: 113-120, 1996.

Finch, G. L., C. H. Hobbs, D. L. Lundgren, J. M. Benson, F. F. Hahn, K. J. Nikula, W. C. Griffith, M. D. Hoover, E. B. Barr, S. A. Belinsky, B. B. Boecker and J. L. Mauderly: Worker Risk Issues for Combined Exposures to Radionuclides and Chemicals - An Experimental Toxicology Approach. To be published in *Proceedings of the ER '95 Meeting*, held in Denver, CO, August 13-18, 1995 (in press).

Finch, G. L., M. D. Hoover, F. F. Hahn, K. J. Nikula, S. A. Belinsky, P. J. Haley and W. C. Griffith: Animal Models of Beryllium-induced Lung Disease. *Environ. Health Perspect. 104(Suppl. 5)*: 973-979, 1996.

Finch, G. L., K. J. Nikula, S. A. Belinsky, E. B. Barr, G. D. Stoner and J. F. Lechner: Failure of Cigarette Smoke to Induce or Promote Lung Cancer in the A/J Mouse. *Cancer Lett. 99*: 161-167, 1996.

Gerde, P., B. A. Muggenburg, J. R. Thornton-Manning, J. L. Lewis, K. H. Pyon and A. R. Dahl: Benzo(a)pyrene Concentrates in Canine Tracheal Epithelium Following Low Level Exposure. *Cancer Res.* (submitted).

Griffith, W. C., B. B. Boecker, C. R. Watson and G. C. Gerber: Possible Uses of Animal Databases for Further Statistical Evaluation and Modeling. In *Radiation Research 1895-1995, Vol. 2: Congress Lectures* (U. Hagen *et al.*, eds.), p. 731-737, 10th ICRR Society, Wurzburg, 1995.

Guilmette, R. A., Y. S. Cheng and W. C. Griffith: Characterizing the Variability in Adult Human Nasal Airway Dimensions. To be published in the *Proceedings of Inhaled Particles VIII*, Cambridge, UK, August 26-30, 1996 (submitted).

Guilmette, R. A. and B. R. Scott: Radiation Toxicology. To be published in the *Encyclopedia of Toxicology* (P. Wexler, ed.), Appleton and Lange, Stamford, CT (submitted).

Hahn, F. F.: Radiation-Induced Adenosquamous Cell Carcinoma, Lung, Rat. In *Respiratory System* (T. C. Jones *et al.*, eds.), pp. 226-229, International Life Sciences Institute, Springer-Verlag, Heidelberg, Germany, 1996.

Hahn, F. F.: Radiation-Induced Squamous Cell Carcinoma, Lung, Rat. In *Respiratory System* (T. C. Jones *et al.*, eds.), pp. 213-218, International Life Sciences Institute, Springer-Verlag, Heidelberg, Germany, 1996.

Hahn, F. F.: Radiation-Induced Adenocarcinoma, Lung, Rat. In *Respiratory System* (T. C. Jones *et al.*, eds.), pp. 218-223, International Life Sciences Institute, Springer-Verlag, Heidelberg, Germany, 1996.

Hahn, F. F.: Radiation-Induced Sarcoma, Lung, Rat. In *Respiratory System* (T. C. Jones *et al.*, eds.), pp. 223-226, International Life Sciences Institute, Springer-Verlag, Heidelberg, Germany, 1996.

Hahn, F. F., B. B. Boecker, W. C. Griffith and B. A. Muggenburg: Biological Effects of Inhaled $^{144}CeCl_3$ in Beagle Dogs. *Radiat. Res.* (in press).

Hahn, F. F. and G. A. Boorman: Neoplasia and Preneoplasia of the Lung. To be published in *Pathology of Neoplasia and Preneoplasia in Rodents, EULEP Color Atlas, Vol. 2* (P. Bannasch, ed.) (in press).

Hahn, F. F., B. A. Muggenburg and B. B. Boecker: Hepatic Neoplasms from Internally Deposited $^{144}CeCl_3$. *Toxicol. Pathol. 24(3)*: 281-289, 1996.

Hahn, F. F., B. A. Muggenburg and W. C. Griffith: Primary Lung Neoplasia in a Beagle Colony. *Vet. Pathol.* (in press).

Harkema, J. R., E. B. Barr and J. A. Hotchkiss: Responses of Rat Nasal Epithelium to Short- and Long-Term Exposures of Ozone: Image Analysis of Epithelial Injury, Adaptation and Repair. *J. Microscopy Res. Tech.* (in press).

Harkema, J. R., J. A. Hotchkiss and W. C. Griffith: Mucous Cell Metaplasia in Rat Nasal Epithelium After a 20 Month Exposure to Ozone: A Morphometric Study of Epithelial Differentiation. *Am. J. Respir. Cell Mol. Biol.* (in press).

Harkema, J. R., J. L. Mauderly and W. C. Griffith: Pulmonary Function Alterations in F344 Rats Following Chronic Ozone Inhalation. *Inhal. Toxicol. 8*: 163-183, 1996.

Harkema, J. R. and J. L. Mauderly: Pulmonary Function Alterations in F344 Rats Following Chronic Ozone Inhalation. In *Tropospheric Ozone: Critical Issues in the Regulatory Process* (J. J. Vostal, ed.), pp. 431-443, Air & Waste Management Assoc., Pittsburgh, PA, 1996.

Harris, C. C., A. M. A. Pfeifer, T. A. Lehman, A. Weston, B. Gerwin and J. F. Lechner: Oncogenes and Tumor Suppressor Genes in Human Carcinogenesis. *Cancer Res. Clin. Oncol.* (in press).

Henderson, R. F.: Particulate Air Pollution and Increased Mortality: Biological Plausibility for Causal Relationship. To be published in the *Proceedings of the Air and Waste Management Association Meeting*, held in San Antonio, TX, June 18-23, 1995 (in press).

Henderson, R. F.: Species Differences in Metabolism of Benzene. *Environ. Health Perspect.* (in press).

Henderson, R. F.: Species Differences in Metabolism of 1,3-Butadiene. In *Biological Reactive Intermediates V* (R. Snyder *et al.*, eds.), pp. 371-376, Plenum Publishing Corporation, New York, NY, 1996.

Henderson, R. F.: Strategies for Use of Biological Markers of Exposure. *Toxicol. Lett. 82/82*: 379-383, 1995.

Henderson, R. F., J. R. Thornton-Manning, W. E. Bechtold and A. R. Dahl: Metabolism of 1,3-Butadiene: Species Differences. *Toxicology* (in press).

Hobbs, C. H.: Research Methodologies for Risk Assessment. To be published in *Proceedings of the Symposium on Acidifying Emissions*, held in Alberta, Canada, April 14-17, 1996 (submitted).

Hobbs, C. H., J. L. Mauderly and M. B. Snipes: Workshop Overview: The Maximum Tolerated Dose for Inhalation Bioassays: Toxicity vs. Overload. *Fundam. Appl. Toxicol. 29*: 155-167, 1996.

Hotchkiss, J. A., J. R. Harkema and N. F. Johnson: Kinetics of Nasal Epithelial Cell Loss and Proliferation in F344 Rats Following a Single Exposure to 0.5 ppm Ozone. *Toxicol. Appl. Pharmacol.* (in press).

Hussain, S. P., C. H. Kennedy, P. Amstad, J. F. Lechner and C. C. Harris: Mutability of p53 Codons 249 and 250 to ^{238}Pu-alpha Particles in Normal Human Bronchial Epithelial Cells. *Carcinogenesis* (in press).

Issa, J. P., S. S. Baylin and S. A. Belinsky: Methylation of the Estrogen Receptor CpG Island in Lung Tumors is Related to the Specific Type of Carcinogen Exposure. *Cancer Res. 56*: 3655-3658, 1996.

Johnson, N. F. and F. F. Hahn: Mesothelioma Induction Following Intrapleural Inoculation of F344 Rats with Silicon Carbide Whiskers and Continuous Ceramic Filaments. *Br. J. Occup. Med.* (in press).

Johnson, N. F., A. W. Hickman, T. R. Carpenter and G. J. Newton: Biodosimetric Approach for Estimating Alpha-Particle Dose to Respiratory Tract Epithelial Cells. To be published in the *Proceedings of the Fifth International Inhalation Symposium "Correlations Between In Vitro and In Vivo Investigations in Inhalation Toxicology,"* held in Hannover, Germany, February 20-24, 1995, International Life Sciences Institutes Press, Washington, DC (in press).

Kelsey, K. T., J. K. Wienecke, J. Ward, W. Bechtold and J. Fajen: Sister-Chromatid Exchanges, Glutathione S-Transferase Theta Deletion and Cytogenic Sensitivity to Diepoxybutane in Lymphocytes from Butadiene Monomer Production Workers. *Mutat. Res. 335*: 267-273, 1995.

Kennedy, C. H. and J. F. Lechner: *In Vitro* Carcinogenesis of Human Bronchial Epithelial Cells. To be published in the *Proceedings of the Fifth International Inhalation Symposium "Correlations Between In Vitro and In Vivo Investigations in Inhalation Toxicology,"* held in Hannover, Germany, February 20-24, 1995, International Life Sciences Institutes Press, Washington, DC (in press).

Kennedy, C. H. and J. F. Lechner: Sequence of Events in Lung Carcinogenesis. To be published in the *Assessment of Carcinogenic Risk from Occupational Exposure to Inorganic Substances* (J. Duffus, ed.), Royal Society of Chemistry, Cambridge, U.K. (submitted).

Kennedy, C. H., C. E. Mitchell, N. H. Fukushima, R. E. Neft and J. F. Lechner: Induction of Genomic Instability in Normal Human Bronchial Epithelial Cells by ^{238}Pu Alpha-Particles. *Carcinogenesis 17(8)*: 1671-1676, 1996.

Kusewitt, D. F., J. L. Lewis, W. C. Griffith and R. D. Ley: Ultraviolet Radiation Exposure and Photoreactivation on Life Span and Tumor Development in the Marsupial *Mondelphis Domestica*. *Radiat. Res.* (in press).

Lechner, J.: Recent Advances in Lung Cancer Biology. In *Third International DOE/CEC Residential Radon Epidemiology Workshop*, DOE/ER-0668, pp. 38-45, NTIS, U. S. Department of Energy, Springfield, VA, 1995.

Lechner, J. F., R. E. Neft, F. D. Gilliland, R. E. Crowell, R. T. Temes, J. M. Samet and S. A. Belinsky: Identification of Trisomy 7 in Cultured Bronchial Cells from Individuals at High Risk for Lung Cancer: Overview and Perspective. *Environ. Health Perspect.* (in press).

Lechner, J. F., J. Tesfaigzi, and B. I. Gerwin: Oncogenes and Tumor Suppressor Genes in Mesothelioma - A Synopsis. *Environ. Health Perspect.* (in press).

Lipscomb, M. F., D. E. Bice, Lyons C. R., M. R. Schuyler and D. and Wilkes: The Regulation of Pulmonary Immunity. In *Advances in Immunology* (F. J. Dixon, ed.), Academic Press, Inc., San Diego, CA, 1995.

Lundgren, D. L., F. F. Hahn, W. W. Carlton, W. C. Griffith, R. A. Guilmette and N. A. Gillett: Dosimetry and Biological Effects of an Inhaled Monodisperse Aerosol of $^{244}Cm_2O_3$ in the Lung, Liver, and Skeleton of F344 Rats. *Radiat. Res.* (submitted).

Lundgren, D. L., F. F. Hahn, W. C. Griffith, A. F. Hubbs, K. J. Nikula, G. J. Newton, R. G. Cuddihy and B. B. Boecker: Pulmonary Carcinogenicity of Relatively Low Doses of Beta-Particle Radiation from Inhaled $^{144}CeO_2$ in Rats. *Radiat. Res.* (in press).

Malkinson, A. M. and S. A. Belinsky: The Use of Animal Models in Preclinical Studies. In *Lung Cancer: Principles and Practice* (H. I. Pass *et al.*, eds.), pp. 271-284, Lippencott-Raven, Philadelphia, PA, 1996.

Mauderly, J. L.: Lung Overload: The Dilemma and Opportunities for Resolution. *Inhal. Toxicol. 8(Suppl)*: 1-28, 1996.

Mauderly, J. L.: Usefulness of Animal Models for Predicting Human Responses to Chronic Inhalation of Particles. *Chest 109(3)*: 655-685, 1996.

Mauderly, J. L. and R. J. McCunney, Eds.: *Particle Overload in the Rat Lung and Lung Cancer: Implications for Human Risk Assessment.* Taylor & Francis, Washington, DC, 298 pp., 1996.

Mauderly, J. L., D. A. Banas, W. C. Griffith, F. F. Hahn, R. F. Henderson and R. O. McClellan: Diesel Exhaust is Not a Pulmonary Carcinogen in CD-1 Mice Exposed Under Conditions Carcinogenic to F344 Rats. *Fundam. Appl. Toxicol. 30*: 233-242, 1996.

Mauderly, J. L., Y. S. Cheng, N. F. Johnson, M. D. Hoover and H. C. Yeh: Particles Inhaled in the Occupational Setting. In *Lung-Particle Interactions* (P. Gehr and J. Hyder, eds.), Marcel Dekker (submitted).

Melo, D. R., J. L. Lipstein, C. A. N. Oliveira, D. L. Lundgren, B. A. Muggenburg and R. A. Guilmette: A Biokinetic Model for ^{137}Cs. *Health Phys.* (in press).

Melo, D. R., D. L. Lundgren, B. A. Muggenburg and R. A. Guilmette: Prussian Blue Decorporation of ^{137}Cs in Beagles of Different Ages. *Health Phys. 71(2):* 190-197, 1996.

Meyer, M. J. and W. E. Bechtold: Protein Adduct Biomarkers: State of the Art. *Environ. Health Perspect.* (submitted).

Muggenburg, B. A., R. A. Guilmette, J. A. Mewhinney, N. A. Gillett, J. L. Mauderly, W. C. Griffith, J. H. Diel, B. R. Scott, F. F. Hahn and B. B. Boecker: Toxicity of Inhaled $^{238}PuO_2$ in Beagle Dogs. *Radiat. Res. 145(4)*: 361-381, 1996.

Muggenburg, B. A., F. F. Hahn, W. C. Griffith, R. D. Lloyd and B. B. Boecker: The Biological Effects of Radium-224 Injected into Dogs. *Radiat. Res. 146*: 171-186, 1996.

Neft, R. E., M. M. Murphy, L. A. Tierney, S. A. Belinsky, M. Anderson, G. Saccomanno, R. Michels, S. Timm, F. D. Gilliland, R. E. Crowell, and J. F. Lechner: Concurrent Fluorescence in *In Situ* Hybridization and Immunochemistry for the Detection of Chromosomal Aberrations in Exfoliated Bronchial Epithelial Cells. *Acta Cytologica* (in press).

Newton, G. J., M. D. Hoover and R. H. Reif: Determination of Aerosol Size Distribution at UMTRA Project Sites. To be published in the *Proceedings of the ER '95 Meeting*, held in Denver, CO, August 13-18, 1995 (in press).

Nikula, K. J., B. A. Muggenburg, W. C. Griffith, W. W. Carlton, T. E. Fritz and B. B. Boecker: Biological Effects of $^{137}CsCl$ Injected in Beagle Dogs of Different Ages. *Radiat. Res.* (in press).

Nikula, K. J., D. S. Swafford, M. D. Hoover, M. D. Tohulka and G. L. Finch: Chronic Granulomatous Pneumonia and Lymphocytic Responses Induced by Inhaled Beryllium Metal in A/J and C3H/HeJ Mice. *Toxicol. Pathol.* (in press).

Ohnuki, Y., R. R. Reddel, S. E. Bates, J. F. Lechner and C. C. Harris: Chromosomal Changes and Progressive Tumorigenesis of Human Bronchial Epithelial Cell Lines. *Cancer Genet. Cytogenet.* (in press).

Radu, C. B., B. R. Scott, A. Grace and C. R. Butler: ITRI Hot Ponds Soil Remediation Based on DOE RESRAD Code. To be published in the *Proceedings of the ER '95 Meeting*, held in Denver, CO, August 13-18, 1995 (in press).

Rothman, N., R. Haas, R. B. Hayes, G. L. Li, J. Wiemels, S. Campelman, P. J. E. Quintana, L. J. Xi, M. Dosemeci, N. Titenko-Holland, K. B. Meyer, W. Lu, L. P. Zhang, W. Bechtold, Y. Z. Wang, P. Kolachana, S. N. Yin, W. Blot and M. T. Smith: Benzene Induces Gene-Duplicating but not Gene-Inactivating Mutations at the Glycophorin A Locus in Exposed Humans. *Proc. Natl. Acad. Sci. USA 92 (9)*: 4069-4073, 1995.

Rothman, N., G. L. Li, M. Dosemeci, W. E. Bechtold, G. Xi, L. Q. Marti, W. Lu, M. T. Smith, N. Titenko-Holland, L. P. Zhang, W. Blot, S. N. Yin and R. B. Hayes: Hematotoxicity Among Chinese Workers Heavily Exposed to Benzene. *Am. J. Ind. Med. 29 (3)*: 236-246, 1996.

Satou, T., K. A. Nielson, B. J. Cummings, F. F. Hahn, E. Head, N. W. Milgram and C. W. Cotman: The Progression of B-Amyloid Deposition in the Frontal Cortex of the Aged Canine. *Brain Pathol.* (submitted).

Schuyler, M., C. R. Lyons, B. J. Masten and D. E. Bice: Immunoglobulin Response to Intrapulmonary Immunization of Asthmatics. *Am. Rev. Respir. Dis.* (submitted).

Scott, B. R.: Biophysical and Biomathematical Adventures in Radiobiology. In *Proceedings of the Fifth Annual College of Sciences' Symposium, Versatility and Wonders of Physics*, pp. 19-56, Southern University and A&M College, Baton Rouge, LA, 1996.

Scott, B. R.: Estimating Lethality Risks for Complex Exposure Patterns. To be published in the *Proceedings of the Workshop on Triage of Irradiated Personnel*, Armed Forces Radiobiology Research Institute (submitted).

Scott, B. R.: A Generic Model for Estimating the Risk of Deterministic Effects of Partial Organ Irradiation by Hot Particles. *Health Phys. 69(6)*: 909-916, 1995.

Scott, B. R., M. D. Hoover and G. J. Newton: On Evaluating Respiratory Tract Intake of High-Specific-Activity Alpha-Emitting Particles for Brief Occupational Exposure. *Radiat. Prot. Dosim.* (in press).

Scott, G. G., K. J. Nikula, J. J. Waide and R. F. Henderson: A Reliable Method Not Requiring Sophisticated Instrumentation for Isolation of a High-Purity Population of Rat Type II Cells. *Toxicol. Meth.* (submitted).

Shen, H., S. Huang, R. P. Benzo, M. R. Schuyler, D. E. Bice and D. N. Weissman: Intrapulmonary Antigen Deposition: Human IgA Responses. *Am. J. Respir. Cell Mol. Biol.* (submitted).

Snipes, M. B.: Current Information on Lung Overload in Nonrodent Mammals: Contrast with Rats. *Inhal. Toxicol. 8(Suppl)*: 91-109, 1996.

Snipes, M. B., J. R. Harkema, J. A. Hotchkiss and D. E. Bice: Pulmonary Retention and Clearance of Particles in F344 Rats after Depletion of Circulating Polymorphonuclear Leukocytes. *Exp. Lung Res.* (submitted).

Snipes, M. B., A. C. James and A. M. Jarabek: The 1994 ICRP66 Human Respiratory Tract Dosimetry Model as a Tool for Predicting Lung Burdens from Exposures to Environmental Aerosols. *Appl. Occup. Environ. Hyg.* (submitted).

Snipes, M. B., J. W. Spoo, B. A. Muggenburg, K. J. Nikula, M. D. Hoover, W. C. Griffith and R. A. Guilmette: Evaluation of the Clearance of Particles Deposited on the Conducting Airways of Beagle Dogs. *J. Aerosol Med.* (in press).

Swafford, D. S., S. K. Middleton, W. A. Palmisano, K. J. Nikula, J. Tesfaigzi, S. B. Baylin, J. G. Herman and S. A. Belinsky: Frequent Aberrant Methylation of $p16^{INK4a}$ in Primary Rat Lung Tumors. *Mol. Cell. Biol.* (submitted).

Tesfaigzi, J. and R. E. Neft: SPR1 Overexpression Induces Tetraploidy and Nuclear Abnormalities in Mouse, Hamster, and Human Cell Lines. *Cancer Res.* (submitted).

Tesfaigzi, J., J. Th'ng, J. A. Hotchkiss, J. R. Harkema and P. S. Wright: A Small Proline-Rich Protein, sPRR1, is Upregulated Early During Tobacco-Smoke-Induced Squamous Metaplasia in Rat Nasal Epithelia. *Am. J. Respir. Cell Mol. Biol. 14*: 478-486, 1996.

Tesfaigzi, J. and D. M. Carlson: Cell Cycle-Specific Expression of G0SPR1 in Chinese Hamster Ovary Cells. *Exp. Cell Res.228:* 277-282, 1996.

Tesfaigzi, J. and D. M. Carlson: Expression of spr1 Gene in Cultured Tracheal Epithelial Cells and its Regulation by Retinoids Before and After Confluence. *J. Cell Physiol. 166(3)*: 480-486, 1996.

Tesfaigzi, J., G. An, R. Wu and D. M. Carlson: Two Nuclear Proteins in Tracheal Epithelial Cells are Recognized by Antibodies Specific to a Squamous Differentiation Marker. *J. Cell Physiol. 164*: 571-578, 1995.

Tesfaigzi, J. and R. J. Jaramillo: Simultaneous Preparation of RNA and Nuclei for Northern Blot and Flow Cytometric Analysis. *Biotechniques 21*: 800-804, 1996.

Tesfaigzi, J., N. F. Johnson and J. F. Lechner: Endotoxin Instillation Induces Alveolar Type II Cell Proliferation in the Rat Lung. *Int. J. Exp. Pathol. 77*: 143-154, 1996.

Thornton-Manning, J. R., A. R. Dahl, W. E. Bechtold, W. C. Griffith and R. F. Henderson: Comparison of the Production and Disposition of Butadiene Epoxides in Rats and Mice Following a Single and Repeated Exposures to 1,3-Butadiene via Inhalation. *Toxicology* (submitted).

Thornton-Manning, J. R., A. R. Dahl, W. E. Bechtold, W. C. Griffith, L. Pei and R. F. Henderson: Gender Differences in the Metabolism of 1,3-Butadiene in Sprague-Dawley Rats Following a Low Level Inhalation Exposure. *Carcinogenesis 16(11)*: 2875-2878, 1995.

Thornton-Manning, J. R., A. R. Dahl, W. E. Bechtold, and R. F. Henderson: Gender and Species Differences in the Metabolism of 1,3-Butadiene to Butadiene Monoepoxide and Butadiene Diepoxide in Rodents Following Low-Level Inhalation Exposures. *Toxicology* (in press).

Thornton-Manning, J. R. and A. R. Dahl: Metabolic Capacity of Nasal Tissue: Interspecies Comparisons of Xenobiotic-Metabolizing Enzymes. *Mutat. Res.* (in press).

Thornton-Manning, J. R. and A. R. Dahl: Nasal Tract, Biochemistry. To be published in *Encyclopedia of Human Biology*, Academic Press, Inc. (in press).

Thornton-Manning, J. R., K. J. Nikula, J. A. Hotchkiss, K. J. Avila, K. D. Rohrbacher, X. Ding and A. R. Dahl: Local Cytochrome P450 2A: Identification, Cellular Localization, and Metabolic Activity Toward Hexamethylphosphoramide, a Known Nasal Carcinogen. *Toxicol. Appl,. Pharmacol.* (in press).

Tierney, L. A., F. F. Hahn and J. F. Lechner: p53, ErbB2 and K-ras Gene Dysfunctions are Rare in Spontaneous and Plutonium-239-Induced Canine Lung Neoplasia. *Radiat. Res. 145*: 181-187, 1996.

Tierney, L. A., R. A. Neft, S. A. Belinsky, F. T. Lauer, F. D. Gilliland, R. E. Crowell and J. F. Lechner: Double-Label Suspension Immunocytochemistry for the Detection of Gene Dysfunction in Sputum. *J. Histotechnology* (in press).

Ward, J. B., M. M. Ammenheuser, Jr., E. B. Whorton, W. E. Bechtold, K. T. Kelsey and M. S. Legator: Biological Monitoring for Mutagenic Effects of Occupational Exposure to Butadiene. *Toxicology* (in press).

APPENDIX F

PRESENTATIONS BEFORE REGIONAL, NATIONAL, OR INTERNATIONAL SCIENTIFIC MEETINGS AND EDUCATIONAL AND SCIENTIFIC SEMINARS

OCTOBER 1, 1995 - SEPTEMBER 30, 1996

Baughman, R. P., J. A. Whitsett, E. Pattishall, D. A. Keeton, J. J. Waide and R. F. Henderson: Serial Determinations of Surfactant in Patients with Acute Respiratory Distress Syndrome. American Thoracic Society/American Lung Association International Conference, New Orleans, LA, May 10-15, 1996.

Baughman, R. P., R. F. Henderson, J. J. Waide, M. Rashkin and E. N. Pattishall: Exogenous Surfactant Replacement for Ventilator-Associated Pneumonia. European Respiratory Society Congress, Stockholm, Sweden, September 7-11, 1996.

Bechtold, W. E., M. R. Strunk and M. J. Meyer: S-Phenylcysteine in Albumin as a Benzene Biomarker. Health Effects Institute Annual Meeting, Ashville, NC, April 28-30, 1996.

Belinsky, S. A., K. J. Nikula, S. B. Baylin and J-P J. Issa: Increased Cytosine DNA Methyltransferase Activity is Target Cell Specific and an Early Event in Lung Cancer. Fourth Specialized Program of Research Excellence (SPORE) Meeting, Rockville, MD, July 14-16, 1996.

Belinsky, S. A.: Species Differences and Similarities in Mechanisms of Lung Cancer. Mechanisms and Prevention of Environmentally Caused Cancer, Santa Fe, NM, October 21-25, 1995.

Benson, J. M., E. B. Barr, D. E. Bice, K. J. Nikula, S. M. Thurlow, S. M. Clarke and D. E. Hilmas: The Effect of Be Inhalation on Humoral and Cell-Mediated Immunity in the C3H Mouse. Annual Meeting of the Society of Toxicology, Anaheim, CA, March 4-7, 1996.

Bice, D. E. Asthma: Role of Pulmonary Immune Responses. Bristol Immunology Group, University of Bristol, Bristol, UK, November 7, 1995.

Bice, D. E.: Basic Mechanisms of Lung Immunity. The Interaction Between Lung Defenses and Bacteria in the Pathogenesis of Infection - Time for a Reappraisal, Ware, UK, November 14, 1995.

Bice, D. E.: Localization of Antibody Production in the Lung: Importance in Asthma. Comparative Respiratory Society, Orlando, FL, January 12, 1996.

Bice, D. E. and B. A. Muggenburg: Long-Term Antibody Production in the Lung is not Dependent on Antigen Retention. American Thoracic Society/American Lung Association International Conference, New Orleans, LA, May 10-15, 1996.

Bice, D. E.: Experimental Design. The Lovelace Institutes, Albuquerque, NM, July 17, 1996.

Boecker, B. B., W. C. Griffith, F. F. Hahn, K. J. Nikula, D. L. Lundgren and B. A. Muggenburg: Lifetime Health Risks from Internally Deposited, Beta-Emitting Radionuclides. 27th Annual Meeting of the European Society of Radiation Biology, Montpellier, France, September 2-4, 1996.

Cheng, Y. S., W. E. Bechtold, C. C. Yu and I. F. Hung: Characterization of Incense Aerosols in Indoor Environments. American Association of Aerosol Research Annual Meeting, Pittsburgh, PA, October 9-13, 1995.

Cheng, Y. S. and E. B. Barr: Generation and Characterization of Bioaerosols for Laser Experiments. Scientific Conference on Chemical and Biological Defense Research, Aberdeen Proving Ground, MD, November 14-17, 1995.

Cheng, Y. S. and E. B. Barr: Generation and Characterization for Multi-Spectral UV Fluorescence Laser Experiments. Scientific Conference on Chemical and Biological Defense Research, Aberdeen Proving Ground, MD, June 25-28, 1996.

Cheng, Y. S. and G. Ponciano-Rodriguez: Measurements of Indoor Radon and Radon Progeny in Mexico City. 1996 Health Physics Society Annual Meeting, Seattle, WA, July 21-25, 1996.

Cheng, Y. S., S. M. Smith and H. C. Yeh: Deposition of Ultrafine Particles in Human Tracheobronchial Airways. Inhaled Particles VIII, Cambridge, UK, August 26-30, 1996.

Crowell, R., F. Gilliland, R. Neft, E. Heaphy, L. Crooks, D. Auckley, R. T. Temes, J. Lechner and S. Belinsky: Transforming Growth Factor Regulation of Bronchial Epithelium. American Association for Cancer Research Meeting, Baltimore, MD, April 21-25, 1996.

Crowell, R., D. Auckley, R. T. Temes, F. Gilliland, R. Neft, E. Heaphy, H. Harms, L. Crooks, J. Lechner and S. Belinsky: Detection of Trisomy 7 in Nonmalignant Bronchial Epithelium from Lung Cancer Patients. American Thoracic Society/American Lung Association International Conference, New Orleans, LA, May 11-15, 1996.

Dahl, A. R., L. K. Brookins, and P. M. Gerde: An Exposure System for Measuring Nasal and Lung Uptake of Vapors in Rats. Society of Toxicology Annual Meeting, Anaheim, CA, March 4-7, 1996.

Dahl, A. R.: Interactions of Xenobiotics with Portal-of-Entry Epithelia. Laboratory of Human Toxicology and Molecular Epidemiology, New York State Department of Health, Albany, NY, May 2, 1996.

Dahl, A. R.: How Toxicants Interact with Lining Epithelia. School of Medicine, University of Louisville, Louisville, KY, August 12, 1996.

Dahl, A. R., B. A. Muggenburg, J. R. Thornton-Manning and P. Gerde: Differences in Lung Local Dosimetry of the Carcinogens Benzo(a)pyrene and NNK. American Chemical Society, Division of Chemical Toxicology Symposium, Orlando, FL, August 25-29, 1996.

Dam, K., K. D. Rohrbacher, A. R. Dahl and J. R. Thornton-Manning: An *In Vitro* Model for Studying the Metabolism and Bioactiviation of Xenobiotics in Canine Olfactory Mucosa. Society of Toxicology Annual Meeting, Anaheim, CA, March 4-7, 1996.

Finch, G. L., K. E. Spencer, M. B. Snipes, W. C. Griffith and K. J. Nikula: Effect of Chronic Cigarette Smoke Inhalation on the Distribution of $^{239}PuO_2$ Particles in Rat Lungs. Society of Toxicology Annual Meeting, Anaheim, CA, March 4-7, 1996.

Gerde, P., B. A. Muggenburg, J. R. Thornton-Manning and A. R. Dahl: Differences in Dosimetry of the Carcinogens Benzo(a)pyrene and NNK in Airway Mucosa. Society of Toxicology Annual Meeting, Anaheim, CA, March 4-7, 1996.

Guilmette, R. A., Y. S. Cheng, and W. C. Griffith: Characterizing the Variability in Adult Human Nasal Airway Dimensions. Inhaled Particles VIII, Cambridge, UK, August 26-30, 1996.

Harkema, J., J. A. Hotchkiss, C. Bresee and E. Barr: Post-Exposure Persistence of Ozone-Induced Nasal Lesions in F344 Rats. American Thoracic Society/American Lung Association International Conference, New Orleans, LA, May 10-15, 1996.

Henderson, R. F., J. Alchowiak and C. Henry: Development of a Risk-Based Environmental Management Process for the United States Department of Energy. Course on Risk Management Strategies Applied to Environmental Cleanup in Central and Eastern Europe, Ettore Majorana Center for Scientific Culture, Erice, Italy, November 22-29, 1995.

Henderson, R. F., F. F. Hahn, L. Pei, J. J. Waide, J. M. Benson, S. A. Belinsky, E. B. Barr, J. R. Thornton-Manning, W. E. Bechtold, and A. R. Dahl: Dosimetry of Butadiene Diepoxide in Blood and Lungs of Rodents Following Various Routes of Exposure. Society of Toxicology Annual Meeting, Anaheim, CA, March 4-7, 1996.

Henderson, R. F., J. M. Benson, E. B. Barr, F. F. Hahn, S. A. Belinsky, J. R. Thornton-Manning, W. E. Bechtold, A. R. Dahl and W. C. Griffith: Study of the Potential Carcinogenicity of Butadiene Diepoxide in Rats and Mice. Health Effects Institute Annual Meeting, Ashville, NC, April 28-30, 1996.

Henderson, R. F., M. S. Moses and C. J. Henry: The Need for Policy and Risk Analysis - The Department of Energy Experience. 15th International Symposium on Toxicologic Pathology and Risk Assessment, Society of Toxicological Pathologists, St. Louis, MO, June 10, 1996.

Hotchkiss, J. A., C. Bresee, E. Barr, and J. Harkema: Long-Lasting Effects of Chronic Ozone Exposure on the Sensitivity of Rat Nasal Epithelium to Re-Exposure. American Thoracic Society/American Lung Association International Conference, New Orleans, LA, May 10-15, 1996.

Johnson, N. F., T. R. Carpenter, A. W. Hickman and R. J. Jaramillo: DNA Damage-Inducible Genes as Biomarkers for Low-Dose Exposures to Ionizing Radiation and Chemical Genotoxicants. Society of Toxicology Annual Meeting, Anaheim, CA, March 4-7, 1996.

Johnson, N. F.: Expression of DNA Damage-Inducible Genes p53, Cip1, and Gadd153. Sixth International Meeting on the Toxicology of Natural and Man-Made Fibrous and Non-Fibrous Particles, Lake Placid, NY, September 15-18, 1996.

Jones, S. E., J. S. Wiest, E. Johanson, W. A. Palmisano, M. W. Anderson, and S. A. Belinsky: Sequence Comparison of the Promoter Region of the K-ras Gene in Two Inbred Mouse Strains. Annual Meeting of the American Association of Cancer Research, Washington, DC, April 20-24, 1996.

Lechner, J. F.: Molecular Assays and Endpoints. World Summit on Molecular Toxicology, Orlando, FL, February 12-14., 1996.

Lechner, J. F.: Some Recent Advances in Lung Cancer Biology. Colorado State University, Ft. Collins, CO, May 6, 1996.

Lechner, J. F.: Recent Advances in Detection of Field Cancerization in Highly Exposed People. Prevention and Early Detection of Lung Cancer - Clinical Aspects. International Workshop, Helsinore, Denmark, June 22-25, 1996.

Lechner, J. F.: Oncogenes and Tumor Suppressor Genes in Fiber-associated Tumors: Review and Perspective. Sixth International Meeting on the Toxicology of Natural and Man-Made Fibrous and Non-Fibrous Particles, Lake Placid, NY, September 15-18, 1996.

Lewis, J. L., E. B. Barr and D. A. Kracko: Entry of Aluminum into the CNS from Inhaled Soluble Particles. Association of Chemoreception Sciences Annual Meeting, Sarasota, FL, April 17-21, 1996.

Liberati, T. A. and N. F. Johnson: Use of Cultured Rat Lung Slices Exposed to Fibrous Particles to Study DNA Damage-Inducible Genes. Sixth International Meeting on the Toxicology of Natural and Man-Made Fibrous and Non-Fibrous Particles, Lake Placid, NY, September 15-18, 1996.

Mauderly, J. L.: Particulate Air Pollution: Biological Plausibility and Regulatory Implications. Conference on Air Pollution: Has Particulate Matter Increased Mortality?, University of Washington, Seattle, WA, November 30, 1995.

Mauderly, J. L.: Studies to Determine the Relevance of Rat Lung Tumors for Estimating Human Lung Cancer Risk from Inhaled Diesel Exhaust. Workshop on Diesel Exhaust Research Needs, German Verband der Automobilindustrie (VDA), Frankfurt, Germany, December 7, 1995.

Mauderly, J. L.: Current Understanding of the Potential Mechanisms of Carcinogenicity of Diesel Exhaust. Workshop on Diesel Exhaust: Considerations in the Use of Epidemiologic Data for Quantitative Risk Assessments, San Francisco, CA, January 29-30, 1996.

Mauderly, J. L.: Implications of Silica-Induced Pulmonary Carcinogenicity in Rats for Human Lung Cancer Risk. American Conference of Governmental Industrial Hygienists (ACGIH) Threshold Limit Committee (TLV) Meeting, Fort Lauderdale, FL, February 3, 1996.

Mauderly, J. L.: Biological Plausibility: What Have We Learned Recently and What Do We Need to Know? American Thoracic Society/American Lung Association International Conference, New Orleans, LA, May 12-15, 1996.

Mauderly, J. L.: Health Effects of Inhaled Diesel Emissions and Ambient Particles. Office of Transportation Technologies, U. S. Department of Energy, Washington, DC, June 20, 1996.

Mauderly, J. L: Current Issues Concerning the Toxicology of Inhaled Particles. Meeting of Presidential Advisory Committee on Gulf War Veterans' Illnesses, Denver, CO, August 6, 1996.

Mauderly, J. L.: Relevance of Particle-Induced Rat Lung Tumors for Assessing Pulmonary Carcinogenesis Hazards and Human Lung Cancer Risks. Sixth International Meeting on the Toxicology of Natural and Man-Made Fibrous and Non-Fibrous Particles, Lake Placid, NY, September 15-18, 1996.

Mitchell, C. E., W. E. Palmisano, J. F. Lechner, S. A. Belinsky, A. Bernards, and L. Weissbach: Altered Expression of the IQGAP1 Gene in Human Lung Cancer Cell Lines. Annual Meeting of the American Association of Cancer Research, Washington, DC, April 20-24, 1996.

Neft, R. E., L. A. Tierney, S. A. Belinsky, F. D. Gilliland, R. E. Crowell, N. Joste, and J. F. Lechner: A Method for Double-Labeling Sputum Cells for p53 and Cytokeratin. Annual Meeting of the American Association of Cancer Research, Washington, DC, April 20-24, 1996.

Nikula, K. J. and S. A. Belinsky: Increased Cytoisine DNA-Methyltransferase Activity and Expression in A/J Mouse Lung Following Carcinogen Exposure and During Tumor Progression. 1995 American College of Veterinary Pathologists/American Society of Veterinary Clinical Pathologists Annual Meeting, Atlanta, GA, November 12-17, 1995.

Nikula, K. J., W. C. Griffith, K. J. Avila and J. L. Mauderly: Sites of Particle Retention and Lung Tissue Responses to Chronically Inhaled Diesel Exhaust and Coal Dust in Rats and Cynomolgus Monkeys. Sixth International Meeting on the Toxicology of Natural and Man-Made Fibrous and Non-Fibrous Particles, Lake Placid, NY, September 15-18, 1996.

Nutt, A. W., J. M. Benson, A. R. Dahl, D. G. Burt, B. A. Muggenburg and J. L. Lewis: Acute Inhalation Toxicity of Carbonyl Sulfide. Society of Toxicology Annual Meeting, Anaheim, CA, March 4-7, 1996.

Palmisano. W. E.: Interindividual Variation in p53 and Cip1 Protein Expression Profiles in Normal Human Fibroblast Strains Following Exposure to Alpha-Particles. Annual Meeting of the American Association of Cancer Research, Washington, DC, April 20-24, 1996.

Pyon, K. H., A. R. Dahl and J. L. Lewis: Entry of Inhaled Xylene and its Metabolites into the Olfactory Bulb. Association of Chemoreception Sciences Annual Meeting, Sarasota, FL, April 17-21, 1996.

Scott, B. R.: Expert Judgment of Uncertainty in Radiation Early Health Effects Risks for Specific Exposure Scenarios. A Joint Teleconference Sponsored by the U. S. Nuclear Regulatory Commission and Commission of European Communities, Albuquerque, NM, March 27, 1996.

Scott, B. R.: Estimating Lethality Risks for Complex Exposure Patterns. Armed Forces Radiobiology Research Institute Workshop on Triage of Irradiated Personnel, Bethesda, MD, September 25-27, 1996.

Snipes, M. B., A. C. James, and A. M. Jarabek: The 1994 ICRP Human Respiratory Tract as a Model Tool for Predicting Lung Burdens from Exposures to Environmental Aerosols. Second Colloquium on Particulate Air Pollution and Health, Parke City, UT, May 1-3, 1996.

Snipes, M. B., K. J. Nikula, and R. A. Guilmette: A Comparison of Observed Particle Retention Patterns in Rat Lungs Fixed by Drying Intravascular Perfusion, and Intra-Airway Infusion. Sixth International Meeting on the Toxicology of Natural and Man-Made Fibrous and Non-Fibrous Particles, Lake Placid, NY, September 15-18, 1996.

Swafford, D. S., J. Tesfaigzi, C. H. Kennedy, S. K. Middleton and S. A. Belinsky: Differential Expression of the $p16^{INK4a}$ Tumor Suppressor Gene in Murine Tumor Cell Lines and Primary Lung Tumors. Cancer Susceptibility Genes and Molecular Carcinogenesis, Keystone, CO, February 19-25, 1996.

Swafford, D. S., J. Tesfaigzi, S. K. Middleton, and S. A. Belinsky: Expression of $p16^{INK4a}$ Tumor Suppressor Gene in Rodent Lung Tumors. Mechanisms and Prevention of Environmentally Caused Cancer, Santa Fe, NM, October 21-25, 1995.

Tesfaigzi, J.: Cell Cycle-Specific Expression of a Squamous Cell Marker, the Small Proline-Rich Protein Gene. College of Pharmacy and Pharmaceuticals, Florida A & M University, Tallahassee, FL, October 6, 1995.

Thornton-Manning, J. R., W. E. Bechtold, W. C. Griffith, A. R. Dahl and R. F. Henderson: Tissue Concentrations of Butadiene Epoxides in Rodents Following Multiple and Single Exposures to 1,3-Butadiene (BD) by Inhalation. Society of Toxicology Annual Meeting, Anaheim, CA, March 4-7, 1996.

Thornton-Manning, J. R., A. R. Dahl, W. E. Bechtold, W. C. Griffith and R. F. Henderson: Disposition of Butadiene Diepoxide in Rats Following Low-Level and High-Level Inhalation Exposures to 1,3-Butadiene. American Chemical Society, Division of Chemical Toxicology Symposium, Orlando, FL, August 25-29, 1996.

Tierney, L. A., F. F. Hahn and J. F. Lechner: p53 Tumor Suppressor Gene and Protein Expression is Altered in Cell Lines Derived from Spontaneous and Alpha-Radiation-Induced Canine Lung Tumors. 1995 American College of Veterinary Pathologists/American Society of Veterinary Clinical Pathologists Annual Meeting, Atlanta, GA, November 12-17, 1995.

Wang, Y., Y. S. Cheng, M. B. Snipes and H. N. Jow: Metabolic Kinetics and Dosimetry of Titanium Tritide Particles in the Lung. 1996 Health Physics Society Annual Meeting, Seattle, WA, July 21-25, 1996.

APPENDIX G

SEMINARS PRESENTED BY VISITING SCIENTISTS

OCTOBER 1, 1995 - SEPTEMBER 30, 1996

Dr. Werner Burkart, Institute for Radiation Hygiene, Fachbereich Strahlenhygiene, Institut fur Starhlenhygiene, Neuherberg, Germany, *How Can We Assess Risk from Combined Exposures to Radiation and Other Toxic Agents,* December 5, 1995.

Dr. Leslie A. Braby, Richland, WA, *Techniques for Understanding Low Dose, High LET Radiation Effects,* December 6, 1995.

Dr. Harrison H. Schmitt, Acting VP and Chief Operating Officer, The Lovelace Institutes, Albuquerque, NM, *Trip to the Moon,* January 18, 1996.

Dr. Eiichi Fukishima, Institute for Basic and Applied Research, The Lovelace Institutes, Albuquerque, NM, *NMR Program at TLI,* April 8, 1996.

Dr. Roger Reddell, Children's Medical Research Institute, Wentworthville, Australia, *Role of Telomers and Tumor Suppressor Genes in Senescence and Imortalization of Human Cells,* April 25, 1996

Dr. Francois Paquet, Laboratoire d'Etudes Appliquees en Radiotoxicologie, Pierrelatte, France, *Metabolism and Toxicity of Neptunium: Recent French Research*, May 16, 1996.

Dr. Shinji Takenaka, GSF-Institute of Inhalation Toxicology, Oberschleissheim, Germany, *Proliferative Changes in the Proximal Alveolar Regions of Beagle Dogs after Long-Term Exposure to Acidic Sulfate and Sulfite Aerosols,* May 17, 1996.

Dr. K. K. Dutta, Industrial Toxicology Research Centre, Lucknow, India, *Bhopal Gas Episode, Past and Present,* May 28, 1996.

Dr. Pang Shek, Defense and Civil Institute of Environmental Medicine, Ontario, Canada, *Liposomes in Pulmonary Drug Delivery*, May 31, 1996.

Dr. Les Recio, Chemical Industry Institute of Toxicology, Research Triangle Park, NC, *Studies of In Vivo Mutagenesis in Transgenic Mice*, June 13, 1996.

Dr. Doyle C. Graham, Vanderbilt University Medical Center, Nashville, TN, *Molecular Pathogenesis of Heaxane and Carbon Disulfide Neurotoxicity,* June 13, 1996.

Dr. B. T. Golding, University of Newcastle, Newcastle upon Tyme, England, *DNA Damage and Repair: Implications of Cancer Therapy*, August 23, 1996.

Graduate Students

The ITRI/UNM Graduate Program provides the opportunity for students to obtain a Ph.D. degree. Course work is completed at UNM, and the research portion of the doctoral degree is carried out at ITRI, with a scientist serving as the research advisor. Two students have completed degrees through this program. Industry has provided support for this program. Lilly Laboratories contributed funds which supported attendance of students at scientific meetings. Funds from Dupont Central Research and Development provided stipend support.

Graduate students attending other universities can also perform research necessary for their graduate degrees at ITRI. All course work for the advanced degree is completed at the university before the student starts research at ITRI. The advanced degree is awarded by the participating university upon completion of all degree requirements. These graduate programs take advantage of the complementary academic resources available at universities and the research resources available at ITRI. For example, we have joint graduate programs in pathology and medicine with the School of Veterinary Medicine at Purdue University. Graduate veterinary students complete the research portion of a Ph.D. degree at ITRI as part of their residency program in pathology or internal medicine. Since 1966, 64 graduate students have conducted all or part of their research at ITRI.

Postgraduate Training

Research appointments are available to recent doctoral graduates to continue their research training. One program, funded by the National Institutes of Health, is the Pulmonary Epidemiology and Toxicology Training Program which is conducted jointly with UNM. Participants choose to specialize in either epidemiology or toxicology and receive cross-training in the other discipline. During FY-1996, three fellows participated in this program.

The second program provides research opportunities at ITRI for students in life science, chemistry, veterinary medicine, or engineering. This program develops research capabilities in inhalation toxicology and one or more areas of basic pulmonary biology. During FY-1996, seven fellows participated in this program.

University Faculty and Industrial Scientists

Opportunities are available for scientists from universities or industry to visit the Institute or collaborate on research at ITRI. The length of these visits ranges from a few days to obtain information or learn techniques, to a year to conduct research. During FY-1996, participants included those listed in Appendix G.

APPENDIX J

AUTHOR INDEX